DEFINING THE RNA INTERACTOME OF *AEDES* MOSQUITOES

Zaydah Rolande de Laurent

September 2025

A thesis submitted in fulfilment for the degree of Doctor of Philosophy

MRC - Centre for Virus Research - School of Infection and Immunity - College of Medical, Veterinary and Life Sciences - University of Glasgow

Abstract

System-wide approaches have uncovered a vast spectrum of RNA-binding proteins (RBPs) in mammals and a few non-mammalian organisms, such as the fruit fly, zebrafish, roundworms, and plants. However, information on RBPs of arboviral vectors remains largely unknown. RNA interactome capture was used to characterise the RBPome in cells of two medically important mosquito vectors, *Aedes aegypti* and *Aedes albopictus*. 852 and 683 RBPs were identified in *Aedes aegypti* and *Aedes albopictus*, respectively. These RBPs exhibited properties similar to those of human RBPs, having low hydrophobicity that favoured solubility; basic pH to enable interactions with RNA; and contained intrinsically disordered regions, low complexity regions, such as the RGG box and poly (K) that allow for dynamically modular interactions. The use of RBDmap to map mosquito RBPs also revealed that sequence conservation was most apparent in the RNA-binding site. Underscoring the evolutionary conservation of RNA–protein interactions. Further profiling of *Aedes aegypti* RPBome during SINV infection using comparative (RIC) identified 219 differentially regulated proteins, seventy-two were upregulated, while 143 proteins were downregulated. Characterisation of these proteins revealed 80% lacked canonical RNA binding domains, $>$25% were metabolic enzymes, and GO terms identified that the proteins were involved in transport, nucleotide degradation, and energy metabolism. Lastly, knockdown of 17 differentially regulated proteins revealed that 15 of 17 candidates were proviral. Knockdown efficiency and duration of transfection influenced the phenotype of screened RBPs. XRN1 and DCP1A were found to be proviral, while AAEL010642, a PABP, was antiviral. This study provides the first comprehensive characterisation of the mosquito RBPome, revealing evolutionary conservation with other organisms, dynamic reprogramming during SINV infection, and identifying host factors that predominantly act as proviral regulators of viral replication.

Contents

List of Figures

List of Tables

Acknowledgments

As Isaac Newton once said, ‘If I have seen further, it is by standing on the shoulders of giants.’ This sentiment perfectly captures my journey through the PhD. The path to completing this work has been shaped not only by my own efforts, but also by the unwavering support, guidance, and encouragement of a remarkable group of people. It is with deep gratitude that I acknowledge their invaluable role in helping me reach this milestone.

To the WT IIB, for without the funding, I would not have been able to leave my country to pursue a PhD. Thank you for making my dream come true.

To Alfredo, thank you for your mentorship throughout my PhD. I believe you can attest to the fact that I have grown as an individual, and I can now boldly speak about my science.

To Alain, for helping me find my way to this PhD project, it has indeed changed my life.

To Wael, for your guidance in the lab and throughout my PhD. Thank you for sharing your wisdom with me and making me the scientist I am today.

To the Castello lab:

Marko - always reminding me it’s all going to be fine.

Enzo – to your gentleness and always saying how great PhD students we are.

Namah – for the hugs you always give when you see me, they have made even the tough times seem easy.

Rozeena – to your exceptional boldness and pranks, this PhD has definitely been fun because of you.

Chenrui – the baby of the team, for your great enthusiasm to learn, it was very refreshing and reminded me why research is worthwhile.

To Louie, thank you for imparting your wisdom, your pep talks; they were really an encouragement.

To Natasha, dearest Natasha, thank you for always checking on me and ensuring that I always had a listening ear. To the steep learning curve and to the best hugs in the entire planet, they made the hardest day fade away. You are just the best.

To Steph, for sharing your experience with mosquitoes, it has saved me a lot of grief with my experiments. Also, for the quote “I cry a lot, but I am so productive it’s an art”, I’m always reminded that crying is part of the process and not a weakness.

To Mary, thank you for always being my biggest supporter, believing in me, and praying for me. Thank you for being a second mom to me you are just the best.

To my BSF and small group, for your constant prayers and encouraging words, they have made this journey way easier. I thank God for you every day.

To Marina, we started this PhD together and clicked from the very first day. You have been such a great encouragement to me, even when times were tough. Thank you for always being willing to listen to me whine and for setting me straight. I believe our friendship goes beyond this PhD.

To Mommy, no words can describe what an amazing mom you are. Thank you for always believing in me, for staying on the phone for hours just to ensure I had company when I was struggling with my PhD. Thank you for consistently praying for me, even when I found it hard to do it myself. For a thousand lifetimes, I would most definitely choose you. I love you with all my heart.

To Chantal, having a twin is the best thing ever; the fact that I don’t have to say a thing and you still get me is mind-blowing. For the long hours on the phone, talking about my PhD, you have done this PhD as much as I have. I love you with every cell of my being, and just like with mommy, for a thousand lifetimes, you are and always will be my person.

Author's declaration

I, Zaydah Rolande de Laurent, declare that, except where explicit reference is made to the contribution of others, this thesis is the result of my work and has not been submitted for any other degree at the University of Glasgow or any other institution.

List of Abbreviations

Abbreviation	Definition
Ae.	*Aedes*
AGO2	Argonaute-2
bp	Base pair
cDNA	Complementary DNA
CHIKV	Chikungunya virus
Dcr2	Dicer-2
DENV	Dengue virus
DDA	Data dependent acquisition
DMEM	Dulbecco's modified eagle medium
DNA	Deoxyribonucleic acid
dNTP	Deoxyribonucleoside triphosphate
dsRNA	Double-stranded RNA
GTP	Guanosine triphosphate
EGFP	Enhanced green fluorescence protein
eIF	Eukaryotic initiation factor
FBS	Foetal bovine serum
FDR	False discovery rate
GO	Gene ontology
gvRNA	Genomic viral RNA
HIV-1	Human immunodeficiency virus type 1
hnRNP	Heterogeneous nuclear ribonucleoprotein
hpi	Hours post infection
hpt	Hours post treatment
IDR	Intrinsically disordered region
IMD	immune deficiency
ISG	IFN-stimulated gene

Abbreviation	Definition
JAK/STAT	Janus kinases/signal transducers and activators of transcription
KD	Knockdown
KH	K-homology domain
LC-MS/MS	Liquid chromatography tandem mass spectrometry
MDA5	melanoma differentiation-associated protein 5
MAPK	Mitogen-activated protein kinases
MAYV	Mayaro virus
miRNA	Micro RNA
MOI	Multiplicity of infection
mRNA	Messenger RNA
MS	Mass spectrometry
NFkB	Nuclear factor kappa-light-chain-enhancer of activated B cells
nt	Nucleotide
ORF	Open reading frame
PABP	Poly(A) binding protein
PAMP	Pathogen-associated molecular patterns
PCA	Principle component analysis
PCR	Polymerase chain reaction
PFU	Plaque forming units
piRNA	PIWI interacting RNA
PKR	Protein kinase R
poly(A)	Polyadenylated
PRR	Pattern recognition receptors
PTM	Post-translational modification
R	R programming language
RBD	RNA binding domain

Abbreviation	Definition
RBP	RNA-binding protein
RBS	RNA binding site
RIC	RNA interactome capture
RIG-I	Retinoic acid-inducible gene I
RLR	RIG-I-like receptors
RNA	Ribonucleic acid
RNAi	Ribonucleic acid interference
RNP	Ribonucleoprotein
RRM	RNA recognition motif
RRV	Ross river virus
RT-qPCR	Reverse transcription quantitative polymerase chain reaction
SARS-CoV-2	Severe acute respiratory syndrome coronavirus 2
SINV	Sindbis virus
SFV	Semliki forest virus
sgRNA	Subgenomic RNA
siRNA	Small Interfering RNA
spp	species
TNF	Tumor necrosis factor

1 Introduction

1.1 Alphaviruses

Arborviruses are a diverse group of viruses maintained in cycles between hematophagous arthropod vectors (for example, mosquitoes and ticks) and vertebrate hosts [1, 4–6]. Medically important arboviruses are mainly found in *Flaviviridae*, *Togaviridae*, and *Bunyaviridae* families and collectively cause diseases ranging from mild febrile illness to hemorrhagic fevers and encephalitis [7]. Arboviruses are typically enzootic and depend on birds and mammals that serve as reservoirs for viral maintenance in nature. Humans are usually incidental hosts, who, developing high viremia, can infect anthropophilic vectors, which then transmit the virus in urban cycles [7]. Alphavirus is one of the two genera within the Togoviridae family. The other genus, Rubivirus, contains a single species Rubella virus, while the Alphavirus encompasses over 30 species that infect a wide range of host and vector species, both aquatic and terrestrial [8–10]. Alphaviruses are zoonotic positive-sense single-stranded viruses that are maintained primarily in rodents, primates, and birds by mosquito vectors. However, aquatic arboviruses have no confirmed arthropod vectors. For instance, salmonid alphavirus (SAV) primary mode of transmission is horizontal transmission through water columns [11], whereas southern elephant seal virus (SESV) is thought to be transmitted by sea lice that parasitise seals [12]. Humans are incidental hosts, often getting infected when they intrude on enzootic transmission habitats or when alphaviruses emerge to cause epizootics and epidemics [10, 13].

Notably, alphaviruses that infect humans can be broadly grouped by their clinical manifestation and geographical location. The New World alphaviruses, which include Venezuelan equine encephalitis virus (VEEV), Eastern equine encephalitis virus (EEEV), and Western equine encephalitis virus (WEEV), are found in North, Central, and South America and typically induce neurological disease with potentially high mortality [14]. In contrast, the Old World alphaviruses, which include Chikungunya (CHIKV), Ross River virus (RRV), ONNV, Mayaro virus (MAYV), and Sindbis virus (SINV), are typically found in Africa, Asia, Europe, and Oceania and induce an

arthritogenic disease characterised by fever, rash, and arthralgia [15]. The primary vectors for these viruses are transmitted by the *Culex* and *Aedes spp*, and they represent a re-emerging public health threat as vector distribution expands [16]. CHIKV is an example of an alphavirus that has been declared a high-risk to public health, with cases and deaths increasing by 4-fold from 2022 to 2023 [17]. This is a result of the geographic expansion of its primary vectors, *Ae. aegypti* and *Ae. albopictus*, due to rising global temperatures [18]. Understanding the interaction between virus and vector is thus critical to developing effective countermeasures.

1.1.1 Human pathogenesis and immunity of alphaviruses

Pathology The outcome of alphavirus infection results from complex interactions between the virus and the host's immune system. The severity of the disease and the duration of infection are dependent on the initial immune response [19]. Besides infecting immune cells, alphaviruses also infect endothelial cells, muscle cells, periosteum, fibroblasts and synovial cells [20, 21]. Alphavirus infections are associated with autoimmune or inflammatory syndromes [16] because they trigger both the innate and adaptive immune factors [22]. Immune factors released from the leukocytes, including reactive oxygen species and prostaglandin, are part of the host's immune response, and likely contribute to the acute symptoms associated with alphaviruses [23].

Disruption of the host's immune defence can also contribute to pathology. For example, impaired chemotaxis of immune cells can lead to increased viral titres, triggering an inflammatory response. Conversely, a robust chemotactic and inflammatory response is likely to be detrimental to the host rather than protective, especially in responses that promote neuroinvasion [24]. Replication in the central nervous system (CNS) tissues typically occurs later in the disease pathology [25]

Arthritogenic alphaviruses, including RRV, CHIKV, MAYV, SFV, SINV, ONNV, and Barmah Forest virus, significantly impact the joints and may cause neurological manifestations. These infections have two distinct phases: acute and chronic. The

acute phase typically manifests 3-10 days post-infection, with a viremic period lasting 4-7 days. Clinical manifestations are nonspecific, often leading to misdiagnosis [15]. The frequency of clinical disease varies among viruses. Most RRV and SINV infections are asymptomatic, while up to 80% of CHIKV and MAYV infections result in clinical symptoms [15, 19, 26]. Infection with Old World alphaviruses can lead to rare but possible fatalities, particularly in neonatal or elderly individuals with comorbidities. Fatal cases are often associated with respiratory, renal, hepatic, and neurological complications, especially in individuals with pre-existing conditions such as hypertension, respiratory, or cardiovascular disease [27–30]. Maternal-fetal transmission of CHIKV carries a risk of approximately 3% for neonatal death, with infants infected later in gestation exhibiting various symptoms such as joint edema, petechiae, rash, thrombocytopenia, disseminated intravascular coagulopathy, and encephalopathy, potentially leading to long-term disabilities [31, 32].

Innate immune responses The innate immune response to alphavirus infection involves several key steps: recognition of viral components by pattern recognition receptors (PRRs), production of interferons and pro-inflammatory cytokines, and the activation and recruitment of immune cells. Alphaviruses are detected by PRRs, including Toll-like receptors (TLRs), retinoic acid-inducible gene I (RIG-I)-like receptors (RLRs), NOD-like receptors (NLRs), and C-type lectin receptors (CLRs) [33, 34]. TLRs and RLRs are key players in sensing viral RNA. TLRs recognize viral RNA in endosomes, while RLRs such as RIG-I and melanoma differentiation-associated protein 5 (MDA5), sense viral RNA within the cytoplasm [35]. NLRs, such as NLRP3 and NLRP1, form multiprotein complexes called inflammasomes, which activate caspase-1 and induce the production of pro-inflammatory cytokines IL-1β and IL-18. Recent studies have implicated NLRP3 and NLRP1 in the recognition of alphaviral pathogen-associated molecular patterns (PAMPs), suggesting their involvement in the induction of inflammatory responses during alphavirus infection [36]. Engagement of PRRs activates signalling cascades leading to the expression of transcription factors, which ultimately induce type I interferons (IFNs), pro-inflammatory cytokines, and

chemokines [33].

Effector cells such as macrophages, dendritic cells (DCs), and natural killer (NK) cells are quickly drawn to the infection site, playing a vital role in either protecting the body or contributing to disease development. Through processes like phagocytosis, cytokine release, and direct killing of infected cells, macrophages, dendritic cells, and NK cells work together to limit and ultimately eliminate the virus [15]. This carefully coordinated immune response is essential for the early detection of aphaviruses; however, excessive activation can lead to immunopathology.

Adaptive responses The adaptive immune response plays a pivotal role in viral clearance and long-term immunity. Upon encountering alphavirus antigens, antigen-presenting cells (APCs) such as DCs and macrophages capture and process viral particles. These APCs migrate to secondary lymphoid organs, where they present viral antigens to naive T lymphocytes via major histocompatibility complex (MHC) molecules. This interaction leads to the activation and differentiation of T cells into effector cells, including cytotoxic CD8+ T lymphocytes (CTLs) and helper CD4+ T cells (Th cells) that migrate to sites of infection to control virus replication [34, 37].

Upon recognition of viral peptides presented by MHC class I molecules, CTLs become activated and release cytotoxic granules containing perforin and granzymes, inducing apoptosis in virus-infected cells. This direct cytotoxicity is essential for controlling viral replication and limiting viral spread [38, 39]. Most pathogen-specific CTL responses start 3–4 days post-infection, peak by 7–10 days, and then decline. Helper CD4+ T cells orchestrate the antiviral immune response by providing essential signals for optimal B and CD8+ T cell responses. In acute CHIKV infection, patients exhibit transient lymphopenia, a phenomenon that may be partially explained by CD4+ T cell apoptosis [37, 40].

Alphavirus antigens trigger the activation and differentiation of B cells into antibody producing plasma cells. Virus-specific antibodies target viral particles, neutralise their infectivity, promote opsonisation and phagocytosis, and activate complement-

mediated lysis of infected cells [41].

1.1.2 Alphavirus genome and life cycle

The virus particle consists of an RNA genome (about 11.7kb) surrounded by a protein capsid shell within a host-derived lipid envelope decorated with glycoprotein spikes [10]. The capsid shell and glycoprotein spikes are arranged into icosahedral particles of about 70 nm diameter. There are 240 copies of the capsid protein arranged in a lattice, with the surface glycoprotein spikes, consisting of envelop glycoproteins E1 and E2, also forming a T=4 structure as 80 trimers of heterodimers (Fig.1.1A). The genome is a single strand of positive-sense RNA that possesses a type 0 5' 7-methyl-GpppA cap and a 3' poly(A) tail (Fig.1.1B). The genome has two open reading frames (ORFs), the second of which is expressed through production of a subgenomic mRNA from an internal promoter in the minus-strand RNA replication intermediate. The second ORF encodes the structural proteins that function in the assembly of new virus particles and the attachment and entry to new cells. The first ORF is translated directly from genomic RNA and encodes the non-structural proteins required for RNA synthesis [42] (Fig.1.1,1.2).

Upon entry into a host cell, the genomic 49S RNA serves as mRNA for the nonstructural polyprotein (nsP1–nsP4), which is translated immediately. These nonstructural proteins assemble into a viral replication complex on host cell membranes, primarily endosomal or plasma membrane-derived vesicles, and synthesise a complementary negative-strand RNA. This negative strand then templates two processes: (i) production of new genomic RNA for packaging into progeny virions, and (ii) transcription of a subgenomic mRNA (26S mRNA) encoding the structural proteins. The structural proteins include the capsid protein, which binds the genomic RNA and forms the nucleocapsid, and the envelope glycoproteins (E1 and E2) that embed in the host-derived lipid envelope. The subgenomic mRNA is translated later in infection to produce these structural components. Alphavirus assembly occurs at the host cell plasma membrane, where capsid proteins encapsidate genomic RNA and associate with the cytoplasmic tails of E2; virions then

bud from the membrane, acquiring their envelope studded with E1/E2 spike proteins. Mature virions (70 nm in diameter) are spherical particles capable of initiating a new infection (Fig.1.1, 1.2) [42–45].

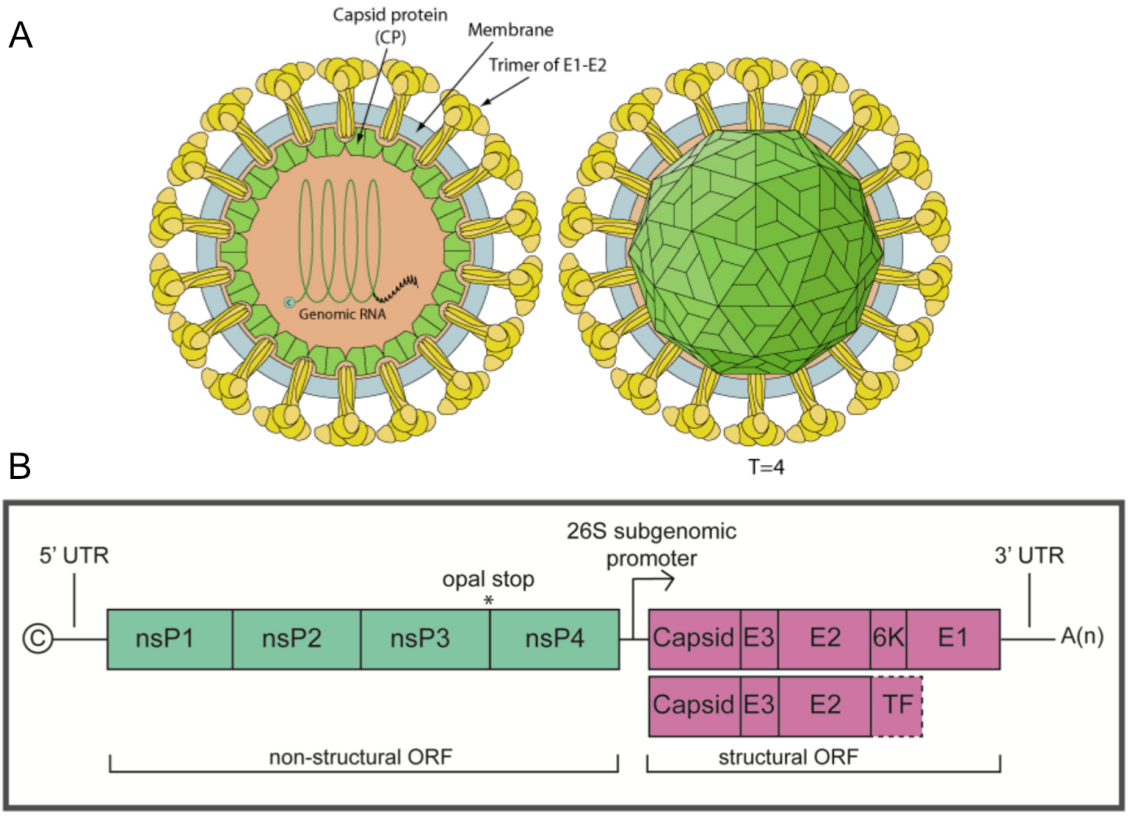

Figure 1.1: Schematic of the alphavirus structure and genome [1]

A)The virus particle consists of an RNA genome surrounded by a protein capsid shell within a host-derived lipid envelope decorated with glycoprotein spikes. The capsid shell and glycoprotein spikes are arranged into icosahedral particles of 70 nm diameter. There are 240 copies of the capsid protein arranged in a T = 4 lattice, with the surface glycoprotein spikes, consisting of E1 and E2, also forming a T = 4 structure as 80 trimers of heterodimers

B) The genome is about 11.7 kb in length and encodes two open reading frames (ORFs) flanked by 5' and 3' untranslated regions (UTRs) and contains a 5' methylguanylate cap and 3' polyadenylated tail. The first ORF encodes a polyprotein that is cleaved into four non-structural proteins (nsP1–4), with cleavage intermediates that function in RNA replication. The second ORF is translated from a subgenomic RNA and encodes the structural polyprotein, which is cleaved into five structural proteins (capsid, E3, E2, 6K, and E1), or, alternatively, a frameshift event leads to a truncated polyprotein that produces capsid, E3, E2, 6K, and TF.

Cell entry is typically via receptor-mediated endocytosis: the E2 glycoprotein on the virion attaches to a host cell receptor, and the virion is internalised into an endosome. Acidification of the endosome triggers conformational changes in E1/E2, leading to membrane fusion and release of the nucleocapsid into the cytosol. Alphavirus replication is cytoplasmic, though the RNA synthesis occurs in protected membrane invaginations known as spherules to shield viral RNA from host defences (Fig.1.2) [44, 46]. A single infected cell can produce thousands of new virions within hours, reflecting the efficiency of the alphavirus replication strategy.

In mosquito vectors, alphaviruses generally establish persistent, non-lethal infections; the virus must infect midgut epithelial cells after ingestion, disseminate to the hemolymph, and ultimately infect the salivary glands to be transmitted in the saliva. In vertebrate hosts, infections are usually acute and immunogenic, with robust interferon responses controlling viremia [47].

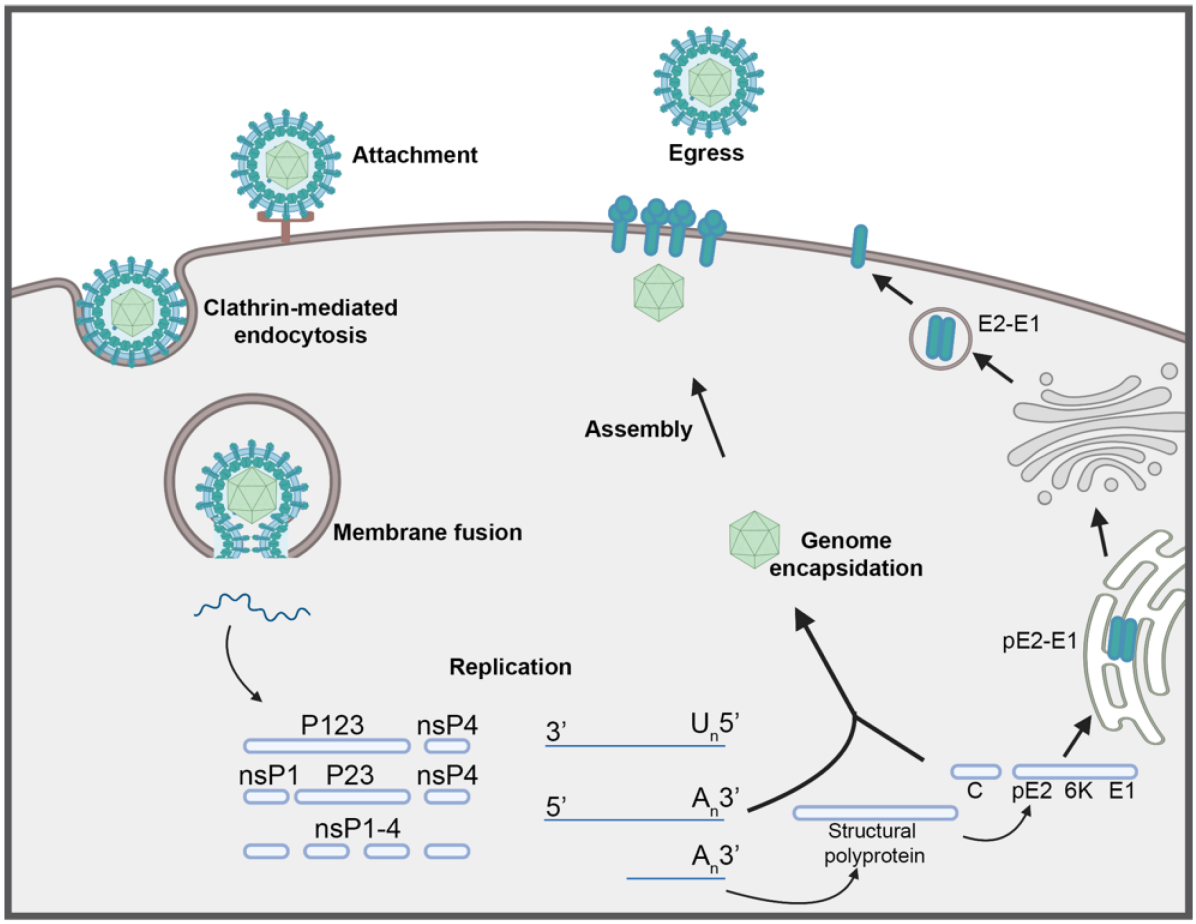

Figure 1.2: Schematic of Alphavirus life cycle [1]

After entry and translation of the genomic RNA, the non-structural polyprotein P1234 is first cleaved to generate P123 and nsP4, which transiently assemble into an early replication complex responsible for negative-strand RNA synthesis. Subsequent trans-cleavage of P123 produces nsP1, P23, and nsP4, shifting the replication complex toward genomic RNA synthesis. Final cleavage into the four individual non-structural proteins (nsP1–4) establishes the mature replication machinery that supports both genomic and subgenomic RNA synthesis. Translation of the subgenomic RNA yields the structural polyprotein, which undergoes coordinated processing for virion assembly. Capsid proteins encapsidate newly synthesised genomic RNA to form cytoplasmic nucleocapsids, while the E1/E2 glycoproteins are processed and trafficked to the plasma membrane. Virion budding occurs at the cell surface, where nucleocapsids acquire their envelope by interacting with the membrane-embedded glycoproteins

1.2 Mosquitoes as a vector

Mosquitoes (Diptera, Nematocera: Culicidae) comprise of over 3,500 known species, organised in 44 genera and 145 sub-genera [48]. Their distribution is quite vast,

being found on every continent except Antarctica. Beyond their ecological ubiquity, mosquitoes have a profound influence on human history and health than any other insect group. Interestingly, only about 5% of species are involved in pathogen transmission. The primary genera of medical importance are *Aedes*, *Anopheles*, and *Culex*, which are responsible for transmitting major diseases such as dengue (DENV), Zika (ZIKV), CHIKV, yellow fever, malaria, West Nile virus (WNV), among others [49,50]. Notably, *Aedes aegypti* (native to Africa) and *Aedes albopictus* (native to Asia) have expanded their range, reaching the Americas and European continents. This invasive spread has been facilitated by globalization and climate change contributing to global resurgence of mosquito-borne epidemics [51–54]. Despite decades of sustained efforts, effective and sustainable mosquito control remains an urgent and elusive challenge in global health.

1.2.1 Mosquito morphology and life cycle

Mosquitoes are tiny insects, typically 0.5 - 1cm long, with the body divided into three parts: head, thorax, and abdomen (Fig.1.3). As members of the order Diptera, they possess a single pair of mesothoracic wings, with hindwings modified into halteres that stabilise flight. Culicidae's defining feature is the proboscis, a piercing-sucking structure used for blood and nectar feeding. Sexual dimorphism is distinctive, with females bearing filiform antennae and short maxillary palps (with the exception of anopheline mosquitoes, where the palp is as long as the proboscis). Meanwhile, males exhibit plumose antennae, elongated palps, and a terminal hypopygium with claws for mating. Adults are covered in scales of varying colouration that, alongside features such as bristle distribution and genital morphology, provide key taxonomic identifiers [55, 56] (Fig.1.3).

Immature stages of mosquitoes are aquatic, characterised by filter feeding, with a distinct head, enlarged thorax, and abdomen terminating in a respiratory siphon or spiracles. Diagnostic features for larval identification include the morphology of antennae, head bristles, abdominal ornamentation, and the structure of the siphon and anal segment. The pupal stage is mobile and aquatic, completing metamorphosis

within 1–2 days [56] (Fig.1.3).

Mosquitoes undergo complete metamorphosis with four distinct stages: egg, larva, pupa, and adult, with each life stages adapted to ecological niches. Gravid females lay eggs in aquatic or semi-aquatic environments and may apply survival strategies such as desiccation-resistance dormancy (e.g. *Aedes spp*). The larvae are aquatic and feed via filter-feeding on microorganisms, moulting through 4 instars before pupation. The pupae are motile but non-feeding and emerge into a flying adult (Fig.1.4). The entire life cycle take 1-2 weeks if the conditions are favourable, such as warm, stable temperatures (24-30ºC) and calm waters that allow for pupae to remain at the water surface [49]. Mating often occurs soon after emergence, with males forming swarms to attract females through visual, chemical, and acoustic cues [57, 58]. Females typically mate once, storing sperm in spermathecae for lifelong use. Mating plugs in some species prevent further copulations. Adult longevity ranges from weeks to several months, with overwintering or aestivation strategies owing for survival in extreme conditions. Only adult females feed on blood, which is essential for egg development. This gonotrophic cycle repeats multiple times in the life of female mosquitoes and is what drives the pathogen transmission cycle. [50, 55].

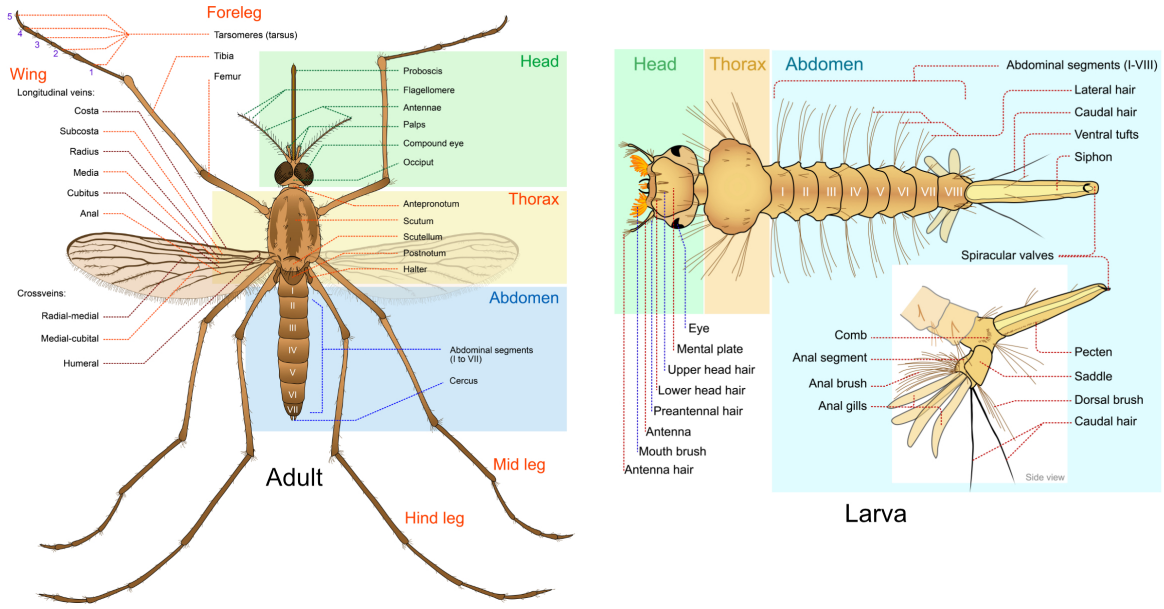

Figure 1.3: Adult and larva mosquito morphology [2]

Adult: Adult mosquitoes are slender insects with a distinct head, thorax, and elongated abdomen. The head bears large compound eyes, multi-segmented antennae, maxillary palps, and a proboscis composed of modified mouthparts (stylets) for blood feeding in females. The thorax is dominated by the mesothorax and supports one pair of scaled wings, halteres, and three pairs of articulated legs. Wing venation and leg scaling are key taxonomic features. The abdomen consists of 7–8 visible segments, with terminal segments housing the genital structures; these show species-specific morphology, particularly in males.

Larva: Mosquito larvae are apodous, aquatic, and characterised by a distinct head, enlarged fused thorax, and nine apparent abdominal segments. The head is dorsoventrally flattened and bears diagnostic setae, antennae, mandibulate mouthparts, and paired larval and developing compound eyes. The thorax forms a single globular unit with prominent setae. The abdomen carries segment-specific setae and ends in anal papillae for osmoregulation. Culicine larvae possess a tubular siphon with apical spiracles and species-specific pecten teeth, whereas Anopheline larvae lack a siphon and breathe via a spiracular plate while resting parallel to the water surface.

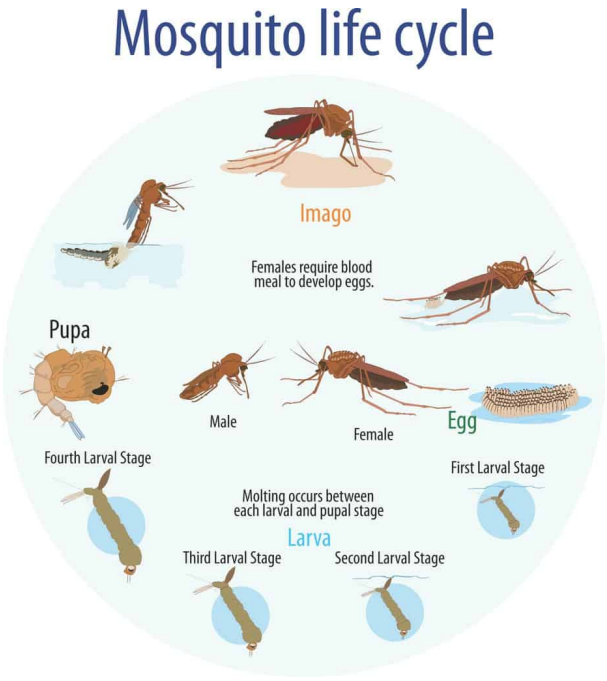

Figure 1.4: Mosquito life cycle [3]

The mosquito life cycle comprises four aquatic-to-terrestrial stages: Eggs are laid on moist surfaces and hatch within 2 days. Larvae develop underwater, breathing at the surface and undergoing four moults before pupation. Pupae remain active but do not feed, with adult development completed in 2–4 days. Adults emerge from the water surface, with males surviving a few days post-mating and females living several weeks to 2 months

1.2.2 Vector competence

For a mosquito to efficiently transmit a virus, it must be vector competent. This journey begins when a female mosquito takes a blood meal from an infected host. The virus in the blood then enters the mosquito's midgut epithelial cells and replicates. Subsequently, the virus spread through the entire body tissues, including the fat bodies, eventually reaching the salivary glands. Finally, upon a subsequent blood meal, the mosquito transmits the virus through its saliva. The time between the ingestion of an infected blood meal and the mosquito becoming infectious is known as the extrinsic incubation period. [59]. For a virus to be successfully transmitted, it must be able to overcome host components. These are anatomical barriers such as the midgut and salivary glands; microbial barriers, these are resident microbes such as *Wolbachia* and insect-specific viruses; and immunological barriers [4] (Fig.1.5), which

will be discussed in detail under mosquito immune pathways later.

In nature, relatively few mosquitoes are competent vectors of specific pathogens. *Ae. aegypti* and *Ae. albopictus*, for example, are the principal urban vectors of DENV, ZIKV, CHIKV, and YFV. On the other hand, *Ae. japonicus*, *Ae. koreicus* and *Culex spp* only play secondary roles. Some flaviviruses, including JEV and WNV, are primarily transmitted by *Culex* mosquitoes. Members of the *Togaviridae* family, CHIKV, Sindbis virus (SINV), Semliki Forest virus (SFV), and Ross River virus (RRV), are primarily transmitted by *Aedes* mosquitoes. The *Anopheles* mosquito, which is the main vector for the parasite *Plasmodium falciparum*, is only known to transmit O'nyong-nyong virus (ONNV) [56, 60]. This illustrates that a mosquito's intrinsic susceptibility to a given virus is shaped by its evolutionary history and genetics. Even within a species, different populations or genetic strains can exhibit varying competence. For instance, certain strains of *Ae. aegypti* are inherently refractory to DENV infection, whereas more susceptible strains show lower antiviral immune activity [4].

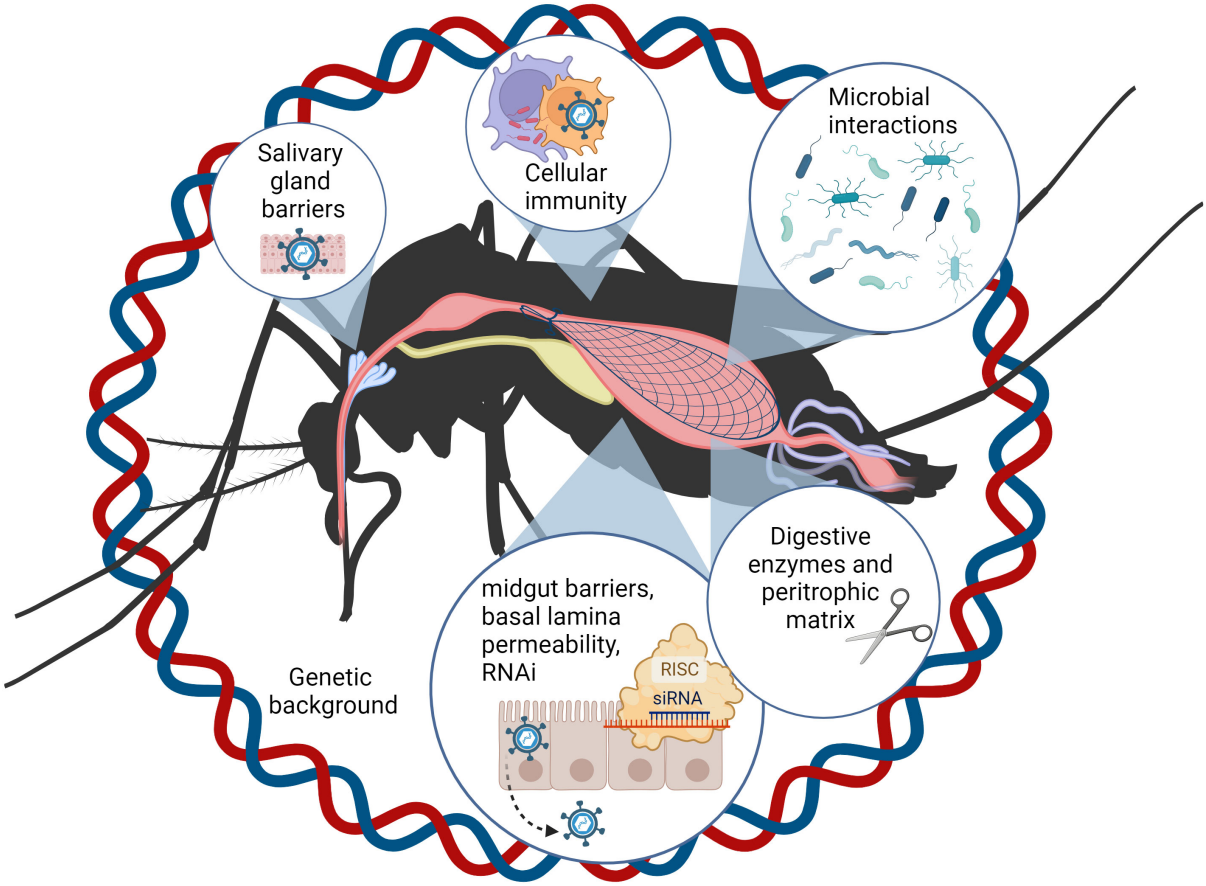

Figure 1.5: Components that determine vector competence [4]

Multiple mosquito-intrinsic factors shape both vector competence and viral evolution. For horizontal transmission to occur, ingested virions must infect and replicate within the midgut epithelium, escape into the hemocoel, disseminate through the body cavity, and subsequently invade the salivary glands, from which they are released in saliva during the next blood meal. At each stage, the virus encounters physical, cellular, microbial, and immune barriers whose effectiveness is strongly influenced by the mosquito's genetics.

1.3 Mosquito innate immune pathways

Mosquitoes lack the adaptive immunity of vertebrates and instead rely entirely on innate immune mechanisms to combat infection. Mosquitoes are constantly being threatened by invading microorganisms and, as a result, have developed immune pathways that target invading pathogens. Key to these are i) the RNA interference (RNAi) pathway, ii) the Janus kinase/signal transducer (JAK-STAT) pathway, iii) the Toll pathway, iv) the immune deficiency (IMD) pathway, and v) the MAPK pathway. The interaction of arborviruses with these pathways is critical in mosquito infection control

strategies. [5, 61].

1.3.1 The RNAi pathway

The RNAi pathway is the main antiviral pathway in mosquitoes. Its primary mode of action involves the targeted degradation of viral RNA molecules, thus inhibiting their replication. Other mechanisms it uses are transposable elements and post-transcriptional gene regulation. The RNAi machinery can be divided into three classes depending on the type of RNA molecule it targets and its primary function:

Micro RNA (miRNA) miRNAs are small noncoding RNAs that are generated in the nucleus from distinct genetic loci. miRNA genes are transcribed into pre-miRNA molecules, which produce stem-loop structures. These pre-miRNAs are then processed in a protein complex known as the microprocessor complex. Here, the ribonuclease III superfamily protein Drosha, along with a double-stranded binding protein, Pasha, cleaves the pre-miRNAs at the stem loop into 70- to 80-nt dsRNAs with a 2- to 3-nt ssRNA overhang. These dsRNAs are then recognised by exportin-5, a RanGTP-dependent dsRNA-binding protein, and transported into the cytoplasm, where they are cleaved by Dcr1 into 22-nt dsRNA duplexes. These dsRNAs are then loaded onto miRNA-specific RISC complexes, where they are separated into two strands. One strand serves as the guide strand that leads to the cleavage of complementary mRNA with Ago1 nuclease. Dcr1 and Ago1 play a role in the miRNA pathway that is analogous to that of Dcr2 and Ago2 in the siRNA pathway [5](Fig.1.6A).

Small interfering RNA (siRNA) The siRNA pathway specifically degrades viral RNA in a sequence-specific manner. Dicer2 (Dcr2), R2D2, and argonaute-2 (Ago2) are the main components of this pathway. The double-stranded RNAs (dsRNAs) that are produced during viral replication are processed by Dcr-2's RNA III domain and the closely associated R2D2 into 21-nucleotide fragments. The fragments are then loaded into the RNA-induced silencing complex (RISC) where they are separated into individual strands. One of the strands is directed for degradation, while the other

remains in the RISC complex and acts as a guide strand. The guide strand then binds to complementary viral RNA that it encounters, and RNA nuclease Ago-2 mediates its cleavage [5](Fig.1.6B).

P-element-induced wimpy testis (PIWI) interacting RNA (piRNA) The piRNA pathway also targets viral RNA; however, its mechanism of action is not yet clearly known. Piwi proteins are key components of this pathway and belong to the Argonaut superfamily. Unlike the siRNA pathway, the piRNA pathway is not conserved in insects, especially within the order Diptera. This suggests a diversification of the pathway [62]. The piRNA targets RNA that is 24-30 nt long and shows uracil bias at nucleotide position 1 at the 5'end, a 10-nucleotide-long complementary sequence to the opposite strand, an adenine bias at nucleotide position 10 of the complementary strand (ping-pong signature), and methylation at the 3'end [5].

Most of our knowledge of the piRNA pathway in mosquitoes is from *Ae. aegypti*, which was found to encode 7 PIWI proteins (PIWI1-7) and Ago3. Based on gene expression data and silencing experiments, different sets of PIWI proteins are used for defence against endogenous transposons and active viral infection. PIWI1-3 and 7 are highly expressed in the germline, whereas PIWI4-6 and Ago3 are expressed in cell lines and somatic tissues. PIWI5 and Ago3 are particularly responsible for the ping-pong amplification-based biogenesis of viral piRNA. PIWI4 is involved in the methylation or maturation of viral piRNA. PIWI4 has also been shown to interact with PIWI5 and PIWI6 and Ago3; as well as with Dcr2 and Ago2. This interactions serves as a connector of the two RNAi pathways [63](Fig.1.6C).

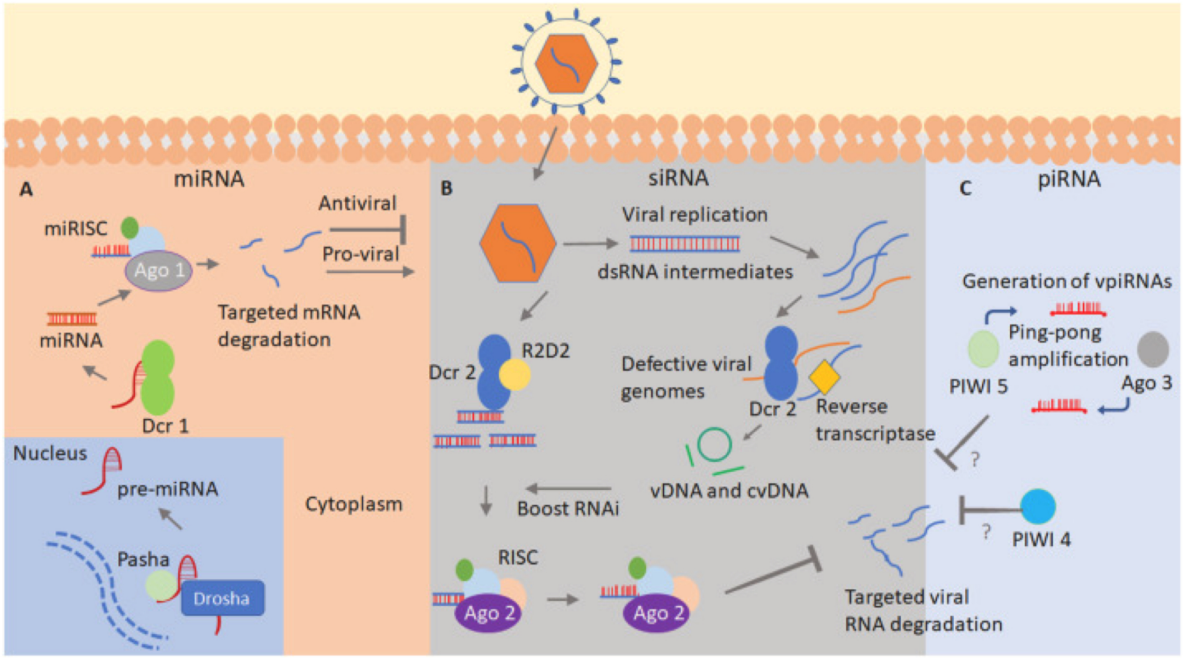

Figure 1.6: The RNAi pathway [5]

A) miRNA pathway: miRNA genes are transcribed as primary miRNAs, processed in the nucleus by Drosha and Pasha into precursor miRNAs (pre-miRNAs), and exported to the cytoplasm via Exportin-5. Dicer-1 cleaves pre-miRNAs to generate miRNA duplexes, which load onto AGO1 to form the miRISC complex that regulates host gene expression through translational repression or mRNA destabilisation.

B) siRNA pathway: dsRNA derived from viral replication intermediates or endogenous sources is processed by Dcr2 into 21-nt siRNA duplexes. These duplexes are transferred to R2D2 and then loaded into AGO2 to form the siRISC complex, which mediates cleavage of complementary viral RNA and is the primary antiviral RNAi response in mosquitoes.

C) piRNA pathway: In the germline and somatic tissues of Aedes mosquitoes, viral and transposon-derived RNAs give rise to 24–30 nt piRNAs. Primary piRNAs are generated through Zucchini-dependent cleavage and load onto PIWI proteins (Piwi5, Piwi6, and Ago3). Secondary piRNAs arise via the ping-pong amplification cycle, characterised by complementary piRNA pairs with a 10-nt overlap. The piRNA pathway contributes to antiviral defence and transposon control.

1.3.2 The JAK/STAT pathway

The JAK/STAT pathway activates signal transcription factors that induce the expression of multiple effector genes that directly target invading microbes. The JAK/STAT pathway is activated when a ligand binds to the receptor Domeless. Once

bound, it is activated through dimerisation, which results in self-phosphorylation of receptor-associated tyrosine kinase Hopscotch (Hop). Phosphorylated Hop then phosphorylates the Domeless receptor, which acts as a docking site for the SH2 domains of the STAT proteins. STATs are transcription factors that lie dormant in the cytoplasm. Once STAT is docked, it is phosphorylated and dimerised. The active dimers are then transported to the nucleus in a RanGTP-dependent manner. In the nucleus, they bind to palindromic sequences in the promoters that regulate the expression of target genes. The JAK/STAT pathway is known to have two negative regulators, suppressor of cytokine signalling (SOCS-1), and protein inhibitor of activated STAT (PIAS-1) [5].

The JAK/STAT pathway has been shown to play an antiviral role against DENV infection in *Ae. aegypti* [41]. dsRNA-mediated silencing of the negative regulator PIAS decreases DENV titres in mosquitoes, whereas silencing of the JAK/STAT receptor Domeless and associated kinase HOP increases DENV titres [41]. Transcriptomics analysis of JAK-STAT-induced and DENV-infected mosquitoes has revealed common DENV restriction factors. Two factors, DENV restriction factor 1 (DVRF1) and 2 (DVRF2), have been shown to exhibit antiviral activity against DENV. Both DVRF1 and DVRF2 have STAT binding sites in their promoter regions. The mode of action of JAK/STAT-induced DVRFs remains unknown [41]. In transgenic *Ae. aegypti* mosquitoes, expression of Domeless and HOP in the fat body has also been successful in reducing DENV titers in multiple mosquito tissues [64]. In addition, another study showed that silencing of the negative regulator PIAS decreases ZIKV infection in the *Ae. aegypti* midgut [65]. The results of these studies indicate the tissue and virus-specificity of the JAK/STAT pathway antiviral response.

1.3.3 Toll pathway

This pathway plays important roles in development, immunity, and metabolism in *Drosophila* and mosquitoes. The Toll pathway acts as a preliminary defence against fungal and bacterial pathogens. However, it plays a key role in mosquito anti-viral defense [66, 67]. The Toll pathway comprises a ligand, receptor, and associated

adaptor proteins, and transcription factors. Spätzle (Spz), a cytokine-like molecule, serves as the central ligand for the Toll pathway. Spz has a prodomain and a hydrophobic C-terminal that recognises Gram-positive and Gram-negative bacteria, and fungal pathogens by various pattern recognition molecules. This recognition leads to proteolytic cleavage of Spz that then activates it by exposing the C-terminal domain. Toll receptor then binds to the C-terminal domains of Spz and is activated. Activated Toll receptor binds to adaptor protein Myd88 and protein kinase Pelle, which phosphorylates Cactus (an I kappa β homolog), allowing it to bind to the Rel1 transcription factor. Phosphorylation of Cactus leads to its degradation, resulting in its dissociation from Rel1. The free Rel1 transcription factor is translocated to the nucleus, where it regulates the gene expression of multiple antimicrobial peptides (AMPs) [68, 69].

The antiviral role of the mosquito Toll pathway was first demonstrated in DENV-infected *Ae. aegypti* mosquitoes [70]. DENV infection upregulates Toll pathway genes and downregulates its negative regulator, Cactus. Silencing MYD88 results in increased DENV titres, whereas silencing Cactus decreases the DENV titre. The antiviral effect of the Toll pathway is also conserved in various laboratory and field-derived strains of *Ae. aegypti*, and is also effective against multiple DENV strains [71]. Gene expression analysis of ZIKV-infected mosquitoes has indicated that Toll pathway-related genes are highly upregulated in ZIKV infection when compared to other immune pathways. Silencing the negative regulators of multiple immune pathways has also shown that the Toll pathway plays a critical role in controlling ZIKV infection in *Ae. aegypti* [65] . However, it appears that this pathway has only a minimal effect on CHIKV infection. Indeed, prior stimulation of the Toll pathway has been shown not to affect CHIKV infection [72]. These studies suggest that the Toll pathway may be specific against flaviviruses, but not active against alphaviruses.

1.3.4 Immune deficiency pathway (IMD)

The IMD is another NF-kB signal transduction pathway that plays a vital role in the antibacterial, antifungal, and anti-plasmodium defence in mosquitoes [73]. The

IMD pathway is comprised of receptors, associated phosphorylation proteins, and caspases, as well as a transcription factor that regulates the expression of multiple AMPs.

In case of *Aedes spp* , the IMD pathway plays a minor role, if any, in the direct response against DENV, CHIKV, or ZIKV infection [65, 70, 72]. However, there is some evidence of a role in antiviral activity in the salivary glands of Aedes mosquitoes [74]. In the case of SINV infection, microbiota-dependent IMD activation has been shown to control viral titers, given that antibiotic treatment prevents the activation of the IMD pathway and increases SINV infection levels [75]. This study showed a tripartite interaction between the microbiota, the IMD pathway, and SINV. The exact mechanism governing this microbiota-mediated antiviral effect is not yet known. In *Culex* mosquitoes, the IMD transcription factor Rel2 has been shown to induce the expression of secretory cytokines such as Vago, with the Rel2 activation controlled by Dcr2 and TNF receptor-associated factor 2 (TRAF 2). Vago, in turn, activates the JAK/STAT pathway and controls WNV infection in *Culex* mosquitoes [76]. This interaction demonstrates a potential crosstalk between the IMD, RNAi, and JAK/STAT pathways.

1.3.5 Mitogen-activated protein kinase pathway (MAPK)

The MAPK pathways are also known to be involved in the antiviral immune response in *Drosophila*, but are less well-characterised in mosquitoes [5]. A few studies have supplied a growing body of evidence supporting their importance in arboviral immunity.

The MAPK/ERK pathway is activated when a ligand binds to the receptor. The binding relays a signal via a phosphorylation cascade that activates ERK-regulated transcription factors and alters the expression of responsive genes. RNAi-mediated depletion of two core components of the ERK pathway has been shown to increase SINV, and Vesicular stomatitis Indiana virus (VSV) infection in *Ae. aegypti* cells [77]. Chemical inhibition of the ERK pathway also results in increased SINV and VSV titers in mosquito cells. It has also been demonstrated that vertebrate insulin activates the ERK pathway and mediates antiviral immunity in mosquito cells [77]. In *Culex*

mosquitoes, vertebrate insulin reduces WNV titres in mosquitoes. In the same study, a parallel comparison between *Drosophila* and *Culex* mosquitoes has suggested that insulin-mediated activation of the ERK pathway ultimately activates the JAK/STAT pathway [78]. Microbiota-mediated priming and virus-induced signalling have both been shown to activate the ERK pathway, which mediates antiviral immunity in the *Drosophila* gut [79]. The microbiota also plays a major role in the antiviral response of vector mosquitoes, either by altering immunity or by secreting antiviral or proviral molecules. All the core proteins required for ERK-mediated priming are present in mosquitoes, suggesting that this response may be conserved in *Drosophila* and mosquitoes [80].

The JNK pathway is another MAPK pathway that plays an important role in apoptosis. This pathway is induced in *Ae. aegypti* salivary glands by DENV, ZIKV, and CHIKV infection [81], suggesting broad antiviral activity for the JNK pathway. Silencing the JNK core component Kayak prior to infection increases viral titers, whereas silencing the negative regulator Puckered leads to decreased viral titers in the salivary glands. The JNK pathway has been shown to induce the antiviral response via apoptosis and the complement-like protein TEP20 [81]. The complement-like system also recognises DENV infection and upregulates AMP expression [82].

The p38s are another set of MAPKs that are highly responsive to external stimuli. The p38 pathway has been implicated in the antiviral defence against invertebrate iridescent virus 6 in *Drosophila* [83]. However, silencing the p38 pathway components in Drosophila cells does not result in a significant increase in the numbers of *Drosophila* C virus (DCV), SINV, or VSV [77], suggesting that the p38 response may be virus-specific in *Drosophila*. In *Anopheles* mosquitoes, the p38 pathway is involved in the immune response against Plasmodium parasites [84]. In *Ae. aegypti* cells, the p38 protein has been shown to regulate the expression of the AMP gene Defensin A [85], but in *Ae. albopictus* cells, p38 acts as a negative regulator of the cecropin A gene [86]. The detailed involvement of this pathway in the antiviral defence in mosquitoes is still unknown.

Overall, mosquitoes have varied tools at their disposal to react and inhibit viral infections. The exact mechanism by which these occur is specific to the tissue and to the virus. In direct contrast to the inhibitory tools mosquitoes have at their disposal, viruses have co-evolved mechanisms to target these pathways. Understanding the virus-host interactions is essential for improving our control strategies.

1.4 Control strategies to control arbovirus infection

While vaccines exist and have been licenced for some alphaviruses (e.g. CHIKV), there is currently no antiviral against alphaviruses, and treatment is based on supportive care [87]. Public health efforts have focused on vector control to mitigate the transmission cycle. A variety of chemical, environmental, and biological approaches have been employed to reduce mosquito populations or inhibit their ability to transmit viruses [88, 89]. Here, major control strategies currently employed will be reviewed, with an emphasis on biological interventions that relate to mosquito-virus interactions and have the potential to target mosquito RNA-binding proteins.

1.4.1 Chemical control

This involves the use of chemical solutions or materials such as organophosphates and pyrethroids to expel or kill mosquitoes. These methods include the use of durable materials, such as insect-treated bed nets; the use of insecticides for peri-domestic space treatment and indoor residual spraying; and the use of larvicidal treatment in water bodies to destroy mosquito breeding habitats. These can be effective in the short term; However the development of insecticide resistance in mosquito populations and the harmful environmental impacts are the major challenges [88, 89].

1.4.2 Environmental control

This aims to eliminate breeding sites. For example, community programs to remove standing water containers, improve water storage, and enhance sanitation to reduce *Aedes* larval habitats. These conventional methods, while important, often struggle

to keep up with *Aedes* mosquitoes in densely populated tropical urban settings, thus spurring interest in more sustainable and targeted biological control tools [88, 89].

1.4.3 Biological control

These largely remain experimental and include the introduction of biological agents such as larvivorous fish or copepods that feed on mosquito larvae. The method, though effective in small settings such as containers, was not sustainable as it required a large coverage of multiple production of larvivorous fish containers to achieve any impact [90]. The use of *Bacillus tungiensis*, a naturally occurring, spore-forming Gram-positive bacterium that produces mosquito-specific larvicidal toxins, has been used to target mosquito larvae effectively. However, its effects on non-target organisms is proving challenging [91]. While the above biological strategies target mosquito larvae, other biological methods targeting the vector are being explored/implemented.

Wolbachia *Wolbachia pipientis* is a naturally occurring intracellular bacterium found in many insects, but notably not in wild *Ae. aegypti*. However, it can be artificially introduced to *Ae. aegypti* from donor species into embryos and establish stable maternally inherited infections [89]. Remarkably, certain *Wolbachia* strains, such as wMel and wAlbB (from *Drosophila* and *Ae. albopictus*, respectively), greatly reduce the replication of arboviruses like DENV, ZIKV, CHIKV, and YFV in *Aedes* mosquitoes. While the exact mechanism is still being elucidated, several hypotheses have been reported, summarised in Table1.1.

Table 1.1: Proposed mechanisms by which *Wolbachia* inhibits arbovirus replication

Mechanism	**Description**	**Effect on Arboviruses**	**Ref**
Competition for intracellular resources	*Wolbachia* induces and manipulates autophagy, restricting access to essential metabolites such as cholesterol and iron required for viral replication.	Deprives viruses of key resources needed for growth.	[92]
Immune priming	Pre-activation of innate immune pathways including Imd, Toll, and JAK-STAT.	Enhances baseline antiviral immunity and reduces infection.	[93]
Phenoloxidase cascade activation	Stimulation of melanisation pathways that deposit melanin around invading pathogens.	Direct antiviral effects through encapsulation/melanisation.	[94]
Modulation of miRNA pathways	Alteration of host miRNA expression to reshape antiviral gene regulation.	Suppresses viral replication via miRNA-mediated immune modulation.	[95]

No matter the mechanism, *Wolbachia*-infected mosquitoes have drastically lower viral loads in salivary glands and thus are much less likely to transmit infection. Another advantageous feature of *Wolbachia* is cytoplasmic incompatibility: infected males sire inviable offspring with uninfected females, giving a reproductive advantage to infected females in a population. This trait allows *Wolbachia* to spread into a mosquito population over time, as releases of infected mosquitoes can result in the *Wolbachia* infection frequency increasing each generation. Field trials have demonstrated the efficacy of *Wolbachia*-based control, for example, releases of *Ae. aegypti* with *Wolbachia* (wMel strain) in Yogyakarta, Indonesia, led to approximately 77% reduction in dengue incidence in treated communities compared to controls [96]. *Wolbachia* deployments by the World Mosquito Program in Australia, Asia, and the Americas have shown sustained establishment of *Wolbachia* in local mosquito populations and corresponding drops in dengue transmission. Notably, this method is self-sustaining after initial releases, since the bacterium is maternally inherited and can persist in the mosquito population without continuous reapplication. Challenges remain,

such as the sensitivity of *Wolbachia* to high temperatures, which can cause infected mosquitoes to lose the infection and the potential for evolutionary pressures on viruses or mosquitoes. Nevertheless, *Wolbachia* appears to be a promising and safe biocontrol strategy [89].

Sterile Insect Technique (SIT) SIT involves the mass-rearing of the target mosquito species in the lab, sterilising the males, usually by irradiation, through chemosterilisation or genetic methods, followed by their release in large numbers into the wild. The sterile males compete with wild males to mate with females; any female that mates with a sterile male will lay eggs that do not hatch, thus reducing the reproductive output of the population [89, 97]. Over time and sufficient coverage, the mosquito population can be suppressed or even locally eliminated by sustained releases. SIT has been successfully used for decades against agricultural insect pests and is now being explored for mosquitoes. For instance, field pilots in parts of China, Malaysia, and Brazil have reported significant reductions in *Ae. aegypti* populations using SIT in combination with other methods [98]. A variation called Incompatible Insect Technique (IIT) uses *Wolbachia*-induced sterility: release of males carrying a *Wolbachia* strain that causes cytoplasmic incompatibility with wild females (effectively a form of sterilisation). This approach has shown success in suppressing *Ae. aegypti* in Guangzhou, China, by over 90% when *Wolbachia*-infected males were released weekly. In practice, modern programs sometimes combine IIT with irradiation (to kill any accidentally released *Wolbachia*-infected females) [98]. However, there are practical challenges with the techniques: rearing and sorting millions of male mosquitoes (separating females is critical to avoid biting mosquitoes in the releases), potential mating competitiveness issues if irradiation weakens males, and the need for repeated large-scale releases as long as there is immigration of fertile mosquitoes. Nevertheless, SIT is gaining momentum as part of integrated vector management, with active programs exploring its feasibility in various regions.

Genetically modified mosquitoes Other genetic approaches include releasing genetically modified mosquitoes (GMM) designed to suppress populations or replace

them with non-competent strains. A known example is the OX513A *Ae. aegypti* developed by Oxitec: males carry a dominant lethal gene that kills offspring, causing a population crash upon sustained release. This approach is a form of RIDL (Release of Insects carrying a Dominant Lethal) and has shown some success in field trials of approximately 80% population reduction in trials in Brazil, but requires continuous releases to maintain suppression. There are also efforts toward gene drives that could spread either a lethal gene or a refractoriness gene through a population, though gene drive use in mosquitoes remain in experimental phases due to ecological and ethical considerations [99, 100].

In summary, current control strategies are increasingly embracing novel biological interventions like *Wolbachia* and SIT, in addition to improved insecticides and community measures. These strategies aim either to reduce mosquito populations or render mosquitoes less competent to transmit pathogens. Each approach has its pros and cons, but collectively they represent essential tools in the fight against arboviruses. Importantly, the success of any strategy may depend on mosquito-pathogen interactions at the molecular level. For example, *Wolbachia's* ability to block viruses presumably taps into mosquito cellular pathways that viruses need, and refractoriness genes often involve immune pathway components or other host factors that inhibit virus development [89]. This connection raises the pertinent question: are there other intrinsic mosquito factors (e.g. mosquito RNA-binding proteins) that modulate vector competence, which could be exploited for control? Recent advances in the study of host-virus interactions suggest that targeting such host factors could complement existing strategies by understanding how they modulate viral infection [101–103]

1.5 RNA-binding Proteins(RBPs)

RNA-binding proteins (RBPs) are proteins that associate with RNA molecules and influence their processing, function, and stability. They participate in every stage of the RNA life cycle, from transcription through translation to degradation. By

forming ribonucleoprotein (RNP) complexes, RBPs regulate key post-transcriptional processes, including splicing, polyadenylation, nuclear export, subcellular localisation, translation, and turnover [104].

Many RBPs achieve RNA recognition through conserved RNA-binding domains (RBDs) [105, 106] detailed in Table1.2.

Table 1.2: Major RBDs and their mechanisms of RNA recognition

RNA-binding domain	**Key Features**	**Mode of RNA Recognition**
RNA Recognition Motif (RRM)	Abundant in spliceosomal and other RNA-processing proteins.	Binds RNA through electrostatic interactions between positively charged residues (Arg, Lys) and the phosphate backbone, complemented by aromatic stacking against nucleobases.
K-Homology (KH) Domain	Found in proteins such as FMR1 and Nova.	Recognises nucleotides via hydrophobic interactions, hydrogen bonding to bases, and structural complementarity with the sugar–phosphate backbone.
Zinc Finger Domains	Includes TFIIIA and related proteins.	Uses electrostatic interactions and zinc coordination to stabilise RNA loop structures and distinguish RNA from DNA.
Double-stranded RNA-binding Domain (dsRBD)	Common in proteins involved in RNA silencing and innate immunity.	Engages RNA in a sequence-independent manner by recognising the 2'-OH groups and the phosphate backbone of A-form dsRNA.

However, the catalogue of RBPs has expanded well beyond proteins containing these classical RBDs. Increasing numbers of proteins have been identified that lack canonical domains, often referred to as enigmRBPs [107] or unconventional RBPs [101, 108]. A striking example is the discovery of metabolic enzymes that "moonlight" as RBPs while lacking obvious RBDs [109, 110]. Such findings underscore that RNA-

binding activity can arise through diverse structural solutions, many of which remain to be uncovered, and highlight that RBPs frequently play multiple roles in the RNA life cycle.

Viruses, and especially RNA viruses, are intimately dependent on host RBPs. As purely intracellular parasites that use RNA as their genetic material, RNA viruses co-opt host RBPs for every stage of their life cycle [101, 102]. RBPs may serve as proviral factors by stabilising viral RNA, aiding in translation or as part of the replication complex; or as antiviral factors that detect viral RNA for degradation. A good example is G3BP (Ras-GAP SH3 domain binding protein), which interacts with alphavirus nsP3 hypervariable domain with tandem FGDF motif. G3BP1 and G3BP2 are host RNA-binding proteins involved in assembling stress granules. Alphaviruses like CHIKV sequester G3BP via nsP3, effectively blocking stress granule formation, thereby preventing an antiviral host response and promoting efficient viral protein translation [111]. Another example is the Staufen protein, which was shown to bind DENV RNA in mosquitoes and restrict its accumulation in multiple *Ae. aegypti* tissues, including the salivary glands [112].

Despite their importance, mosquito RBPs remain relatively understudied. Most of our understanding of RBPs in host-virus interaction comes from mammalian cell cultures [101, 103, 113–115]. However, mosquitoes are evolutionarily distant from humans and have distinct sets of RBPs and behave in a manner that tolerates viral infection. A recent study by Yeh and colleagues, using RNA affinity-pulldown, identified 14 RBPs in *Ae. aegypti* cells. They showed that AePur (Purine-rich element binding protein) had affinity to DENV just like the human homolog; however, the anti-viral function was specific to the mosquito. [112]. This shows that some RBPs may have divergent role and host-specific studies are needed.

1.5.1 Strategies employed to uncover RBPs

The first techniques used to discover RBPs were by protein microarray and RNA probes, and by stable isotope labelling of amino acids and mass spectrometry

[116–118]. However, this approach could not reliably distinguish proteins that interact directly with RNA from those that are recovered indirectly through protein–protein associations with bona fide RBPs. In addition, they did not discriminate between genuine physiological RNA-binding activity and non-specific or artificial interactions. Furthermore, the above-mentioned techniques were performed *in vitro* with limited RNA subtypes and did not account for cellular factors (e.g. stress conditions, RNA secondary structure, subcellular compartmentalisation and chemical modifications) affecting RNA-protein interactions *in vivo*.

Identification of RNA *in vivo* came with the development of RNA interactome capture (RIC) [119, 120]. In RIC, ultraviolet irradiation was used to covalently link proteins to RNA positioned at zero distance (2 angstroms). This was followed by the pulldown of the protein-RNA complex by oligo(dT) beads under chaotropic conditions. The bound proteins were subsequently identified by mass spectrometry. Castello and team used both conventional crosslinking, which relies on the excitability of nucleoside bases by 254 nm ultraviolet light, and photoactivatable ribonucleoside-enhanced crosslinking (PAR-CL) that utilises the nucleoside analogue 4-thiouridine (4SU) [119]. In this method, 4SU is incorporated into nascent RNA within the cells, allowing for more efficient and selective crosslinking of RNA-protein complexes using UV light at 365 nm. This enhances the ability to capture RBPs in a physiological context and increases crosslinking efficiency [119]. In parallel, Baltz and team used 4SU in combination with 6-thioguanosine labelling, exploiting the U-C transitions occurring as a consequence of crosslinking between 4SU and the RBP to globally analyse the RNA interactome [120]. Both studies were able to identify 860 RBPs in HeLa cells and 791 RBPs in HEK293, respectively.

Since the innovative development of RIC the breadth of RBPs has dramatically expanded to include studies from different species such as *Mus musculus* [121], *Saccharomyces cerevisiae* [122], *Drosophila melanogaster* [107], *Caenorhabditis elegans* [123, 124], zebrafish [125], plants [126–128] and parasites (*Plasmodiun falciparum* and *Leishmania donovani*) [129, 130]. Interestingly, comparative analysis of RBPs across species showed that hundreds of RBPs appear to be conserved

across species suggesting an evolutionary pressure to conserve their roles in cellular metabolism [122, 130, 131].

While RIC is effective in capturing RBPs, it is subject to biases arising from exclusively capturing poly(A) tailed RNA, protein abundance, molecular size, and the physicochemical properties of their tryptic peptides. UV irradiation generates RNA–protein crosslinks with high specificity, as it requires zero-distance interactions between nucleotides and amino acids. However, this specificity comes at the cost of reduced efficiency compared with chemical crosslinkers such as formaldehyde. In particular, UV cross-linking performs poorly in detecting transient interactions or contacts involving the ribose–phosphate backbone, since the cross-link is predominantly mediated through nucleotide bases [106]. Several methods have been developed to try and mitigate some, if not all, of these biases [132]. Techniques such as RNA Interactome Using Click Chemistry (RICK) [133], Click Chemistry-Assisted RNA-Interactome Capture (CARIC) [134], complex capture 2C method [135], Total RNA-Associated Protein Purification (TRAPP) [136], Viral Cross-Linking and Solid Phase Purification (VIR-CLASP) [137], Protein-Cross-Linked RNA eXtraction (XRNAX) [138], Orthogonal Organic Phase Separation (OOPS) [139], and Phenol-Toluol Extraction (PTex) [140] have been used for bulk RBP capture. Individually, *in vitro* and *in vivo* techniques have their respective challenges; however, combining methods can provide a more accurate understanding. Below is a table summarising the pros and cons of the different techniques and how they can be applied (Table1.3).

Table 1.3: Comparison of RBP capture methods

Method	RNA Target	Advantage	Disadvantage	Cell Type
RIC	Poly(A)-tailed RNA	Isolates only mRNA complexes (if subset is of interest). Widely used protocol.	Isolates only mRNA complexes. Low signal-to-noise ratios. Additionally, co-purification of non-cross-linked (free) RNA. Can purify off-target RNA containing poly(A) stretches within its sequence.	All poly(A)-tailed organisms
e/cRIC	Poly(A)-tailed RNA	Isolates only mRNA complexes (if subset is of interest). Better signal-to-noise ratios than RIC.	Isolates only mRNA complexes. Additionally, co-purification of free RNA. Can purify off-target RNA containing poly(A) stretches within its sequence.	All poly(A)-tailed organisms
CARIC	Newly transcribed RNA	All RNA types. RNP monitoring through time.	Use of nucleoside analogs. Potential co-purification of naturally biotinylated proteins. Additionally, co-purification of free RNA.	Limited to cell cultures receptive for nucleoside analogs
RICK	Newly transcribed RNA	All RNA types. RNP monitoring through time.	Use of nucleoside analogs. Potential co-purification of naturally biotinylated proteins. Additionally, co-purification of free RNA.	Limited to cell cultures receptive for nucleoside analogs

Method	RNA Target	Advantage	Disadvantage	Cell Type
2C	All RNPs	Fast and cost-effective method.	Contamination of both free protein and free RNA. Dependent on the scale of the silica columns. A nucleotide-size limitation can occur inherent to silica matrices.	All cell types and tissue
(PAR)-TRAPP	All RNPs	Cost-effective method. Scalable protocol.	DNA is co-eluted. Additionally, co-purification of free RNA. A nucleotide-size limitation can occur inherent to silica matrices.	All cell types and tissue
VIR-CLASP	Pre-replicated viral RNPs	Study of early-stage viral infection. Theoretically adaptable to every type of *in vitro* transcribed RNA molecule. Cost-effective method.	Current field of application is small but highly interesting. SPRI beads can have size-selective artefacts.	Limited to cell cultures receptive for nucleoside analogs
XRNAX	All RNPs	All RNA types. Little free RNA. Cost-effective method. Easily scalable. Good starting point for more specific techniques.	Glycoproteins and RNA–protein adducts cannot be distinguished. Technically challenging. Crude fraction.	All cell types and tissue
OOPS	All RNPs	All RNA types. Cost-effective method. Easily scalable.	Technically challenging. Cannot be used as a starting point for more specific techniques.	All cell types and tissue

Method	RNA Target	Advantage	Disadvantage	Cell Type
PTex	All RNPs > 30 bp	All RNA types. Little free RNA. Cost-effective method. Easily scalable. Good starting point for more specific techniques.	Glycoproteins and RNA–protein adducts cannot be distinguished. Technically challenging. 25–30% recovery.	All cell types and tissue

RIC - RNA interactome capture, e/cRIC - Enhanced/comparative RNA interactome capture,

CARIC - Click Chemistry-Assisted RNA-Interactome Capture,

RICK - RNA Interactome Using Click Chemistry,

2C - complex capture 2C method,

PAR-TRAPP - Total RNA-Associated Protein Purification,

VIR-CLASP - Viral Cross-Linking and Solid Phase Purification,

XRANAX - Protein-Cross-Linked RNA eXtraction,

OOPS – Orthogonal Organic Phase Separation,

PTex - Phenol-Toluol Extraction

1.5.2 Plasticity of RBPs

The binding of RBPs to RNA is consistently changing in a cell, and with it, the repertoire of the RNA interactome is determined by physiological cues. While housekeeping RBPs may always be active, many RBPs are more restricted to expression patterns, and their RNA-binding activity may be regulated by post-transcriptional modifications, cofactors, binding, or protein-protein interactions. Moreover, some RBPs can lie dormant for the lack of an RNA target. For example, cellular sensors against viral infection, such as interferon-induced, dsRNA-activated protein kinase (PKR), retinoic acid-inducible gene I protein (RIG-I), or toll-like receptors, can only be activated by products or viral RNA replication, such as dsRNA or triphosphate 5' ends [141–143].

RIC has been adapted to investigate changes in RNA-binding proteomes in response to physiological and environmental cues. It was applied to murine macrophages responding to lipopolysaccharide stimulation, to primary mouse embryo fibroblasts (MEFs) treated with the DNA-damage inducing agent etoposide, and to fruitfly and zebrafish embryos at different stages of development and in mammalian cells infected with viruses [101, 102, 114, 131, 144]. In each of these scenarios, most of the RBPome remodelling was stimulus-specific. For example, in virus-infected cells, many of the proteins with altered RNA binding were linked to antiviral or proviral responses [101]. Garcia-Mareno's study on how SINV alters the RPBome showed that infection, rather than protein abundance, influences the RPBome. However, this is not unusual as infection induces massive cellular host shut-off while redirecting resources for viral replication and proliferation [101]. This shows RIC is a useful tool to study RBP dynamics in different biological scenarios, such as infection.

Early studies of RBPs in viral infection largely focused on individual proteins, chosen for investigation based on their presumed mode of action. It was not until the last decade that methods to unbiasedly identify viral RBPs were implemented, as reviewed in Iselin and colleagues [145]. These techniques have four key components: infection, protein-RNA cross-linking, RNA isolation or capture, and mass

spectrometry. The techniques reviewed in the above mentioned paper differed in the protein-RNA crosslinking and the method of RNA isolation. Protein crosslinking is achieved through different methods. One approach uses 4-thiouridine (4SU), which selectively labels viral RNA and requires higher energy ultraviolet light (365 nm) for crosslinking. This method prevents the crosslinking of unlabelled, natural RNA. Another approach is formaldehyde cross-linking, which is less specific because it captures both RNA–protein and protein–protein interactions.

Three proteome-wide approaches have been recently used to elucidate the composition of alphavirus RNPs. These include viral crosslinking and solid-phase purification (VIR-CLASP), crosslink-assisted messenger RNP purification (CLAMP), and vRNA interactome capture (vRIC). Kim and group used VIR-CLASP to capture the early events viral infection by infecting unlabelled host cells with 4SU-labeled viral RNA, followed by UV cross-linking and solid-phase purification [146]. This method enabled the identification of hundreds of host RBPs interacting with incoming CHIKV RNA, including the unexpected discovery of fatty acid synthase (FASN) as a direct viral interactor with a proviral role. However, VIR-CLASP is restricted to the initial stages of infection and does not capture interactions during later stages of the viral life cycle.

To extend the analysis to post-entry events, CLAMP was used to profile viral ribonucleoprotein complexes (vRNPs) at later time points [147]. In this method, cellular transcription is halted with actinomycin before 4SU labelling, crosslinking is achieved with formaldehyde, and vRNPs are purified using biotin-based chemistry and streptavidin precipitation. CLAMP was first applied to SINV and later expanded to a comparative analysis of CHIKV, SINV, and VEEV, identifying 108 conserved host RBPs across these viruses [148]. Among these, hnRNP K was validated as a key interactor with alphavirus subgenomic RNA, with functional studies showing its proviral role. Nonetheless, CLAMP datasets contained relatively few bona fide RBPs, likely due to the promiscuous nature of formaldehyde crosslinking and limited purification specificity [145].

More recently, vRIC was developed to address limitations in capturing post-replicative

alphavirus RBPs. Originally applied to SARS-CoV-2 [113] and later to SINV [103], vRIC uses 4SU-labelled vRNA coupled with oligo(dT)-based capture. In SINV, this method identified approximately 400 host RBPs, with comparative analyses highlighting enrichment of post-translational modification enzymes, such as kinases, and differences in translation initiation factors between viral and cellular RNPs. These findings support earlier reports of non-canonical cap-dependent translation mechanisms in SINV [149, 150]. Together, these complementary approaches provide a temporal framework for mapping viral RPBs.

Altogether, the different RBPs discovery methods have expanded our understanding of host protein and viral RNA interactions. The different methodologies have their individual caveats; however, together they paint a clear picture of how host RBPs are hijacked by the virus to sustain infection and further indicate how host immunity reacts to address the growing cellular threat. Unfortunately, all the above studies focused on the same host, human cell lines. Understanding how the virus behaves in humans can aid in developing new antiviral therapeutics. However, understanding how the virus interacts with the vectors that transmit human infection will be essential in developing a sustainable vector management system.

1.6 Objective of the study

The overarching research question for this study is whether mosquito RBPs that are critical in virus-vector interactions can be identified, and whether manipulation of these RBPs can be used to block viral replication. Based on the background discussed, mosquito RBPs represent a relatively untapped facet of vector biology that might be leveraged to interfere with viruses in the vector, complementing strategies like *Wolbachia*.

Three objectives were set to address this question:

1. Profile the mRNA-binding proteome (RBPome) of mosquitoes, with a focus on the arboviral vector *Ae. aegypti* and *Ae. albopictus*. RNA interactome capture will be applied to *Aedes* cell lines (Aag2-AF5 for *Ae. aegypti* and U4.4 for *Ae.*

albopictus) to comprehensively catalogue RBPs in these vector species. This will establish which proteins are normally bound to mRNA in mosquito cells, providing a baseline for comparison and revealing how similar or divergent the mosquito RBP repertoire is relative to model organisms, the human RBPome.

2. Determine how the mosquito RBPome is remodelled during alphavirus infection. Using the SINV as a model arbovirus, Comparative RNA interactome capture will be perfomed on infected versus uninfected mosquitoes *Ae. aegypi* Aag2-AF5 cells. Quantitative mass spectrometry will identify RBPs that show differential enrichment. By profiling these changes, the aim is to pinpoint candidate RBPs that either facilitate viral replication or are suppressed by the virus.

3. Functionally evaluate the role of selected RBPs in alphavirus infection by RNA interference (RNAi)-mediated silencing. From the RBPome obtained in objective 2, a subset of RBPs that are regulated during infection and use RNAi-mediated silencing to assess their impact on SINV infection by RT-qPCR.

2 Materials

2.1 Reagents

Table 2.1: Reagents

Reagent	**Supplier**	**CAT. #**
Leibovitz's L-15 Medium	Gibco	11415060
DMEM	Gibco	10569010
OptiMEM	Gibco	51985034
Triptose phosphate broth	Gibco	18950039
Fetal bovine serum HI	Gibco	A5670801
Penicillin-Steptomycin (10,000 U/ml)	Gibco	15140122
IGEPAL CA-630	Sigma-Aldrich	I8896
DMSO	Sigma-Aldrich	D2260
DTT	Sigma Aldrich	D1532
Lithium chloride	Sigma-Aldrich	310468
Lithium dodecyl sulfate	Sigma-Aldrich	L5901
Luna Universal One-step RT-qPCR kit	NEB	E3005E
Oligo(dT)25 beads	NEB	S1419S
NEBNext High-Fidelity 2X PCR Master Mix	NEB	M0541
XhoI	NEB	R0146S
HiScribe T7 Arca	NEB	E2065
100bp DNA Ladder	NEB	M3231
NuPage LDS Sample Buffer (4x)	Invitrogen	NP0007
NuPAGE MOPS SDS Running Buffer (20x)	Invitrogen	NP0001
NuPAGE Bis-Tris Mini Protein Gels, 4–12%	Invitrogen	NP0322BOX
Qubit Protein Broad Range Assay Kit	Invitrogen	A50669
Trypan Blue Stain (0.4%)	Invitrogen	T10282
SilverQuest staining kit	Invitrogen	LC6070

Random Hexamers (50µM)	Invitrogen	N8080127
RNaseOUT Recombinant Ribonuclease Inhibitor	Invitrogen	10777019
MEGAscript RNAi Kit	Invitrogen	AM1626
UltraPure 1 M Tris-HCl Buffer, pH 7.5	Invitrogen	15567027
NaCl (5M) RNase-free	Invitrogen	AM9760G
EDTA (0.5M), pH 8.0	Invitrogen	AM9260G
Superscript III	Thermo Fisher	18080-044
Deoxynucleotide (dNTP) Solution Mix	NEB	N0447S
X-tremeGENE 360 Transfection Reagent	Roche	XTG360-RO
AEBSF	BioChemica	A14210100
Triton X-100	Promega	H5141

2.2 Consumables

Table 2.2: Consumables

Item	**Supplier**	**CAT. #**
Cell culture flask T-175	SARSTEDT	83.3912.300
Cell culture flask T-175	SARSTEDT	83.3911.302
Cell culture flask T-175	SARSTEDT	83.3910.302
MicroAmp Optical 96-Well Plate	Applied Biosystems	N8010560
MicroAmp Optical Adhesive Film	Applied Biosystems	4360954
PCR Tube 0.2ml, 8-Strip Flat Caps	Starlab	A1402-3700c
10µl Grad filter tips sterile racked	Starlab	S1120-3810
20µl Grad filter tips sterile racked	Starlab	S1120-1810
200µl Grad filter tips sterile racked	Starlab	S1128-8810
1000µl Grad filter tips sterile racked	Starlab	S1122-1830
Cell Scrapper	Corning	3010 SLS
Falcon 50 ml conical bottom	Corning	352070
1.5ml Protein LoBind Tubes	Eppendorf	00030108116

2.3 Equipment

Table 2.3: Equipment

Instrument	**Supplier**
Countess II FL Automated Cell Counter	Thermo Fisher
EVOS M5000	Thermo Fisher
GelDoc Imaging System	BioRad
NanoDrop Microvolume Spectrophotometer	Thermo Fisher
Odyssey CLx Imaging System	LiCor
PCR machine	ABI
PowerPac Basic Power Supply	BioRad
QuantStudio3 real-time PCR system	Applied Biosystems
Qubit Fluorometer	Thermo Fisher
Transblot Turbo Transfer System	BioRad
254nm UV Crosslinker	Roth Selection
EASY-nano-LC 1000 system	Thermofisher scientific

2.4 Software

Table 2.4: Software

Software	**Version**	**Purpose**
MobiDB-lite	v3.8.4	Prediction of intrinsically disordered regions
InterProScan	v5.64-96.0	Protein domain annotation and functional prediction
ChimeraX	v1.9	Protein visualisation and structural analysis
AlphaFold3	2024 release	Structure prediction
Rstudio	Version 2025	Statistical analysis and plotting

2.5 In house buffers

Table 2.5: In house buffers

Buffer	**Components**
RIC lysis buffer	20mM Tris-HCl, 500mM LiCl, 0.5% LiDs, 1mM EDTA, 5mM DTT, 0.1% IGEPAL, double distilled water
RIC Buffer 1	20mM Tris-HCl, 500mM LiCl, 0.1% LiDs, 1mM EDTA, 5mM DTT, 0.1% IGEPAL, double distilled water
RIC Buffer 2	20mM Tris-HCl, 500mM LiCl, 1mM EDTA, 5mM DTT, 0.1% IGEPAL, double distilled water
RIC Buffer 3	20mM Tris-HCl, 200mM LiCl, 1mM EDTA, 5mM DTT, double distilled water
RIC Elution Buffer	20mM Tris-HCl, 1mM EDTA, double distilled water
RIPA buffer	10mM Tris-HCl, 150 mM NaCl, 0.5 mM EDTA, 0.1% SDS, 1% Triton X-100, 1% sodium deoxycholate
Blocking buffer	5% W/V Skim milk, 0.1% Tween 20

2.6 Cell lines & Viruses

Table 2.6: Cell Lines

Cell line or virus	**Source**	**Modified? or backbone**
HEK293	ECACC #85120602	Parental
VeroE6	Castello lab	Parental
BHK	Castello lab	Parental
Aag2-AF5	Lab of Alain Kohl	Parental
U4.4	Lab of Alain Kohl	Parental
pT7-SVnsP3Scarlet	Castello lab	pTE32J1
pT7-SVwt	Lab of L. Carrasco	pTE32J1

2.7 dsRNA oligonucleotides with T7 promoter sequence

Table 2.7: dsRNA Oligonucleotides

Oligonucleotides	Sequence
T7AEDCP1A-FWD	.TAATACGACTCACTATAGGGTAAAGCCATCATCATCGTCG
T7AENOVA1-FWD	TAATACGACTCACTATAGGGAAAGCAAGCCGAGAAAACAA
T7AETDRD7-FWD	TAATACGACTCACTATAGGGTTGGAAAAAGCTGCCAGAGT
T7AEPRP16-FWD	TAATACGACTCACTATAGGGACTTTCACCATTCCAGGTCG
T7AEPANK1-FWD	TAATACGACTCACTATAGGGGCGGTACCTGACGAAACACT
T7AELENG8-FWD	TAATACGACTCACTATAGGGGAATGTTCCGCCAGGTCTAA
T7AEPSMD6-FWD	TAATACGACTCACTATAGGGTTGGAACTGGCACAAATCAA
T7AETCRG1-FWD	TAATACGACTCACTATAGGGCGGAATACCTGGACTGGCTA
T7AESET1B-FWD	TAATACGACTCACTATAGGGCGGTCTTGGACGATTCAGAT
T7AESF3B4-FWD	TAATACGACTCACTATAGGGTATTTGTGTAACCGGCCCAT
T7AAEL025565-FWD	TAATACGACTCACTATAGGGTCTCATCGCACTACCGTCTG
T7AAEL001397-FWD	TAATACGACTCACTATAGGGCAGAATAAGGCAGCTTTGGC
T7AAEL025697-FWD	TAATACGACTCACTATAGGGGGCCTACGGTATGGACAAGA
T7AAEL025553-FWD	TAATACGACTCACTATAGGGGTCAGTGTCAAACCTCCCGT
T7AAEL025569-FWD	TAATACGACTCACTATAGGGGGAATACGGATCCTGAAGCA
T7AAEL023209-FWD	TAATACGACTCACTATAGGGTGTTCTGAACTTAGCGTGCG
T7AAEL008063-FWD	TAATACGACTCACTATAGGGACGCGAGGTAAAAAGCTTCA
T7AEDCP1A-RVS	TAATACGACTCACTATAGGGGGCGGTGTTGAATGTGTAGA

T7AENOVA1-RVS	TAATACGACTCACTATAGGGGCGTTCGATGGCTATTCATT
T7AETDRD7-RVS	TAATACGACTCACTATAGGGAATAGCTGGTGCGCTTGTCT
T7AEPRP16-RVS	TAATACGACTCACTATAGGGCGGTGTTGGCTAGATTGGTT
T7AEPANK1-RVS	TAATACGACTCACTATAGGGGCTGTATCGCTTCCTCGAAC
T7AELENG8-RVS	TAATACGACTCACTATAGGGACTGCGCTCCATGAAGTTCT
T7AEPSMD6-RVS	TAATACGACTCACTATAGGGAATCGCCACACAATAGGCTC
T7AETCRG1-RVS	TAATACGACTCACTATAGGGCTTCCACGTCGGTTTTGAAT
T7AESET1B-RVS	TAATACGACTCACTATAGGGGATGACAGACTGGACAGCGA
T7AESF3B4-RVS	TAATACGACTCACTATAGGGCGCTCCCTAGAAATTGAACG
T7AAEL025565-RVS	TAATACGACTCACTATAGGGAAGTGGTGAATTCGTCGTCC
T7AAEL001397-RVS	TAATACGACTCACTATAGGGCCATTCAATGATCTCCGCTT
T7AAEL025697-RVS	TAATACGACTCACTATAGGGGAAGATGTCCTGCACGGTTT
T7AAEL025553-RVS	TAATACGACTCACTATAGGGAGTTCAGCACACGGAGACCT
T7AAEL025569-RVS	TAATACGACTCACTATAGGGCGAATTCCGAGAAGCTCAAC
T7AAEL023209-RVS	TAATACGACTCACTATAGGGTCCTGCTGCTGTAAAAGCCT
T7AAEL008063-RVS	TAATACGACTCACTATAGGGGTCAACTTTCCTCTCGGCTG
T7-SINV-FWD	TAATACGACTCACTATAGGGTATATCTCCCGGCGTTGCAC
T7-SINV-RVS	TAATACGACTCACTATAGGGCCGTGGCTAGTATCGGTTCC

2.8 qPCR *Ae. aegypti* oligonucleotides

Table 2.8: qPCR oligonucleotides

Oligonucleotides	**Sequence**
qAEDCP1A-FWD	ACCCATTGCTCAACAGTTCC
qAENOVA1-FWD	GCGACTCAACGTGAGAATGA
qAETDRD7-FWD	CACACGTTGATGATTCTGGG
qAEPRP16-FWD	GCCCTCCAAATTCATCTTCA
qAEPANK1-FWD	TCGAGGGAAGCGTAGTGAGT
qAELENG8-FWD	GCCAGACTTGAGCAAACCTC
qAEPSMD6-FWD	CTTCCGGAACATAACCAGGA
qAETCRG1-FWD	GAGGACAAGCAGAACCGAAG
qAESET1B-FWD	AGCCTATGGCTGGTATGGTG
qAESF3B4-FWD	TGACGCTCGTTTTCTGTCAC
qAAEL025565-FWD	GGTCCCTTCTGGATGAAACA
qAAEL001397-FWD	CCTGGACGTTTCACCGTACT
qAAEL025697-FWD	AGCTAGTTCCCTGCTCTCCC
qAAEL025553-FWD	CTTATGTGAACAGCCAGCGA
qAAEL025569-FWD	GTGTCTAGAAGGACCGCAGC
qAAEL023209-FWD	TGTTCTGAACTTAGCGTGCG
qAAEL008063-FWD	TCAGAAAAAGGCCTGCTCAT
qAEDCP1A-RVS	GCACTGGCAAATAAATCGGT
qAENOVA1-RVS	GGGGTATCGAACAAGCAAAA
qAETDRD7-RVS	CAGCTGATGTGCAGACGATT
qAEPRP16-RVS	GTCGGACGGAAGTTGTGAAT
qAEPANK1-RVS	AAACGAATTTGCCTACACCG
qAELENG8-RVS	CGGTAGGATTGTTGAAGGGA
qAEPSMD6-RVS	TTGACCTCCTTCATATCGGC
qAETCRG1-RVS	ATCCTCACGCAGAGCTGAAT

qAESET1B-RVS	GTAATCAGAAGCGCCGTAGC
qAESF3B4-RVS	GGAACTCCACGAAACCGTAA
qAAEL025565-RVS	AAGTGGTGAATTCGTCGTCC
qAAEL001397-RVS	TTACAGCTCAATGCGTCGTC
qAAEL025697-RVS	TTACGTACCAATAAGCCGCC
qAAEL025553-RVS	CAGCAGATAGCGCATCACAT
qAAEL025569-RVS	GCATTATGGGAGCTGGTGTT
qAAEL023209-RVS	GGTGATGTAACATTGCGTCG
qAAEL008063-RVS	TGAAGCTTTTTACCTCGCGT
qSINV-FWD	TATATCTCCCGGCGTTGCAC
qSINV-RVS	CCGTGGCTAGTATCGGTTCC

3 Methods

3.1 Cell Biology

3.1.1 Cell culture

Mammalian cells (BHK21, Vero, and HEK 293 cells) were incubated at 37°C in a humidified atmosphere with 5% CO_2. These cells were maintained in Dulbecco's modified Eagle medium (DMEM) GlutaMax supplemented with 10% fetal bovine serum (FBS), and 1X penicillin-streptomycin. The cells were passaged regularly to maintain a confluency of 80-90% confluency. To split the cells, the media was first removed, and the cells were washed with 1X PBS. Trypsin-EDTA 0.25% was added to the cells and incubated for 3 min. The cells were then resuspended in DMEM supplemented with 10% FBS and seeded as desired. Cell stocks were made by resuspending cells in FBS supplemented with 5% DMSO and stored either at -80°C or in liquid nitrogen.

Mosquito cells (Aag2-AF5 - *Aedes aegypti* and U4.4 - *Aedes albopictus* cells) were incubated at 28°C without CO_2. These cells were maintained in Leibovitz's L-15 medium with 2mM glutamine, 0.1 mM non-essential amino acid, 10% tryptose phosphate broth, 10% fetal bovine serum, and 1X penicillin-streptomycin. The cells were passaged regularly to maintain a confluency of 80-90% confluency. To split the cells, a cell scraper was used to detach adherent cells, the medium was mixed up and down to ensure cell homogeneity, fresh 10% Leibovitz L-15 medium was added (1:1), and cells were seeded as desired. Cell stocks were made by resuspending cells in FBS supplemented with 5% DMSO and complement medium (1:1) and stored at -80°C or in liquid nitrogen.

When needed, human and mosquito cells were counted using 0.4% Trypan Blue Stain and the Countess II FL automated cell counter.

3.1.2 Virus Generation

SINV was generated from a plasmid or by expanding pre-existing viral stock. Plasmid DNA was linearised using the XhoI restriction endonuclease (New England Biolabs).

Briefly, 1 µg of plasmid DNA was incubated in a 50 µl reaction containing 10X rCutSmart Buffer and 10 U XhoI. The mix was incubated at 37°C for 15 min, followed by 65°C for 20 min to inactivate the enzyme. With the linearised plasmid, mRNA was synthesised using the HiScribe T7 ARCA mRNA Kit (New England Biolabs) following the manufacturer's instructions. Briefly, linearised DNA templates containing a T7 promoter were incubated in a 20 µl transcription reaction comprising ARCA cap analogue, NTP mix, reaction buffer, and T7 RNA polymerase enzyme mix. Reactions were incubated at 37°C for 2 h to allow transcription. Following RNA synthesis, DNA templates were removed by DNase I treatment at 37°C for 15 min. Poly(A) tailing was performed by adding Poly(A) Polymerase and tailing buffer directly to the transcription reaction and incubating at 37°C for an additional 30 min.

After mRNA synthesis, 2 µl of DNase I was added to the reaction mix and incubated at 37°C for 15 min. The RNA was then purified using the Zymo Research RNA Clean and Concentrator-5 kit. Briefly, two volumes of RNA-binding buffer were added to the DNase-treated mRNA, followed by an equal volume of absolute ethanol. The mixture was transferred to a Zymo spin IC column and centrifuged at 16,000 × g for 30 s. The column was subsequently washed by adding 400 µl of RNA prep buffer and centrifuging for 30 s, followed by 700 µl of RNA wash buffer and another centrifugation for 30 s. A final wash with 400 µl of RNA wash buffer was performed and the column centrifuged at 16,000 × g for 1 min to ensure complete removal of residual buffer. The column was then placed into a clean RNase-free tube, and the RNA was eluted by adding 15 µl of nuclease-free water and centrifuging for 1 min. Transfection was performed in BHK21 exhibiting 70-90% confluency with 2.5µg of mRNA in a T175 flask using Lipofectamine 3000 kit according to the manufacturer's instructions. Briefly, Lipofectamine 3000 reagent mix and P3000 reagent mix were mixed and incubated for 15 min at room temperature. The cells were incubated at 37°C in a humidified atmosphere with 5% CO_2 for 24-48 hours or until cytopathic effect (CPE) was observed, after which the cells were harvested.

To harvest, the supernatant was transferred to a Falcon tube, and if the solution was acidic (yellow) HEPES solution was added to a final concentration of 500 mM. The

supernatant was centrifuged at 1000rpm for 5 minutes to remove cell debris and was filtered through a 0.45µM filter. Single-use aliquots were stored at -80°C. For expansion stocks, a T175 flask of BHK21 cells was infected with virus at an MOI of 0.1 in 15ml DMEM. Cells were incubated for 48 hours (37°C, 5% CO_2) and harvested as described above. No more than one round of expansion was performed for tagged virus stocks.

3.1.3 Virus Titration

SINV was titrated by plaque assay. 1×10^5 Vero cells per well were seeded in a 24-well plate in DMEM (10% FBS, 1x P/S) and incubated overnight. Serial dilutions of virus stock or prepared in serum-free DMEM with 1X penicillin-streptomycin. The media was carefully removed from the 24-well plate, and 100µl of virus stock serial dilution was added to each well. Cells were incubated for 1 hour (37°C, 5% CO_2) before 1ml of prepared 0.6% Avicell overlay was added. Cells were gently shaken to distribute the overlay evenly. After 2 days of incubation (37°C, 5% CO_2), Avicell was removed and 500µl 8% Formaldehyde was added to each well. Plates were incubated in the fume hood for 1 hour, then rinsed twice with PBS. 100µl of crystal violet stain was added and incubated for 1 hour, before the plates were washed in water and plaques were counted. Viral titre was calculated as per the formula:

$$PFU/ml = \frac{Averagenumberofplaques}{Stockdilution\times Volumeofinoculum}$$

3.1.4 Translation Shutoff using click-chemistry

Aag2-AF5 and HEK 293 cells were infected with SINV (MOI 1) and left and incubate as per the cells' requirements mentioned above for 16 hours. Starvation of cells was done for 1 h by incubating in methionine/cysteine-free media, supplemented with 1X NEAA, glutamine, sodium pyruvate, 2% FBS. Cells were then incubated with the same medium supplemented with the Click-IT-AHA (L-Azidohoalanine) reagent for 4 h. The cells were lysed in a solution containing 1% SDS, 50mM Tris-HCl HCL pH 8, with protease and phosphatase inhibitors. Click chemistry reaction for protein detection

was performed using biotin alkyne according to the manufacturer's instructions using the Click-IT protein reaction buffer kit. Briefly, 50 µl of labelled protein was mixed with 100 µl of Click-iT reaction buffer and 160 µl of double-distilled water, and the mixture was vortexed for 5 s. Subsequently, 10 µl of $CuSO_4$ was added and vortexed briefly, followed by the addition of 10 µl of Click-iT reaction additive 1 solution. After vortexing for 5 s, the reaction was incubated for 3–5 min at room temperature. A further 20 µl of Click-iT reaction buffer additive 2 solution was then added, and the mixture was vortexed continuously for 20 min, during which the solution developed a bright orange colour. The reaction was quenched by adding 600 µl of methanol, followed by 150 µl of chloroform and 400 µl of double-distilled water, with brief vortexing after each addition. The sample was centrifuged at 13,000 × g for 5 min, and the upper aqueous phase was carefully removed, leaving the protein precipitate at the interphase undisturbed. The precipitate was washed twice with 450 µl of methanol, each time vortexing and centrifuging at 13,000 × g for 5 min before discarding the supernatant. The pellet was then air-dried for at least 15 min, resuspended in 4× sample loading buffer, and heated at 70°C with shaking at 1000 rpm for 10 min. Proteins were subsequently resolved by SDS-PAGE and transferred onto a cellulose membrane for downstream analysis. Labelled proteins were incubated in a solution containing 1% BSA with streptavidin-HRP for subsequent visualisation with the Odyssey CLx Imaging System.

3.1.5 dsRNA Knockdowns

dsRNA primer design was done using Snapdragon, a web-based tool used for designing long double-stranded RNAs (dsRNAs) to facilitate RNA interference (RNAi) gene knockdown experiments [151]. To each primer T7 promoter sequence was added.

Preparation of DNA template Complementary DNA (cDNA) was synthesised from total RNA using the SuperScript III First-Strand Synthesis System (Thermo Fisher Scientific) according to the manufacturer's protocol. Briefly, 1 µg of DNase-treated RNA was mixed with 1 µl oligo(dT) primers, 1 µl 10 mM dNTP mix, and nuclease-free water to a volume of 10 µl. The mixture was heated to 65°C for 5 min and placed on

ice for at least 1 min. First-strand synthesis was performed by adding 10 µl of cDNA synthesis mix containing 2× First-Strand Buffer, 0.1 M DTT, RNaseOUT recombinant RNase inhibitor, and 200 U SuperScript III Reverse Transcriptase. Reactions were incubated at 50°C for 50 min, followed by enzyme inactivation at 70°C for 15 min.

dsRNA synthesis Double-stranded RNA (dsRNA) was generated using the MEGAscript RNAi Kit (Invitrogen) following the manufacturer's instructions. Briefly, gene-specific primers were designed with T7 promoter sequences appended to the 5' ends. PCR products were purified and used as templates for in vitro transcription. Each transcription reaction (20 µl) contained the purified DNA template, reaction buffer, ribonucleotide mix, and T7 RNA polymerase mix, and was incubated at 37°C for 4 h to allow RNA synthesis. Following transcription, RNA strands were annealed by incubating the reaction at 75°C for 5 min and slowly cooling to room temperature. The RNA annealed RNA reactions were treated with DNase I and RNase for 15 min at 37°C to remove the DNA template and ssRNA, after which complementary dsRNA was purified using the kit's column-based system, eluted in nuclease-free water, and quantified by using qubit. RNA integrity was confirmed by agarose gel electrophoresis before use in downstream knockdown assays.

3.2 Biochemical and molecular techniques

3.2.1 Western blot

Preparation of the samples involved mixing with NuPAGE 4x LDS sample buffer (Invitrogen) and heating at 95°C for 5 minutes, followed by loading them into the precast NuPAGE Bis-Tris Mini Protein Gels, 4–12%, 1.0–1.5 mm (Invitrogen). The proteins were separated by SDS-PAGE at 180 volts for 1 hour and transferred to nitrocellulose membranes using the Trans-Blot Turbo transfer system (Bio-Rad). Membranes were blocked using 5% skim milk in 0.1% PBST (blocking buffer) for 1 hour at room temperature. The blocking buffer was also used to dilute the primary and secondary antibodies. The membranes were incubated overnight at 4°C with the primary antibody. A further incubation with the appropriate secondary antibody

was done for 1 hour at room temperature in a dark room. After each incubation, the membranes were washed 3 times with 0.1% PBST. Imaging was performed on the LI-COR Odyssey CLx.

3.2.2 Silver staining

NuPAGE 4x LDS sample buffer (Invitrogen) was mixed with the sample and heated to 95°C for 5 minutes. This was then loaded into the precast NuPAGE Bis-Tris Mini Protein Gels, 4–12%, 1.0–1.5 mm (Invitrogen). The proteins were separated by SDS-PAGE at 180 volts for 1 hour. Silver staining was performed on the gel using the SilverQuest Kit as per the manufacturer's instructions.

3.2.3 RNA interactome capture (RIC)

Sample harvesting

To determine the repertoire of mosquito RNA-binding proteins. Three T175 per mosquito cell type (Aag2-AF5 and U4.4) and per UV treatment (treated and untreated) were seeded with mosquito cells were incubated at 28°C in the absence of CO_2. These cells were maintained in Leibovitz's L-15 medium (10% FBS, 10% TPB, 1xP/S). After 48 hours or until confluency, the media was aspirated and cells washed with PBS. Cells were trypsinized for approximately 5 minutes, and resuspended in 10 ml Leibovitz's L-15 medium (10% FBS, 10% TPB, 1xP/S). The resuspended cells were transferred into a 50 ml Eppendorf tube and centrifuged at 5000 xg for 10 minutes. The media was discarded, leaving the pellet, which was resuspended in 10 ml PBS. The resuspended cells were then transferred to a 50 cm^2 petri-dish, placed on ice, and UV crosslinked at 254 nm, with the cover off. The crosslinked cells were then transferred into a 50 ml Eppendorf tube and centrifuged at 5000 xg for 10 minutes to pellet the cells. The supernatant was discarded, and the samples were stored at $-$80°C until further processing.

To determine how RBPs modulate infection (cRIC). Three T175 per condition were seeded with Aag2-AF5 mosquito cells were incubated at 28°C in the absence of CO_2.

These cells were maintained in Leibovitz's L-15 medium (10% FBS, 10% TPB, 1xP/S). After 48 hours or until confluency, the media was aspirated, 15 ml Serum-free media containing SINV (MOI = 1) was added for an hour. The media was then replaced with Leibovitz's L-15 medium (10% FBS, 10% TPB, 1xP/S). Samples were harvested at 8, 16, and 24 hours post-infection. The media was aspirated and cells were washed with PBS, cells were trypsinized for approximately 5 minutes, and resuspended in 10 mL Leibovitz's L-15 medium (10% FBS, 10% TPB, 1xP/S). The resuspended cells were transferred into a 50 ml Eppendorf tube and centrifuged at 5000 xg for 10 minutes. The media was discarded, leaving the pellet, which was resuspended in 10 ml PBS. The resuspended cells were then transferred to a 50 cm^2 petri-dish, placed on ice, and UV crosslinked at 254 nm, with the cover off. The crosslinked cells were then transferred into a 50 ml Eppendorf tube and centrifuged at 5000 xg for 10 minutes to pellet the cells. The supernatant was discarded, and the samples were stored at $-80^{\circ}\mathrm{C}$ until further processing.

RIC and cRIC

Thawed pellets were resuspended in 5ml of lysis buffer (20mM Tris-HCl pH 7.5, 500mM LiCl, 0.5% LiDS Wt/Vol, 1mM EDTA, 0.1% IGEPAL (NP-40) and 5mM DTT). Lysates were pelleted homogenized by passing them through a 27G needle, this process was repeated until the viscosity of the lysate was low. 200ml of lysate was aliquoted for total proteome analysis. To the remaining lysate, 500 µl of oligo$(dT)_{25}$ magnetic beads was added (New England Biolabs, #14195S) and incubated for 1h at $4^{\circ}\mathrm{C}$ with gentle rotation. The lysate with oligo $(DT)_{25}$was placed on an appropriate magnetic stand, and the supernatant(lysate) was collected into a different tube 500 µl of oligo$(dT)_{25}$ magnetic beads were added, and further incubation for 1h at $4^{\circ}\mathrm{C}$ with gentle rotation was carried out. The separated oligo $(DT)_{25}$from the supernatant(lysate), was resuspended in lysis buffer and incubated on ice for 5 minutes with occasional pipetting to ensure proper mixing. This was followed by 2 washes each with 5mL: buffer 1(20 mM Tris-HCl pH 7.5, 500 mM LiCl, 0.1% LiDS wt/vol, 1 mM EDTA, 0.1% IGEPAL and 5 mM DTT) on ice, buffer 2 (20 mM Tris-HCl pH 7.5, 500 mM LiCl, 1 mM EDTA, 0.01% IGEPAL and 5 mM DTT) on ice, and buffer 3 (20

mM Tris-HCl pH 7.5, 200 mM LiCl, 1mM EDTA and 5 mM DTT) at room temperature. All washes were followed by 5 minutes of incubation, with occasional mixing to ensure homogeneity and placement on the appropriate magnetic stand to discard the wash buffer. The beads were resuspended in 150mL of elution buffer and incubated for 5 minutes at 55°C with agitation. The process was repeated for the second lysate and eluates combined and stored at -80°C. 50ml of eluate was used QC checks, which involved Western blot and silver staining.

Mass spectrophotometry

RIC eluates were processed with a single pot solid phase enhanced sample preparation (SP3) protocol using 70% acetonitrile for protein binding [152]. All samples were acidified with 5% formic acid prior to mass spectrometric analysis. For RIC eluates, liquid chromatography (LC) was performed using an EASY-nano-LC 1000 system (Thermo Fisher Scientific) in which peptides were initially trapped on a 75 µm internal diameter guard column packed with Reprosil Gold 120 C18, 3 µm, 120 angstrom pores (Dr. Maisch GmbH, r13.9g) in solvent A using a constant pressure of 500 bar. Peptides were then separated on a 45°C heated EASY-Spray column (50 cm x 75 m ID, PepMap RSLC C18, 2 m, Thermo Fisher Scientific no.164540) using a 3 h linear 8%˘30% [vol/vol] acetonitrile gradient and constant 200 nl/min flow rate. Peptides were introduced via an EASY-Spray nano-electrospray ion source into an Orbitrap Elite mass spectrometer (Thermo Fisher Scientific). Spectra were acquired with resolution 30000, m/z range 350$-$1500, AGC target 1x106, maximum injection time 250 ms. The 20 most abundant peaks were fragmented using CID (AGC target 5x103, maximum injection time 100 ms, normalised collision energy 35%) in a data-dependent decision tree method.

3.3 Data analysis

3.3.1 Ortholog identification

To define orthologs, Vectorbase gene IDs for *Aedes* mosquitoes were used in InParanoid-DIAMOND to identify complex orthologous relationships between protein

sequences from different genomes within Docker.

3.3.2 GO terms

GO enrichment analyses were performed using G:profiler (https://biit.cs.ut.ee/gprofiler/gost). The use of the "highlighted" column was used to collapse GO terms with similar functions. A p-value cut-off of 0.01 was used.

3.3.3 Hydrophobicity and Isoelectric Points

The Peptides R package [153] that calculates theoretical physicochemical properties of protein sequences was used to calculate hydrophobicity using the scale “KyteDoolittle” and Isoelectric point using pKscale “EMBOSS”.

3.3.4 Intrinsically disordered regions

To predict protein disorder, MobiDB-lite v3.8.4 [154] (a long disorder predictor that runs on Python) was used to determine regions of disorder in our sequences. The sequence output (a fasta file with D for disordered amino acids and S for ordered amino acids) was used to calculate the disordered content of each protein.

3.3.5 Proteins domains

To identify what domains are present in our proteins, InterProScan v5.64-96.0 [155, 156] was run, restricting the output to PFAM domains. If a protein had multiple domains, priority was given to classical, then non-classical, and then unknown. This was based on the literature by Castello and team [157]

3.3.6 RBDmapping

RBDpep from RBDmap [158], were used to identify RNA binding sites. Multiple sequence alignment on *Aedes* mosquito protein sequences from the proteomics data was performed to predict possible regions of binding. For every site predicted a

percentage conservation score was assigned. The higher the conservation score, the more similar the alignment and vice versa.

3.3.7 Proteomics

Peptide identification and quantitation of all proteomics experiments were then performed using MaxQuant (v1.5.0.35) [159]. Data were searched against the *Aedes aegypti* and *Aedes albopictus* from Vectorbase for (version, January 2022), and for cRIC data, were searched against the *Aedes aegypti* from Vectorbase (version, January 2022) and SINV from the Uniprot database. False discovery rate (FDR) was set at 1% and 10%, using both peptide and protein identification, and 'match between runs' was turned on. Otherwise, default parameters were used.

Data analysis of ProteinGroups file from MaxQuant was performed in R. Data was normalised using the 'vsn' package. Rows were filtered to remove any with $>$2 NA values for the RIC and $>$6 for cRIC in each condition under study. Minimum value imputation was performed for on/off changes (all NA values in one condition and $<$2 NA values in the other). Only values for replicates corresponding to non-NA values in the other condition were imputed. Fold-changes and p-values were calculated using the limma package [160], with replicate included as a block in the regression analysis, and FDR was calculated from p-values using the fdrtool package.

3.3.8 Statistical analysis

Statistical analysis was performed using R packages ggsignif and rstatix. The Wilcox test was used to compare two groups with uneven distributions, and the paired t tests were used to compare the test and control samples. Statistical significance is denoted as: $P < 0.05$; *, $P < 0.01$; **, $P < 0.001$, ***.

3.3.9 Data visualization

RStudio was used to make all the plots in the thesis, ChimeraX v.1.9 was used for protein structures, and Biorender was used for schematic diagrams. Compilation of

figures and images was done on Affinity Designer, and cropping of gel images.

4 The complement of *Aedes* mosquito RBPs

4.1 Introduction

RBPs are central to virtually all stages of RNA metabolism, from synthesis in the nucleus to decay in the cytoplasm [104, 161]. Over the past decade, technological advances have significantly expanded our understanding of the RBPome. These methods often rely on chemical or photochemical crosslinking followed by enrichment of protein-RNA complexes using antisense probes, oligo(dT) beads, or biotin-streptavidin system, reviewed in [132, 145]. Among these techniques, RNA interactome capture (RIC) has emerged as the gold standard for global and unbiased identification of RBPs. RIC involves Ultraviolet (UV) crosslinking to induce *in vivo* covalent bonding of proteins to RNA that are at zero distance, usually 2 angstrom, followed by the selective capture of polyadenylated (PolyA) RNA using oligo(dT) beads under denaturing conditions and the identification of proteins by mass spectrometry [119, 120]. This approach offers key advantages: UV light only promotes covalent crosslinking of native RBPs and RNA at zero-distance while avoiding protein-protein interactions, and the hybridisation of RNA to oligo(dT) beads allows the use of high-salt and chaotropic buffers to eliminate non-convalently linked proteins (piggback riders). However, a known limitation is its bias towards polyadenylated RNA, with mRNA being the dorminant species (about 70%) excluding interactions with non-polyadenylated species, such as tRNA, rRNA and other non-polyadenylated non-coding RNA.

RIC has been successfully used to characterize RBPs in several model organisms such as *Homo sapiens* [119, 122], *Mus musculus* [121], *Danio rerio* [125], *Drosophila melanogaster* [107], *Caenorhabditis elegans* [123, 124], *Saccharomyces cerevisiae* [122], and plants [126–128]. These studies have revealed that the RBPome is broader than previously anticipated including proteins with no recognisable RNA-binding domains, often harbouring enzymatic domains, protein-protein interaction domains or intrinsically disordered regions (IDRs). A large proportion of these are evolutionarily conserved in their ability to bind RNA and share physicochemical properties such as low complexity regions or overall positive charge. Resources such as RBPbase [162],

RBPDB [163], and RBP2GO [164] consolidate these findings, offering centralized repositories of experimentally supported protein-RNA interactions across species.

Despite these advances, the RNA-binding proteomes of non-model organisms, particularly arthropod viral vectors, remain poorly characterised. This gap is particularly evident in mosquitoes such as *Aedes (Ae.) aegypti* and *Ae. albopictus*, both of which are vectors of arboviruses, including DENV, CHIKV, ZIKV, and YFV [88, 165, 166]. Given the essential roles of RBPs in regulating viral replication, immune responses, and gene expression [101, 113, 167–169], a detailed characterisation of the mosquito RBPome is critical in elucidating the mechanisms of vector competence and host-pathogen interactions at the post-transcriptional level.

In this chapter, RIC and mass spectrometry will be employed to comprehensively characterise RNA-binding proteins (RBPs) in *Ae. aegypti* and *Ae. albopictus*. The characterisation will include analyses of domain architecture, biochemical properties, and conservation with respect to human RBPs.

4.2 Results

4.2.1 RNA interactome capture (RIC) specifically enriches for mosquito RNA-binding proteins (RBPs)

As modulators and regulators of gene expression, RBPs are crucial in all living cells, by ensuring physiological processes for normal cell function, development, and response to environmental stress take place. Characterising mosquito RPBs in two mosquito species of medical concern will provide the basis for functional studies during infection. To comprehensively and systematically characterise RBPs in mosquitoes, RIC was employed [119, 120], a stringent proteomics-based technique that identifies proteins interacting with poly(A) RNA in cells. Briefly, cells were irradiated with 150mJ/cm^2 UV light at a wavelength of 254nm. The cells were then lysed under denaturing conditions and homogenised by passing them through a 26G needle. This ensures that the DNA is sheared to reduce the viscosity of the sample. The covalently linked protein-RNA complexes were then isolated, using oligo(dT)$_{25}$ magnetic beads that bind the poly(A) tailed RNA. Under denaturing conditions, the beads were washed first with a high-salt buffer and high concentrations of chaotropic detergents to remove non-covalently bound proteins. This was followed by a low-salt buffer. This allowed for the removal of unbound proteins and RNAs, respectively. The crosslinked proteins were eluted from the beads by heating at 55°C. The eluate was then digested using a combination of RNase A and RNase T1 to release the proteins (Fig.4.1).

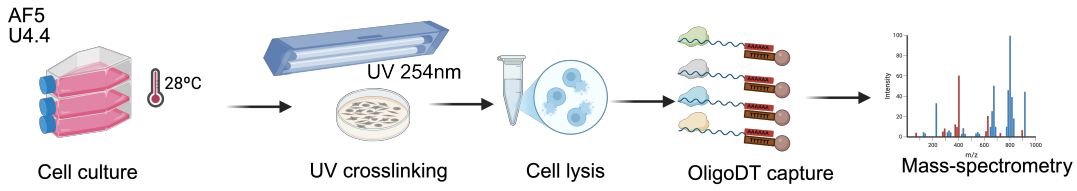

Figure 4.1: Schematic representation of RNA intractome capture (RIC)
mRNA-protein complexes are formed by employing UV-irradiation to proliferating mosquito cells. These complexes are isolated by pulldown with oligo(dT)$_{25}$ magnetic beads, stringent washes with high salt buffers, and subsequent low salt buffers. The bound protein is eluted with RNase and identified by mass spectrometry.

Two mosquito cell lines were used, *Ae. aegypti* (Aag2-AF5) and *Ae. albopictus* (U4.4). These cell lines were selected because they are derived from two key mosquito vectors of medical importance known to transmit viruses such as CHIKV and DENV [166]. Additionally, they are immunocompetent cells, having a functional RNAi pathway that limits viral propagation [5,170]. The use of immunocompetent cell lines is important for capturing a comprehensive repertoire of RBPs, including those involved in antiviral response. Moreover, to ensure sufficient protein yield for downstream mass spectrometry, all experiments were conducted in three biological replicates, with each replicate comprising pooled lysates from three T175 flasks. Biological replicates were generated for each cell line, Aag2-AF5 and U4.4. Each replicate included a non-irradiated sample (-UV) as a negative control for identifying background protein co-isolated with RNA in a cross-linking independent manner. A second control was taken following UV irradiation but prior to oligo(dT)$_{25}$ capture, referred to as the input, to represent the whole cell lysate. A third set of controls included RNase treatment prior to oligo(dT)$_{25}$ capture in both UV-irradiated and non-irradiated conditions. This was used to assess the dependence of protein enrichment on RNA integrity (not cross-linking as above). The RNAse-treated samples were denoted as +RNase, while the untreated controls were denoted as -RNase.

To assess the quality of RIC enrichment, whole cell lysates/input and eluates were confirmed by SDS-PAGE gel electrophoresis followed by silver staining. From the silver-stained gels, UV-irradiated (+UV) inputs and eluates showed distinct banding patterns, with eluates showing a distinctive but less complex pattern than that of inputs, indicative of specific enrichment (Fig.4.2A and B). The resulting pattern showed similarities to previous RIC experiments [122, 123, 158]. Notably, the +UV eluates displayed consistent banding patterns across replicates for both mosquito cell lines, reinforcing the reproducibility of the RIC protocol (Fig.4.2B). In contrast, the non-irradiated (-UV) eluates lack visible protein bands, except for the prominent RNase band at the bottom of the gel (Fig.4.2B). This suggests minimal non-specific isolation of proteins non-covalently bound to RNA. The input profiles from +UV and -UV conditions were similar, suggesting overall protein composition in the inputs remained unaffected

by irradiation, and that enrichment was oligo(dT)$_{25}$-dependent (Fig.4.2A).

To test if the adaptation of RIC is dependent on RNA isolation as a result of the formation of protein-RNA complexes by UV-irradiation, the effects of RNase treatment was examined. SDS-PAGE gel electrophoresis and silver staining were performed on eluates from +UV and -UV samples, with (+RNase) or without (-RNase) RNase digestion. +RNase samples were largely devoid of protein bands apart from the RNase band itself, whereas the -RNase samples showed complex protein profiles compatible with the cellular pool of RBPs (Fig.4.2C). This confirms that protein recovery is only possible if cellular RNA is intact, highlighting the strong RNA dependency of our assay. Together, these results confirm the robustness of RIC in enriching for bona fide RBPs.

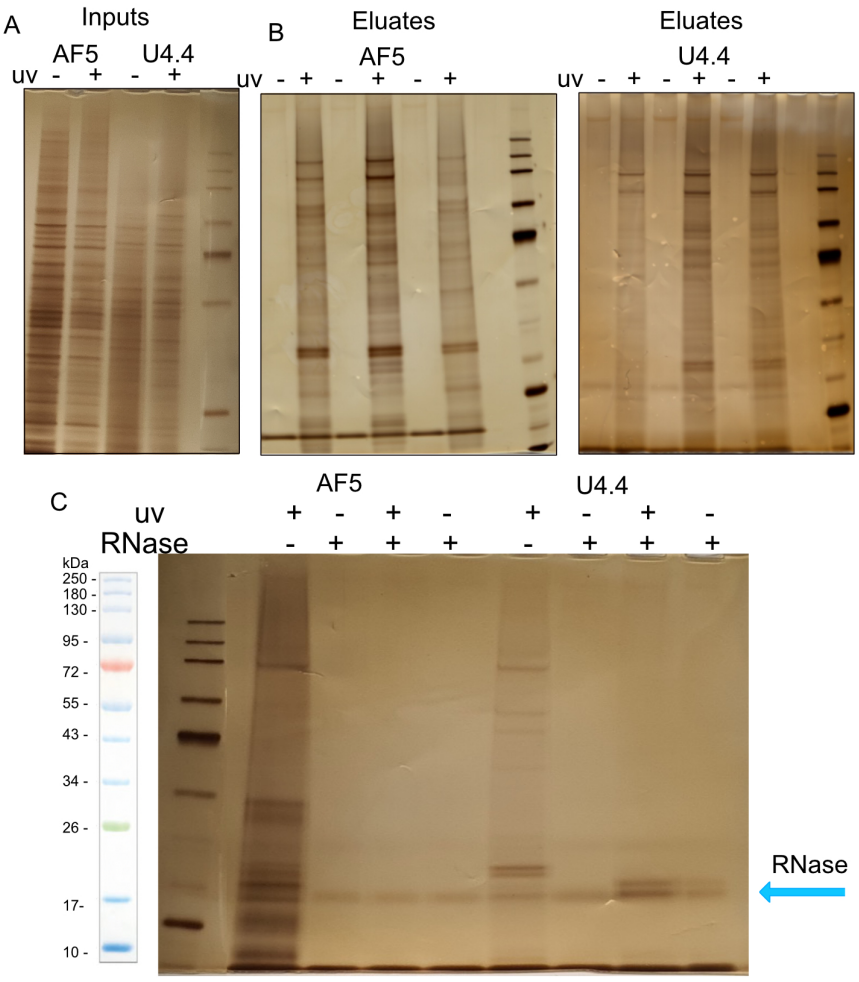

Figure 4.2: Validation of RIC enrichment in mosquito cell lines by silver staining

A) Analysis of whole cell inputs and eluates from UV-irradiated (+UV) and non-irradiated (-UV) samples. Input profiles from +UV and -UV conditions showed similar banding patterns in both *Ae. aegypti* Aag2-AF5 and *Ae. albopictus* U4.4 cells, suggesting protein composition remained unaffected. U4.4 bands were not as intense as Aag2-AF5 cells due to differences in cell count, which is influenced by growth patterns. Aag2-AF5 tend to clump up while U4.4 are more spread out on the plate surface. B) +UV and oligo(dT) eluates showed distinct and reproducible banding patterns across replicates, indicating specific enrichment of RNA-binding proteins. -UV and oligo(dT) eluates were largely devoid of protein bands, except for an RNase band, suggesting minimal non-specific isolation. These patterns were observed in both Aag2-AF5 and U4.4 cells. C) Comparison of RNase-treated (+RNase) and untreated (-RNase) eluates. +RNase samples lacked visible protein bands except for the RNAse band at about 13kDa, confirming that protein enrichment is RNA-dependent. This image is a representative of 3 replicates that were tested. This was observed in both Aag2-AF5 and U4.4 cells.

To identify systematically and comprehensively the scope of mosquito RBPs, the

eluates were subsequently processed for proteomics on an LC-MS/MS in collaboration with Dr Yana Demyanenko, Dr. Wael Kamel, and Prof. Shabaz Mohammed at the Roslin Franklin Institute. Peptides and proteins were determined and quantified by MaxQuant 2.0 [159]. The analysis revealed, 1,545 RBPs were enriched in both *Ae. aegypti* (852) and *Ae. albopictus* (683) over the negative. Data analysis was conducted under the supervision of Dr. Wael Kamel. The distribution of protein intensities in the UV-irradiated (+UV) samples was consistent across biological replicates in both the *Aedes* species, while the non-irradiated (-UV) samples showed markedly lower intensities (Fig.4.3A), consistent with what was observed in the silver stains (Fig.4.2B). Principal component analysis (PCA) further demonstrated clear separation of -UV and +UV samples (Fig.4.3B), supporting the UV-dependent isolation of proteins.

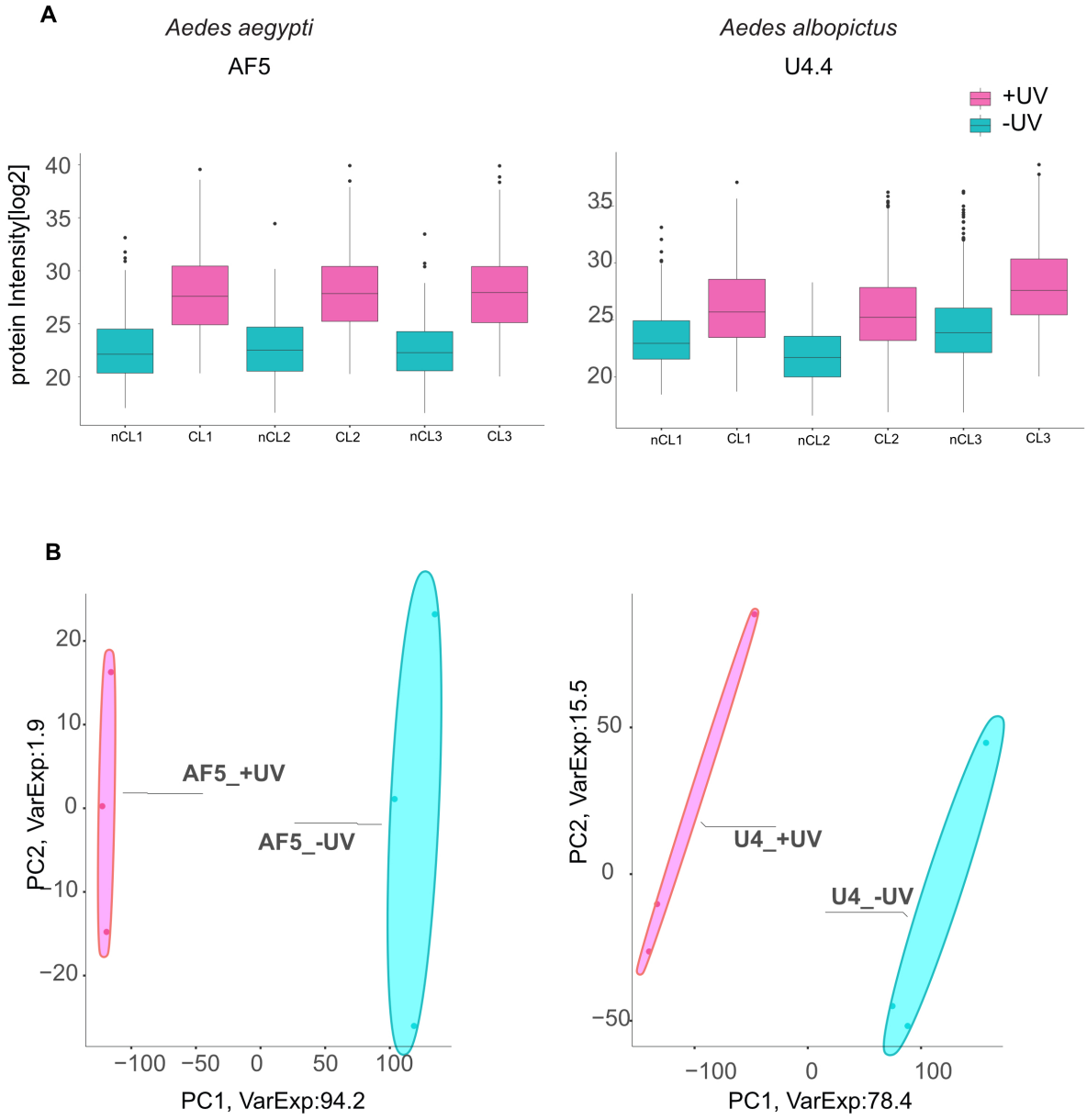

Figure 4.3: Protein intensity distribution and principal component analysis (PCA) of RIC enriched mosquito RBPs

Quality assessment of proteomics data. A) Protein intensities were consistent across all three replicates in both conditions (+UV and -UV) in *Ae. aegypti* Aag2-AF5 and *Ae. albopictus* U4.4 cell lines. The -UV had lower intensities compared to the +UV samples. B) PCA revealed clear separation between the -UV and +UV samples. Together, these confirm the UV-dependent protein enrichment of RIC.

To identify bona fide RPBs in *Ae. aegypti* and *Ae. albopictus*, a moderated t-test was applied, followed by p-values adjustment using the limma R package [160].

This analysis identified 852 and 683 significantly enriched proteins over the non-irradiated control (-UV) in *Ae. aegypti* and *Ae. albopictus*, respectively. These enriched proteins displayed a clear shift towards the UV-irradiated (+UV) condition, as shown on the volcano plot (Fig.4.4A). Proteins that were significantly enriched at 10% FDR in both mosquito species were considered high-confidence RBPs, while those present only in one mosquito species were considered candidate RBPs. These results support the effectiveness of the RIC technique in enriching for RBPs, consistent with protein patterns observed in silver-stained gels (Fig.4.2B). Further comparison of the two mosquitoes identified 396 RBPs that were shared between *Ae. aegypti* and *Ae. albopictus*, with 33 unique to *Ae. albopictus* (Fig.4.4B). The overlap in RBP composition across mosquito species identifies conserved RBPs, while RPBs unique to each mosquito exemplifies species-specific expression or culture conditions that favour specific RBPs binding to RNA.

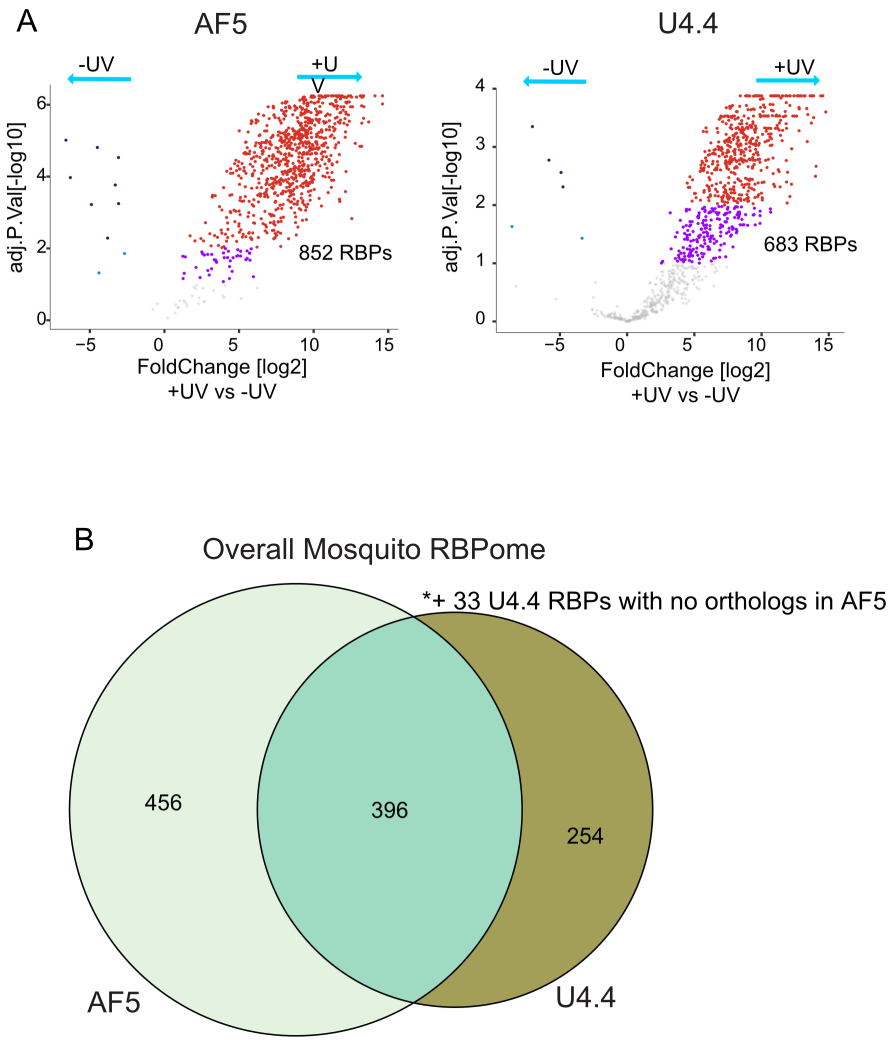

Figure 4.4: Identification of RNA-binding proteins by quantitative proteomics and orthologs between *Aedes* mosquitoes

A) Volcano plots showing differential protein enrichment between UV-irradiated (+UV) and non-irradiated (-UV) conditions for *Ae. aegypti* and *Ae. albopictus*. Proteins significantly enriched at 10% FDR (purple) and 1% FDR (red) were considered candidate RBPs. Enrichment toward the +UV condition supports UV-dependent capture of RNA-binding proteins by RIC.

B) Venn diagram showing overlap of identified RBPs between *Ae. aegypti* and *Ae. albopictus*. A total of 396 RBPs were shared, with 33 found exclusively in *Ae. albopictus*, highlighting both conserved and species-specific components of the mosquito RBP repertoire

4.2.2 Analysis of RNA-binding domains (RBDs) in mosquitoes RBPs

Given the considerable overlap in RBPs between *Ae. aegypti* and *Ae. albopictus*, RBDs were investigated to determine whether they were conserved. First,

InterProScan v5.64-96.0 was run [155, 156], restricting the output to PFAM domains, then using list of protein domain from published work by Castello et al. and Lunde et al [105, 119], RBPs were classified based on the presence or absence of known RBDs. Consistent with published literature, RBDs were classified into classical and non-classical categories. Approximately 50% harboured either classical (having specific sequence and architecture) or non-classified (containing enzymatic domains and intrinsically disordered regions) RBPs, while the other half lacked recognisable RBDs (Fig.4.5). This large proportion of "orphan" RBPs (proteins with unrecognisable RBDs) is similar to what has been reported in humans and the fruitfly [107,119]. These findings suggest that a substantial number of RBPs may interact with RNA through unconventional domains, highlighting the potential for the discovery of novel RNA-binding domains in mosquitoes.

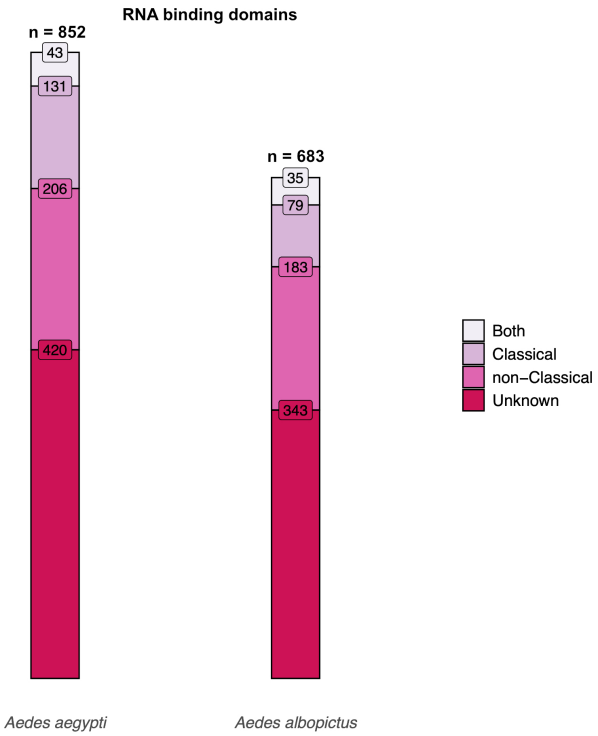

Figure 4.5: Classification of mosquito RBPs by RNA-binding domains RBDs

Mosquito RBPs were grouped based on the presence of classical (light pink), non-classical (pink), or unknown (red) RNA-binding domains, as defined in previous studies. Approximately half of the identified RBPs contained known RBDs, while the other half lacked any annotated domains, consistent with what is described in human and fruitfly proteomes. These findings suggest widespread RNA binding beyond currently known domain families. Protein PFAM ids from 852 and 683 for *Ae. aegypti* and *Ae. albopictus*, respectively, were used to classify these domains.

To further characterise the RBD landscape, the frequency of individual domains among the mosquito RBPs was plotted. Similar to findings in other species, the most prevalent classical RBPs were RNA recognition motifs (RRMs), K-homology (KH) domains, and DEAD box helicase domains (Fig.4.6A). In the non-classical RBD group, ribosomal proteins, spectrin proteins, and zinc finger proteins were the most prominent (Fig.4.6B). This domain distribution suggests that mosquito RBPs are architecturally similar to other organisms, which is consistent with the evolutionarily conserved biochemical needs of RNA binding.

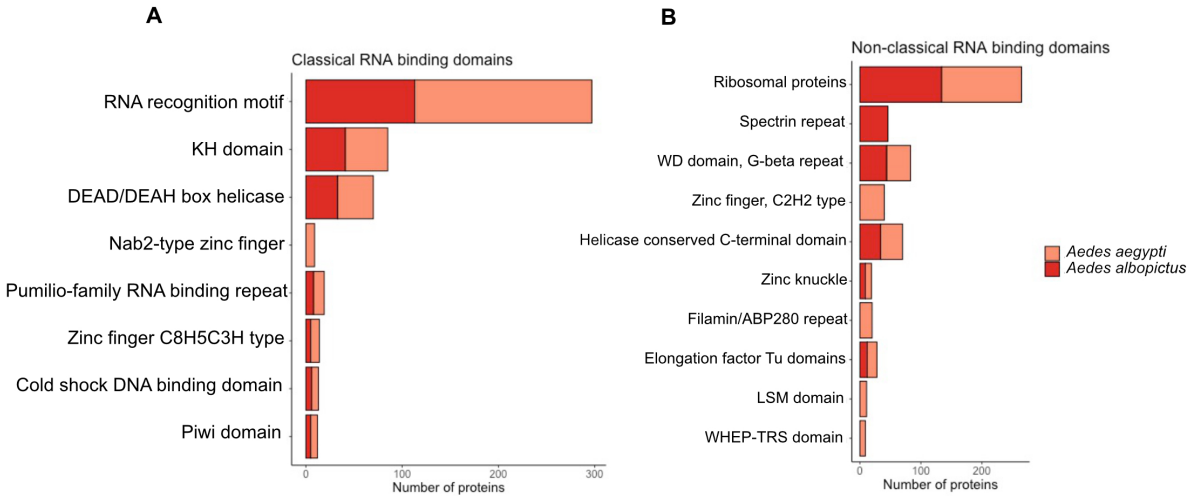

Figure 4.6: Distribution of RNA-binding domains types in mosquito RBPs

Bar plot showing the most frequent RNA-binding domains among identified RBPs in *Ae. aegypti* (brick red) and *Ae. albopictus* (orange). A) Classical domains, such as RRMs, KH domains, and DEAD-box helicases, were the most abundant. B) Non-classical domains included ribosomal proteins, spectrin repeats, and zinc finger motifs. The observed pattern mirrors domain usage in other species, suggesting evolutionary conservation of RNA-binding architecture.

4.2.3 The physicochemical and structural properties of RNA-binding proteins in mosquitoes

To validate the mosquito RBPome, physicochemical and structural properties of identified RBPs was assessed to determine if they exhibited characteristics of known RBPs. For comparative analysis, the human RBPome derived from HeLa cells was. The human RBPome has been extensively studied and provides a robust reference [119]. Specifically, features that are commonly found in mammalian RBPs were examined, including key physicochemical properties such as hydrophobicity (HI) and isoelectric point (pI), and intrinsically disordered regions (IDRs) and specific IDRs motifs. These features are known to contribute to RNA binding function and provide an additional layer of evidence for the accuracy and biological relevance of *Aedes* mosquito RBPome.

Hydrophobicity (HI) and Isoelectric points (pI) Effective RNA binding requires proteins to have specific physicochemical properties: Low HI, which contributes to

their solubility and explains why they are not typically associated with membranes, and basic pI due to the abundance of positively charged amino acids that enable electrostatic interactions with the negatively charged RNA backbone. To assess these parameters in mosquito RBPs, the Peptides R package was used [153], which calculates HI and pI from protein sequences. The results showed that RBPs in both mosquito species were less hydrophobic than their whole proteome, similar to human RBPs (Fig.4.7A). The pI of mosquito RBPs was generally more basic than that of the whole proteome and closely resembled the human RBPs (Fig.4.7B). These findings suggest that mosquito RBPs are biochemically optimised for electrostatic interactions with RNA while maintaining solubility in the aqueous intracellular environment, consistent with what is observed in the human RBPome.

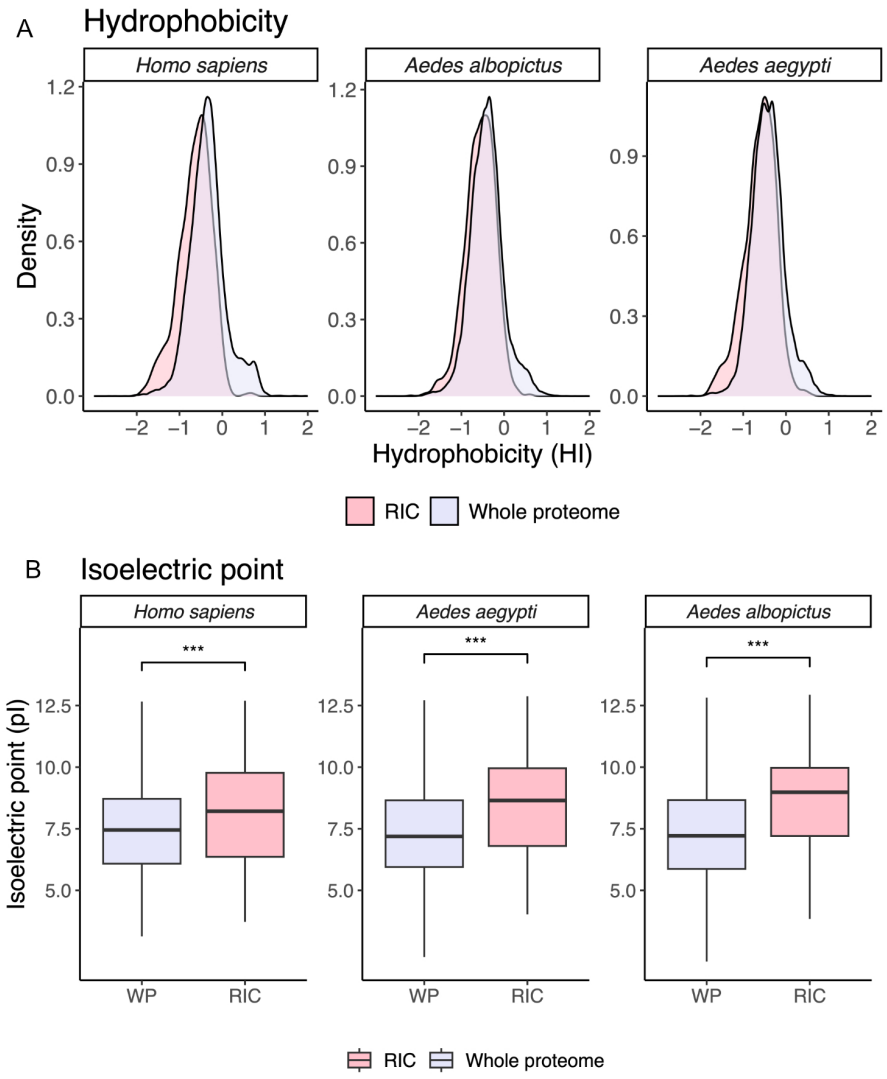

Figure 4.7: Physicochemical properties of mosquito RBPs

A) Density plots showing the hydrophobicity of the RNA-bound (RIC) proteome (pink) to be less hydrophobic than the whole proteome (lavender).

B) Isoelectric points showing RBPs (RIC) (pink) to be more basic than their whole proteome counterparts (lavender), which was significant $p < 0.001$, ***. These properties ensure interactions between protein and RNA. WP - whole proteome, RIC - RNA interactome capture

Intrinsically disordered regions/domains (IDRs/IDDs) A large proportion of human RBPs contain extensive intrinsically disordered regions (IDRs), which lack stable 3D structure. These flexible regions can participate in non-canonical modes of RNA binding and, in some cases, promote co-folding of the protein and RNA upon interaction [119, 131]. To identify IDRs, mobiDBlite v3.8.4 was used [154], an *in silico* Python tool that integrates nine different predictors to estimate disordered consensus

regions of at least 20 residues. The analysis revealed that RBPs in both *Ae. aegypti* and *Ae. albopictus* were more disordered compared to the overall proteome, although the difference was not statistically significant in *Ae. albopictus*. This is consistent with what was observed in humans (Fig.4.8).

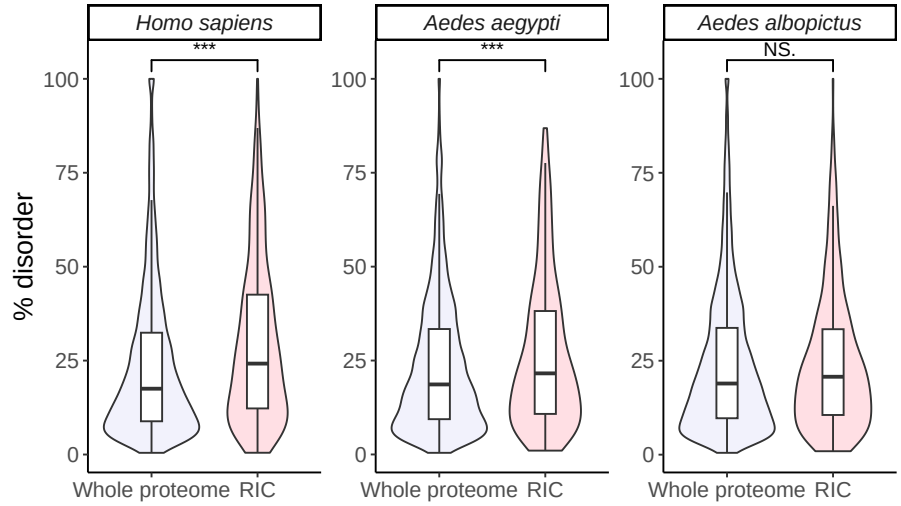

Figure 4.8: Violin plots showing the distribution of intrinsically disordered regions in RBPs

Proportion of Intrinsically disordered regions (IDRs) in *Homo sapiens*, *Ae. aegypti*, and *Ae. albopictus* RBPs (pink) compared to the whole proteome (lavender), showing higher disorder in RBPs. In *Homo sapiens* and the *Ae. aegypti* the difference was significant with a $p > 0.001$, ***, whereas that of *Ae. albopictus* was not significant (NS).

RIC - RNA interactome capture

IDRs can be classified on the basis of sequence motif with enrichment of residues such as serine (S), proline (P), glycine (G), arginine (R) and glutamine (Q) [119, 131]. Upon examining for specific short sequence motifs within IDRs, the RGG box was the most abundant motif observed, which is also very frequent in human RBPs. Interestingly, other glycine rich motifs such as YGG, GYG, GYS, SYG, and SYS boxes were identified in mosquitoes just like in humans (Fig.4.9). This motif is known to mediate RNA binding and induce molecular condensates [171]. Other well-established motifs in humans, such as the SR and poly (K) motifs, were also observed in the mosquito datasets. The presence and evolutionary conservation of these low-complexity motifs suggest they may play crucial roles in RNA biology.

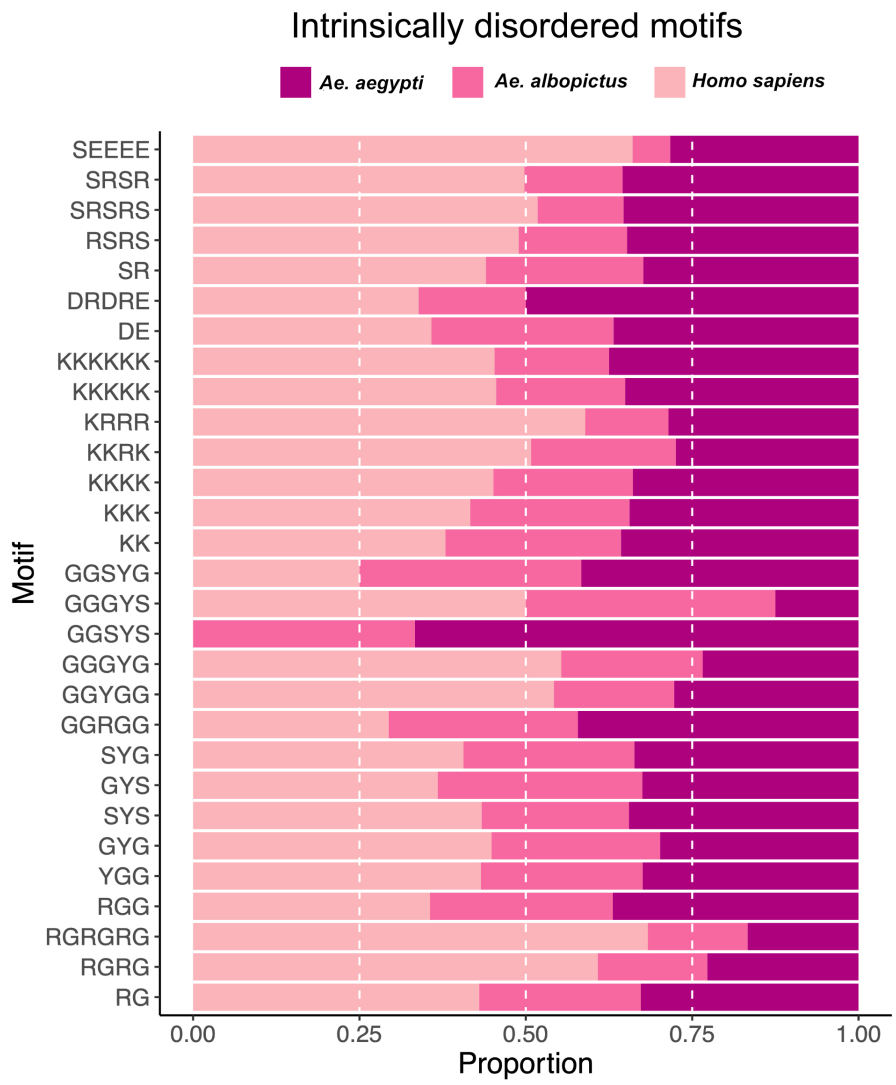

Figure 4.9: Intrinsically disordered motifs in mosquito and human RBPs

Barplot showing the proportions of motifs associated with intrinsically disordered regions. Glycine (G), serine (S), lysine (K), and arginine (R) -rich motifs were the motifs observed in *Aedes* mosquito RBPs and were comparable to *Homo sapiens* RBPs, although some motifs were preferentially enriched in mosquitoes, such as the SYG, GGRGG, and GGSYS. These low complexity motifs seem to influence RBP function.

4.2.4 Conservation of mosquito RBPs

To assess whether discovered RBPs are conserved across species, a systematic ortholog prediction using both mosquito species (*Ae. aegypti* and *Ae. albopictus*) and human was used, for which the RNA-bound proteome (RBPome) is well characterised. To circumvent the limitation due to different numbers of paralogs and orthologs between species, the InParanoid-DIAMOND algorithm was used [172]. This analysis was performed using HeLa RBPome as a reference for human proteins, as this is a highly benchmarked and validated resource that sets the basis for a high-quality dataset [119]. The analysis revealed that 79% (n=662) of *Ae. aegypti* and 78% (n=537) *Ae. albopictus* has human orthologs (Fig.4.10A). High incidence of orthologs suggests overall functional conservation between mosquitoes and humans, supporting the use of human RBP data to inform hypotheses in mosquitoes. GO term analysis further revealed functions related to RNA biology, such as processing, modification, translation and turnover (Fig.4.10B). This further ascertains the robustness of RIC to enrich for RBPs.

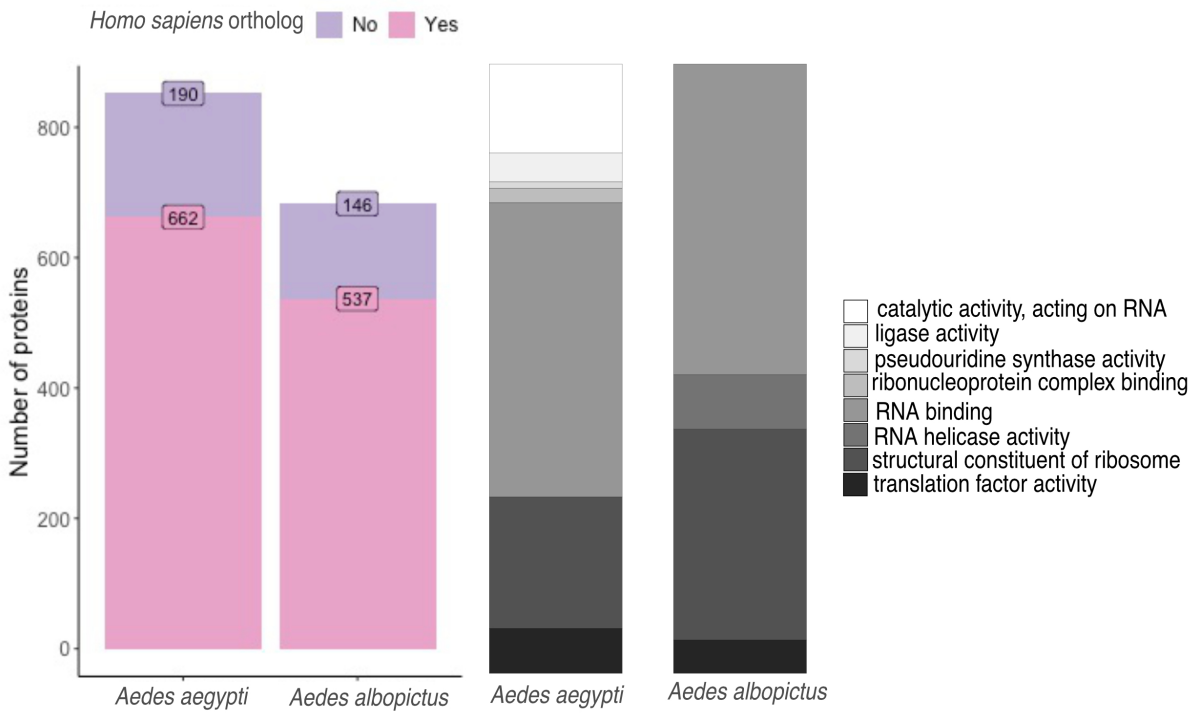

Figure 4.10: Orthologous relationships, species-specific overlap, and GO processes of mosquito RBPs

A) Proportion of RBPs from mosquitoes with predicted orthologs in the human RNA-bound proteome. Approximately 79% (n = 662) and 78% (n = 537) of RBPs in *Ae. aegypti* and *Ae. albopictus*, respectively. *Homo sapiens* orthologs (pink) and without (purple). This indicates that the majority of RBPs identified in *Aedes* mosquitoes are shared with *Homo sapiens*.

B) GOterms showing processes involving RNA, such as translation, RNA binding and RNA helicase activity in *Ae. albopictus* and *Ae. aegypti*.

4.2.5 RNA-binding sites (RBS) are evolutionarily conserved

Protein regions involved in RNA interaction are biochemically constrained, and based on the hypothesis that RBS must be, on average, more conserved than other RBP regions, RBS sequences were assessed for level of conservation. With the assistance of Rozeena Arif, RBDmap data from HeLa cells was utilised. In brief, RBDmap combines protein–RNA UV crosslinking, limited proteolysis, and mass spectrometry to globally map protein segments directly involved in RNA binding (Fig.4.11A) [106]. The analysis revealed that RNA-binding regions are by far more conserved than other protein sequences in the RBPs (Fig.4.11B). These results validate the hypothesis,

reinforcing the idea that RNA-binding regions are more constrained biochemically than other RBP regions.

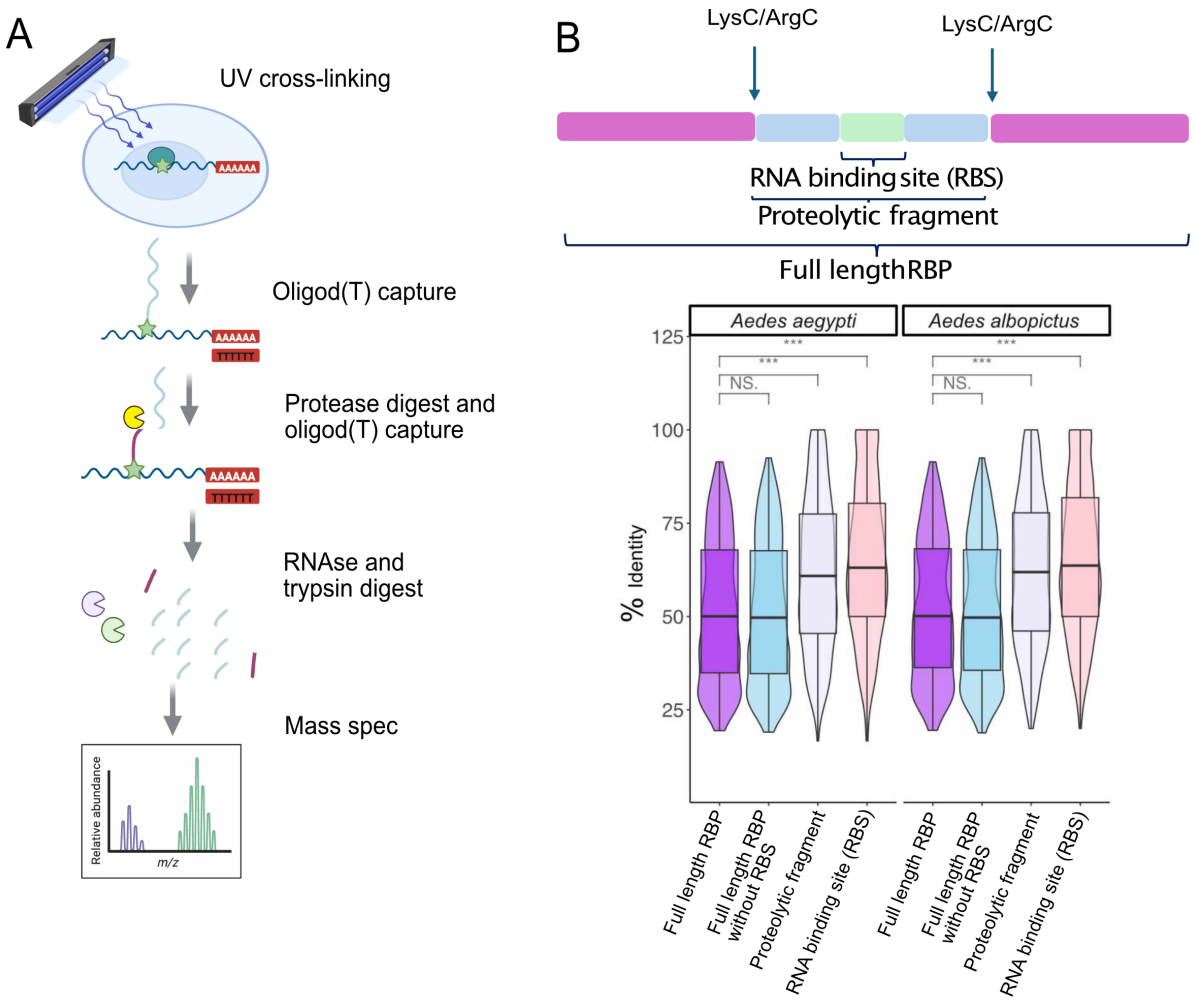

Figure 4.11: RBDmap schematic and sequence conservation of RBPs in mosquitoes

A) Schematic of RBDmap showing the UV crosslinking of protein to RNA, followed by oligo(dT) capture. An additional protease digestion was performed that targets lysine (Lys) and arginine (Arg), followed by a second oligo(dT) capture and mass spectrometry.

B) Violin plots showing sequence conservation increases with proximity to the RNA-binding site (RBS), emphasising the importance of sequence conservation in ensuring proper function of RBPs. Full length RBP (purple), Full length RBP without RBS (blue), proteolytic fragment (lavender), RNA binding site (pink). $P < 0.001$, *** , is significant, while NS was not significant.

RBDmap was generated in human cells, and based on the hypothesis that the high level of interspecies conservation would allow for the identification of RBS in relevant mosquito RBPs. As a proof of principle, DHX15 and TOP3B were chosen because

they are known to play regulatory roles during viral infection, and there is a human RBDmap dataset available [106, 168, 169]. Protein domain annotations were obtained using InterProScan v5.64 [155, 156], which provided tabular domain information based on protein sequences. After mapping the human RBDmap sequences to mosquito orthologs, this regions were visualised and highlighted using ChimeraX [173]. PFAM domain analysis showed that domain architecture was largely conserved across *Ae. aegypti*, *Ae. albopictus*, and *Homo sapiens* (Fig.4.12 A, DHX15 and TOP3B). DHX15 was highly conserved across species, both in sequence and domain architecture (Fig.4.12). In contrast, TOP3B exhibited an additional domain in humans that was absent or truncated in both Aedes mosquitoes (Fig.4.12). This suggests a loss of domain in mosquitoes or gain in domain in humans over evolutionary time.

RBDmap RNA-binding site (RBS) showed DHX15 RNA binding activity to be located in the DEAH helicase domain (PF00270) (Fig.4.12B, DHX15). By contrast, TOP3B, with unorthodox RBP with no recognisable RBD. The analysis revealed the RNA-binding site to be located in the topoisomerase domain (PF01131) that is highly conserved from mosquito to human (Fig.4.12 B, TOP3B). This conservation analysis was consistent in human and the *Aedes* mosquitoes, highlighting the power of evolutionary analysis at identifying RBDs given their biochemical constraints.

By performing multiple sequence alignment using the MSA R package, and visualising using amino acid conservation with the "prettyshade" parameter [174], sequence similarity between the human and mosquito RBPs at the RBS was quantified. *Ae. aegypti* and *Ae. albopictus* DHX15 RBS had 100% sequence identity, although a few conservative substitutions were observed in humans (i.e., biochemical properties were maintained) (Fig.4.12C, DHX15). Similarly, TOP3B RBS had 100% identity, with few conservative substitutions in humans (Fig.4.12C, TOP3B). These results suggest sequences can vary at RBS across evolution, but the overall biochemical properties are conserved to some extent.

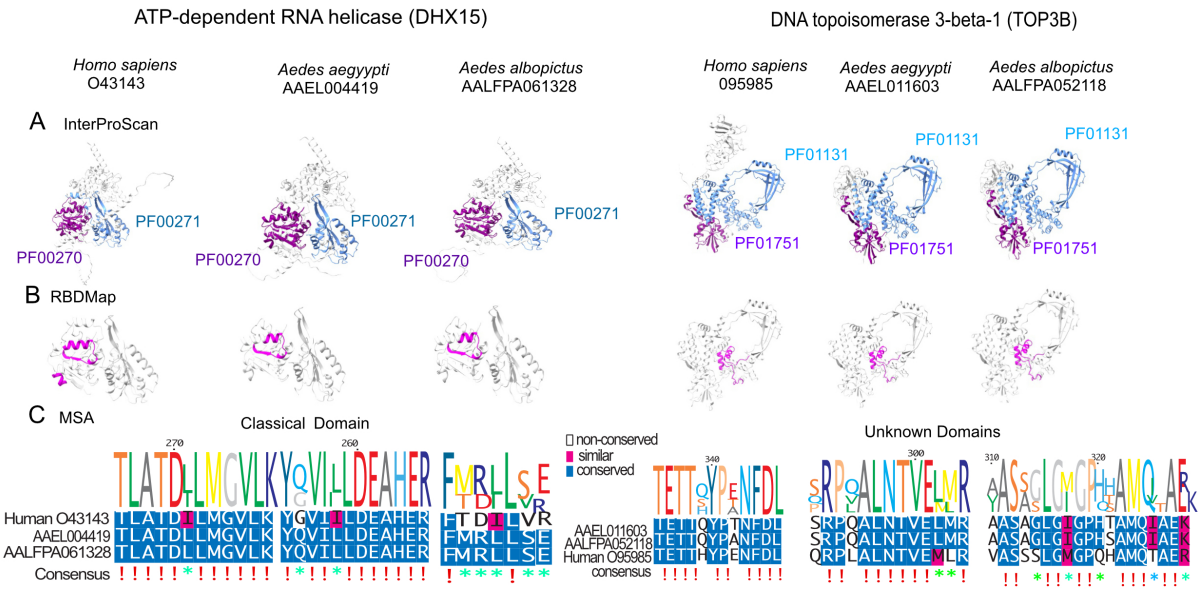

Figure 4.12: RNA binding domains, RNA binding sites, and their sequences

A) Comparison of RBPs, DHX15 and TOP3B, across species (human and mosquitoes), showing their PFAM domains as predicted by InterProScan, highlighted in blue and purple,

B) RNA binding site (RSB) as predicted by RBDMap mapping highlighted in magenta, and

C) Sequence alignment showing degree of conservation with blue showing conserved sequences, pink showing sequence similarity and white showing no sequence conservation.

4.3 Discussion

4.3.1 Conservation of RBPs

This study provides the first comprehensive study of RBPs in mosquitoes, which is a major vector of medical concern. Particularly, high-quality RPB resources for both *Ae. aegypti* and *Ae. albopictus* was generated, offering potential avenues for vector control interventions. Using RNA interactome capture [119, 120], over a thousand RBPs were identified in both species. Remarkably, approximately 78% had orthologs in human RBPs, suggesting a degree of evolutionary conservation and reinforcing the notion that core RNA processing components are maintained even in taxa as divergent as insects and mammals. This is consistent with cross-species analysis in yeast and nematodes, where they found 56% of nematode RBPome to match yeast and 62% of yeast RBPome to match that of nematodes [124]; in the *Drosophila* RBPome, 148 RBPs were found to be shared by at least three species (mouse, nematodes and humans) [107]. Reinforcing that even across evolutionary distance, species RBPs appear to be retained, suggesting strong selective pressure to maintain RNA-protein interactions.

Interestingly, these shared RBPs that appeared to be in all interactomes have been shown to be predominantly proteins previously known and are involved in core processes of RNA metabolism, such as translation and processing, whereas species-specific proteins are enriched for novel RBPs [107]. In the mosquito data sets, 396 proteins were shared between *Ae. aegypti* and *Ae. albopictus*, with 33 RBPs *Ae. albopictus* having no ortholog in *Ae. aegypti*. While the 33 show possible novel species-specific RBP enrichment, overall, the overlap shows that RBPs are highly conserved, as their biological functions need to be maintained.

4.3.2 Known (Classical and non-classical RBDs) vs unknown (unconventional RBDs) RBPs

Another important observation in the mosquito data set was the identification of known or unknown RBDs. Known are those with known RBDs, while those with

unrecognisable RBDs are unconventional. Remarkably, about 50% of RBPs identified in mosquitoes have known RBDs, which contain classical or non-classical RBDs that have been previously identified [105,119] while the remaining 50% represent unknown RBDs. This mirror findings from humans, where 53% of the RBPs were found to have known RBDs and 47% to have unknown [106]. Similarly, another study reported that approximately 60% of yeast RBPs and about 70% of human RBPs contain known RNA-binding domains [122]In Drosophila, only 14% of fly-specific RBPs carried known RBDs, whereas among RBPs conserved across species, 86% possessed identifiable RBDs [107]. This concordant observation in human, fly, yeast and now mosquitoes indicates that roughly about 50% of cellular RBPs fall outside the scope of typical RBDs. This, therefore, presents the notion that the majority of RBPs bind RNA through diverse domains such as enzymatic domains and regions of low complexity rather than dedicated domains [106, 119, 131]

The repertoire of classical RBDs detected in mosquitoes is identical to that in other species, reflecting the evolutionary conservation of RNA-binding architecture. RRMs were the most predominant domains in the mosquito RBPome, followed by well known KH domain and DEAD/DEAH-box helicase. This matches the profile of mammalian, yeast, flies and nematode RBPomes, where RMMs, KH domains and DEAD-box helicase proteins were prevalent domains [106, 107, 121–123]. This widespread presence of RRMs, KH domains and helicase domains emphasises their ancient origin and indispensable role in binding and remodelling RNA. Non-classical RBDs, such as zinc fingers, ribosomal proteins, and spectrin proteins, were among RBPs present in mosquitoes. This analysis classified known RBPs as classical or non-classical based on prior definition by Castello and team [106], and found similar proportions of these RBPs to be reported in HeLa cells and *Drosophila* [106, 107]. Such RBPs represent a class of RBPs that also play a role in the binding and remodelling of RNA.

4.3.3 Biochemical features of mosquito RBPs

Biochemical properties also offer evidence for the validation and conservation of mosquito RBPs identified. Like in human and yeast RBPome [106, 107] where

biochemical properties are intrinsically tied to RNA binding function, low HI was observed in mosquito RBPome, which is to be expected as RBPs need to remain soluble in the cytoplasm or nucleoplasm and to easily shuttle between compartments. In Castello and colleagues' HeLa cells study, they showed that hydrophobic proteins were underrepresented in the captured fraction of RBPs relative to the whole proteome [119]. The mosquito RBPome aligns with this trend, reinforcing that RBPomes are inherently enriched for soluble, hydrophilic proteins across species.

Another feature of RBPs is the overall basic (positively charged) character, measured by pI. RNA is a polyanion; amino acid residues such as lysine and arginine in proteins allow for effective binding by mediating electrostatic contact with the RNA backbone. The mosquito RBPome was found to have a more basic pI than the whole proteome, reaffirming that mosquito RBPs are enriched in positively charged amino acids. This closely resembles that of human RBPs, which was shifted toward basic pI when compared to non-RBPs [106, 119]. Nematodes and *Drosophila* also showed a similar trend of basic RBPs [107, 123]. This convergence in pI suggests a biochemical optimisation for RNA binding across evolution, where RBPs accumulate basic residues to bind negatively charged RNA.

Another key feature is that RBPs tend to contain intrinsically disordered regions (IDRs). These are regions in the protein that lack a fixed 3D structure and often facilitate RNA-binding in many proteins, providing scaffolds and low-affinity interaction interfaces that can accommodate a plethora of RNA [106]. In the mosquito RBPome, RBPs were found to be more disordered than typical proteins. This aligns with findings in human cells where more than half of RBSs in the human RBP lie within IDRs [119]. This shows that IDRs are common in the RBPome world and allow for dynamic interaction of RBPs. Like in other species, the detection low-complexity motifs within the mosquito RBPs was observed. For instance, RGG boxes were the most abundant motifs in mosquitoes, and have been observed in human, mouse and yeast [122, 158, 175]. These RGG/RG motifs are known to contribute to RNA binding and phase separation, such as stress granule formation, due to their biochemical properties [131, 176]. YGG, GYG, GYS, SYG and SYS motifs were also observed to be present in mosquito RBPs

just like in humans. These glycine, tyrosine and serine subsets of low complexity motifs are thought to work similarly as RGG boxes. Other low complexity motifs, such as poly(K), SR-rich motifs that were present in mosquito RBPs are also common in mammals [119, 175].

4.3.4 Domain and RBS conservation

Looking at specific examples, to assess how well the domain architecture and RBS are conserved across mosquitoes to humans, focus was given to two proteins, DHX15 and TOP3B, which have both been functionally implicated to be antiviral [168, 169]. This provides a contrast between conventional vs unconventional RBPs. DHX15 contains a known helicase (DEAH-box) domain often found in RNA-binding helicases, whereas TOP3B is an unconventional RBP, a topoisomerase enzyme not classically categorised as an RNA-binding protein.

Using InterProScan for domain annotation, RBDMap HeLa data as a guide for RBS, and Alphafold models. DHX15, a DEAD box helicase involved in splicing quality control, suppresses transcription upon detection of widespread intron retention [177]. DHX15 has been reported to recognise viral RNA and modulate anti-viral signalling in mosquito cells by regulating glycosylation during DENV and CHIKV infection [169]. DHX15 showed remarkable conservation of the RNA-binding site in the helicase domain (PF00270) across mosquitoes and humans. TOP3B, a DNA/RNA topoisomerase, has been shown to form a complex with RDRD3 and facilitate gene transcription and resolution R-loops [178] and to have anti-viral activity in tick cells by impairing the production of viral particles [168]. TOP3B contained its RNA-binding site in the topoisomerase (PF01131) domain across mosquitoes and humans. However, the mosquito TOP3B structures had a truncated domain/region that only appears in the human TOP3B. The loss of a domain could reflect divergence in the biological role of TOP3B; perhaps in vertebrates, it acquired an additional regulatory domain for RNA or protein interactions that insects do not require. However, the core architecture of the RNA-binding site remains conserved. This aligns with the RBDmap study in human cells that reported RBD to have a high degree of evolutionary conservation, with many

critical RBD residues being similar biochemically across species [106].

4.3.5 Limitations of the study and future work

While RIC is highly effective in capturing mRNA-bound proteome, it is inherently biased to polyadenylated RNA, which means RBPs that act on rRNA, tRNA and snRNA are underrepresented or absent. This may be valuable when studying mRNA-associated proteins; however, if the intent is to capture the total RBPome, complementary methods, such as enhanced RIC, are advisable. The identified RBPs in mosquito cells, while insightful, do not give a clear picture of what happens in different tissues, where the physiological composition is different and future experiments should work on the whole mosquito.

Future work should expand RBP discovery and focus on functional characterisation, particularly of unconventional and mosquito-specific RBPs. Key questions include whether unconventional RBPs bind RNA sequence-specifically or act as chaperones. Approaches like CLIP-seq or RIP-seq will be crucial to map these interactions and uncover links between metabolism and gene regulation in mosquitoes.

In conclusion, mosquito RBPs retain core architectural and biochemical features observed in higher organisms, including conserved RBDs, enrichment of IDRs, and preservation of RNA-binding sites. This evolutionary convergence speaks to the fundamental role of RBPs across species. Furthermore, the identification of species-specific and unconventional RBPs offers insight into mosquito-specific RBPs as targets for vector or antiviral strategies. In the next chapter, the remodelling of the mosquito RBPome during viral infection will be investigated.

5 The remodelling of *Ae. aegypti* RBPs by SINV virus

5.1 Introduction

Over the years, the study of protein interactions was limited to individual proteins. A systematic search for classical RNA-binding domains, such as RNA recognition motifs and KH domains, facilitated the identification of RBPs [105]. These classical RBDs often have a modular architecture that enhances affinity and specificity [179]. However, over the last two decades, it has become apparent that non-canonical RBPs can also mediate interactions with RNA with unusual topologies and RNA binding modes [180, 181]. The discovery of these unorthodox RNA binders highlights the existence of a broader universe of RBPs that remain unknown.

The establishment of RIC led to the unbiased identification of RBPs [119, 120, 182]. RIC takes advantage of the photo-reactivity of nucleotide bases to UV irradiation to covalently bind RNA and proteins at zero distance. This is followed by the capture of polyadenylated RNA by hybridisation to Oligo(dT) magnetic beads under denaturing conditions. When RIC was applied to HeLa cells, 800 RPBs were identified, where two-thirds of them lacked canonical RBDs [119]. Adjusting the RIC protocol by adding a partial proteolytic step revealed that newly identified RBPs interact with RNA through catalytic cores, protein-protein surfaces and intrinsically disordered regions (IDRs) [106, 183]. Application or RIC to other systems, including tissues, revealed that the RNA interactome is very diverse but highly conserved across species [107,184,185]. Evolution of RNA-protein capture methods, such as protein-crosslinked RNA eXtraction (XRNAX) to capture total RNA as opposed to only poly(A) RNA, identified proteins that largely overlap those captured by RIC [138]. RIC has also been applied to identify RBPs influenced by physiological and pathological cues. In *Drosophila* embryonic development, it was observed that the maternal zygotic transition correlates with hundreds of changes in RBPs associated with RNA. The changes were mostly related to protein abundance as a result of proteomic alterations associated with embryonic development [107].

Viruses are expected to dynamically interact with host dependency and antiviral factors, which provides an excellent context for RIC to profile cellular RBPs dynamically. In mammalian cells, RIC has been used to characterise the cellular RBPome during infection with SINV, SARS-CoV-2, and influenza virus (IAV) [101, 113, 114]. Notably, these studies showed an alteration of the RBPome as infection progressed, with over 30% RBPs exhibiting changes in RNA binding activity at later time points [101, 113, 114]. Investigation of RNA transcripts using RNA-seq further revealed that SINV infection resulted in widespread degradation of cellular housekeeping genes, and viral RNA became the most abundant RNA species in cells (70%) [101]. RIC in infection also revealed many relevant antiviral and dependency proteins. For example, Interferon-gamma inducible factor 16 (IFI16) was one of the early responders to SINV infection. IFI16 has been shown to bind DNA [186]; However, RIC also shows it binds RNA [101]. Previous studies have also demonstrated that IFI16 interacts with CHIKV RNA and suppresses infection [187]. These confirm how antiviral proteins like IFI16 are vital in antiviral defences to modulate virus success during infection. Dependency RBPs, such as 5'-3' exonuclease 1 (XRN1) were also upregulated during infection. XRN1 was shown to play a pivotal role in SINV and SARS-CoV-2 infection, where its depletion led to cells being refractory to infection [101, 188]. Activation of XRN1 could explain the degradation of cellular RNA observed during SINV and SARS-CoV-2.

This demonstrates the applicability of comparative RIC as a powerful tool for elucidating the RBPome under diverse conditions, including during infections with different viruses, across multiple cell types such as mosquito cells, and following experimental conditions such as interferon stimulation. Such experiments broaden our understanding of the complex interactions between viruses and their hosts.

In this chapter, The aim is to define the atlas of RNA-binding proteins in *Ae. aegypti* Aag2-AF5 cells at 8, 16, and 24 hpi (hours post-infection) using comparative RIC. By profiling host RBPs over the course of infection will aid in determining what factors drive viral replication in mosquitoes.

5.2 Results

5.2.1 Infection kinetics in *Ae. aegypti* derived Aag2-AF5 cell line

Mosquitoes often show little to no cytopathic effect during infection, establishing persistent, non-lethal infection, unlike in mammalian cells [189]. To characterise infection kinetics in mosquitoes, two components were considered in the study design: firstly, the cell line to use, *Ae. aegypti* Aag2-AF5 cells were selected due to their monoclonal nature and a functional RNAi system [190]; second, the choice of virus, SINV was chosen as a representative of alphavirus due to its tractability and widespread use in arbovirus research [16,43,101,169,189,190]. The infection kinetics were then conducted over an 18-day time course. Briefly, cells were infected with SINV, and samples were collected (every day and every other day after day 10) to assess viral replication and cell viability. Specifically, supernatants were harvested to quantify viral titres, while cell pellets were used for viable cell counts, quantitative reverse transcription polymerase chain reaction (RT-qPCR) to evaluate viral gene expression. All infections were performed in a T25 flask, with three biological replicates per condition, mock (uninfected) and SINV-infected (28°C, 0% CO_2). Cells were infected at a multiplicity of infection (MOI) of 1.

To assess the impact of infection on cell viability, samples were stained with trypan blue and counted. A two-sample t-test ($p > 0.01$) on the mock and infected was calculated for each time point. The results indicated minimal cell death across all time points in both uninfected (mock) and SINV-infected conditions, with 93% or higher cell viability being observed. There were no statistically significant differences between mock and infected except on days 1 and 9. These findings suggest that cell death observed during the time course was not driven by viral infection, but was likely due to baseline cellular turnover and environmental stress associated with the harvesting process and long-term culture (Fig.5.1).

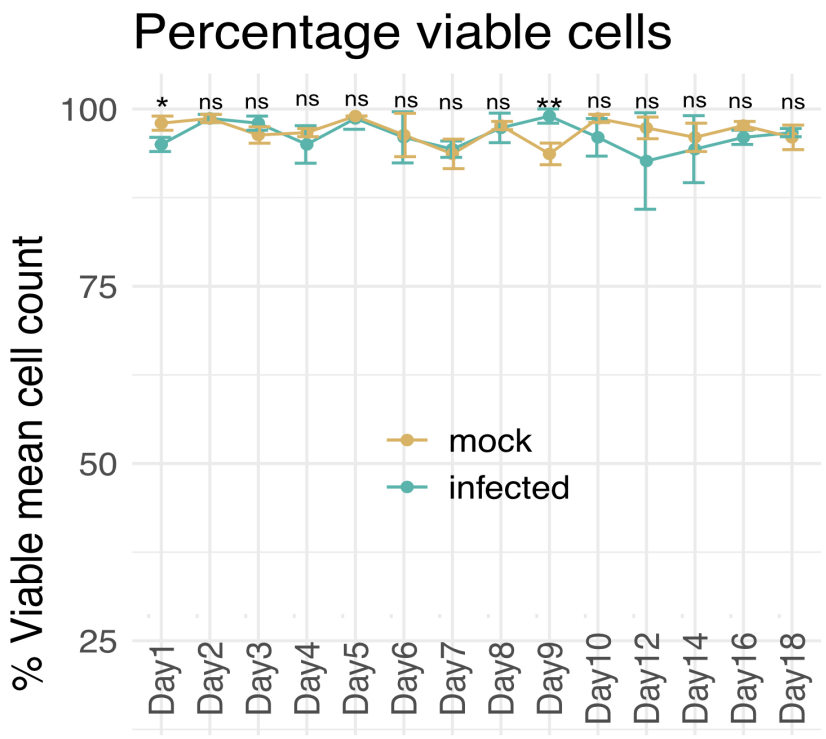

Figure 5.1: SINV infection does not significantly affect cell viability in Aag2-AF5 cells

Percentage viable cell counts were measured at multiple time points over an 18-day infection time course by staining cells with trypan blue. SINV-infected (green) and mock/uninfected (gold) *Ae. aegypti* Aag2-AF5 cells exhibited minimal differences in viability across all time points. Using a paired t-test and mean and SD error bars for triplicate samples showed that mock vs infected cells did not differ significantly except on days 1 and 9 ($p < 0.1$, *, and $p < 0.05$, **, not significant, ns). This suggests that SINV infection does not induce significant cytopathic effects and that any difference in cell viability was likely due to routine cellular turnover.

Infectious particle release over time Formation of viral particles indicates that the virus is replicating and spreading. To estimate the number of infectious particles released into the culture medium, plaque assays were performed on mammalian Vero cells using the supernatants collected at each time point. Viral titres were calculated in plaque-forming units per millilitre (PFU/ml) as described in the methods. The results revealed a logarithmic increase in PFU/ml up to day 2, indicative of rapid viral replication and release in the early stages of infection. This was followed by a gradual decline from days 3 to 6 (2-fold decrease), with the exception of a transient increase on day 5 (approx. 0.5 increase), though it did not reach the levels observed in early

infection. A secondary increase in viral load was observed on days 7 and 8 (about 2-fold), followed by a decline on day 9, where it eventually stabilises for the remainder of the experiment (Fig.5.2). These temporal dynamics suggest a biphasic infection profile: an acute phase, corresponding to two replication cycles, characterised by high viral replication and release; and a subsequent persistent phase, also spanning two replication cycles, marked by lower and relatively stable viral titres. This reflects the persistent pattern of infection generally observed in mosquito cells [189].

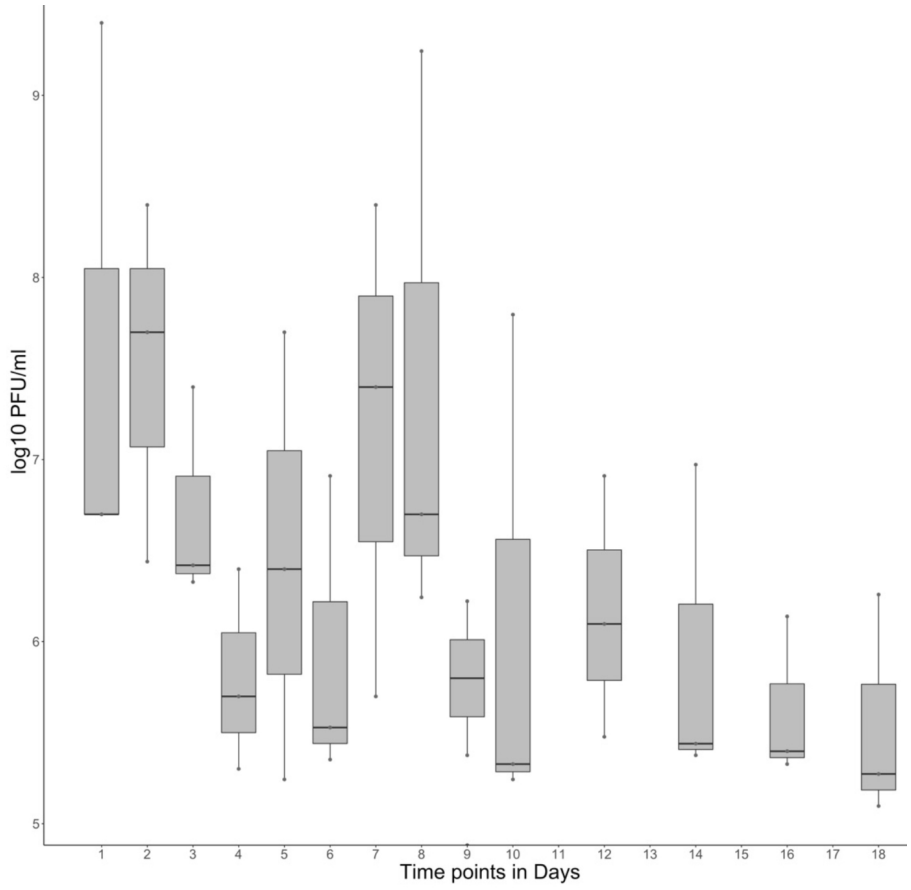

Figure 5.2: Temporal profile of infectious virus release measured by plaque assay

Boxplot of quantified SINV viral particles from supernatants collected from infected Aag2-AF5 cells passaged with virus over an 18-day time course using plaque assays on Vero cells, the error bars showing mean and SD of triplicate samples. Viral titres (PFU/mL) increased exponentially, peaking at day 2 post-infection, followed by a gradual decline from days 3 to 6 (with a transient increase on day 5). A secondary increase in viral load was observed on days 7 and 8, followed by a decline on day 9 and stabilisation from day 10 onwards. These dynamics indicate a biphasic infection pattern comprising an acute phase of high replication and a persistent phase with lower, stable viral production.

Viral RNA gene expression over time Upon alphavirus entry into the host cell, they hijack the host proteins for their replication. The process begins with the translation of non-structural polyproteins (nsPs), which are synthesised to form new viral RNA. Subsequently, synthesis of subgenomic RNA follows to produce structural proteins [42]. To characterise viral replication kinetics, the expression of genomic (g) (non-structural protein) and subgenomic (sg) (structural protein) viral RNA (vRNA) was assessed by RT-qPCR over the 18-day time course. The results show that gvRNA levels were lowest on day 1, peaked sharply on day 2, and then gradually declined until day 6 by 1.5 fold, after which they remained relatively stable (Fig.5.3a). In contrast, sgvRNA levels were highest on day 1, followed by more than a 5-fold decrease on day 2, which continued to decline gradually to day 6, then rose gradually before stabilising (Fig.5.3b). This suggests that the formation of new viral RNA occurs at the onset of infection, as gvRNA levels are much higher, while sgvRNA levels occur later on [42]. The eventual stable state of both the genomic and subgenomic RNA suggests a persistent infection, which was also evident from the viral titres (Fig.5.2) .

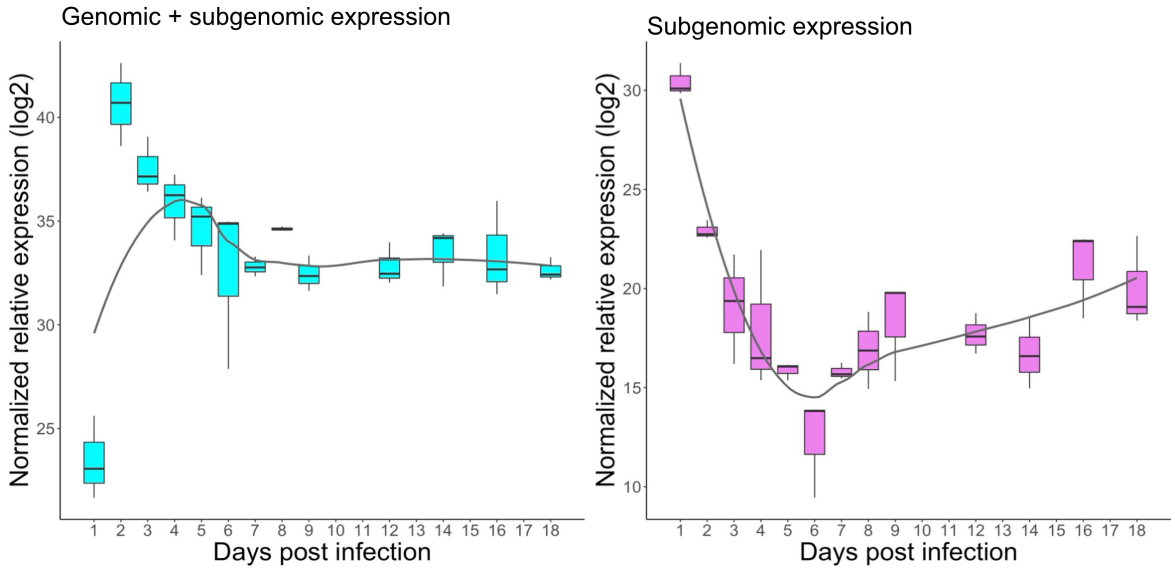

Figure 5.3: Genomic and subgenomic viral RNA dynamics during SINV infection in Aag2-AF5 cells

Box of the expression of SINV genomic + subgenomic RNA (genomic) and subgenomic RNA showing mean and SD from triplicate samples from each time point up to 18 days of infection. Genomic RNA levels were lowest at day 1, peaked sharply at day 2, and gradually declined until day 6 before stabilising. In contrast, Subgenomic RNA levels were highest on day 1 and decreased by more than 5-fold on day 2, followed by a slow and steady decline that reached its lowest at day six, and then began to steadily rise and then stabilise onwards throughout the infection. The presence of genomic RNA reflects ongoing viral replication, while the Subgenomic formation of virus particles. Together, these results reflect dynamic regulation of the SINV replication cycle in mosquito cells. Primers targeting nsP2 were used to target genomic and subgenomic RNA while primers targeting the capsid were used to target the subgenomic RNA.

5.2.2 Translation dynamics in mosquito and human

Viral infection in mammalian cells is lytic, while in mosquito cells is non-lytic [189]. To assess the impact of SINV infection on host translation in arthropod versus human cells, comparison of the global protein synthesis in Aag2-AF5 cells and human HEK293 cells under uninfected (mock) and SINV-infected conditions. Both cell lines were infected with SINV at an MOI of 1 for 16 hours, which ensured minimal cytopathic effect in the HEK cells. To label the newly synthesised proteins, cells were treated with a methionine analogue, L-Azidohoalanine (AHA) , which could later be conjugated

to biotin for protein visualisation. In the HEK293 cells, robust protein synthesis was observed in the uninfected (-) cells as indicated by the diverse banding pattern. In contrast, the SINV-infected (+) HEK293 cell displayed a single band corresponding to the viral capsid protein, suggesting host translational shutoff and redirection of cellular resources to viral protein production (Fig.5.4). In Aag2-AF5 cells, both uninfected (-) and SINV-infected (+) cells exhibited comparable banding patterns, similar to that observed in uninfected (-) HEK293 cells. This indicates that SINV infection does not induce shutoff of host protein synthesis in mosquito cells, and that translation remains active during infection (Fig.5.4). These results highlight the fundamental differences between mammalian and mosquito cells, with arthropod cells supporting persistent infection (which is shown earlier Fig.5.2) without repression of translational activity.

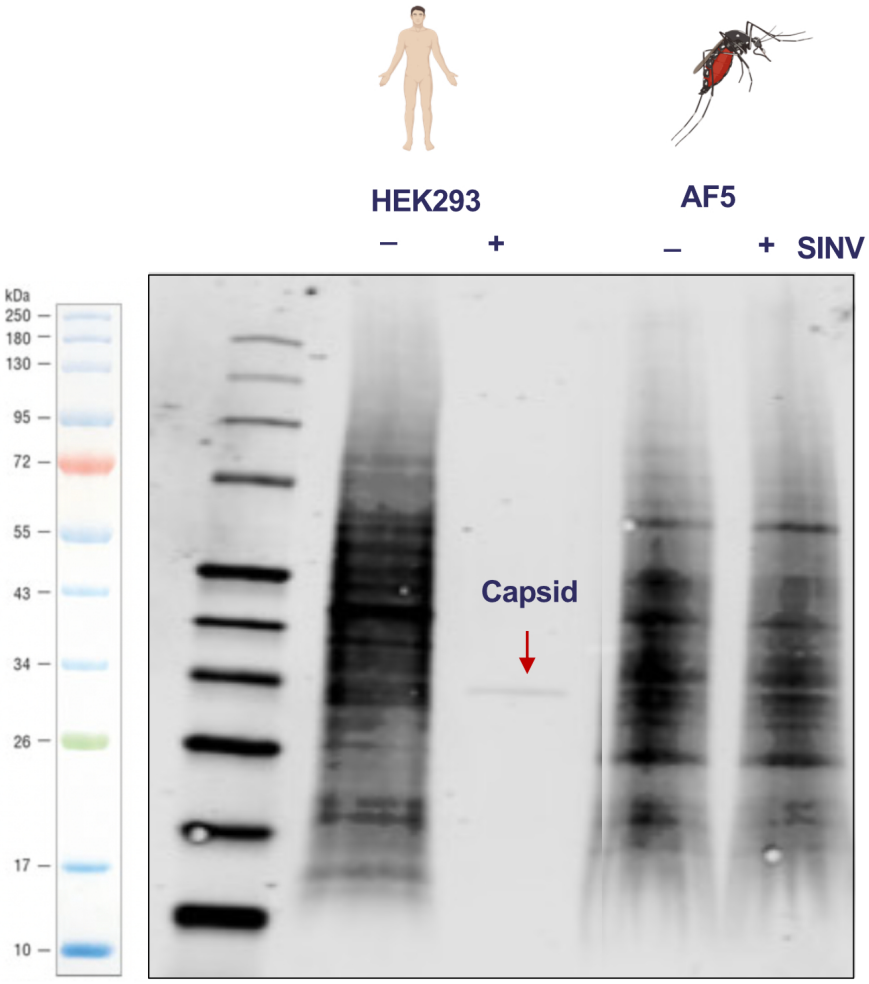

Figure 5.4: Comparison of host protein synthesis in infected and SINV-infected (+) and uninfected (-) HEK293 and Aag2-AF5 cells

Cells were infected with SINV (MOI = 1) for 16 hours (to ensure minimal cytopathic effect on the HEK cells), followed by a 1-hour methionine/cysteine starvation and a 4-hour pulse with AHA. Newly synthesized proteins were detected using a biotin-azide click chemistry reaction and visualized by streptavidin-HRP on a nitrocellulose membrane. In HEK293 cells, SINV infection led to suppression of host translation, evidenced by a loss of banding and a single capsid band (30 kDA). In contrast, Aag2-AF5 cells showed no apparent change in translation profile between mock and infected conditions, indicating preserved host translation during infection.

5.2.3 Viral infection determines the RNA-bound proteome

Having observed that mosquitoes sustain persistent infection without an apparent fitness cost and with translation remaining unhampered, it is evident that mosquito infection dynamics differ from those in mammalian systems. Viruses are obligate

intracellular parasites that rely heavily on host machinery for genome replication and virion assembly. RNA-binding proteins (RBPs) exemplify such host factors frequently co-opted during infection. The roles of RBPs have been extensively characterised in mammalian systems [101, 113]. Based on the hypothesis that RBP dynamics in mosquitoes will differ from those observed in mammals, comparative RNA interactome capture (cRIC) was performed in *Ae. aegypti* Aag2-AF5 cells infected with SINV and uninfected. For cRIC, Aag2-AF5 cells were seeded and infected at approximately 80% confluency with SINV at a multiplicity of infection (MOI) of 1. Cells were harvested at 8, 16, and 24 hours post-infection (hpi). All experiments were conducted in three biological replicates, each replicate comprising pooled lysates from three T175 flasks to ensure sufficient material for proteomic analysis. RIC was then performed as described in the previous chapter and in the Methods section (Fig.5.5).

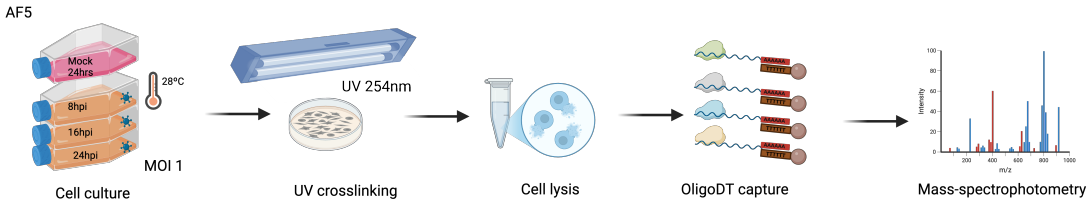

Figure 5.5: Schematic of the cRIC workflow

Overview of the comparative RNA interactome capture (cRIC) methodology. SINV infected Aag2-AF5 cells were UV-crosslinked at 254 nm to covalently link RNA-protein complexes, followed by lysis, oligo(dT) magnetic bead pulldown of poly(A)-RNA, stringent high salt washing, and RNase digestion to release crosslinked proteins for proteomic analysis.

Quality of protein enrichment To confirm successful SINV infection, western blotting was performed for the viral capsid protein. Capsid levels increased with time, peaking at 24 hpi, while tubulin levels remained unchanged, serving as a loading control and representative housekeeping protein. As expected, capsid was absent in mock controls (Fig.5.6A). The success of RIC enrichment was confirmed by SDS-PAGE followed by silver staining. Eluates displayed distinct banding patterns (Fig.5.6 C) compared to input, indicating specific enrichment of RNA-bound proteins (Fig.5.6

B). Notably, eluate profiles were consistent across all infection time points (Fig.5.6 C), suggesting that abundant, constitutive RBPs remain stable during infection [101].

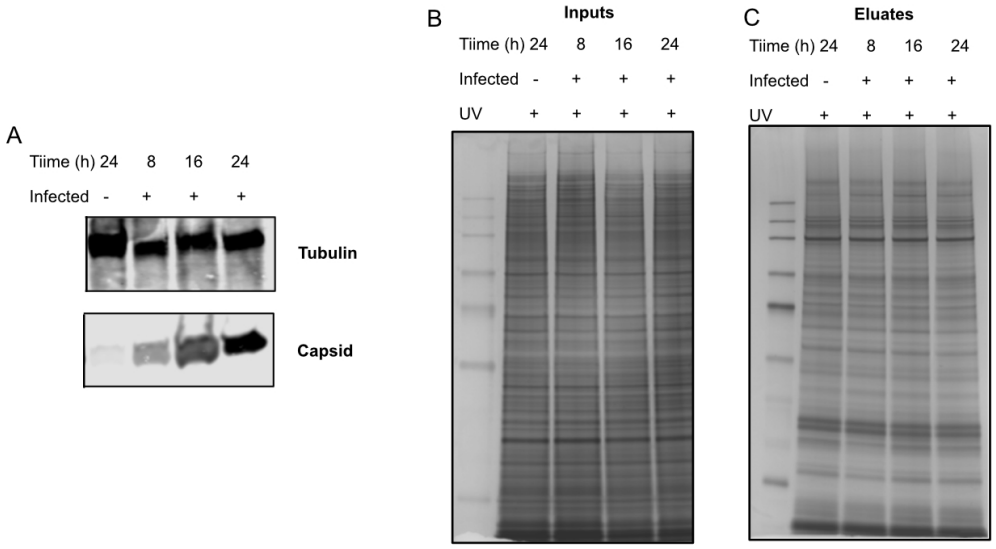

Figure 5.6: Western blot and Silver staining of input inputs and cRIC eluates

A)Western blot analysis of cRIC eluates probed with antibodies against SINV capsid and tubulin (housekeeping protein). Capsid protein levels increase with time, peaking at 24 hpi, confirming active infection. Tubulin levels remain consistent across all samples, serving as a loading control. No capsid is detected in the mock/control.

B-C) SDS-PAGE followed by silver staining of inputs and eluates from uninfected/mock (-) and SINV-infected (+) Aag2-AF5 cells. Eluates show distinct banding profiles from input, indicating specific enrichment of RNA-binding proteins. Eluate banding patterns are consistent across 8, 16, and 24 hpi, suggesting stable RBP profiles during infection.

Eluates were then processed for LC-MS/MS-based proteomic analysis in collaboration with Dr. Yana Demyanenko and Prof. Shabaz Mohammed at the Rosalind Franklin Institute. Protein identification and quantification were performed using MaxQuant v2.0 [159] and data acquisition was done using label-free data-dependent acquisition (DDA) , identifying 1,556 proteins. Instances of protein intensity values not being present (missing value) were evaluated across replicates. Missing values show variability across replicates at each time point (Fig.5.7 left). To account for missing values, data were normalized using variance stabilization normalization (vsn) in R

[191]. By examining the protein intensities before and after normalisation (Fig.5.7), it is evident that missing values account for variability in replicates and necessitate normalisation for ease of downstream analysis. This variation could be a result of biological variability, such as inherent cell heterogeneity or on/off scenarios (present in mock and not infected or vice versa), or technical issues during sample processing and/or equipment performance.

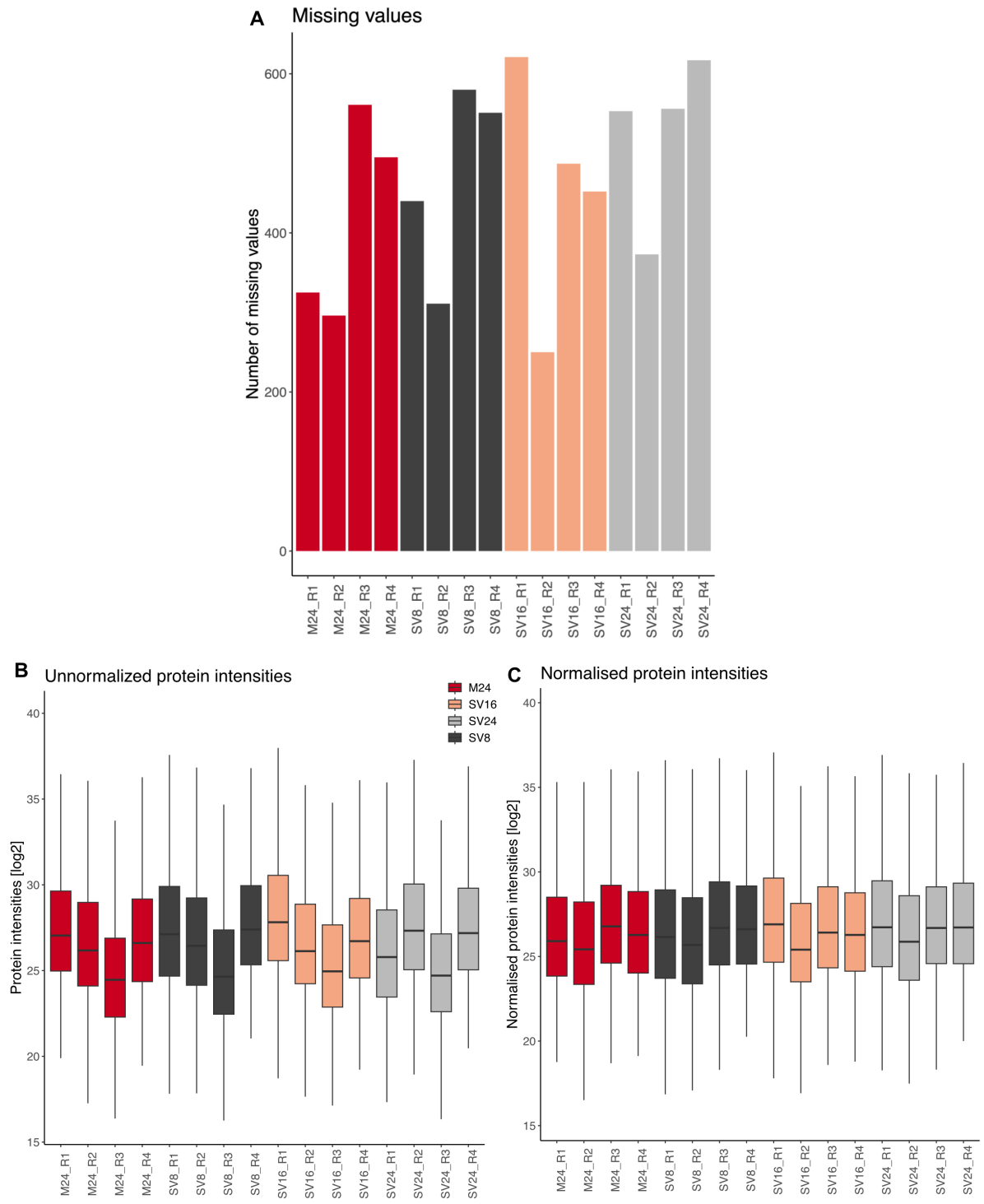

Figure 5.7: Quality of proteins by mass spectrometry

A) Barplot showing the instances where protein was not present (missing values), variability within and across replicates was evident(left). B) Boxplot of log2-transformed protein intensities identified by LC-MS/MS in cRIC eluates at 8, 16, and 24 hours post-infection (hpi) before normalisation and, C) after normalisation. Upon normalisation, the distribution remains consistent across all time points, indicating reproducible protein enrichment and stable recovery of RBPs over time. M24 - Mock, SV8 - 8hpi, SV16 - 16hpi and SV24 - 24hpi.

Remodelling of RBPs during infection In order to estimate the statistically significant changes during infection, data was analysed relative to mock (uninfected) by performing a moderated t-test using the limma R package [192]. To correct for multiple testing, p-values from limma were corrected using FDRtool in R [193] and False discovery rate (FDR) 1% and FDR 10% estimated in the data (Fig.5.9A). This analysis revealed 215 proteins with altered RNA-binding activity at 8, 16, and 24 hours post-infection (hpi). 143 downregulated, whereas 72 were upregulated (Fig.5.9B). The number of upregulated proteins declined over time, whereas downregulated proteins progressively increased, suggesting that host defence mechanisms are activated as infection progresses. Interestingly, the 16 hpi displayed fewer altered proteins compared to the other time points examined (Fig.5.9B), possibly suggesting a transition phase infection dynamics, from acute to persistent infection.

The abundance of proteins may be influenced by the metabolic processes that occur in cells. To delineate the steps of viral replication and transcription, viral temporal changes were examined using protein intensities. Capsid increased during the course of infection, while nsP1 decreased (Fig.5.8). E2 and nsP1-2 did not follow any particular trend over the course of infection (Fig.5.8). However, the pattern exhibited by Capsid and nsP1 aligns with the canonical alphavirus replication strategy, in which translation of genomic (non-structural) proteins precedes that of subgenomic (structural) proteins [45, 194].

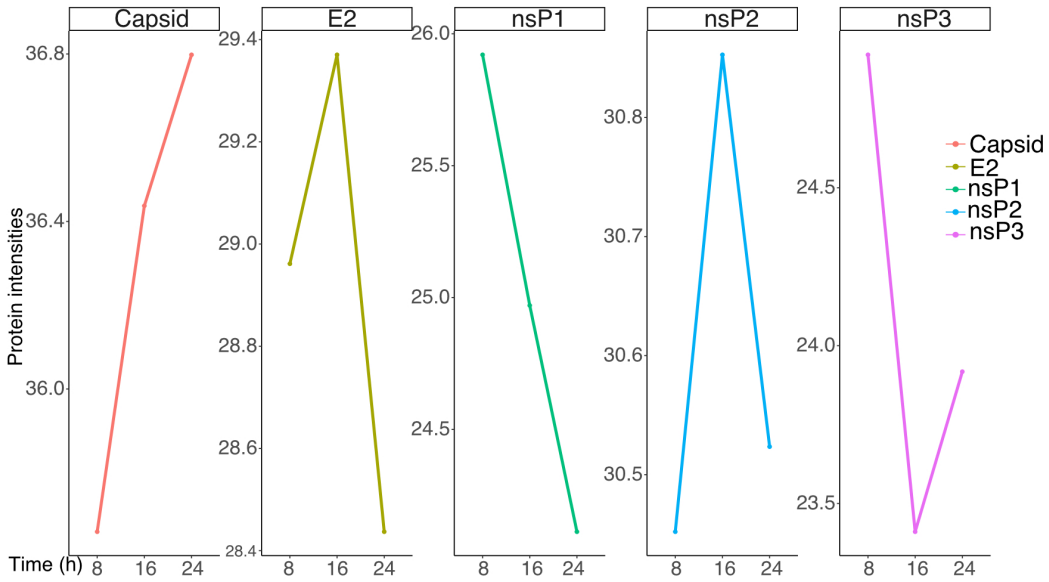

Figure 5.8: Temporal changes in viral protein intensities

Viral protein intensities obtained from normalised mass spectrometry data were plotted for 8, 16 and 24 hpi.Changes in protein intensities of viral proteins over time, showed capsid was increasing while nsP2 was decreasing. This is in line with the normal viral life cycle, where non-structural proteins are produced first, followed by structural proteins later on. The rest of the viral proteins did not follow a particular trend.

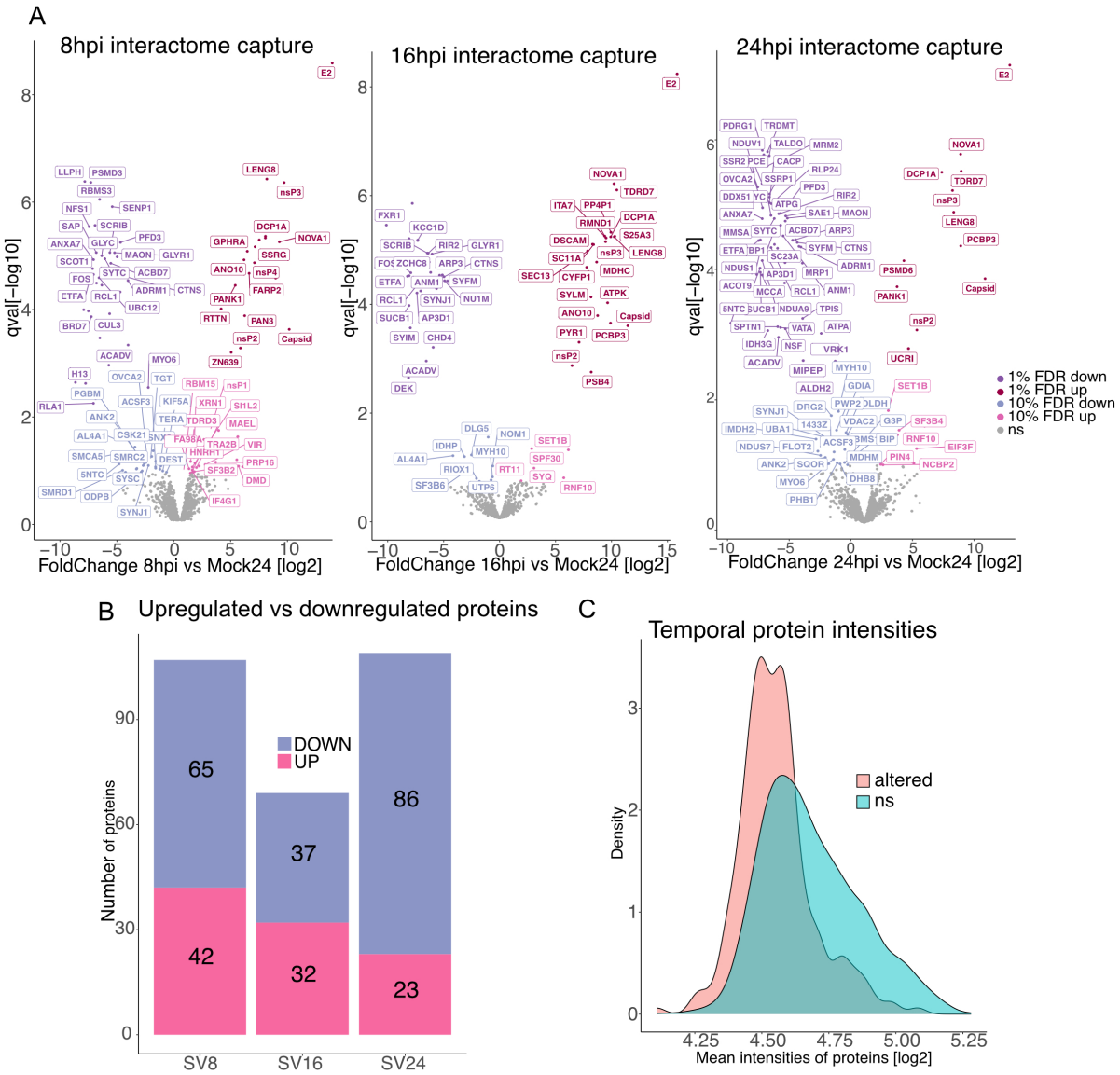

Figure 5.9: Protein abundance during SINV infection of *Ae. aegypti* cells

A) Volcano plots highlighting regulated proteins at 10% FDR (light pink upregulated, blue downregulated), and 1% FDR (Dark pink upregulated, purple downregulated) during active infection with SINV at 8, 16 and 24 hpi.

B) Bar plot showing the number of upregulated and downregulated proteins over time (8, 16, and 24 hpi) during infection with SINV. The number of upregulated proteins decreased over time, while the opposite was true for downregulated proteins, except at 16 hpi where it was lower than either 8 or 24 hpi, suggesting a possible transition between the acute and persistent phase of infection.

C) Density plot showing the distribution of significantly altered proteins (pink) vs unaltered proteins. This shows that most of the proteins were not changing.

Across time points, only 7 upregulated proteins were shared, 4 of which were viral

proteins (Fig.5.10A), while 7 were shared from the downregulated proteins (Fig.5.10B). This suggests that most responses were time-specific. Heat map and clustering analysis of shared proteins revealed three groups: two clusters that were indicative of downregulation and one that showed upregulation as the infection progressed (Fig.5.10C-D). The heat map (Fig.5.10C) and density plot (Fig.5.9C) also suggest that only very few RBPs are changed during viral infection, while the majority of proteins are unaffected (Fig.5.10C-D). This is supported by the translation shutoff experiment, where no difference in translation for the infected and non-infected was observed (Fig.5.4). Collectively, the few proteins that change exhibit pronounced temporal dynamics, characterised by rapid turnover and clear time-dependent modulation of relative abundance. (Fig.5.10C-D).

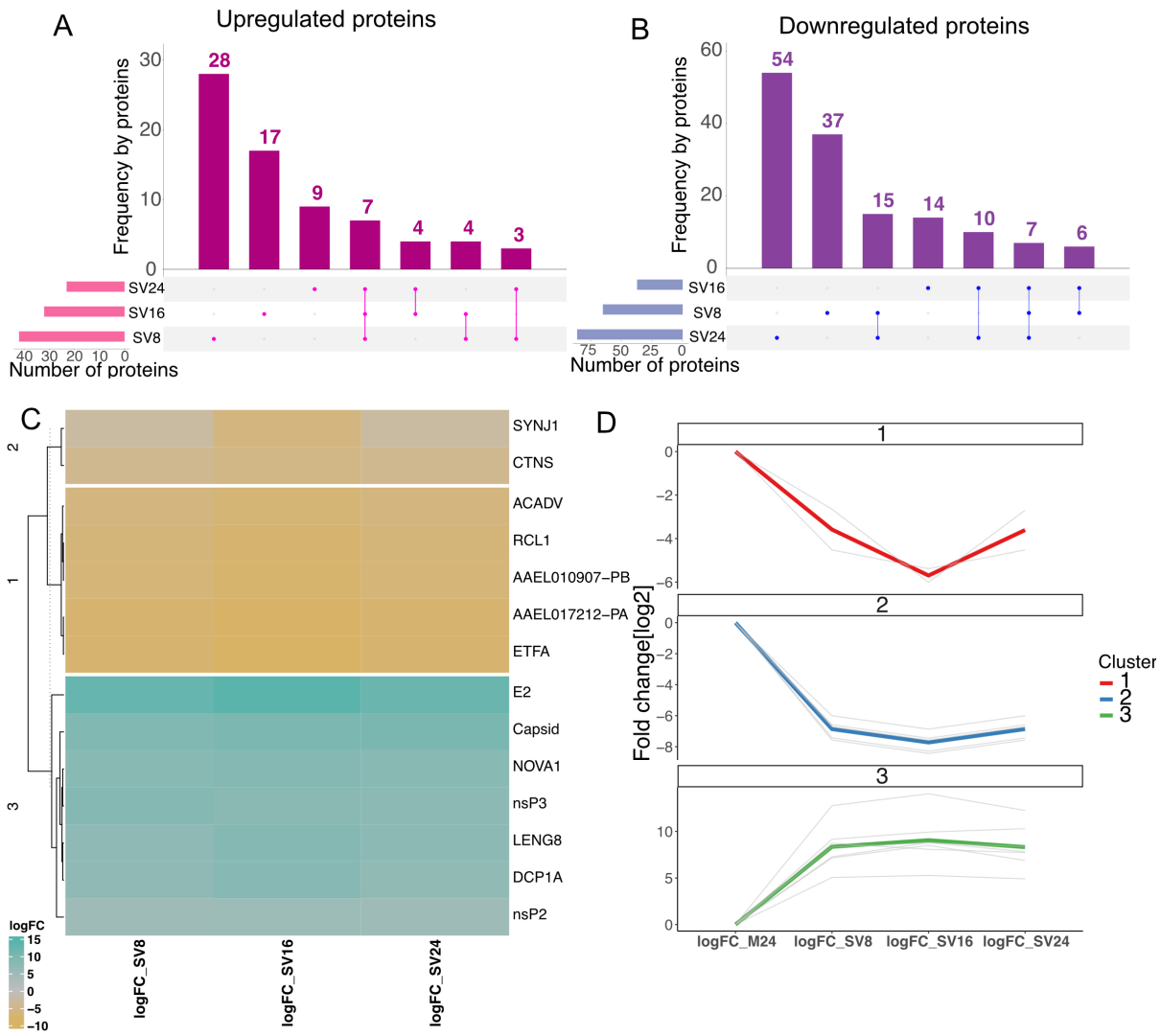

Figure 5.10: Quantitative overview of altered proteins during Sinbis infection of *Ae. aegypti* cells

A-B) Upset plots of up- and down-regulated proteins showing the degree of intersection (shared RBPs) over the course of infection. Most RBPs were regulated in a time-specific manner, with 7 upregulated and 7 downregulated proteins being shared across time points.

C) Heatmap of 14 protein groups without missing values clustered according to their abundance patterns over time,

D) Clusters of abundance profiles of 14 proteins (shared across time points) over time. Clusters 1 and 2 are declining as infection progresses, with cluster 1 increasing slightly at 24 hpi. Cluster 3 proteins increase as infection progresses. This suggests a temporal dynamic of protein regulation that is influenced by both host and virus.

Function characterisation of altered RBPs The altered RBPs were subjected to further characterisation. Firstly, gene ontology (GO) enrichment was performed using G: Profiler [195]. GO enrichment analysis revealed several categories that were altered during infection (Fig.5.11A). Among them were: RNA binding, reflecting the role of RBPs in viral replication and host defence; proton transmembrane activity, suggesting the modulation of ion transport processes that maybe necessary for maintaining homeostasis during infection; oxidoreductase activity and nucleotide bind, suggesting changes in redox metabolism and nucleotide associated processes; ligase activity, which may indicated remodelling of modification pathways, such as ubiquitination: heterocyclic binding and anion binding, were also represented, consistent with broad metabolic and structural adjustments occurring during infection.

KEGG pathway analysis further revealed that RNA degradation pathway to be upregulated, suggesting infection affects the RNA turnover mechanism. Pathways such as valine, leucine, and isoleucine degradation and biosynthesis of amino acids related to amino acid metabolism were identified. In addition, pathways central to energy metabolism, including the TCA cycle, carbon metabolism, and oxidative phosphorylation, were altered during infection, suggesting the virus also requires modulation of these resources for its survival (Fig.5.11B).

Given that RNA-binding proteins harbour an array of RNA-binding domains, both canonical and non-canonical [106], the identified RBPs were analysed for the domains they harboured. Strikingly, more than 80% harboured non-canonical domains, suggesting the involvement of unconventional RNA-binding mechanisms (Fig.5.11C).

Previous studies have demonstrated that enzymes frequently moonlight as RBPs despite lacking conventional RBDs [109, 110]. To further characterise the functional profile of the significantly altered proteins, they were classified based on their enzyme class. Approximately 25% could be assigned to six major classes: hydrolases, ligases, lyases, transferases, oxidoreductases, and isomerases (Fig.5.11D). To assess whether these RBPs were preferentially upregulated or downregulated, a forest plot of odds ratios comparing up vs downregulated RBPs was generated (Fig.5.11D).

This revealed that most classes showed an odds ratio below 1, indicating a trend towards downregulation during alphavirus infection (Fig.5.11D and Appendix. 8.4). In particular, Ligase tended toward upregulation with RBPs belonging to the class of aminoacyl-tRNA synthetases (aaRSs), which are enzymes that catalyse the attachment of specific amino acids to their corresponding tRNAs, lyase and hydrolases were more or less evenly distributed between up- and downregulated proteins, while oxidoreductases displayed strong (significant) downregulation (Fig.5.11D and Appendix. 8.4).

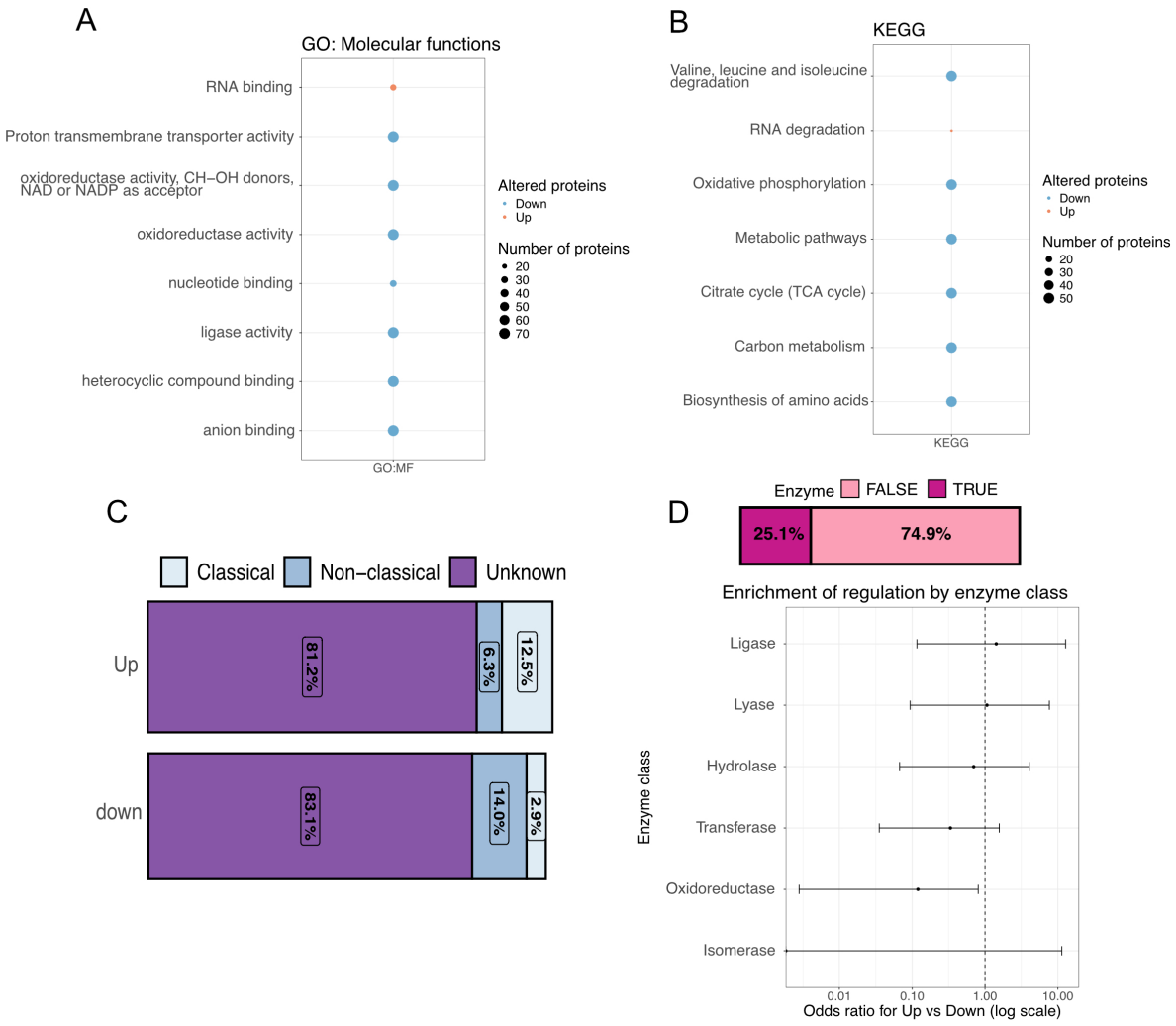

Figure 5.11: Characterisation of Altered RBDs during SINV Infection

A) Dot plot showing GO Molecular function enrichment. Most categories involved RNA processing, metabolism, and transport. The size of the dot represents the number of proteins, blue represents upregulated proteins, and orange represents downregulated proteins.

B) Dot plot of KEGG analysis pathways. This revealed pathway is involved in amino acid metabolism and energy metabolism. The size of the dot represents the number of proteins, blue represents upregulated proteins, and orange represents downregulated proteins.

C) Barplot showing classification of RBPs based on RNA-binding domains (RBDs). More than 80% significantly regulated RBPs contained non-canonical RBDs

D) Barplot showing proportion of RBPs that are enzymes (25%) and forest plot showing up- and down-regulated enzymes during infection. Odds ratios >1 represent preferential upregulation and < 1 represent preferential downregulation of proteins. Ligases tend towards upregulation (not significant), lyase and hydrolase had no bias, while oxidoreductase significantly downregulated, and transferase tends towards downregulation (not significant).

5.3 Discussion

In this chapter, three key features of infection in *Ae. aegypti* mosquito cells are highlighted. Firstly, how infection in mosquito cells alternates between acute (high rate of viral replication) and persistent (low rates of replication) phases over 18 days and with minimal effects on cell viability. Secondly, translation dynamics in human and mosquito cells during infection are vastly different. In human cells, total translation shut-off is observed, while in mosquito cells, translation proceeded as normal. Thirdly, using proteomics, 215 mosquito RNA-binding proteins were remodelled during an arboviral infection. These RBPs exhibited time-specific RBPs, RNA-binding activity that was evident from the GO term and KEGG analysis; RBPs with unconventional RNA-binding domains were the most abundant, of which over 25% were enzymes. Overall, this chapter shows that viral replication in mosquitoes is biphasic, going through periods of high and low viral replication; mosquitoes can overcome virus-induced stress and therefore do not exhibit translation shutoff; and the repertoire of RBPs during infection is altered.

5.3.1 Alphavirus infection dynamics in mosquito cells

The findings show that SINV infection in Aag2-AF5 cells follows a biphasic course characterised by an acute replication phase that eventually establishes persistence. Of note, this transition occurred with minimal loss of cell viability, despite the continuous detection of viral RNA. This contrasts with vertebrate cells, where virus infection results in cytopathic effect [189]. Similar biphasic dynamics have been reported in mosquitoes infected with alphavirus such as SINV and CHIKV, where the infection eventually stabilised into persistence, which allows for long-term viral maintenance with no debilitating effects to the host [196, 197]. This difference reflects distinct evolutionary pressures acting on arborviruses in their vertebrate and mosquito hosts. In vertebrates, the virus encounters strong innate immune responses, particularly the interferon-mediated pathways, where recognition of viral RNA by host pattern recognition receptors such as RIG-I, MDA5, and TLRs induces type I interferons and downstream expression of interferon-stimulated genes (ISGs). To evade this host

response, alphaviruses have evolved immune evasion strategies that shut down host transcription and translation. Viral nsP2 degrades RNA polymerase II and halts host mRNA synthesis, while repurposing host translation machinery for its replication [196]. By contrast, mosquitoes' antiviral defence relies heavily on RNA interference (RNAi), which regulates but does not clear the infection. As a result, tolerance has been established between the alphavirus and mosquito that allows for sustained levels of virus replication [170, 198].

In the time-course analysis, viral genomic RNA levels peaked at day 2 and declined approximately fivefold by day 6, whereas subgenomic mRNA reached its maximum at day 1, declined about fifteenfold by day 6, and then stabilised. This expression pattern is consistent with the canonical alphavirus replication cycle, in which genomic RNA is first translated to produce the nonstructural polyproteins (nsP1–4) that drive RNA synthesis, followed by the generation of subgenomic RNA encoding the structural proteins required for virion assembly [43,199]. Importantly, the decline and subsequent stabilisation of viral RNA coincided with viral titre plateauing at relatively low levels, providing a strong argument for the establishment of persistence in Aag2-AF5 cells. Together, mosquitoes exhibit a biphasic mode of infection, characterised by an initial acute phase followed by persistence. This adaptive co-evolution between the mosquito and virus enables tolerance, ensuring mosquito survival and long-term transmission potential.

5.3.2 Translation shut-off or tolerance as a coping mechanism

Protein synthesis in vertebrates and mosquitoes is strikingly different during infection. In vertebrate cells, alphaviruses induce profound transcriptional and translational shut-off. This process is primarily mediated by the viral nonstructural protein 2 (nsP2), which translocates into the nucleus and promotes the degradation of the largest subunit of RNA polymerase II (RPB1), thereby preventing host mRNA synthesis [196, 200–202]. In addition, the inhibition of translation is induced by the induction of protein kinase R (PKR) by dsRNA viral RNA. The binding of PKR to dsRNA leads to conformation changes that result in autophosphorylation of PKR, which subsequently

phosphorylates eIF2α. Phosphorylation of eIF2α blocks the binding of GTP to intiate MET-tRNA to start translation. As a result, global cap-dependent translation initiation is shut off [196, 203]. This results in the collapse of host protein synthesis, while translation of viral RNA progresses due to structural differences in the viral subgenomic RNA that enable ribosomes to bypass this inhibitory pathway [204]. The HEK cells infection experiment confirmed this phenomenon by showing a single protein viral band (capsid) on the nitrocellulose membrane, indicative of host translational shut-off. This reflects the virus strategy to maximize production of viral proteins while crippling the mammalian host antiviral defense [205].

In contrast, mosquito Aag2-AF5 cells did not exhibit translation shut-off upon SINV infection. Labelling of metabolic proteins showed indistinguishable protein profiles between the infected and uninfected. This indicates mosquito global translation is unaffected even as viral proteins are being produced. Mechanistically, this suggests that mosquito immune defence is fundamentally different from mammals. Pathways such as the PKR sensing of dsRNA may be absent or function differently [150, 201]. The mosquito antiviral strategy, RNAi, employs viral degradation rather than shutting down host translation, which ensures viral production is controlled while global translation is unhampered [196, 206–209]. Taken together, this highlights the central theme of arbovirus biology. Alphaviruses induce strong shut-off in vertebrate hosts to evade antiviral defences, whereas in mosquitoes, infection proceeds in a translation-permissive state without compromising the host. To achieve this arboviruses co-opt host factors such as RBPs; thus, understanding host-virus interaction is crucial for identifying targets that could potentially control the spread of alphaviruses.

5.3.3 Proteomic remodelling of RBPs in *Ae. aegypti* cells (Aag2-AF5) during an alpha virus infection

Given that SINV infection in mosquito cells does not obliterate host biosynthesis, shows thatRBPs could be used to foster a tolerance state of infection among other mechanisms, such as the RNAi pathway. Using RIC, identified 1556 RPBs with only 215 being significantly altered in at least one of the time points, 8, 16, and 24 hpi. This

suggests that the global landscape of RBPs remains largely unaltered during SINV infection. Viral proteins (nsP1-4, capsid, E2) were among the 72 RBPs that were upregulated, and 143 RBPs were downregulated over time, indicating that infection in mosquitoes moves towards suppression as infection progresses. The highest numbers of changes were observed at 8 and 24 hpi, with fewer alterations at 16 hpi, suggesting a translational phase between the acute and persistent phases of infection. A similar pattern has been observed in CHIKV infection of *Ae. aegypti* cells, which induced relatively few proteomic changes at early time points but had a marked increase of altered proteins at 36 hpi, an indication of host progressive remodelling RPBs during infection [210].

This study also aligns with proteome-wide studies in virus-induced RBPome changes. In mammalian cells, SINV infection resulted in a similar scale of altered proteins during infection, 247 RBPs [101]. Changes in the RBPome were mainly driven by loss of cellular RNA and emergence of viral RNA, due to host transcriptional shut-off and increased viral transcripts. Indeed, Garcia-Meoreno *et al.* identified key regulators such as XRN1, an exonuclease that localises with viral particles and promotes SINV infection, and GEMINI5, a small nucleolar ribonucleoprotein that acts as a negative regulator of viral gene expression [101]. Hydrolases, e.g., XRN1, were uniquely identified at 8 hpi in the proteomics data, suggesting a similar role in promoting viral infection, however, transiently. This indicates that the host or virus reconfigures RBPs based on their needs, albeit with different outcomes. In mammals, a lytic infection is observed, while in mosquitoes, it is nonlytic, leading to persistence.

The proteomic data also captured the temporal dynamics of viral proteins. However, they were consistently changing during the course of infection. In particular, nsP1 decreased with time while capsid increased over time, conforming to typical alphavirus replication where nonstructural polyproteins (nsP1-4) are translated immediately to form the replicase complex, while structural proteins are produced later on during infection [197]. This detection of viral proteins in the RBPome confirms that these proteins are inherently associated with viral genomic and subgenomic RNA during infection, thus emphasising their role as central RNA binding hubs that coordinate

replication and transcription of the viral genomes [43, 46]. RPBs that co-purify with viral proteins are therefore potential cofactors of viral replication. [148].

Notably, several host RBPs altered at all time points may represent key factors in the mosquito response to infection. Among those consistently upregulated were NOVA1, DCP1A, and LENG8, proteins associated with RNA metabolism and processing. For example, DCPIA is a core activator of the mRNA decapping complex usually associated with XRN1. XRN1 has been shown to be viral dependency factors in mammalian cells favouring viral replication, often colocalising with viral particles and providing free nucleotides from the degradation often host cellular mRNA [101, 211]. In contrast, consistently downregulated proteins included ACADV, CTNS, SYNJ1, and RCL; however, their association with infection is not known. For example, ACADV is an acyl-CoA dehydrogenase involved in fatty acid metabolism and is likely to provide energy; however, the host likely regulates its production to control viral replication [212].

Overall, these findings demonstrate that SINV virus infection triggers progressive and selective remodelling of the mosquito RNA-binding proteome, with early upregulation of supportive factors giving way to later host-driven suppression, consistent with the establishment of persistence.

5.3.4 Function and pathway analysis of altered RBPs

Viral replication is an energy-intensive process and could explain why processes such as the TCA cycle, carbon metabolism, oxidoreductase activity, and oxidative phosphorylation appear among the GO and KEGG terms. To meet their replication needs, viruses must reprogram host cell metabolism. One pathway that viruses frequently exploit is oxidative phosphorylation, a mitochondrial process that generates ATP through electron transport and proton gradient formation. This modulation ensures a steady supply of energy required for replication [213]. In mammalian systems, modulation of mitochondrial function during SINV infection has been shown to be a necessary mechanism to drive viral replication [214]. A direct consequence

of increased oxidative phosphorylation is the generation of reactive oxygen species (ROS). Moderate ROS levels can be proviral by activating transcription factors such as NF-κB, which support viral replication. However, excessive ROS is detrimental, leading to host cell damage [189]. NF-kB is a nuclear transcription factor often activated by viral dsRNA translocating to the nucleus and upregulating proinflammatory cytokines, chemokines, and adhesion molecules that strengthen the host's innate defence against viruses. However, in mammals, viruses have evolved strategies to hijack NF-kB, usually by harbouring NF-kB binding sites that induce transcription factors indirectly through host-produced pro-inflammatory chemokines or directly by viral products, resulting in the trans-activation of kB containing viral promoter that enhances viral transcription [215].

Conversely, in mosquitoes, arboviruses adopt a more balanced strategy. Cappuccio and colleagues showed that SINV infection in *Ae. albopictus* cells leads to metabolic adjustments that favour persistence rather than the extreme alterations that are detrimental to the host, usually by controlling oxidative activity to maintain moderate oxidative stress [189]. This is likely why downregulation of oxidative and energy pathways is observed, providing an environment where the virus can replicate at controlled levels. At the same time, the mosquito host tolerates infection without adverse effects. This balance is likely what enables mosquitoes to maintain lifelong infections that facilitate viral transmission while remaining unaffected themselves.

5.3.5 Characterisation of RNA-binding domains

Further analysis of the altered RBPs revealed that approximately 80% lacked canonical RNA-binding domains (RBDs). This observation agrees with global interactome capture studies, where a significant fraction of RBPs were found to lack canonical domains but could still bind RNA through low complexity regions or enzyme active sites [109, 110, 122]. Such non-canonical RBPs often emerge as regulators of RNA stability, translation, or localisation during viral infection [131]. Their enrichment in our dataset suggests that SINV recruits a broad spectrum of host proteins, many of which are not traditionally annotated as RBPs, to facilitate or modulate infection in

mosquitoes.

Classification of RBPs by function revealed 25% of the altered RBPs to be enzymes. Representation of metabolic enzymes among RPBs underscores the dual functionality of many proteins at the intersection of metabolism and RNA regulation. Dehydrogenases such as ALDH2 were identified, linked with reducing oxidative stress in HBV infection [216], CTBP1 in redox sensing in adenovirus infections [217], and G3P/GAPDH glycolytic enzyme. This enzyme has been shown to have dual activity: as an enzyme catalysing the conversion of Glyceradehyde 3 phosphate to 1,3 bisphosphoglycerate with concomitant NADH production; as an RBP where it has been reported to bind mRNA, tRNA and viral RNA [110]. A notable example is its role within the IFNγ-activated GAIT complex, where GAPDH, together with EPRS, SNCRIP/hnRNPQ and ribosomal proteins L3a, regulate selective translation of inflammatory mRNAs in myeloid cells [218]. GAPDH also bind AU-rich element (AREs) in 3' UTRs through its N-terminal Rossmann fold, a domain that also binds NAD^+/NADH. Competition between these dinucleotides and RNA suggests a molecular mechanism for switching between enzymatic and RNA-regulatory roles [110]. Viruses have been shown to exploit the moonlighting activity of GAPDH. For example, in human parainfluenza virus type 3 (HPIV3), GAPDH was found to co-localise with viral RNPs in the perinuclear region and regulate HPIV3 infection [219]. GAPDH has been implicated as inhibitor of coronaviruses as it acts as a negative transcriptional regulator of AT1R (angiotensin II receptor 1) thus preventing their entry as they cannot bind angiotesin converting enzyme 2 (ACE2) [220]. The presence of these enzyme-RBPs in mosquito cells suggests that SINV may co-opt metabolic proteins to stabilise viral RNA, promote translation, or remodel host energy flux. Indeed, the concurrent downregulation of major metabolic pathways in our KEGG analysis suggests that some enzymes may be diverted from their canonical functions into RNA-binding roles during infection.

The dominance of non-canonical and enzymatic RBPs among the altered proteins in the dataset indicates that the mosquito RBPome undergoes substantial functional diversification during SINV infection. Rather than relying solely on classical RBPs,

the virus appears to exploit multifunctional proteins that link RNA metabolism to energy production and stress responses. This broadening of the RNA-binding landscape may be critical for maintaining infection without overwhelming the host cell, thereby supporting the long-term persistence that characterises arbovirus–mosquito interactions.

5.4 Limitations and future directions

A key limitation of the study is that cRIC has a bias towards protein abundance, size, and the physicochemical properties of their tryptic peptide sequences; thus, RBPs lacking these features may be poorly enriched. Although cRIC initiates the capture of protein-linked to RNA at zero distance and is therefore highly specific, this comes at the cost of missing proteins that are not in close proximity to RNA. In this regard, methods that use formaldehyde have an advantage. On the specificity spectrum, cRIC also enriches for poly(A)-bound proteins. This was not a concern in the experiment, as SINV is a polyadenylated virus; however, one must consider study design carefully when working with non-poly(A) viruses, where alternative methods such as probe-based approaches may be more suitable. It is also important to note that cRIC does not capture transient changes, and thus some proteins may be missed depending on timing. In this study, multiple time points were selected for harvesting to mitigate this.

5.4.1 Conclusion

SINV establishes a persistent infection in *Aedes* cells, with canonical replication dynamics, preserved translation, and selective proteomic remodelling. Host responses favoured RNA-binding enrichment and RNA degradation, while metabolic suppression aligned with transition to persistence. The dominance of non-canonical and enzymatic RBPs highlights previously unappreciated layers of virus–host interaction. Together, these findings support the model that mosquitoes strike an evolutionary balance with arboviruses, enabling lifelong transmission while avoiding cytopathology. In the next chapter, knockdown of the altered proteins will be performed to observe what effects

they have on SINV yield.

6 RNAi gene mediated silencing on *Ae. aegypti* RBPs regulated during SINV infection

6.1 Introduction

RNA viruses are obligate intracellular parasites that rely heavily on host factors throughout their life cycle, from replication to packing [221]. As mentioned earlier, RNA-binding proteins (RBPs) are critical regulators of RNA metabolism, influencing RNA stability, localisation, translation, and decay, and are frequently co-opted by viruses to promote infection or antagonised as part of host defence response [101,102, 222]. In mammalian systems, RBPs such as G3BP1 and G3BP2 support alphaviruses by scaffolding replication complexes [204], Cyclophilin A is also recruited during SINV infection to promote viral replication [101], hnRNP1 K and PCBP1 regulate translation and RNA stability during picornavirus infection [223]. In contrast, other RBPs have antiviral activity, for example, ZAP restrict alphaviruses by targeting CpG-enriched viral RNA for degradation [224].

The knowledge we have on RBPs and their implications in mosquito infection is limited. Argonaute-2 (AGO2) and DICER-2 (Dcr-2) are well-studied RBPs that are central to the RNA interference (RNAi) pathway, which plays a key antiviral role in mosquitoes [225–228]. Unlike in vertebrates, which rely heavily on interferon induction, mosquitoes use RNAi to control viral infection. Central to this pathway is the recognition of dsRNA, an obligatory intermediate of viral replication. In siRNA pathway, the dsRNA is cleaved by Dcr-2 into 21 nt, which is then loaded into the RNA-induced silencing complex (RISC). Here AGO2 serves as a catalytic silencer by guided base pairing of viral RNA for degradation. Beyond siRNA, miRNA that targets viral RNA employs Drosha and Pasha to cleave dsRNA to about 70 nt before being introduced to the siRNA pathway. piRNA is also another pathway, where the generation of virus derived RNAs are sent for degradation. Other RBPs implicated in mosquito infection, such as loquacious and Sec61 A1, have been shown to promote DENV infection [229]. These demonstrate that RBPs can work for or against viral replication, and their functions in infection require

characterisation, especially in arthropod vectors, where little is known about RBPs.

Building on the previous chapter, where cRIC was employed to map the RBP landscape during SINV infection, 215 RBPs were identified that had altered RNA-activity. While this highlights widespread regulation of host RBPs, it does not reveal their specific role in viral infection. To address this gap, RNAi offers a powerful strategy to probe for function.

RNAi is a naturally occurring defence mechanism against foreign genetic material that is widely exploited as a molecular tool for loss of function studies by post-transcriptional gene silencing [230–233]. Introduction of long double-stranded RNA (dsRNA) into cells (typically 300-600 nucleotides long) triggers the RNAi pathway, initiating the degradation of complementary transcripts [73, 234, 235]. Other techniques employing different RNAi architectures, usually 21-24 nucleotides, such as siRNA and short hairpin RNA (shRNA), can be used to trigger the RNA pathway [231, 236].

The successful use of RNAi in loss of function studies has been carried out in arthropods, including mosquitoes [72, 227, 237–239]. More recently, RNAi-based approaches have gained recognition as potential pest control strategies owing to their high specificity [240–242].

In this chapter, dsRNA-mediated silencing was employed on candidate RBPs identified in the previous chapter to assess their impact on SINV infection.

6.2 Results

6.2.1 Selection and synthesis of knockdown screens

As described in Chapter 5, proteomic analysis revealed that RNA-binding proteins (RBPs) are differentially regulated in response to viral infection. The responses observed were highly time-specific, with minimal overlap of regulated RBPs across time points. To investigate whether these RBPs impact viral replication, 17 candidate proteins were selected for a small-scale target screen.

Candidate RBPs were selected based on the following criteria:

1. **RBPs regulated during the persistent phase of infection**. Proteins upregulated at 24 hours post-infection were chosen as this time point represents the beginning of the persistent phase. These proteins are thus expected to be involved in tolerance mechanisms. From this dataset, only RBPs that were significantly upregulated were considered. Among these, several were also consistently detected at earlier time points: four proteins were shared between 16 hpi and 24 hpi, while three were shared between 8 hpi and 24 hpi. Proteins with consistent kinetics were prioritised, as their detection relies on two or more experimental points (Fig6.1A).

2. **Known RNAi activity**. DICER2 (Dcr-2) and argonaute-2 (AGO2) were included as positive controls, since they are core components of the siRNA pathway and are well established as antiviral effectors in mosquitoes [243], despite not being significantly enriched in the dataset.

3. **Literature**. In addition, DHX15 was selected, informed by previous studies that reported their antiviral activity in mosquitoes during DENV and CHIKV infection [169] , as well as TOP3B as it showed a phenotype in tick cells infected with uukunyemi virus [168]. Although not detected in the cRIC dataset, they could act as a reference point for antiviral activity across viral species.

Together, these criteria allowed the inclusion of both proteomics-identified candidates and well-characterised RBPs with known or putative antiviral roles, providing a set of

proteins for functional validation.

To generate knockdown screens, dsRNA constructs targeting 400 to 600 bp regions of each gene were designed using Snapdragon [151] and incorporating the T7 promoter sequence. Using the MEGAscript RNAi kit as per the manufacturer's instructions, dsRNAs were generated. Briefly, cDNA templates containing the T7 promoter sequence were synthesised to generate dsRNA, followed by enzymatic digestion with an RNase and a DNase to remove DNA and single-stranded RNA (ssRNA). Purification of dsRNA using spin columns was performed to remove proteins, free nucleotides, and degraded dsRNA products. Upon transfection of dsRNA and infection, RT-qPCR was used to assess their knockdown (KD) efficiency and impact on viral replication (Fig.6.1B).

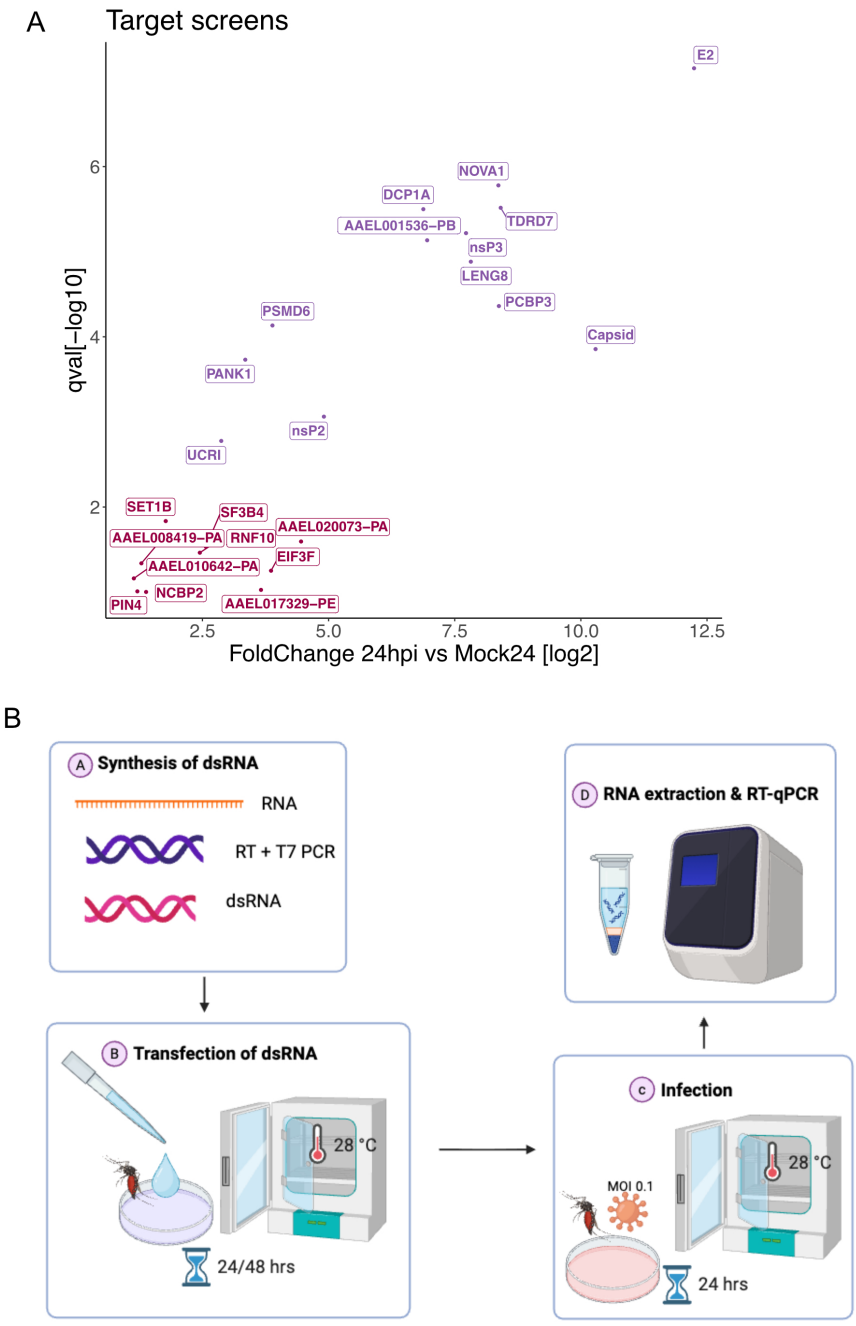

Figure 6.1: Target RNAi screens and Workflow of Knockdown (KD) synthesis

A) Candidate RBPs were selected based on proteomics at 24 hpi, representing the persistent phase of infection. Upregulated proteins shared across earlier time points were prioritised, alongside inclusion of AGO2 and Dcr2 (RNAi controls) and DHX15 and TOP3B, previously reported with antiviral activity. Purple represents proteins at 1% FDR, while pink represents proteins at 10% FDR. FDR - False discovery rate.

B) Schematic workflow of the RNAi screens, from synthesis of dsRNA, transfection and infection, and finally determination of regulatory activity by RT-qPCR.

6.2.2 Optimising RBP knockdown in mosquitoes

dsRNA can be introduced into cells directly or by the use of transfection reagents. However, because dsRNA stability is often affected by RNases and changes in pH, carrier systems are required to ensure effective cellular delivery [244]. To develop a protocol for efficient transfection in *Ae. aegypti* Aag2-AF5 cells, Two commercial transfection reagents were compared: Lipofectamine 3000 (Invitrogen), a lipid-based transfection reagent, and XtremeGENE 360 (ROCHE), a non-liposomal formulation. Transfections were performed with 100, 200, and 300 ng dsRNA targeting AGO2, DHX15, and SINV, with dsEGFP included as a non-targeting control. Each condition was performed in biological triplicate, using 24-well plates seeded with 5.0×10^5 cells/mL and left for two days to achieve confluency.

KD efficiency was determined by RT-qPCR, with Ct values normalised to a housekeeping gene (actin) (ΔCt) and fold-change calculated using the $\Delta\Delta$Ct method relative to dsEGFP. Results are presented as mean $\pm$ SD, and a pairwise t-test was used to determine significance (p-value $<$ 0.05). Across all conditions, XtremeGENE 360 consistently outperformed Lipofectamine 3000 (Fig.6.2A-B). XtremeGENE 360 achieved $>$75% KD at 100 ng, whereas Lipofectamine 300 required 300 ng to reach comparable efficacy (Fig.6.2A-B). Notably, AGO2 KD failed in lipofectamine-treated cells, with Ct values $>$29 (Appendix. 8.2) and the sample was excluded from the lipofectamine analysis. These results established that XtremeGENE 360 is a more efficient transfection reagent than Lipofectamine 3000, achieving robust knockdown at lower dsRNA concentrations.

To evaluate the functional consequences of KD, cells were subsequently infected with SINV at an MOI of 0.1 for 24 hours, and RT-qPCR was performed to quantify viral RNA levels. Using XtremeGENE 360, silencing AGO2 led to an increase in viral replication, even at moderate KD efficiency (55%), confirming AGO2's strong antiviral role in mosquitoes as a component of RNAi (Fig.6.2C and Appendix. 8.1). DHX15 displayed a KD efficiency-dependent effect: strong KD ($>$85%) reduced viral replication, whereas partial KD (76%) produced the opposite effect, suggesting the

incomplete silencing may disrupt normal antiviral signalling. A similar trend was observed with Lipofectamine 3000, though KD efficiencies were lower (Fig.6.2D and Appendix. 8.1). In all cases, an increase in viral replication did not exceed 0.5-fold relative to the dsEGFP baseline, indicating modest effects (Fig.6.2C-D). As expected, SINV-targeting dsRNA produced consistent viral suppression across both reagents, with the extent of effect on virus to proportional to KD efficiency (Fig.6.2C-D). It was also evident that an increase in transfection reagent influenced viral replication, especially that of DHX15 (Fig.6.2C-D). These results show that KD efficiency and transfection reagents impact viral replication, reinforcing the importance of standardising both reagent and concentration for reliable interpretation (Fig.6.2A-D).

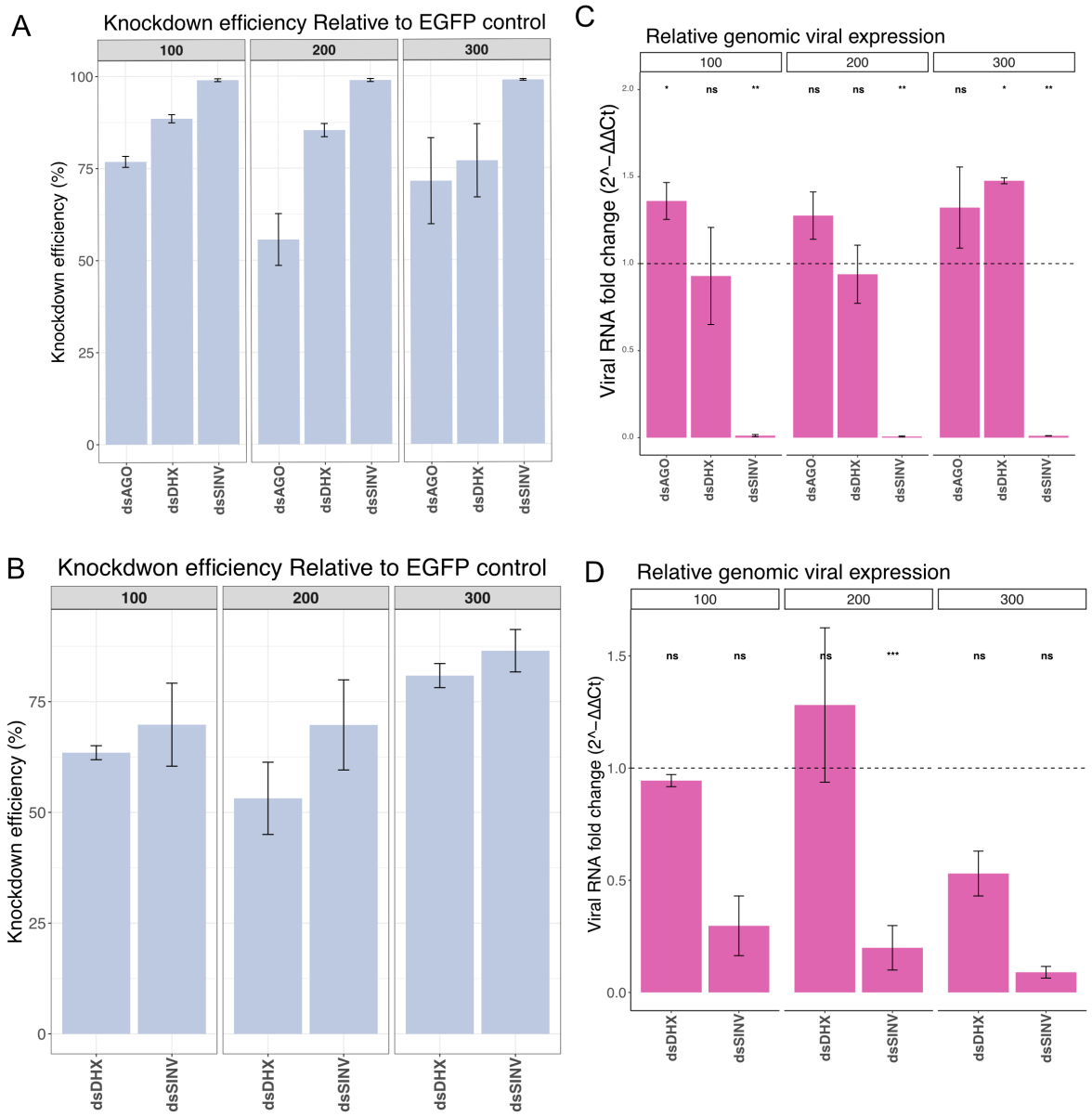

Figure 6.2: Optimisation of knockdown (KD) screens

A-B) Bar plot showing knockdown (KD) efficiency by RT-qPCR after silencing of indicated targets at different concentrations of dsRNA using XtremeGENE 360 and Lipofectamine 3000, respectively, with mean and SD error bars plotted.

C-D) Quantification of genomic SINV RNA levels by RT-qPCR after silencing of the indicated genes in Aag2-AF5 cells at different concentrations of dsRNA using XtremeGENE 360 and Lipofectamine 3000, respectively. The 1-fold point on the linear scale is indicated by the dashed line, which represents the baseline, dsEGFP. Paired t-test of eGFP and target was calculated with P < 0.001, ***, P ,0.05, **, and P < 0.1, *, and not significant (ns) indicated.

6.2.3 Impact of RBP knockdown on SINV replication

Having established optimal conditions for the RNAi screens (use of XtremeGENE 360 and 100 ng of dsRNA), The role of 17 candidates RBPs were investigate during SINV infection. Aag2-AF5 cells were transfected with dsRNA targeting individual candidates for either 24 or 48 hours prior to 24-hour infection (24 hpi) with SINV at an MOI of 0.1. Each experiment was performed in triplicate, and KD efficiency as well as viral RNA levels were quantified as detailed above. The choice of transfection duration is a critical parameter, as it allows not only the induction of the RNAi silencing complex and degradation of mRNA targets, but also sufficient time for existing proteins to undergo turnover, enabling the knockdown effect to manifest at the protein level before viral challenge.

To address this, firstly, 24-hour transfection (24 hpt) of Aag2-AF5 cells was assessed prior to infection. It was observed that at least 14 of the 20 targets achieved a KD efficiency of at least 50%, with two targets below 25% KD efficiency, and with one (SF3B4) failing (Fig.6.3A), indicating that RNAi induction was generally effective. Next, the impact of these KD efficiencies on viral genomic RNA levels was examined. Except for SF3B4 whose KD failed, AGO-2, Drc2, AAEL008419, AAEL010642, AAEL020073, PCBP3, PSMD6, and RNF10 showed increased viral genomic RNA levels upon their depletion, consistent with antiviral activity (Fig.6.3B). Conversely, KDs of AAEL001536, EIF3F, LENG8, PANK1, SET1B, TDRD7, UCRI, and XRN1 resulted in a decrease of viral RNA levels, an indication of their "proviral" activity (Fig.6.3B). However, the decrease was very subtle and non-significant, and below 0.5 fold change relative to dsEGFP. TOP3B KD achieved 85% efficiency but did not affect viral RNA levels (Fig.6.3A-B and Appendix. 8.3).

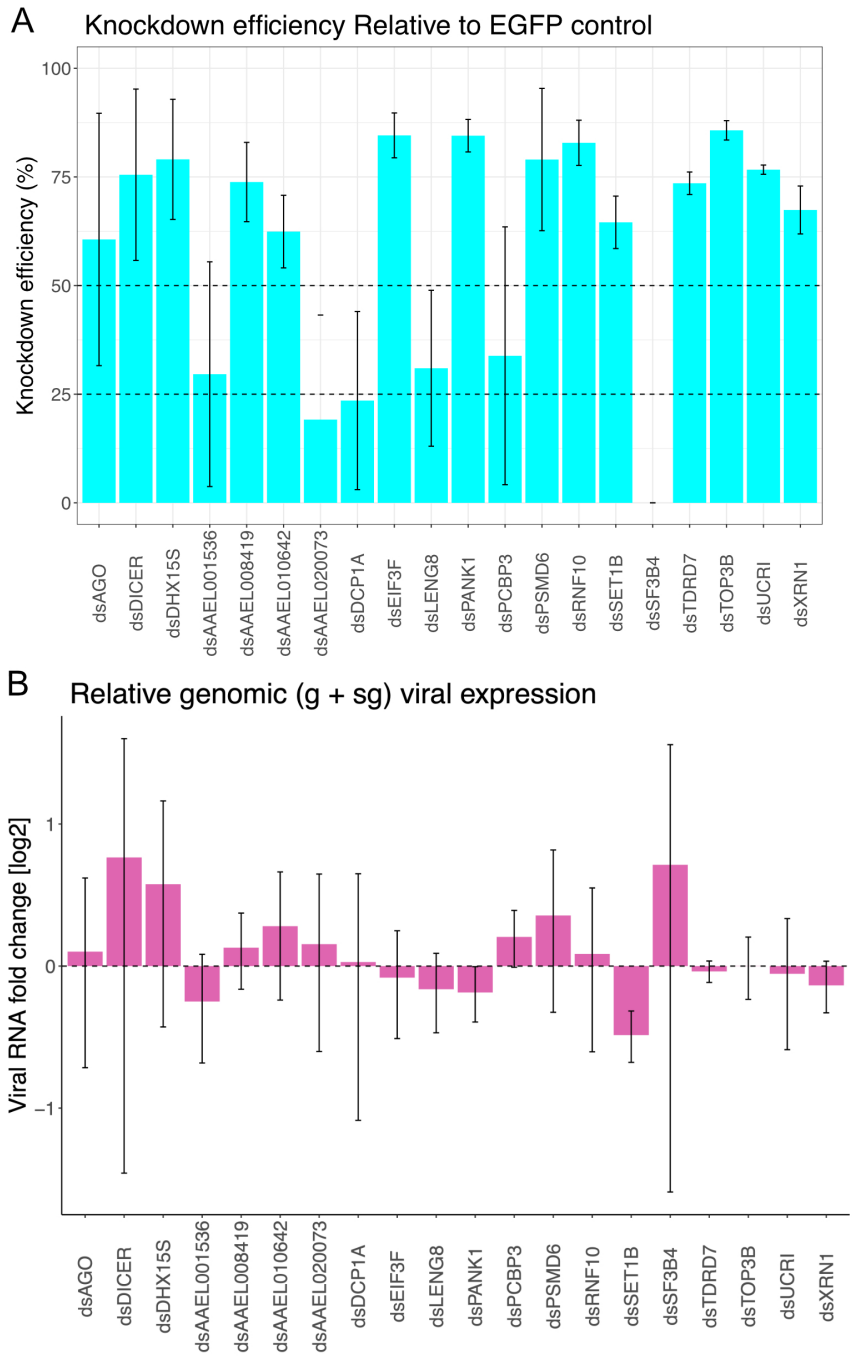

Figure 6.3: Targets RNAi screen and their impact on SINV infection 24 hpt

A) Barplot showing knockdown (KD) efficiency by RT-qPCR after silencing of indicated targets. The 25% and 50% points on the linear scale indicate 25% and 50% KD efficiency. Each target was done in triplicate and with mean and SD error bars plotted. B) Quantification of genomic SINV RNA levels by RT-qPCR after silencing of the indicated genes in Aag2-AF5 cells across the datasets. The 1-fold point on the linear scale is indicated by the dashed line, which represents the baseline, dsEGFP. Each target was tested in triplicate relative to eGFP, and the mean and SD were plotted.

NB: Table in Appendix 8.3 shows proviral and antiviral RBPs with significant values indicated.

Secondly, Transfection at 48 hours was assessed prior to infection using two independent biological replicate sets. KD efficiencies were comparable to the 24 hpt condition in at least one of the sets, 15 of 20 RBPs tested achieving at least 25% KD. SF3B4 failed in one of the sets (also failed in the 24 hpt), LENG8 and XRN1 showed poor silencing in one of the sets, below 10% (Fig.6.4).

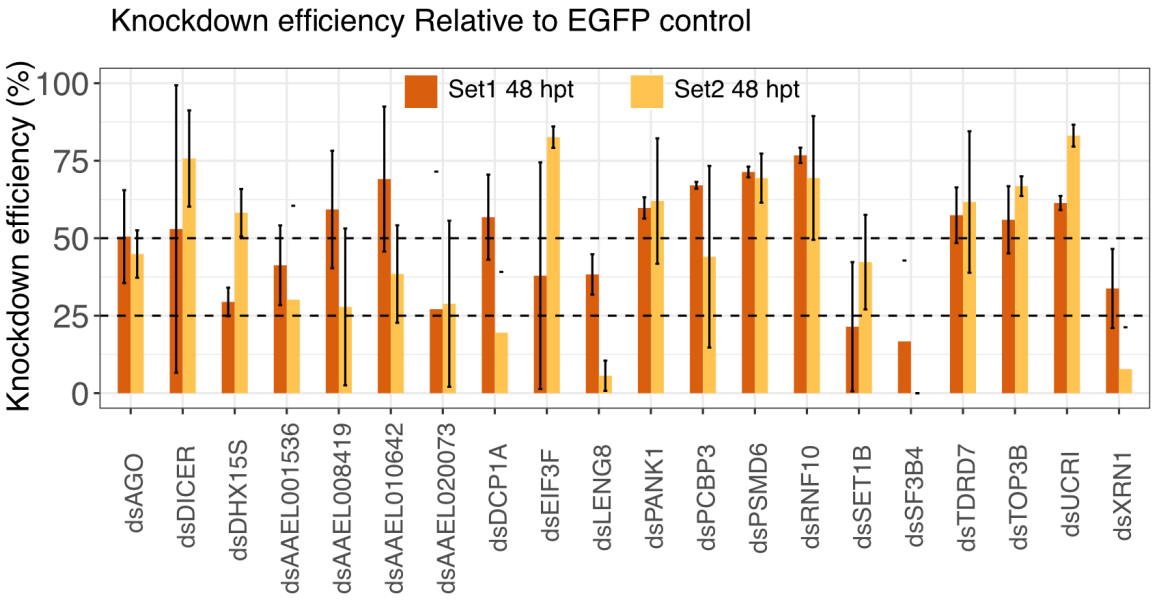

Figure 6.4: KD efficiency 48 hpt

Barplot showing knockdown (KD) efficiency by RT-qPCR after silencing of indicated targets. The 25% and 50% points on the linear scale indicate 25% and 50% KD efficiency. The error bars represent the mean and SD of triplicated sample tested.

Analysis of viral RNA levels revealed that KD of most RBPs reduced both genomic and subgenomic RNA (Fig.6.5A-B and table in appendix 8.3). Specifically, genomic RNA was reduced following KD of AAEL001536, AAEL020073, DCP1A, PCBP3, PSMD6, TDRD7 and UCRI, suggesting their proviral activity (Fig.6.5A). Interestingly, AAEL020073, PCBP3, and PSMD6 did not replicate the 24 hpt trends despite them having similar KD efficiencies, suggesting they may require a longer time post-transfection to observe the effects of the RBP depletion (Fig.6.5A, and 6.3A-B). KD of LENG8 and XRN1 also showed a decrease in mRNA levels at >25% KD, consistent with proviral activity, though variability between replicate sets indicated sensitivity to KD efficiency (Fig. 6.4 and 6.5A).

AGO2 and Dcr2 showed little to no inhibition of viral replication at KD efficiencies $\leq$50%, whereas at 24 hpt antiviral activity was observed once KD exceeded 55%, indicating a KD efficiency–dependent effect or possible recovery of the RNAi pathway (Fig. 6.4 and 6.5A, and 6.3A-B). EIF3F and SET1B displayed KD efficiency–dependent effects, acting as proviral factors only when KD exceeded 40%, which was consistent with observations at 24 hpt (Fig.6.5A, and 6.3A-B).PANK1 and TOP3B showed both decreases and increases in mRNA levels; however, these changes did not correlate with KD efficiency, suggesting they likely reflect experimental variability rather than a true KD effect (Fig.6.5A, and 6.3A-B). In contrast, DHX15 and AAEL010642 showed increased viral replication, which is consistent with what was observed at 24 hpt (Fig.6.5A and 6.3A-B). These results reinforce the idea that these are antiviral factors.

Subgenomic RNA levels consistently mirrored genomic RNA for most KDs. Notably, DHX15 KD increased subgenomic RNA, while Dcr2, PCBP2, RNF10, SET1B, and TOP3B showed inconsistent patterns (Fig.6.5B). However, variability between replicates was high, and further investigation is required to draw a conclusion. Together, the 48 hpt data support that most RBPs tested are proviral dependency factors for SINV replication, while also highlighting the influence of KD efficiency and the depletion time frame on the observed outcomes.

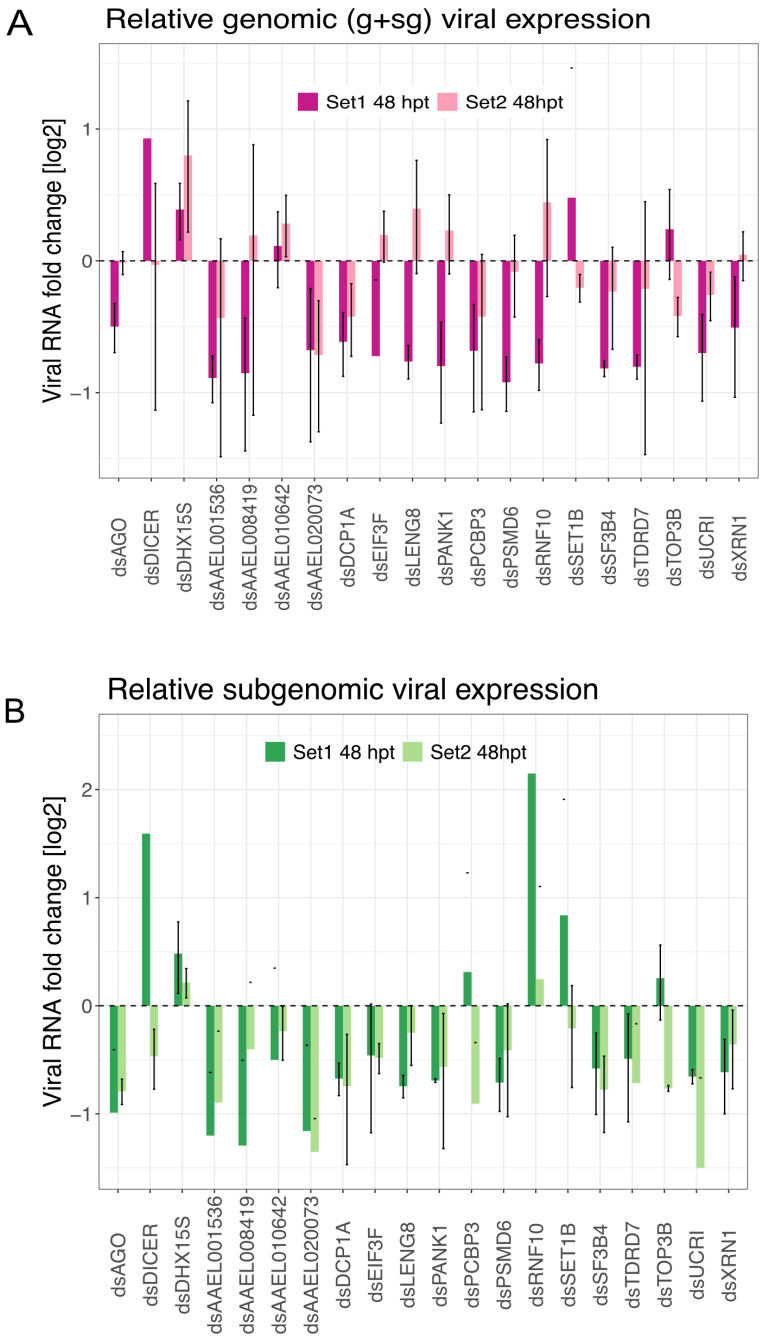

Figure 6.5: A targeted RNAi screen identifies RNA-binding proteins (RBPs) that control arbovirus replication in cells

A) Quantification of genomic RNA by qRT-PCR after silencing of the indicated genes in Aag2-AF5 cells across the datasets. The 1-fold point on the linear scale is indicated by the dashed line, which represents the baseline, dsEGFP. Mean and SD error bars represent triplicate samples tested.

B) Quantification of subgenomic RNA by qRT-PCR after silencing of the indicated genes in Aag2-AF5 cells across the datasets. The 1-fold point on the linear scale is indicated by the dashed line, which represents the baseline, dsEGFP. Error bars showing the mean and SD of triplicate samples tested.

NB: Table in appendix 8.3 shows proviral and antiviral RBPs with significant values indicated.

6.3 Discussion

Delivery of intact dsRNA into cells is crucial to induce the RNAi pathway, which in turn aids deciphering the functions of intended targets [244]. The data revealed that XtremeGENE 360 transfection reagent to Lipofectamine 3000 transfection reagent, allowing for the silencing of target genes at lower doses. Upon examining the effect of KD on candidate targets during SINV infection revealed that most of the genes were proviral; however, the duration of transfection and KD efficiency influenced viral RNA levels.

6.3.1 Optimising dsRNA delivery in Aag2-AF5 cells

Introduction of exogenous dsRNA into cells may prove challenging, as nucleases and pH can affect their stability [244]. Carrier systems such as polymers, peptides, liposomes, and nanoparticles are commercially available and can shield dsRNA from degradation and facilitate its entry into cells [245]. In the optimization, 100 ng of dsRNA with XtremeGENE 360 achieved $>$75% KD of target mRNAs, whereas Lipofectamine 3000 required 300 ng of dsRNA to reach comparable depletion levels. This superior efficiency of XtremeGENE 360 may be due to its formulation causing less toxicity or promoting more efficient dsRNA uptake. In a study that evaluated the effects of eight commercially available transfection reagents in mosquito cells C6/36 and U4.4 to identify the most effective and less toxic reagent, showed Lipofectamine RNAiMAX and Lipofectamine 2000 were found to have low to moderate complexing capacity and were more cytotoxic compared to other formulations they tested (K4 and Metafectenes) [246]. Another study using zebrafish cells compared the efficiency of four transfection reagents showed XtremeGENE HP to provide the best transfection results compared to Lipofectamine LTX, JetPrime, and Matra-A [247]. In mammalian systems, Lipofectamine generally provides high transfection efficiency, but it can be cytotoxic. Non-liposomal reagents, such as FuGENE, are typically less cytotoxic; however, their transfection efficiency has been reported as either good or poor depending on the cell type, including in HeLa cells [245]. The data shows that, like other non-liposomal reagents (e.g. FuGENE and XtremeGENE HP),

XtremeGENE360 had better transfection efficiency as they tend to be less cytotoxic compared to liposomal reagents, in this case, Lipofectamine 3000. These results underscore the importance of testing multiple transfection reagents in mosquito cells to maximise dsRNA uptake efficiency. By choosing XtremeGENE 360 and 100 ng of dsRNA, efficient KD was guaranteed while minimising reagent-induced variability.

6.3.2 Mosquito RBPs as factors that promote SINV infection

The majority of candidate RBPs tested promoted viral infection. This is perhaps unsurprising, as candidate selection was based on RBPs that were upregulated during the 24 hpi in the cRIC analysis, a bias that likely enriched for host factors that support viral replication. Many of these proteins are linked to translation and metabolic pathways, consistent with the idea that SINV co-opts core cellular processes to sustain its life cycle [101, 102]. Specific examples are discussed below:

EIF3F (Eukaryotic initiation factor 3 subunit F) is one of the RBPs that consistently reduced viral RNA, even at moderate KD efficiency of about 40%. EIF3F is one of the 13 subunits of the EIF3 complex, which is critical for ribosomal recruitment during cap-dependent translation initiation [248, 249]. Positioned near the mRNA entry channel of the 40S ribosome, EIF3F contributes to mRNA recruitment and scanning, and interacts with EIF3H and EIF3K to stabilise the complex [250]. Because SINV has a capped genome, it depends on host cap-dependent translation, and the loss of EIF3F likely disrupts ribosome recruitment, impairing protein synthesis and viral replication. This is consistent with the general dependence of RNA viruses on host translational apparatus, where many, such as poliovirus, co-opt initiation factors for internal ribosome entry sites (IRES)- or cap-dependent translation of their polyproteins [248]. Thus, the reduction in SINV RNA upon EIF3F knockdown highlights EIF3F as essential for maintaining EIF3 integrity and for recruiting viral mRNAs to ribosomes, thereby promoting replication.

PCBP3 is a poly(C)-binding protein. In the data, it emerged as a proviral factor. PCPB family of proteins are a group of versatile RBPs known to bind poly(C) motifs and

regulate stability and/or translation of target mRNAs [251, 252]. In picornaviruses, PCBPs are essential for host co-factors: for example, poliovirus requires PCBP2 for genomic RNA stability, IRES-dependent translation initiation, and to form replication complexes [223]. Moreover, PCBP2 binds the 5' cloverleaf of poliovirus RNA and helps recruit polymerase for negative-strand synthesis [223]. Additionally, PCBP1/2 can modulate antiviral signalling in mammalian cells, where PCBP2 negatively regulates RIG-I/MAVS and cGAS-STING pathways [253]. In *Aedes* cells, SINV has a 5' cap (no IRES), but PCPB3 might still bind viral UTRs or modulate host mRNAs. The screens showed PCBP3 KD to consistently suppress SINV replication at 48 hpt, even at $<$ 25%. This indicates PCBP3 normally enhances infection, possibly by stabilising viral RNA or aiding translation. Interestingly, in the 24 hpt experiment, PCBP3 KD did not initially lower viral RNA, but in the 48 hpt experiment, the proviral effect became evident. This suggests PCBP3's impact may require longer depletion to manifest, perhaps due to protein stability. Given that PCBP plays a multitude of roles in the cell, mechanistic studies are required to identify the exact mechanism SINV uses to enhance its replication. However, SINV's reliance on PCBP3 suggests that it binds this host protein to promote its own gene expression.

Two candidate RBPs in the data, namely, XRN1 and DCP1A, are known core components of the 5'–3' mRNA degradation machinery. XRN1 is a cytoplasmic exonuclease that degrades RNA after removal of the cap structure by DCP2/DCP1 complex or other decapping enzymes. In this study, KD of XRN1 and DCP1A reduced SINV RNA levels, suggesting that the mRNA decay pathway is required for efficient viral replication. This aligns with findings by García-Moreno *et al.* showing that SINV replication was impaired in XRN1-deficient HEK293 cells. Moreover, that study showed that XRN1 localise to viral replication factories in SINV-infected cells. [101]. More recently, Ruscica *et al.* proposed that XRN1 requirement for viral infection is due to its role in causing the degradation of cellular RNAs. Loss of cellular transcripts causes an increase in free nucleotides that can be used to fuel viral replication [211]. In addition, flaviviruses stall XRN1 on their 3' UTR to generate subgenomic RNAs, which are used to hijack antiviral factors and prevent innate immune signalling [254].

Taken together, this findings support a model in which SINV co-opts host mRNA degradation machinery, probably to aid replication through cellular mRNA degradation and nucleotide recycling, where loss of either the decapping enzyme DCP1A or the exonuclease XRN1 impairs replication.

PSMD6 is a subunit of the 26S proteasome regulatory complex and was another dependency factor revealed in this study. Its depletion resulted in decreased viral RNA levels, suggesting that the ubiquitin-proteasome system (UPS) is important in SINV. This aligns with findings for mayaro virus (MAYV), another alphavirus, where proteasome inhibition of UPS by MG132, a proteasome inhibitor, resulted in decreased viral replication [255]. Viruses often exploit UPS for entry, uncoating or remodelling host proteins [256]. One possible mechanism SINV could exploit is the proteosome-mediated degradation of host restriction factors, such as antiviral RBPs or interferon-stimulated gene products, which would otherwise suppress viral replication. By targeting these factors for ubiquitination and subsequent degradation, SINV may overcome intrinsic immune barriers and create a more permissive environment for its replication [196, 203, 257]. In addition, the UPS may contribute to the dynamic regulation of viral replication complexes (VRCs). VRCs are membrane-associated organelles that undergo continual assembly and disassembly during infection. Proteosome-dependent turnover of misfolded proteins or obsolete viral proteins may help maintain functional VRCs, thereby facilitating efficient viral RNA synthesis [257, 258]. This supports the notion that PSMD6 is a proviral factor in SINV infection. Conversely, in mammalian cells, UPS have been implicated in antiviral defence. For example, TRIM25 mediates the ubiquitination of RIG-I, ZAP, and ZC3HAV1, all of which are key antiviral factors in SINV [101]. This highlights the dual nature of UPS as a double-edged sword, where it can be co-opted to favour viral replication, yet also act to repress infection. Further investigation is required to understand its exact role in mosquitoes during viral infection.

TDRD7 (Tudor domain-containing protein 7) was another provial RBP in this dataset. Knockdown of TDRD7 reduced viral replication, indicating that viruses replicate more efficiently in its presence. In mammals, TDRD7 has been characterised as an

interferon-stimulated gene that restricts viral replication by binding to the cellular kinase AMP-activated protein kinase (AMPK) and inactivating it, thereby blocking virus-induced autophagy [259,260]. Arboviruses such as DENV and ZIKV exploit autophagy by inducing the formation of autophagosomes to promote viral replication [261, 262]. These indicate that SINV sequesters TDRD7 to prevent inhibition of AMPK, thereby facilitating autophagosome formation and supporting its replication. This hypothesis merits further investigation to elucidate the pathway by which TDRD7 acts as a proviral factor.

Ubiquinol-cytochrome c reductase complex (UCRI) is part of mitochondrial complex III, and is essential for electron transport and ATP production. As a metabolic enzyme, UCR1 may have a moonlight role in infection, which is governed by its interaction with RNA. A clear example of riboregulation in human cells is the binding of vault RNA 1-1 to p62, a key regulator of autophagy, which prevents p62 from fulfilling its function [263]. In this study, UCRI depletion led to reduced mRNA levels, suggesting that SINV relies on the mitochondrial electron transport chain, possibly to sustain ATP production necessary for replication. These findings highlight the importance of mitochondrial homeostasis in mosquito cells for efficient viral replication.

Pantothenate kinase 1 (PANK1), a cytosolic enzyme catalysing the first step in coenzyme A (CoA) biosynthesis, represents another metabolic enzyme potentially linked to viral replication. Because alphavirus replication is energy and lipid-intensive, requiring abundant ATP and biosynthetic precursors to form membrane-bound replication factories [264, 265], and disruption of PANK1 may limit CoA availability, hindering fatty acid synthesis needed for new viral membranous structures. In this study, depletion of PANK1 showed proviral activity at 24 hpt but gave inconclusive results at 48 hpt, possibly reflecting pathway recovery or a compensatory pathway being induced. These results support the notion that viruses reshape host metabolic pathways for their replication; however, further investigation is required to determine if PANK1 acts directly through riboregulatory mechanisms or indirectly through its role in metabolism.

Knocking down SF3B4 (a splicing factor) also reduced SINV RNA levels, suggesting its role as a dependency factor. SF3B4 is a component of the SF3B complex within the U2 small nucleolar ribonucleoprotein (snRNP), which is required for recognition and stabilisation of the branch point sequence during pre-mRNA splicing [266, 267]. In mammalian systems, SINV infection causes U2 snRNP/SF3B to relocalize to viral replication organelles (VROs), where it exerts an antiviral function by repressing viral replication and gene expression [103, 268]. In mosquito cells, by contrast, SF3B4 depletion reduced viral replication, implying that its presence favours infections. One possible explanation is that the non-lytic nature of mosquito infection prevents U2 snRNP relocalisation to VROs, thereby limiting the antiviral effects observed in mammalian cells. Further investigation is necessary to determine how a nuclear splicing factor functions as a proviral protein in mosquitoes.

SET1B is a histone H3K4 methyltransferase involved in adding methyl groups to histone H3 at lysine 4 (H3K4), which marks genomic regions of active transcription. SET1B operates as part of the COMPASS complex and plays a significant role in regulating gene expression, influencing developmental processes in cells [269]. Beyond its role in development, SET1B has been shown to drive gene expression by recruiting hypoxia-inducible factors to gene promoter sites, which drive expression under stressful conditions [270]. In the analysis, depletion of SET1B resulted in reduced viral mRNA levels, suggesting that SET1B may influence viral replication indirectly by altering the cellular environment through chromatin remodelling and regulating host stress-response genes. While its role in infection remains poorly understood, this study shows that SET1B is a dependency factor in SINV infection, warranting further investigation.

Knockdown of LENG8 and the homeobox protein (AAEL001536) each produced modest reductions in viral RNA levels. Homeobox proteins function as sequence-specific transcription factors that regulate gene expression programs [271], Although their role in SINV infection is likely indirect, it is possible that the virus exploits products of these pathways to support replication. However, little is currently known about such interactions, and detailed mechanistic studies will be required to identify their roles.

6.3.3 Mosquito RBPs that act as antiviral factors during SINV infection

While the majority of tested RBPs functioned as proviral factors, a subset exhibited antiviral activity, as their presence restricted SINV replication. Knockdown of these candidates resulted in elevated viral RNA levels relative to controls, indicating that under normal conditions, these proteins act as intrinsic restriction factors that limit viral replication. Notably, the magnitude of viral increase upon silencing these antiviral RBPs was relatively small (0.5 to 1 fold change).

AAEL010642, a putative poly(A)-binding protein (PABP), showed increased viral RNA levels upon KD, suggesting an antiviral role. PABP normally binds the 3' poly(A) tail of mRNAs and interacts with EIF4G at the 5' end to form a closed-looped mRNP that enhances translation initiation and stabilises transcripts [272]. Viruses frequently target PABP to suppress host translation and redirect resources for their own replication [149]. Given its central role in cap-dependent translation initiation, the observed restriction is unexpected. One possibility is that PAPB has dual functionality: it may cooperate with factors such as EIF3F to promote viral translation, but also engage other pathways that destabilise or degrade viral mRNAs. This warrants further investigation into the roles of PABP during infection.

As expected, the siRNA-mediated antiviral pathway was represented by AGO2 and DCR-2. AGO2, the slicer endonuclease of the RNA-induced silencing complex (RISC), is a well-established antiviral effector in mosquitoes. It directly cleaves viral RNAs complementary to virus-derived siRNAs, thereby suppressing infection. DCR-2, which generates siRNAs from viral dsRNA, is equally critical for antiviral defense [5, 198, 207, 273]. In the knockdown screens of AGO2 and DCR-2 there was no marked increase SINV RNA unless the knockdown efficiency was high ($>$55%). This is consistent with previous reports demonstrating that AGO2 functions as a major antiviral factor: for example, partial knockdown of AGO2 led to increased viral replication in CHIKV [72]. Similar observations have been reported for SFV, DENV, SINV, and BUNV [225–228]. Interestingly, Varjak and colleagues showed that AGO2 knockdown reduced genomic ZIKV RNA levels [274], suggesting context-specific outcomes that may depend on

virus type, timing, or cellular environment. This may also explain why SINV RNA levels reduced at 48 hpt, where partial knockdown might not fully disrupt the RNAi pathway, and compensatory mechanisms may be triggered. A complete knockout would likely reveal a more pronounced phenotype. Indeed, Varjak et al. also demonstrated that DCR-2 knockout led to reduced AGO2 expression, confirming the central role of DCR-2 in maintaining siRNA pathway integrity. In the results, the duration of transfection was particularly critical for AGO2, as 48 hpt prior to infection appeared to allow either recovery of the siRNA pathway or activation of compensatory mechanisms.

TOP3B is a DNA/RNA topoisomerase whose function on mRNA is linked to polyribosomes and the fragile X mental retardation protein (FMRP), where it regulates translation. In addition, TOP3B interacts with the RNA-induced silencing complex (RISC), contributing to heterochromatin formation and transcriptional silencing [275, 276]. TOP3B has also been implicated in the regulation of flavivirus infection [167]. In that study, deletion of the TOP3B–TDRD3 complex did not impair viral RNA transcription or translation but significantly reduced the production of infectious particles. A similar phenotype was reported in tick cells, where knockdown of TOP3B did not alter UUKV RNA levels but decreased infectious virus yield [168]. In the SINV screens, TOP3B knockdown had no detectable effect on viral RNA replication at 24 hpt; however, measurements at 48 hpt were highly variable and therefore inconclusive. These results suggest that while viral RNA synthesis may be unaffected, TOP3B could be required at later stages of the viral life cycle, such as assembly or production of infectious virions. A limitation of this study is that plaque assays were not perfomed, which would have allowed direct quantification of infectious particle output. Further investigation is warranted to clarify the role of TOP3B in mosquito infection.

Depletion of DHX15 caused increased SINV replication even when the protein was reduced partially (<50%), reinforcing it proposed role as antiviral factor [169]. These results support recent work on *Ae. aegypti* Aag2 cells, where DHX15 was identified as an antiviral factor in SINV-infected cells [169] . In the same study, they also showed that DHX15 depletion increases the replication of DENV and CHIKV viruses, indicating that DHX15 is a broad-spectrum antiviral factor in mosquitoes. The authors suggested that

DHX15 restricts viral replication by regulating glycolysis. In mammalian cells, DHX15 is also known for its antiviral activity, however, via a different mechanism. DHX15 in humans interacts with RIG-I-like receptors to promote interferon signalling [277, 278]. Thus, DHX15 has conserved antiviral activity across species, albeit via different mechanisms.

6.3.4 Protein turnover and its effect on viral mRNA

Duration of knockdown prior to infection was relevant for several targets. Comparing KD at 24 hpt and 48 hpt showed that certain RBPs only had observable effects at the longer time. For instance, PCBP3 and PSMD6 knockdown did not significantly suppress the virus when transfected 24 hpt before infection. This is perhaps because their RNA levels had not dropped enough, or the cells hadn't had time to exhaust existing protein pools, but at 48 hpt pre-infection, their knockdown clearly reduced viral RNA. This indicates some proteins have slow turnover, or the cells need more time to manifest functional deficits after their mRNA is knocked down. In contrast, other targets such as DCP1A, DHX15 showed effects even at 24 hpt KD, implying a faster turnover or more immediate impact on virus processes. Experimental timing is therefore critical: Performing a screen at only 24 hpt might have missed certain provial hits. By also examining 48 hpt, improved the chance to catch late-arising phenotypes. However, extended knockdown can also introduce secondary effects; cells may adapt over 48 hpt to the loss of a protein, potentially activating compensatory pathways or stress responses that can influence virus replication. Thus, there is a trade-off between giving sufficient time for knockdown vs. introducing additional variables. In this case, using two time points and two biological replicates helped distinguish true effects from noise. For example, LENG8 and XRN1 had one replicate with poor KD at 48 hpt and another with good KD; by noting the correlation with KD efficiency, it can be inferred that their proviral roles are real but sensitive to the efficiency of KD. Reproducibility across replicates and conditions strengthened confidence in assignments of pro/antiviral function.

6.3.5 Limitations and future works

While this targeted RBP knockdown screen yielded valuable insights, there are several limitations to acknowledge. First, the screen was limited to the testing of 17 candidates (plus controls), chosen based on specific criteria. This is not an exhaustive survey of the RBPome, and undoubtedly other important RBPs were not tested. The criteria may have missed factors that are not strongly upregulated at 24 hpi but still play critical roles. For example, a protein sharply upregulated at 8 hpi and then returning to baseline might be very important for initial infection but not essential in the persistent phase. A larger-scale screen could uncover additional host factors of up- and down-regulated genes.

Second, the readouts focused on viral RNA levels by RT-qPCR. While this is a convenient as it is a sensitive measure of replication, it does not directly measure production of viral proteins or infectious virus particles. Lack of function can, for example, lead to the accumulation of defective viral RNA or non-infectious particles that inflate the RNA count without an equivalent increase in infectious titre. In this case, all changes in viral RNA were moderate, mostly +/-0.5-fold of the control, indicating only modest effects. It is possible that at the level of the infectious virus, these differences could be larger or smaller. To address this, future experiments should include assays such as plaque assays or TCID50 measurements for each knockdown condition. If a depletion of RBP truly suppresses the virus, it should result in lower plaque-forming units. These data would validate whether the changes observed in RNA translate to meaningful functional differences in virus propagation.

Third, all experiments were conducted in Aag2-AF5, an *Ae. aegypti*-derived cell line. Cell lines are useful models but may not fully recapitulate the complexity of an intact mosquito, where tissue-specific factors and systemic immunity come into play. The roles of certain RBPs might differ *in vivo*, for example, an RBP that is proviral in cell culture might be less important in an adult mosquito if that protein is not expressed in the midgut or salivary glands. Future work should test key candidates *in vivo* to evaluate their role in infection and how transmission is altered in mosquitoes. Along

the same lines, time and dose of infection in the study were constrained (24 h post-infection at MOI 0.1). It's possible that some RBPs have a more significant effect at later stages of infection or at different virus doses. For instance, a modest 0.5-fold change in viral RNA at 24 hpi might translate to a much larger difference in cumulative virus production over a longer infection period. Extending the time course and measuring infectious output would therefore provide greater insight.

In conclusion, this discussion has delineated how a small-scale RBP knockdown screen advanced our understanding of SINV-host interactions in Aedes cells. Proviral RBPs identified highlight the host pathways, such as mRNA translation and decay and metabolic pathways that SINV leverages, many of which are common across viruses. This study also confirmed DHX15 and discovered AAEL010462 as antiviral factors. The results also emphasise the importance of knockdown efficacy and duration of transfection prior to infection when deciding on the experimental design in uncovering functional roles. There remain limitations, but this has paved the way for targeted follow-up experiments. Ultimately, unravelling how each of these RBPs contributes to the infection puzzle will deepen our understanding of arboviral persistence in vectors and could reveal novel targets to interfere with the virus life cycle either in the mosquito or possibly in human infection. By identifying which host proteins tip the balance in favour of the virus or the host, we move closer to strategies that can reduce arbovirus burden.

7 General Discussion

7.1 Summary

This thesis outlines the contributions made toward uncovering RBPs in *Aedes* mosquitoes both under basal conditions and during infection. RIC was employed to identify mosquito RBPs, followed by cRIC to determine those differentially regulated during SINV infection. To explore their functional relevance, RNAi-mediated silencing was used for a subset of these RBPs. The findings revealed that mosquito RBPs share strong similarities with those in mammalian systems and yeast, suggesting evolutionary pressure to preserve their biochemical properties and overall domain architecture. Furthermore, viruses also exploit these host RBPs in mosquito vectors to support their own replication cycle, while mosquito cells also employ RNA binders to counteract infection.

Firstly, The complement of RBPs in two mosquito cell lines, *Ae. aegypt* Aag2-AF5 and *Ae. albopictus* U4.4 cell lines was identified. These two species are vectors of significant importance due to their ability to transmit viruses such as DENV, CHIKV, and other arboviruses of concern [166]. This study identified 852 RBPs in *Aedes aegypti* and 683 RBPs in *Ae. albopictus*. Remarkably, comparison of these proteins to human RBPs indicated 78% of these RBPs were conserved, which indicates an evolutionary pressure to maintain their function even across taxa. Upon further characterisation, 50% of these proteins contained canonical RBDs, with RRMs, KH domains and DEAD-box helicases being the most represented domains. The remaining half lacked canonical RBDs, suggesting that they interact with RNA through alternative yet unknown RNA-binding mechanisms. The number of "unorthodox" RBPs is in line with studies in mammalian cells. These unorthodox RBPs include metabolic enzymes and membrane proteins, whose biological functions are already well understood. However, their interaction with RNA introduces a moonlighting activity that is likely controlled by RNA, a phenomenon known as riboregulation [279]. Biochemical properties of RBPs identified showed that RBPs were less hydrophobic, had a basic isoelectric point (pH$>$7), and had regions of low complexity. These properties allowed for a modular

configuration that facilitates RBP interactions with RNA and other molecules. Using RBPmap peptides [106], RNA-binding sites(RBS) were identified, which revealed sequence identity to be highest at the RBS.

With the established repertoire of mosquito RBPs, the next step was to identify RBPs that are co-opted for virus replication. Here, cRIC was employed on Aag2-AF5 cells with SINV kinetics at 8, 16, and 24 hpi. 215 of 1556 RBPs were identified as differentially expressed, with 72 upregulated and 143 downregulated. Interestingly, only 14 RBPs were shared across all time points, 4 of which were viral proteins, emphasising how viral RBPs play an important role during the infection process. Furthermore, over 80% of these proteins lacked conventional RBDs, 25% of which were metabolic enzymes. These enzymes include ligases, lyases and oxidoreductases and are typically found in RNA interactome experiments [106, 121]. Interestingly, oxidoreductases tended toward downregulation, a trend consistent with the concept that excessive oxidative stress is generally harmful to the host cell and virus. For successful persistent infection, viruses generally depend on maintaining homeostasis rather than inducing damaging oxidative environments. Notably, one of the oxidoreductases identified was GAPDH (a dehydrogenase), an essential housekeeping gene. GAPDH has an AU-rich element in its Rossmann domain that mediates RNA binding [110]. This interaction can alter its canonical metabolic function, giving rise to its moonlighting activity as an RBP. For example, in coronaviruses, GAPDH binds AT1 and inhibits viral entry [220]. The continued identification of noncanonical RBPs keeps expanding as technologies advance and more organisms are being analysed; thus, there is a need for further characterisation and determination of functions of these proteins to establish their roles in infection and cellular regulation.

Building on the cRIC data, A functional assay using dsRNA-mediated silencing was used to determine the roles of a subset of RBPs that had been identified. The selection of RBPs to test was based on the persistent phase of infection (characterised by low viral titers) and proteins that were consistently upregulated at 8, 16, 24 hpi. From this,17 candidates were identified for screening; 15 of the 17 were proviral, including XRN1 and DCP1A, which are core components of the 5'-3' mRNA

degradation machinery. These RBPs were broadly considered antiviral, as antiviral endonucleases such as RNaseL still rely on endogenous exonucleases to eliminate the resulting RNA fragments [280]. However, they have recently been implicated in flaviviruses and alphaviruses as essential dependency factors, being recruited to viral factories where they degrade cellular mRNA to generate free nucleotides to fuel viral replication [101, 211]. These latter results agree with the study's observations, suggesting that XRN1 and DCP1A are proviral factors that facilitate viral replication. This data thus support the notion that the role of the 5'-to-3' degradation machinery to provide nucleotides might be conserved in arthropods and mammals. As a control, DHX15 was included, which has been suggested to have antiviral activity against SINV, CHIKV, and DENV by regulating glycolysis. Knockdown of DHX15 hampers the expression of genes encoding core enzymes of the glycolytic pathway [169]. The results further confirmed the antiviral phenotype of DHX15, validating orthogonally these earlier observations. AAEL010642 is a homolog of the human PABP1 protein, which binds to the poly(A) tails of cellular mRNAs and increases their stability and translation. These experiments revealed an antiviral role, perhaps preventing cellular mRNA degradation in infected cells and reducing the availability of nucleotides.

Another interesting finding from the dsRNA silencing experiments was that knockdown (KD) efficiency and the duration of transfection significantly influenced the observed SINV phenotype. For example, depletion of RBPs such as PCBP1 and PSMD6 appeared to favour viral replication after shorter transfection (24 hpt); however, extending the transfection (48 hpt) resulted in reduced viral mRNA levels. This highlights that proteins differ in their half-lives, with stability and turnover rates determining how quickly the effects of RNA depletion become evident. Sufficient time is therefore required not only for degradation of target mRNAs but also for the natural turnover of pre-existing proteins, ensuring that the phenotype truly reflects the knockdown effect. These findings underscore the importance of considering both RNA and protein stability when designing RNAi experiments to achieve accurate interpretation of outcomes.

Altogether, this study confirmed that RIC is an effective technique for identifying

RBPs in mosquito cells. This method focuses preferentially on poly(A)-associated proteins; therefore, complementary approaches could be considered in the future to survey the scope of RBPs binding to non-polyadenylated proteins. Such methods include protein-crosslinked RNA eXtraction (XRNAX) and orthogonal organic phase separation (OOPS), which capture global protein-RNA complexes [138, 139]. Bona fide RBPs were identified, 1545 RBPs belonging to *Aedes* mosquitoes and 215 related to infection. This has expanded our knowledge of RBPs, particularly in mosquitoes, and opened avenues for studying the infection of other viruses in this model, thereby improving our understanding of RBP regulation and its biological relevance.

7.2 The future of mosquito biology

The publication of entire mosquito genomes, such as *Ae. aegypti* in 2007 and the improvement of its annotation in 2018 has provided foundations to identify genetically encoded molecular factors that influence all aspects of mosquito biology, including vector competence at molecular-level resolution [281, 282]. In parallel, advances in omics techniques, such as whole genome sequencing, RNA sequencing, and protein sequencing, have broadened our knowledge of molecular biology. The open-access repositories compiling genomic, transcriptomic, and proteomic data have enabled the identification of molecular factors that are associated with vector competence and provide a stepping stone in subsequent functional characterisations.

While providing avenues for exploration, many mosquito genes are annotated as hypothetical or unknown and for less studied mosquitoes, this proportion could even be wider, resulting in difficulties when trying to determine function. Another challenge is the bias towards model organisms; for example, most of what we know of insect biology is drawn from *Drosophila melanogaster* [283]. Mosquito data must often be extrapolated from *Drosophila*, which may not always hold true given differences in vector physiology and virus susceptibility. This bias means certain RBPs critical in mosquitoes may be novel or divergent, and thus overlooked if only searches rely on homology [284]. Another hindrance is in the bioinformatic

pipelines that are often optimised for model organisms and do not work optimally for mosquitoes or other arthropods. The need for specialised data-mining tools is needed to make maximal use of new insect genome resources [284]. For example, functional enrichment analyses or pathway databases may have sparse coverage for mosquito genes, forcing researchers to map mosquito gene IDs to *Drosophila* or human orthologs to infer function. Case in point, the analysis of the *Ae. albopictus* data necessitated the use of orthologs from *Ae. aegypti* to carry out gene function as it is better annotated. Addressing these issues requires joint efforts in genome curation, community annotation and the development of more databases that are designed for vector research, such as Vectorbase and FlyBase. Initiatives such as i5K project for sequencing arthropods go a long way in setting a baseline for characterisation of mosquitoes [285].

The use of high-throughput studies such as RNA sequencing and transcriptomics has allowed for mosquitoes to be studied in unprecedented detail. In this case, the use of RIC to profile proteins in *Aedes* mosquitoes in an unbiased manner provided the first set of bona fide RBPs in mosquitoes. A further layer of mosquito RBPs involved during infection highlighted the mosquito-virus interactome. While this provided an inventory of the protein interactome in mosquitoes, integrating these data with transcript-level analysis would have given a more comprehensive understanding of the mosquito RBPome. One such approach would be the use of UV cross-linking and immunoprecipitation (iCLIP), which allows for the identification of the exact RNA site bound by specific RBPs *in vivo*. In practice, the method involves UV-cross-linking RNA and protein, immunoprecipitation of particular RBPs of interest using antibodies or tagged versions of the proteins, and then sequencing the co-precipitated RNA fragment [286]. This gives a base-pair resolution map of where the RBP binds to transcripts across the transcriptome, for example, in mammalian cells, GEMIN5 was shown to bind 5' UTR of SINV RNA, thus modulating translation, and this explains its role in repressing viral translation [101]. Such insight is helpful in determining whether RBPs act directly on viral RNA or indirectly. Other RNA-centric methods [132] or methods that enrich for only viral proteins [145] could further expand our knowledge

of the mosquito-virus interactome.

The discovery of RBP is only the start, and a critical step is determining the function of these proteins. Methods commonly used are: RNAi-mediated silencing, which was applied to a subset of RBPs identified during infection. RNAi is used transiently to silence genes by introducing specific RNA molecules; however, this method induces only partial silencing of gene expression that may sometimes be impossible to reproduce, leading to an ambiguous interpretation of the role of the target gene [287]. CRISPR/CA9 is a precise genome editing tool that is used to knock out or knock in target genes, introducing mutant alleles into the germline, thereby allowing for the generation of stable mutant lines. A drawback to CRISPR is that knockout of essential genes may lead to non-viable mutants, which has limited its application [288]. However, some studies have demonstrated its feasibility in mosquito cell lines and developed tools optimised for genome-scale screening in vectors [288]. Such tools hold great potential for genome-wide scale investigation of mosquito-virus interactions.

Another consideration to note is that cell lines do not always recapitulate a whole mosquito, as protein composition may vary from tissue to tissue. On the other hand, the genetic diversity observed in wild mosquito populations also offers another complication on the use of laboratory-established mosquitoes [289]. Although they still provide insightful information, this calls for a change in approach that ensures a more collaborative type of research, ultimately integrating field studies.

By pursuing these directions, we will be better equipped to unravel the complex web of mosquito–virus interactions. Ultimately, such knowledge could inform the development of novel antiviral strategies or genetic interventions that disrupt the viral life cycle within mosquitoes, thereby reducing disease transmission.

8 Appendices

8.1 XtremeGENE 360 data

name	conc	target.x	CT.x	target.y	replicat	CT.y	DCT	meanGFP	DDCT	M2DDCT	Kdpercentage
dsAGO	100	AGO	21.3132629	ACTIN	1	15.9182596	5.39500332	3.180679	2.21432432	0.21548744	0.78451256
dsAGO	100	AGO	19.9605446	ACTIN	2	14.7493401	5.21120453	3.180679	2.03052553	0.2447659	0.755234102
dsAGO	100	AGO	21.0871983	ACTIN	3	15.8186436	5.26855469	3.180679	2.08787568	0.2352268	0.764773205
dsAGO	200	AGO	20.7719421	ACTIN	1	15.8072119	4.96473026	3.67127959	1.29345067	0.40797406	0.592025941
dsAGO	200	AGO	20.8036613	ACTIN	2	15.805727	4.99793434	3.67127959	1.32665475	0.39869164	0.601308363
dsAGO	200	AGO	20.4675331	ACTIN	3	15.8666124	4.60092068	3.67127959	0.92964109	0.52498893	0.475011068
dsAGO	300	AGO	20.7621861	ACTIN	1	15.9350834	4.82710266	3.41805967	1.40904299	0.37656139	0.623438606
dsAGO	300	AGO	21.9323959	ACTIN	2	15.8112087	6.12118721	3.41805967	2.70312754	0.1535598	0.846440204
dsAGO	300	AGO	20.553093	ACTIN	3	15.5180464	5.03504658	3.41805967	1.61698691	0.32601564	0.673984358
dsDHX	100	DHX	22.6892548	ACTIN	1	16.8151207	5.87413406	2.64459769	3.22953637	0.10661362	0.893386383
dsDHX	100	DHX	21.9942665	ACTIN	2	16.1769028	5.81736374	2.64459769	3.17276605	0.11089252	0.889107481
dsDHX	100	DHX	21.6532574	ACTIN	3	16.0391254	5.61413193	2.64459769	2.96953424	0.12766773	0.872332275
dsDHX	200	DHX	21.5587711	ACTIN	1	16.042511	5.51626015	2.69016933	2.82609081	0.14101389	0.858986109
dsDHX	200	DHX	22.3346252	ACTIN	2	16.7331028	5.60152245	2.69016933	2.91135311	0.13292155	0.867078453
dsDHX	200	DHX	21.4769783	ACTIN	3	16.2070103	5.26996803	2.69016933	2.5797987	0.16726428	0.832735719
dsDHX	300	DHX	20.9167728	ACTIN	1	16.4412098	4.47556305	2.53185654	1.94370651	0.25994773	0.740052265
dsDHX	300	DHX	21.1817169	ACTIN	2	16.9667187	4.21499825	2.53185654	1.68314171	0.31140376	0.688596235
dsDHX	300	DHX	21.5487766	ACTIN	3	15.9505005	5.59827614	2.53185654	3.0664196	0.11937564	0.880624358
dsGFP	100	AGO	19.1533546	ACTIN	1	15.882926	3.27042866	3.180679	0.08974965	0.9396858	0.060314205
dsGFP	100	DHX	18.5477142	ACTIN	1	15.882926	2.66478825	2.64459769	0.02019056	0.98610245	0.013897552
dsGFP	100	SINV	9.36977386	ACTIN	1	15.882926	-6.5131521	-6.7031326	0.18998051	0.87661757	0.123382434
dsGFP	100	SINV	9.12932777	ACTIN	2	16.029541	-6.9002132	-6.7031326	-0.1970806	1.14637624	-0.14637624
dsGFP	100	AGO	19.1043625	ACTIN	2	16.029541	3.07482147	3.180679	-0.1058575	1.07613385	-0.07613385
dsGFP	100	DHX	18.6568203	ACTIN	2	16.029541	2.62727928	2.64459769	-0.0173184	1.01207655	-0.01207655
dsGFP	100	SINV	9.38864422	ACTIN	3	16.0846767	-6.6960325	-6.7031326	0.00710011	0.99509067	0.004909328
dsGFP	100	DHX	18.7264023	ACTIN	3	16.0846767	2.64172554	2.64459769	-0.0028721	1.00199281	-0.00199281
dsGFP	100	AGO	19.2814636	ACTIN	3	16.0846767	3.19678688	3.180679	0.01610788	0.98889697	0.011103031
dsGFP	200	DHX	18.9156303	ACTIN	1	16.0866165	2.82901382	2.69016933	0.13884449	0.90824631	0.091753687
dsGFP	200	SINV	9.8197937	ACTIN	1	16.0866165	-6.2668228	-6.2813212	0.01449839	0.99000081	0.009999192
dsGFP	200	AGO	19.685564	ACTIN	1	16.0866165	3.59894753	3.67127959	-0.0723321	1.05141488	-0.05141488
dsGFP	200	AGO	19.2793484	ACTIN	2	15.6758909	3.60345745	3.67127959	-0.0678221	1.04813325	-0.04813325
dsGFP	200	DHX	18.2565804	ACTIN	2	15.6758909	2.58068943	2.69016933	-0.1094799	1.07883924	-0.07883924
dsGFP	200	SINV	9.61213112	ACTIN	2	15.6758909	-6.0637598	-6.2813212	0.2175614	0.8600179	0.139982098
dsGFP	200	SINV	10.9958887	ACTIN	3	17.5092697	-6.513381	-6.2813212	-0.2320598	1.17451065	-0.17451065
dsGFP	200	AGO	21.3207035	ACTIN	3	17.5092697	3.81143379	3.67127959	0.1401542	0.90742216	0.09257784
dsGFP	200	DHX	20.1700745	ACTIN	3	17.5092697	2.66080475	2.69016933	-0.0293646	1.02056253	-0.02056253
dsGFP	300	SINV	9.38049126	ACTIN	1	16.036335	-6.6558437	-6.4939283	-0.1619155	1.11877154	-0.11877154
dsGFP	300	DHX	18.6258202	ACTIN	1	16.036335	2.58948517	2.53185654	0.05762863	0.96084217	0.039157835
dsGFP	300	AGO	19.3443222	ACTIN	1	16.036335	3.30798721	3.41805967	-0.1100725	1.07928244	-0.07928244
dsGFP	300	SINV	9.37058449	ACTIN	2	16.0833626	-6.7127781	-6.4939283	-0.2188498	1.16380538	-0.16380538
dsGFP	300	DHX	18.4512291	ACTIN	2	16.0833626	2.36786652	2.53185654	-0.16399	1.12038146	-0.12038146
dsGFP	300	AGO	19.4642735	ACTIN	2	16.0833626	3.38091087	3.41805967	-0.0371488	1.02608397	-0.02608397
dsGFP	300	DHX	18.6900005	ACTIN	3	16.0517826	2.63821793	2.53185654	0.10636139	0.92892795	0.071072048
dsGFP	300	AGO	19.6170635	ACTIN	3	16.0517826	3.56528091	3.41805967	0.14722125	0.90298802	0.09701198
dsGFP	300	SINV	9.93861961	ACTIN	3	16.0517826	-6.113163	-6.4939283	0.38076528	0.76803008	0.23196992
dsSINV	100	SINV	15.4393044	ACTIN	1	15.898243	-0.4589386	-6.7031326	6.24419403	0.01319199	0.98680801
dsSINV	100	SINV	15.8010435	ACTIN	2	16.2023582	-0.4013147	-6.7031326	6.30181789	0.01267546	0.987324538
dsSINV	100	SINV	16.0731659	ACTIN	3	15.4606009	0.61256504	-6.7031326	7.31569767	0.00627705	0.99372295
dsSINV	200	SINV	15.5927134	ACTIN	1	15.3551226	0.23759079	-6.2813212	6.518912	0.01090466	0.989095345
dsSINV	200	SINV	16.5812969	ACTIN	3	15.834631	0.74666595	-6.2813212	7.02798716	0.0076624	0.992337596
dsSINV	200	SINV	15.544364	ACTIN	3	15.834631	-0.290267	-6.2813212	5.99105422	0.01572219	0.984277812
dsSINV	300	SINV	15.9733591	ACTIN	1	16.147831	-0.1744719	-6.4939283	6.31945642	0.01252143	0.987478566
dsSINV	300	SINV	15.6433926	ACTIN	2	15.7474918	-0.1040993	-6.4939283	6.389829	0.01192531	0.988074687
dsSINV	300	SINV	16.1275024	ACTIN	3	15.7218904	0.40561199	-6.4939283	6.89954027	0.0083759	0.991624101

8.2 Lipofectamine data

name	dsconcn	target.x	CT.x	target.y	CT.y	DCT	meanGFP	DDCT	M2DDCT	pereff
dsAGO	100	AGO	29.1062355	ACTIN	16.8414288	12.2648068	14.1758614	-1.9110546	3.76083917	0
dsAGO	100	AGO	29.9648762	ACTIN	15.9836226	13.9812536	14.1758614	-0.1946077	1.14441296	0
dsAGO	100	AGO	30.3512974	ACTIN	16.2424145	14.1088829	14.1758614	-0.0669785	1.04752048	0
dsAGO	200	AGO	31.0527706	ACTIN	15.2906017	15.7621689	19.461689	-3.6995201	12.9917161	0
dsAGO	200	AGO	31.8077717	ACTIN	15.3639469	16.4438248	19.461689	-3.0178642	8.09967616	0
dsAGO	200	AGO	31.3853474	ACTIN	16.0044193	15.380928	19.461689	-4.080761	16.9212115	0
dsAGO	300	AGO	30.5005436	ACTIN	16.283205	14.2173386	18.8907576	-4.673419	25.5175692	0
dsAGO	300	AGO	30.5953674	ACTIN	15.6072035	14.988164	18.8907576	-3.9025936	14.9553898	0
dsAGO	300	AGO	30.7931309	ACTIN	15.5291882	15.2639427	18.8907576	-3.6268148	12.3532166	0
dsDHX	100	DHX	21.1767712	ACTIN	16.0019665	5.17480469	3.79114087	1.38366381	0.38324429	61.6755714
dsDHX	100	DHX	21.8803787	ACTIN	16.6107693	5.26960945	3.79114087	1.47846858	0.35886955	64.113045
dsDHX	100	DHX	22.0816078	ACTIN	16.7907524	5.29085541	3.79114087	1.49971453	0.35362336	64.6376645
dsDHX	200	DHX	22.4487667	ACTIN	16.9649105	5.4838562	4.65313339	0.83072281	0.56224748	43.7752522
dsDHX	200	DHX	20.4664021	ACTIN	14.549201	5.91720104	4.65313339	1.26406765	0.41636836	58.3631639
dsDHX	200	DHX	21.4138699	ACTIN	15.5301542	5.88371563	4.65313339	1.23058224	0.42614543	57.3854571
dsDHX	300	DHX	21.9655914	ACTIN	15.2861528	6.67943859	4.34163698	2.33780162	0.19781152	80.2188476
dsDHX	300	DHX	22.1414909	ACTIN	15.5782919	6.56319904	4.34163698	2.22156207	0.21440908	78.5590917
dsDHX	300	DHX	22.2917061	ACTIN	15.318347	6.97335911	4.34163698	2.63172213	0.16135139	83.8648615
dsGFP	100	AGO	33.9853745	ACTIN	19.9524345	14.0329399	14.1758614	-0.1429214	1.10413873	0
dsGFP	100	DHX	23.5336266	ACTIN	19.9524345	3.58119202	3.79114087	-0.2099489	1.15664718	0
dsGFP	100	SINV	13.0231314	ACTIN	19.9524345	-6.9293032	-5.8374446	-1.0918585	2.13148447	0
dsGFP	100	AGO	31.1887493	ACTIN	16.1891327	14.9996166	14.1758614	0.82375526	0.56496944	43.5030561
dsGFP	100	DHX	19.9866867	ACTIN	16.1891327	3.79755402	3.79114087	0.00641314	0.99556461	0.44353857
dsGFP	100	SINV	11.2235489	ACTIN	16.1891327	-4.9655838	-5.8374446	0.87186082	0.54644158	45.3558417
dsGFP	100	AGO	30.2194061	ACTIN	16.7243786	13.4950275	14.1758614	-0.6808338	1.60306599	-60.306599
dsGFP	100	DHX	20.7190552	ACTIN	16.7243786	3.99467659	3.79114087	0.20353572	0.86841966	13.1580345
dsGFP	100	SINV	11.1069317	ACTIN	16.7243786	-5.6174469	-5.8374446	0.21999772	0.85856679	14.1433209
dsGFP	200	AGO	36.9865646	ACTIN	16.0167294	20.9698353	19.461689	1.50814629	0.35156265	64.843735
dsGFP	200	SINV	11.7566366	ACTIN	16.0167294	-4.2600927	-4.3296541	0.06956132	0.95292771	4.70722911
dsGFP	200	DHX	20.7140369	ACTIN	16.0167294	4.69730759	4.65313339	0.04417419	0.9698448	3.0155198
dsGFP	200	AGO	33.8189812	ACTIN	15.3680534	18.4509277	19.461689	-1.0107613	2.01497405	0
dsGFP	200	DHX	19.9095116	ACTIN	15.3680534	4.54145813	4.65313339	-0.1116753	1.08048217	0
dsGFP	200	SINV	11.0082398	ACTIN	15.3680534	-4.3598137	-4.3296541	-0.0301596	1.02112511	0
dsGFP	200	AGO	34.2200203	ACTIN	15.2557163	18.964304	19.461689	-0.497385	1.41165253	0
dsGFP	200	DHX	19.9763508	ACTIN	15.2557163	4.72063446	4.65313339	0.06750107	0.95428952	4.57104815
dsGFP	200	SINV	10.8866606	ACTIN	15.2557163	-4.3690557	-4.3296541	-0.0394017	1.02768754	0
dsGFP	300	AGO	35.9536972	ACTIN	19.9364109	16.0172863	18.8907576	-2.8734713	7.3282629	0
dsGFP	300	DHX	23.9620953	ACTIN	19.9364109	4.02568436	4.34163698	-0.3159526	1.24483335	0
dsGFP	300	SINV	13.4786911	ACTIN	19.9364109	-6.4577198	-5.1890434	-1.2686764	2.4094042	0
dsGFP	300	AGO	34.787014	ACTIN	15.3380423	19.4489718	18.8907576	0.55821419	0.67914231	32.0857693
dsGFP	300	DHX	19.7764301	ACTIN	15.3380423	4.43838787	4.34163698	0.0967509	0.93513665	6.48633496
dsGFP	300	SINV	11.1336737	ACTIN	15.3380423	-4.2043686	-5.1890434	0.98467477	0.50533963	49.466037
dsGFP	300	AGO	36.6283417	ACTIN	15.422327	21.2060146	18.8907576	2.31525707	0.20092694	79.9073059
dsGFP	300	DHX	19.9831657	ACTIN	15.422327	4.5608387	4.34163698	0.21920172	0.85904063	14.0959368
dsGFP	300	SINV	10.5172854	ACTIN	15.422327	-4.9050417	-5.1890434	0.28400167	0.82130975	17.8690249
dsSINV	100	SINV	13.1417894	ACTIN	16.6551914	-3.513402	-5.8374446	2.32404264	0.19970708	80.0292923
dsSINV	100	SINV	11.4417858	ACTIN	15.8969641	-4.4551783	-5.8374446	1.38226636	0.38361569	61.6384309
dsSINV	100	SINV	11.6088839	ACTIN	15.8145561	-4.2056723	-5.8374446	1.63177236	0.32269154	67.7308464
dsSINV	200	SINV	13.9347382	ACTIN	15.9862232	-2.0514851	-4.3296541	2.278169	0.20615924	79.3840764
dsSINV	200	SINV	12.8667097	ACTIN	15.9060497	-3.03934	-4.3296541	1.29031404	0.40886202	59.1137979
dsSINV	200	SINV	12.6055574	ACTIN	15.1624041	-2.5568466	-4.3296541	1.77280744	0.29263872	70.7361283
dsSINV	300	SINV	14.9809141	ACTIN	16.5482407	-1.5673265	-5.1890434	3.62171682	0.08123714	91.8762864
dsSINV	300	SINV	12.7130384	ACTIN	15.3720903	-2.6590519	-5.1890434	2.52999147	0.17313971	82.6860293
dsSINV	300	SINV	12.7645168	ACTIN	15.2225914	-2.4580746	-5.1890434	2.73096879	0.1506248	84.9375203

8.3 Screened targets data

#	ds	exp	mean.FCDD	sd.FCDDCT	p.signif	activity	mean.KD.perctage	sd.KD.percentage
1	dsAAEL001536	24 hpt	0.841	0.218	ns	proviral	29.606	25.857
2	dsAAEL001536	Set1 48hpt	0.54	0.066	ns	proviral	41.279	12.849
3	dsAAEL001536	Set2 48hpt	0.74	0.383	ns	proviral	30.152	30.31
4	dsAAEL008419	24 hpt	1.094	0.201	ns	anti-viral	73.824	9.126
5	dsAAEL008419	Set1 48hpt	0.554	0.186	ns	proviral	59.269	18.956
6	dsAAEL008419	Set2 48hpt	1.143	0.699	ns	anti-viral	27.84	25.306
7	dsAAEL010642	24 hpt	1.215	0.368	ns	anti-viral	62.421	8.356
8	dsAAEL010642	Set1 48hpt	1.081	0.213	ns	anti-viral	69.082	23.387
9	dsAAEL010642	Set2 48hpt	1.217	0.195	*	anti-viral	38.442	15.722
10	dsAAEL020073	24 hpt	1.113	0.454	ns	anti-viral	19.154	24.062
11	dsAAEL020073	Set1 48hpt	0.625	0.239	ns	proviral	27.102	44.384
12	dsAAEL020073	Set2 48hpt	0.609	0.202	ns	proviral	28.844	26.783
13	dsAGO	24 hpt	1.073	0.464	ns	anti-viral	60.614	29.04
14	dsAGO	Set1 48hpt	0.708	0.091	ns	proviral	50.514	14.99
15	dsAGO	Set2 48hpt	0.99	0.06	ns	proviral	44.901	7.646
16	dsDCP1A	24 hpt	1.02	0.549	ns	proviral	23.532	20.494
17	dsDCP1A	Set1 48hpt	0.653	0.108	ns	proviral	56.788	13.729
18	dsDCP1A	Set2 48hpt	0.746	0.141	ns	proviral	19.531	19.602
19	dsDHX15S	24 hpt	1.491	0.748	ns	anti-viral	79.042	13.825
20	dsDHX15S	Set1 48hpt	1.31	0.193	ns	anti-viral	29.451	4.605
21	dsDHX15S	Set2 48hpt	1.741	0.578	ns	anti-viral	58.209	7.667
22	dsDICER	24 hpt	1.699	1.335	ns	anti-viral	75.502	19.716
23	dsDICER	Set1 48hpt	1.904	2.68	ns	anti-viral	52.959	46.382
24	dsDICER	Set2 48hpt	0.979	0.523	ns	proviral	75.716	15.516
25	dsEGFP	24 hpt	1.018	0.236		control	NA	NA
26	dsEGFP	Set1 48hpt	1.002	0.073		control	NA	NA
27	dsEGFP	Set2 48hpt	1.011	0.182		control	NA	NA
28	dsEIF3F	24 hpt	0.945	0.243	ns	proviral	84.559	5.161
29	dsEIF3F	Set1 48hpt	0.606	0.299	ns	proviral	37.913	36.563
30	dsEIF3F	Set2 48hpt	1.146	0.153	*	anti-viral	82.602	3.458
31	dsLENG8	24 hpt	0.893	0.171	ns	proviral	30.972	17.942
32	dsLENG8	Set1 48hpt	0.589	0.052	ns	proviral	38.308	6.515
33	dsLENG8	Set2 48hpt	1.316	0.381	ns	anti-viral	5.628	4.878
34	dsPANK1	24 hpt	0.879	0.118	ns	proviral	84.492	3.742
35	dsPANK1	Set1 48hpt	0.575	0.149	ns	proviral	59.768	3.438
36	dsPANK1	Set2 48hpt	1.174	0.241	ns	anti-viral	61.996	20.232
37	dsPCBP3	24 hpt	1.153	0.159	ns	anti-viral	33.84	29.667
38	dsPCBP3	Set1 48hpt	0.623	0.171	ns	proviral	67.054	1.102
39	dsPCBP3	Set2 48hpt	0.746	0.289	ns	proviral	44.016	29.303
40	dsPSMD6	24 hpt	1.28	0.482	ns	anti-viral	79.002	16.376
41	dsPSMD6	Set1 48hpt	0.528	0.075	ns	proviral	71.374	1.735
42	dsPSMD6	Set2 48hpt	0.944	0.2	ns	proviral	69.384	7.911
43	dsRNF10	24 hpt	1.061	0.403	*	anti-viral	82.851	5.201
44	dsRNF10	Set1 48hpt	0.583	0.077	ns	proviral	76.738	2.467
45	dsRNF10	Set2 48hpt	1.361	0.532	ns	anti-viral	69.437	19.963
46	dsSET1B	24 hpt	0.714	0.089	ns	proviral	64.551	6.036
47	dsSET1B	Set1 48hpt	1.394	1.363	ns	anti-viral	21.444	20.849
48	dsSET1B	Set2 48hpt	0.868	0.063	*	proviral	42.284	15.255
49	dsSF3B4	24 hpt	1.639	1.307	ns		0	0
50	dsSF3B4	Set1 48hpt	0.568	0.024	ns	proviral	16.699	26.114
51	dsSF3B4	Set2 48hpt	0.851	0.223	ns		0	0
52	dsSINV	24 hpt	0.003	0.001	ns	postivecontrol	99.79	0.041
53	dsSINV	Set1 48hpt	0.008	0.001	ns	postivecontrol	99.102	0.194
54	dsSINV	Set2 48hpt	0.007	0.002	ns	postivecontrol	99.262	0.277
55	dsTDRD7	24 hpt	0.974	0.051	ns	proviral	73.542	2.59
56	dsTDRD7	Set1 48hpt	0.573	0.036	ns	proviral	57.425	8.961
57	dsTDRD7	Set2 48hpt	0.863	0.502	*	proviral	61.688	22.814
58	dsTOP3B	24 hpt	1.001	0.151	ns	proviral	85.721	2.229
59	dsTOP3B	Set1 48hpt	1.181	0.274	ns	anti-viral	55.945	10.836
60	dsTOP3B	Set2 48hpt	0.748	0.077	ns	proviral	66.789	3.17
61	dsUCRI	24 hpt	0.963	0.298	ns	proviral	76.671	1.063
62	dsUCRI	Set1 48hpt	0.616	0.138	ns	proviral	61.361	2.284
63	dsUCRI	Set2 48hpt	0.836	0.106	ns	proviral	83.098	3.529
64	dsXRN1	24 hpt	0.91	0.114	ns	proviral	67.396	5.514
65	dsXRN1	Set1 48hpt	0.704	0.216	ns	proviral	33.778	12.755
66	dsXRN1	Set2 48hpt	1.033	0.132	ns	proviral	7.781	13.477

8.4 Enrichment of enzyme classes (odds ratios)

Enzyme class	OR	CI_low	CI_high	p	$n_{\text{in class}}$	$p_{\text{adj (BH)}}$
Oxidoreductase (EC 1)	0.120	0.002 80	0.806	0.0141	17	0.0848
Transferase (EC 2)	0.335	0.0353	1.57	0.234	14	0.701
Ligase (EC 6)	1.43	0.116	12.8	0.656	5	1
Lyase (EC 4)	1.06	0.0938	7.64	1	6	1
Hydrolase (EC 3)	0.700	0.0672	4.06	1	8	1
Isomerase (EC 5)	0	0	11.3	1	1	1

9 References

[1] Margarita V Rangel, Kenneth A Stapleford, Tuli Mukhopadhyay, and Tem Morrison. Alphavirus Virulence Determinants. *Pathogens 2021, Vol. 10, Page 981*, 10(8):981, 8 2021.

[2] https://zanzare.ipla.org/index.php/en/the-mosquitoes/the-morphology. Mosquito morphology, 2025.

[3] https://www.nemassmosquito.org/mosquitos/pages/mosquito-life-cycle. Mosquito Life Cycle, 2025.

[4] Juliette Lewis, Emily N. Gallichotte, Jenna Randall, Arielle Glass, Brian D. Foy, Gregory D. Ebel, and Rebekah C. Kading. Intrinsic factors driving mosquito vector competence and viral evolution: a review. *Frontiers in Cellular and Infection Microbiology*, 13:1330600, 2023.

[5] Chinmay V. Tikhe and George Dimopoulos. Mosquito antiviral immune pathways. *Developmental and Comparative Immunology*, 116:103964, 3 2021.

[6] Scott C. Weaver and William K. Reisen. Present and future arboviral threats. *Antiviral Research*, 85(2):328–345, 2 2010.

[7] Duane J. Gubler. The Global Emergence/Resurgence of Arboviral Diseases As Public Health Problems. *Archives of Medical Research*, 33(4):330–342, 7 2002.

[8] Ann M. Powers, Aaron C. Brault, Yukio Shirako, Ellen G. Strauss, WenLi Kang, James H. Strauss, and Scott C. Weaver. Evolutionary Relationships and Systematics of the Alphaviruses. *Journal of Virology*, 75(21):10118–10131, 11 2001.

[9] A.M. Powers. Togaviruses: Alphaviruses. *Reference Module in Biomedical Sciences*, 1 2014.

[10] Scott C. Weaver, Robert B. Tesh, and Robert E. Shope. Alphavirus Infections. *Tropical Infectious Diseases: Principles, Pathogens, & Practice, 2-Volume Set with CD-ROM*, pages 831–838, 1 2006.

[11] Mia C. Hikke, Marjan Verest, Just M. Vlak, and Gorben P. Pijlman. Salmonid alphavirus replication in mosquito cells: towards a novel vaccine production system. *Microbial Biotechnology*, 7(5):480, 2014.

[12] N. L. Forrester, G. Palacios, R. B. Tesh, N. Savji, H. Guzman, M. Sherman, S. C. Weaver, and W. I. Lipkin. Genome-Scale Phylogeny of the Alphavirus Genus Suggests a Marine Origin. *Journal of Virology*, 86(5):2729–2738, 3 2012.

[13] Diane E. Griffin. Alphaviruses. *Wiley Encyclopedia of Molecular Medicine*, 1 2002.

[14] Bradley S. Hollidge, Francisco González-Scarano, and Samantha S. Soldan. Arboviral Encephalitides: Transmission, Emergence, and Pathogenesis. *Journal of Neuroimmune Pharmacology*, 5(3):428, 9 2010.

[15] Andreas Suhrbier, Marie Christine Jaffar-Bandjee, and Philippe Gasque. Arthritogenic alphaviruses-an overview. *Nature Reviews Rheumatology*, 8(7):420–429, 7 2012.

[16] Victoria K. Baxter and Mark T. Heise. Immunopathogenesis of alphaviruses. *Advances in Virus Research*, 2020.

[17] Alyssa M. Lantz and Victoria K. Baxter. Neuropathogenesis of Old World Alphaviruses: Considerations for the Development of Medical Countermeasures. *Viruses*, 17(2):261, 2 2025.

[18] Marcos A. Espinal, Jon K. Andrus, Barbara Jauregui, Stephen Hull Waterman, David Michael Morens, Jose Ignacio Santos, Olaf Horstick, Lorraine Ayana Francis, and Daniel Olson. Emerging and reemerging aedes-transmitted arbovirus infections in the region of the americas: Implications for health policy. *American Journal of Public Health*, 109(3):387–392, 2019.

[19] Israel Guerrero-Arguero, Claudia M. Tellez-Freitas, K. Scott Weber, Bradford K. Berges, Richard A. Robison, and Brett E. Pickett. Alphaviruses: Host pathogenesis, immune response, and vaccine & treatment updates. *Journal of General Virology*, 102(8):001644, 8 2021.

[20] Thomas E. Morrison, Alan C. Whitmore, Reed S. Shabman, Brett A. Lidbury, Suresh Mahalingam, and Mark T. Heise. Characterization of Ross River Virus Tropism and Virus-Induced Inflammation in a Mouse Model of Viral Arthritis and Myositis. *Journal of Virology*, 80(2):737–749, 1 2006.

[21] Simona Ozden, Michel Huerre, Jean Pierre Riviere, Lark L. Coffey, Philippe V. Afonso, Vincent Mouly, Jean de Monredon, Jean Christophe Roger, Mohamed El Amrani, Jean Luc Yvin, Marie Christine Jaffar, Marie Pascale Frenkiel, Marion Sourisseau, Olivier Schwartz, Gillian Butler-Browne, Philippe Desprès, Antoine Gessain, and Pierre Emmanuel Ceccaldi. Human Muscle Satellite Cells as Targets of Chikungunya Virus Infection. *PLoS ONE*, 2(6), 2007.

[22] Esposito Danillo Lucas Alves and Fonseca Benedito Antonio Lopes da. Characterization of the immune response following in vitro mayaro and chikungunya viruses (Alphavirus, Togaviridae) infection of mononuclear cells. *Virus Research*, 256:166–173, 9 2018.

[23] Sarah A. Steer and John A. Corbett. The Role and Regulation of COX-2 during Viral Infection. *Viral Immunology*, 16(4):447–460, 2003.

[24] Ruo Yan Ong, Fok Moon Lum, and Lisa F.P. Ng. The Fine Line between Protection and Pathology in Neurotropic Flavivirus and Alphavirus Infections. *Future Virology*, 9(3):313–330, 2014.

[25] Kate D. Ryman and William B. Klimstra. Host responses to alphavirus infection. *Immunological Reviews*, 225(1):27–45, 10 2008.

[26] Sathya Prakash Manimunda, Paluru Vijayachari, Raghuraj Uppoor, Attayur Purushottaman Sugunan, Shiv Shankar Singh, Subhodh Kumar Rai, Anakkathil Balan Sudeep, Nagarajan Muruganandam, Itta Krishna Chaitanya, and Dev Reddy Guruprasad. Clinical progression of chikungunya fever during acute and chronic arthritic stages and the changes in joint morphology as revealed by imaging. *Transactions of the Royal Society of Tropical Medicine and Hygiene*, 104(6):392–399, 6 2010.

[27] A. Economopoulou, M. Dominguez, B. Helynck, D. Sissoko, O. Wichmann, P. Quenel, P. Germonneau, and I. Quatresous. Atypical Chikungunya virus infections: Clinical manifestations, mortality and risk factors for severe disease during the 2005-2006 outbreak on Réunion. *Epidemiology and Infection*, 137(4):534–541, 2009.

[28] Babasaheb V. Tandale, Padmakar S. Sathe, Vidya A. Arankalle, R. S. Wadia, Rahul Kulkarni, Sudhir V. Shah, Sanjeev K. Shah, Jay K. Sheth, A. B. Sudeep, Anuradha S. Tripathy, and Akhilesh C. Mishra. Systemic involvements and fatalities during Chikungunya epidemic in India, 2006. *Journal of Clinical Virology*, 46(2):145–149, 10 2009.

[29] Juan M. de la Hoz, Brayan Bayona, Samir Viloria, José L. Accini, Homero San Juan-Vergara, and Diego Viasus. Fatal cases of Chikungunya virus infection in Colombia: Diagnostic and treatment challenges. *Journal of Clinical Virology*, 69:27–29, 8 2015.

[30] Marcela Mercado, Jorge Acosta-Reyes, Edgar Parra, Luis Guzmán, Mauricio Beltrán, Philippe Gasque, Carlos Mejía-García, and Diego Viasus. Renal involvement in fatal cases of chikungunya virus infection. *Journal of Clinical Virology*, 103:16–18, 6 2018.

[31] Yasmina Touret, Hanitra Randrianaivo, Alain Michault, Isabelle Schuffenecker, Edouard Kauffmann, Yann Lenglet, Georges Barau, and Alain Fourmaintraux. Early maternal-fetal transmission of the Chikungunya virus. *Presse Medicale*, 35(11 I):1656–1658, 2006.

[32] Patrick Gérardin, Georges Barau, Alain Michault, Marc Bintner, Hanitra Randrianaivo, Ghassan Choker, Yann Lenglet, Yasmina Touret, Anne Bouveret, Philippe Grivard, Karin Le Roux, Séverine Blanc, Isabelle Schuffenecker, Thérèse Couderc, Fernando Arenzana-Seisdedos, Marc Lecuit, and Pierre Yves Robillard. Multidisciplinary prospective study of mother-to-child chikungunya virus infections on the island of La Réunion. *PLoS Medicine*, 5(3):0413–0423, 3 2008.

[33] Kathryn S. Carpentier and Thomas E. Morrison. Innate immune control of alphavirus infection. *Current Opinion in Virology*, 28:53–60, 2 2018.

[34] Natasha M. Kafai, Michael S. Diamond, and Julie M. Fox. Distinct Cellular Tropism and Immune Responses to Alphavirus Infection. *Annual Review of Immunology*, 40:615–649, 2022.

[35] Martin Schlee and Gunther Hartmann. Discriminating self from non-self in nucleic acid sensing. *Nature Reviews Immunology*, 16(9):566–580, 8 2016.

[36] Lea Marie Jenster, Karl Elmar Lange, Sabine Normann, Anja Vom Hemdt, Jennifer D. Wuerth, Lisa D.J. Schiffelers, Yonas M. Tesfamariam, Florian N. Gohr, Laura Klein, Ines H. Kaltheuner, Stefan Ebner, Dorothee J. Lapp, Jacob Mayer, Jonas Moecking, Hidde L. Ploegh, Eicke Latz, Felix Meissner, Matthias Geyer, Beate M. Kümmerer, and Florian I. Schmidt. P38 kinases mediate NLRP1 inflammasome activation after ribotoxic stress response and virus infection. *Journal of Experimental Medicine*, 220(1), 1 2023.

[37] Nadia Wauquier, Pierre Becquart, Dieudonné Nkoghe, Cindy Padilla, Angélique Ndjoyi-Mbiguino, and Eric M. Leroy. The acute phase of Chikungunya virus infection in humans is associated with strong innate immunity and T CD8 cell activation. *Journal of Infectious Diseases*, 204(1):115–123, 7 2011.

[38] Cinthia Nóbrega de Sousa Dias, Bruna Macêdo Gois, Viviane Silva Lima, Isabel Cristina Guerra-Gomes, Josélio Maria Galvão Araújo, Juliana de Assis Silva Gomes, Demétrius Antônio Machado Araújo, Isac Almeida Medeiros, Fátima de Lourdes Assunção Araújo de Azevedo, Robson Cavalcanti Veras, Daniele Idalino Janebro, Ian Porto Gurgel do Amaral, and Tatjana Souza Lima Keesen. Human CD8 T-cell activation in acute and chronic chikungunya infection. *Immunology*, 155(4):499–504, 12 2018.

[39] Bennett J. Davenport, Christopher Bullock, Mary K. McCarthy, David W. Hawman, Kenneth M. Murphy, Ross M. Kedl, Michael S. Diamond, and Thomas E. Morrison. Chikungunya Virus Evades Antiviral CD8 + T Cell

Responses To Establish Persistent Infection in Joint-Associated Tissues . *Journal of Virology*, 94(9), 4 2020.

[40] May La Linn, L. Mateo, J. Gardner, and A. Suhrbier. Alphavirus-Specific Cytotoxic T Lymphocytes Recognize a Cross-Reactive Epitope from the Capsid Protein and Can Eliminate Virus from Persistently Infected Macrophages. *Journal of Virology*, 72(6):5146–5153, 6 1998.

[41] Jayme A. Souza-Neto, Shuzhen Sim, and George Dimopoulos. An evolutionary conserved function of the JAK-STAT pathway in anti-dengue defense. *Proceedings of the National Academy of Sciences of the United States of America*, 106(42):17841–17846, 10 2009.

[42] Jonathan C. Rupp, Kevin J. Sokoloski, Natasha N. Gebhart, and Richard W. Hardy. Alphavirus RNA synthesis and non-structural protein functions. *The Journal of General Virology*, 96(Pt 9):2483, 9 2015.

[43] Joyce Jose, Aaron B. Taylor, and Richard J. Kuhn. Spatial and temporal analysis of alphavirus replication and assembly in mammalian and mosquito cells. *mBio*, 8(1), 1 2017.

[44] Ofer Zimmerman, Autumn C. Holmes, Natasha M. Kafai, Lucas J. Adams, and Michael S. Diamond. Entry receptors — the gateway to alphavirus infection. *The Journal of Clinical Investigation*, 133(2):e165307, 1 2023.

[45] Joyce Jose, Jonathan E. Snyder, and Richard Kuhn. A structural and functional perspective of alphavirus replication and assembly. *Future Microbiology*, 4(7):837–856, 2009.

[46] Luis Carrasco, Miguel Angel Sanz, and Esther González-Almela. The Regulation of Translation in Alphavirus-Infected Cells. *Viruses*, 10(2):70, 2 2018.

[47] Liming Zhang, Yibin Zhu, and Gong Cheng. Comparison of innate immune responses against arboviruses in mammalian hosts and mosquito vectors. *hLife*, 3(6):258–274, 6 2025.

[48] Ralph E Harbach. The Culicidae (Diptera): a review of taxonomy, classification and phylogeny*. *Zootaxa*, 1668:591–638, 2007.

[49] Norbert Becker, Dušan Petrić, Marija Zgomba, Clive Boase, Minoo B. Madon, Christine Dahl, and Achim Kaiser. Mosquitoes. 2020.

[50] Frances M. Hawkes and Richard J. Hopkins. The mosquito. *Mosquitopia*, pages 16–31, 7 2022.

[51] Moritz U.G. Kraemer, Robert C. Reiner, Oliver J. Brady, Jane P. Messina, Marius Gilbert, David M. Pigott, Dingdong Yi, Kimberly Johnson, Lucas Earl, Laurie B. Marczak, Shreya Shirude, Nicole Davis Weaver, Donal Bisanzio, T. Alex Perkins, Shengjie Lai, Xin Lu, Peter Jones, Giovanini E. Coelho, Roberta G. Carvalho, Wim Van Bortel, Cedric Marsboom, Guy Hendrickx, Francis Schaffner, Chester G. Moore, Heinrich H. Nax, Linus Bengtsson, Erik Wetter, Andrew J. Tatem, John S. Brownstein, David L. Smith, Louis Lambrechts, Simon Cauchemez, Catherine Linard, Nuno R. Faria, Oliver G. Pybus, Thomas W. Scott, Qiyong Liu, Hongjie Yu, G. R.William Wint, Simon I. Hay, and Nick Golding. Publisher Correction: Past and future spread of the arbovirus vectors Aedes aegypti and Aedes albopictus. *Nature Microbiology*, 4(5):900, 5 2019.

[52] Giovanni Benelli, André B.B. Wilke, and John C. Beier. Aedes albopictus (Asian Tiger Mosquito). *Trends in Parasitology*, 36(11):942–943, 11 2020.

[53] Moritz U.G. Kraemer, Marianne E. Sinka, Kirsten A. Duda, Adrian Q.N. Mylne, Freya M. Shearer, Christopher M. Barker, Chester G. Moore, Roberta G. Carvalho, Giovanini E. Coelho, Wim Van Bortel, Guy Hendrickx, Francis Schaffner, Iqbal Rf Elyazar, Hwa Jen Teng, Oliver J. Brady, Jane P. Messina, David M. Pigott, Thomas W. Scott, David L. Smith, G. R. William Wint, Nick Golding, and Simon I. Hay. The global distribution of the arbovirus vectors Aedes aegypti and Ae. albopictus. *eLife*, 4(JUNE2015):e08347, 6 2015.

[54] Jesús Veiga, Mario Garrido, Marta Garrigós, Carolina R.F. Chagas, and Josué

Martínez-de la Puente. A Literature Review on the Role of the Invasive Aedes albopictus in the Transmission of Avian Malaria Parasites. *Animals 2024, Vol. 14, Page 2019*, 14(14):2019, 7 2024.

[55] A.N. Clements. The Biology of Mosquitoes, Volume 2: Sensory Reception and Behaviour. *The Biology of Mosquitoes, Volume 2: Sensory Reception and Behaviour*, 6 1999.

[56] Marco Pombi and Fabrizio Montarsi. Mosquitoes (Culicidae). *Encyclopedia of Infection and Immunity: Volumes 1-4*, 2:801–818, 1 2022.

[57] Gabriella Gibson, Ben Warren, and Ian J. Russell. Humming in tune: Sex and species recognition by mosquitoes on the wing. *JARO - Journal of the Association for Research in Otolaryngology*, 11(4):527–540, 12 2010.

[58] Lauren J. Cator, Ben J. Arthur, Laura C. Harrington, and Ronald R. Hoy. Harmonic convergence in the love songs of the dengue vector mosquito. *Science*, 323(5917):1077–1079, 2 2009.

[59] Laura D. Kramer and Alexander T. Ciota. Dissecting vectorial capacity for mosquito-borne viruses. *Current opinion in virology*, 15:112, 12 2015.

[60] Solène Cottis, Adrien A. Blisnick, Anna Bella Failloux, and Kenneth D. Vernick. Determinants of Chikungunya and O'nyong-Nyong Virus Specificity for Infection of Aedes and Anopheles Mosquito Vectors. *Viruses*, 15(3), 3 2023.

[61] Ankit Kumar, Priyanshu Srivastava, P. D.N.N. Sirisena, Sunil Kumar Dubey, Ramesh Kumar, Jatin Shrinet, and Sujatha Sunil. Mosquito Innate Immunity. *Insects*, 9(3):1000097, 9 2018.

[62] Samuel H Lewis, Heli Salmela, and Darren J Obbard. Duplication and Diversification of Dipteran Argonaute Genes, and the Evolutionary Divergence of Piwi and Aubergine.

[63] Pascal Miesen, Erika Girardi, and Ronald P Van Rij. Distinct sets of PIWI proteins produce arbovirus and transposon-derived piRNAs in Aedes aegypti

mosquito cells. *Nucleic Acids Research*, 43(13):6545–6556, 2015.

[64] Natapong Jupatanakul, Shuzhen Sim, Yesseinia I. Angleró-Rodríguez, Jayme Souza-Neto, Suchismita Das, Kristin E. Poti, Shannan L. Rossi, Nicholas Bergren, Nikos Vasilakis, and George Dimopoulos. Engineered Aedes aegypti JAK/STAT Pathway-Mediated Immunity to Dengue Virus. *PLOS Neglected Tropical Diseases*, 11(1):e0005187, 1 2017.

[65] Yesseinia I. Angleró-Rodríguez, Hannah J. MacLeod, Seokyoung Kang, Jenny S. Carlson, Natapong Jupatanakul, and George Dimopoulos. Aedes aegypti molecular responses to Zika Virus: Modulation of infection by the toll and Jak/Stat immune pathways and virus host factors. *Frontiers in Microbiology*, 8(OCT):288406, 10 2017.

[66] Gee W. Lau, Boyan C. Goumnerov, Cynthia L. Walendziewicz, Jennifer Hewitson, Wenzhong Xiao, Shalina Mahajan-Miklos, Ronald G. Tompkins, Lizabeth A. Perkins, and Laurence G. Rahme. The Drosophila melanogaster toll pathway participates in resistance to infection by the gram-negative human pathogen Pseudomonas aeruginosa. *Infection and Immunity*, 71(7):4059–4066, 7 2003.

[67] Woon Shin Sang, Vladimir Kokoza, Guowu Bian, Hyang Mi Cheon, Jung Kim Yu, and Alexander S. Raikhel. REL1, a Homologue of Drosophila Dorsal, Regulates Toll Antifungal Immune Pathway in the Female Mosquito Aedes aegypti. *Journal of Biological Chemistry*, 280(16):16499–16507, 4 2005.

[68] Alexander N.R. Weber, Servane Tauszig-Delamasure, Jules A. Hoffmann, Eric Lelièvre, Hugues Gascan, Keith P. Ray, Mary A. Morse, Jean Luc Imler, and Nicholas J. Gay. Binding of the Drosophila cytokine Spätzle to Toll is direct and establishes signaling. *Nature Immunology*, 4(8):794–800, 8 2003.

[69] Susanna Valanne, Jing-Huan Wang, and Mika Rämet. The Drosophila Toll Signaling Pathway. *The Journal of Immunology*, 186(2):649–656, 1 2011.

[70] Zhiyong Xi, Jose L. Ramirez, and George Dimopoulos. The Aedes aegypti toll pathway controls dengue virus infection. *PLoS Pathogens*, 4(7), 7 2008.

[71] Jose L. Ramirez and George Dimopoulos. The Toll immune signaling pathway control conserved anti-dengue defenses across diverse Ae. aegypti strains and against multiple dengue virus serotypes. *Developmental & Comparative Immunology*, 34(6):625–629, 6 2010.

[72] Melanie Mcfarlane, Camilo Arias-Goeta, Estelle Martin 2¤, Zoe O'hara, Aleksei Lulla, Laurence Mousson, Stephanie M Rainey, Suzana Misbah, Esther Schnettler, Claire L Donald, Andres Merits, Alain Kohl, Anna-Bella Failloux, and Eva Harris. Characterization of Aedes aegypti Innate-Immune Pathways that Limit Chikungunya Virus Replication.

[73] Gunter Meister and Thomas Tuschl. Mechanisms of gene silencing by double-stranded RNA. *Nature*, 431(7006):343–349, 9 2004.

[74] Natthanej Luplertlop, Pornapat Surasombatpattana, Degrees Patramool, Emilie Dumas, Ladawan Wasinpiyamongkol, Laure Saune, Rodolphe Hamel, Eric Bernard, Denis Sereno, Frédé Ric Thomas, David Piquemal, Hans Yssel, Laurence Briant, and Dorothée Missé. Induction of a Peptide with Activity against a Broad Spectrum of Pathogens in the Aedes aegypti Salivary Gland, following Infection with Dengue Virus. *PLoS Pathogens*, 7(1):e1001252, 1 2011.

[75] Ana Beatriz Ferreira Barletta, Maria Clara L. Nascimento-Silva, Octávio A.C. Talyuli, José Henrique M. Oliveira, Luiza Oliveira Ramos Pereira, Pedro L. Oliveira, and Marcos Henrique F. Sorgine. Microbiota activates IMD pathway and limits Sindbis infection in Aedes aegypti. *Parasites and Vectors*, 10(1):1–9, 2 2017.

[76] Prasad N. Paradkar, Lee Trinidad, Rhonda Voysey, Jean Bernard Duchemin, and Peter J. Walker. Secreted Vago restricts West Nile virus infection in Culex mosquito cells by activating the Jak-STAT pathway. *Proceedings of the National*

Academy of Sciences of the United States of America, 109(46):18915–18920, 11 2012.

[77] Jie Xu, Kaycie Hopkins, Leah Sabin, Ari Yasunaga, Harry Subramanian, Ian Lamborn, Beth Gordesky-Gold, and Sara Cherry. ERK signaling couples nutrient status to antiviral defense in the insect gut. *Proceedings of the National Academy of Sciences of the United States of America*, 110(37):15025–15030, 9 2013.

[78] Laura R.H. Ahlers, Chasity E. Trammell, Grace F. Carrell, Sophie Mackinnon, Brandi K. Torrevillas, Clement Y. Chow, Shirley Luckhart, and Alan G. Goodman. Insulin Potentiates JAK/STAT Signaling to Broadly Inhibit Flavivirus Replication in Insect Vectors. *Cell Reports*, 29(7):1946–1960, 11 2019.

[79] Christine L. Sansone, Jonathan Cohen, Ari Yasunaga, Jie Xu, Greg Osborn, Harry Subramanian, Beth Gold, Nicolas Buchon, and Sara Cherry. Microbiota-Dependent Priming of Antiviral Intestinal Immunity in Drosophila. *Cell Host & Microbe*, 18(5):571–581, 11 2015.

[80] Eric P. Caragata, Chinmay V. Tikhe, and George Dimopoulos. Curious entanglements: interactions between mosquitoes, their microbiota, and arboviruses. *Current Opinion in Virology*, 37:26–36, 8 2019.

[81] Avisha Chowdhury, Cassandra M. Modahl, Siok Thing Tan, Benjamin Wong Wei Xiang, Dorothée Missé, Thomas Vial, R. Manjunatha Kini, and Julien Francis Pompon. JNK pathway restricts DENV2, ZIKV and CHIKV infection by activating complement and apoptosis in mosquito salivary glands. *PLoS Pathogens*, 16(8):e1008754, 8 2020.

[82] Xiaoping Xiao, Yang Liu, Xiaoyan Zhang, Jing Wang, Zuofeng Li, Xiaojing Pang, Penghua Wang, and Gong Cheng. Complement-Related Proteins Control the Flavivirus Infection of Aedes aegypti by Inducing Antimicrobial Peptides. *PLOS Pathogens*, 10(4):e1004027, 2014.

[83] Cara West and Neal Silverman. p38b and JAK-STAT signaling protect against

Invertebrate iridescent virus 6 infection in Drosophila. *PLOS Pathogens*, 14(5):e1007020, 5 2018.

[84] Bo Wang, Nazzy Pakpour, Eleonora Napoli, Anna Drexler, Elizabeth K.K. Glennon, Win Surachetpong, Kong Cheung, Alejandro Aguirre, John M. Klyver, Edwin E. Lewis, Richard Eigenheer, Brett S. Phinney, Cecilia Giulivi, and Shirley Luckhart. Anopheles stephensi p38 MAPK signaling regulates innate immunity and bioenergetics during Plasmodium falciparum infection. *Parasites and Vectors*, 8(1):1–21, 8 2015.

[85] R. Chen-Chih Wu, M. F. Shaio, and W. L. Cho. A p38 MAP kinase regulates the expression of the Aedes aegypti defensin gene in mosquito cells. *Insect Molecular Biology*, 16(4):389–399, 8 2007.

[86] Alice E. Moon, Anthony J. Walker, and Stephen Goodbourn. Regulation of transcription of the Aedes albopictus cecropin A1 gene: A role for p38 mitogen-activated protein kinase. *Insect Biochemistry and Molecular Biology*, 41(8):628–636, 8 2011.

[87] Cláudio Antônio de Moura Pereira, Renata Pessôa Germano Mendes, Poliana Gomes da Silva, Elton José Ferreira Chaves, and Lindomar José Pena. Vaccines Against Urban Epidemic Arboviruses: The State of the Art. *Viruses*, 17(3):382, 3 2025.

[88] Hudson Onen, Miryam M. Luzala, Stephen Kigozi, Rebecca M. Sikumbili, Claude Josué K. Muanga, Eunice N. Zola, Sébastien N. Wendji, Aristote B. Buya, Aiste Balciunaitiene, Jonas Viškelis, Martha A. Kaddumukasa, and Patrick B. Memvanga. Mosquito-Borne Diseases and Their Control Strategies: An Overview Focused on Green Synthesized Plant-Based Metallic Nanoparticles. *Insects*, 14(3):221, 3 2023.

[89] Samson T. Ogunlade, Michael T. Meehan, Adeshina I. Adekunle, Diana P. Rojas, Oyelola A. Adegboye, and Emma S. McBryde. A Review: Aedes-Borne Arboviral

Infections, Controls and Wolbachia-Based Strategies. *Vaccines 2021, Vol. 9, Page 32*, 9(1):32, 1 2021.

[90] W. W. Han, A. Lazaro, P. J. Mccall, L. George, S. Runge-Ranzinger, J. Toledo, R. Velayudhan, and O. Horstick. Efficacy and community effectiveness of larvivorous fish for dengue vector control. *Tropical Medicine and International Health*, 20(9):1239–1256, 9 2015.

[91] Magnus Land, Mirco Bundschuh, Richard J. Hopkins, Brigitte Poulin, and Brendan G. McKie. Effects of mosquito control using the microbial agent Bacillus thuringiensis israelensis (Bti) on aquatic and terrestrial ecosystems: a systematic review. *Environmental Evidence*, 12(1), 12 2023.

[92] Denis Voronin, Darren A.N. Cook, Andrew Steven, and Mark J. Taylor. Autophagy regulates Wolbachia populations across diverse symbiotic associations. *Proceedings of the National Academy of Sciences of the United States of America*, 109(25), 6 2012.

[93] Joseph Kamtchum-Tatuene, Benjamin L. Makepeace, Laura Benjamin, Matthew Baylis, and Tom Solomon. The potential role of Wolbachia in controlling the transmission of emerging human arboviral infections. *Current Opinion in Infectious Diseases*, 30(1):108–116, 2017.

[94] Pune Thomas, Nichola Kenny, Darryl Eyles, Luciano A. Moreira, Scott L. O'Neill, and Sassan Asgari. Infection with the wMel and wMelPop strains of Wolbachia leads to higher levels of melanization in the hemolymph of Drosophila melanogaster, Drosophila simulans and Aedes aegypti. *Developmental and Comparative Immunology*, 35(3):360–365, 2011.

[95] Mazhar Hussain, Francesca D. Frentiu, Luciano A. Moreira, Scott L. O'Neill, and Sassan Asgari. Wolbachia uses host microRNAs to manipulate host gene expression and facilitate colonization of the dengue vector Aedes aegypti. *Proceedings of the National Academy of Sciences of the United States of America*, 108(22):9250–9255, 5 2011.

[96] Cameron P Simmons, Jeremy J Farrar, Nguyen van Vinh Chau, Bridget Wills, Ben Ham Tu, and Ho Chi Minh City. Dengue. *New England Journal of Medicine*, 366(15):1423–1432, 4 2012.

[97] Rachel Morreale, Danilo O. Carvalho, Steven Stenhouse, Johanna Bajonero, Rui Pereira, Daniel A. Hahn, Aaron Lloyd, and David F. Hoel. Suppression of Aedes aegypti by the sterile insect technique on Captiva Island, Florida, USA from 2020 to 2022. *PLOS Neglected Tropical Diseases*, 19(7):e0013256, 7 2025.

[98] Adi Utarini, Citra Indriani, Riris A. Ahmad, Warsito Tantowijoyo, Eggi Arguni, M. Ridwan Ansari, Endah Supriyati, D. Satria Wardana, Yeti Meitika, Inggrid Ernesia, Indah Nurhayati, Equatori Prabowo, Bekti Andari, Benjamin R. Green, Lauren Hodgson, Zoe Cutcher, Edwige Rancès, Peter A. Ryan, Scott L. O'Neill, Suzanne M. Dufault, Stephanie K. Tanamas, Nicholas P. Jewell, Katherine L. Anders, and Cameron P. Simmons. Efficacy of Wolbachia-Infected Mosquito Deployments for the Control of Dengue. *New England Journal of Medicine*, 384(23):2177–2186, 6 2021.

[99] Cynthia E. Schairer, James Najera, Anthony A. James, Omar S. Akbari, and Cinnamon S. Bloss. Oxitec and MosquitoMate in the United States: lessons for the future of gene drive mosquito control. *Pathogens and Global Health*, 115(6):365, 2021.

[100] Paulo Paes De Andrade, Francisco José Lima Aragão, Walter Colli, Odir Antônio Dellagostin, Flávio Finardi-Filho, Mario Hiroyuki Hirata, Amaro De Castro Lira-Neto, Marcia Almeida De Melo, Alexandre Lima Nepomuceno, Francisco Gorgônio Da Nóbrega, Gutemberg Delfino De Sousa, Fernando Hercos Valicente, and Maria Helena Bodanese Zanettini. Use of transgenic Aedes aegypti in Brazil: risk perception and assessment. *Bulletin of the World Health Organization*, 94(10):766, 10 2016.

[101] Manuel Garcia-Moreno, Marko Noerenberg, Shuai Ni, Aino I. Järvelin, Esther González-Almela, Caroline E. Lenz, Marcel Bach-Pages, Victoria Cox, Rosario

Avolio, Thomas Davis, Svenja Hester, Thibault J.M. Sohier, Bingnan Li, Gregory Heikel, Gracjan Michlewski, Miguel A. Sanz, Luis Carrasco, Emiliano P. Ricci, Vicent Pelechano, Ilan Davis, Bernd Fischer, Shabaz Mohammed, and Alfredo Castello. System-wide Profiling of RNA-Binding Proteins Uncovers Key Regulators of Virus Infection. *Molecular cell*, 74(1):196–211, 4 2019.

[102] Wael Kamel, Vincenzo Ruscica, Manuel Garcia-Moreno, Natasha Palmalux, Louisa Iselin, Maximilian Hannan, Aino Järvelin, Marko Noerenberg, Samantha Moore, Andres Merits, Ilan Davis, Javier Martinez, Shabaz Mohammed, and Alfredo Castello. Compositional analysis of Sindbis virus ribonucleoproteins reveals an extensive co-opting of key nuclear RNA-binding proteins. *bioRxiv*, page 2021.10.06.463336, 10 2021.

[103] Wael Kamel, Vincenzo Ruscica, Azman Embarc-Buh, Zaydah R. de Laurent, Manuel Garcia-Moreno, Yana Demyanenko, Richard J. Orton, Marko Noerenberg, Meghana Madhusudhan, Louisa Iselin, Aino I. Järvelin, Maximilian Hannan, Eduardo Kitano, Samantha Moore, Andres Merits, Ilan Davis, Shabaz Mohammed, and Alfredo Castello. Alphavirus infection triggers selective cytoplasmic translocation of nuclear RBPs with moonlighting antiviral roles. *Molecular Cell*, 84(24):4896–4911, 12 2024.

[104] Tina Glisovic, Jennifer L. Bachorik, Jeongsik Yong, and Gideon Dreyfuss. RNA-binding proteins and post-transcriptional gene regulation. *FEBS letters*, 582(14):1977, 6 2008.

[105] Bradley M Lunde, Claire Moore, and Gabriele Varani. RNA-binding proteins: modular design for efficient function. *Nat Rev Mol Cell Biol*, 2007.

[106] Alfredo Castello, Bernd Fischer, Christian K. Frese, Rastislav Horos, Anne Marie Alleaume, Sophia Foehr, Tomaz Curk, Jeroen Krijgsveld, and Matthias W. Hentze. Comprehensive Identification of RNA-Binding Domains in Human Cells. *Molecular Cell*, 63(4):696, 8 2016.

[107] Vasiliy O. Sysoev, Bernd Fischer, Christian K. Frese, Ishaan Gupta, Jeroen

Krijgsveld, Matthias W. Hentze, Alfredo Castello, and Anne Ephrussi. Global changes of the RNA-bound proteome during the maternal-to-zygotic transition in Drosophila. *Nature Communications 2016 7:1*, 7(1):1–11, 7 2016.

[108] Debashish Ray, Kaitlin U Laverty, Arttu Jolma, Kate Nie, Reuben Samson, Sara E Pour, Cyrus L Tam, Niklas Von Krosigk, Syed Nabeel-Shah, Mihai Albu, Hong Zheng, Gabrielle Perron, Hyunmin Lee, Hamed Najafabadi, Benjamin Blencowe, Jack Greenblatt, Quaid Morris, and Timothy R Hughes. RNA-binding proteins that lack canonical RNA-binding domains are rarely sequence-specific. 123.

[109] Nicole J. Curtis and Constance J. Jeffery. The expanding world of metabolic enzymes moonlighting as RNA binding proteins. *Biochemical Society Transactions*, 49(3):1099–1108, 6 2021.

[110] Alfredo Castello, Matthias W. Hentze, and Thomas Preiss. Metabolic Enzymes Enjoying New Partnerships as RNA-Binding Proteins. *Trends in Endocrinology and Metabolism*, 26(12):746, 12 2015.

[111] Tim Schulte, Lifeng Liu, Marc D. Panas, Bastian Thaa, Nicole Dickson, Benjamin Götte, Adnane Achour, and Gerald M. McInerney. Combined structural, biochemical and cellular evidence demonstrates that both FGDF motifs in alphavirus nsP3 are required for efficient replication. *Open Biology*, 6(7):160078, 7 2016.

[112] Shih-Chia Yeh, Mayra Diosa-Toro, Wei-Lian Tan, Florian Rachenne, Arthur Hain, Celestia Pei Xuan Yeo, Inès Bribes, Benjamin Wong Wei Xiang, Gayathiri Sathiamoorthy Kannan, Menchie Casayuran Manuel, Dorothé Missé, Yu Keung Mok, and Julien ID Pompon. Characterization of dengue virus 3'UTR RNA binding proteins in mosquitoes reveals that AeStaufen reduces subgenomic flaviviral RNA in saliva. *PLOS Pathogens*, 18(9):e1010427, 9 2022.

[113] Wael Kamel, Marko Noerenberg, Berati Cerikan, Honglin Chen, Aino I. Järvelin, Mohamed Kammoun, Jeffrey Y. Lee, Ni Shuai, Manuel Garcia-Moreno, Anna

Andrejeva, Michael J. Deery, Natasha Johnson, Christopher J. Neufeldt, Mirko Cortese, Michael L. Knight, Kathryn S. Lilley, Javier Martinez, Ilan Davis, Ralf Bartenschlager, Shabaz Mohammed, and Alfredo Castello. Global analysis of protein-RNA interactions in SARS-CoV-2-infected cells reveals key regulators of infection. *Molecular cell*, 81(13):2851–2867, 7 2021.

[114] Stefano Bonazza, Hannah Leigh Coutts, Swathi Sukumar, Hannah Louise Turkington, and David Gary Courtney. Identifying cellular RNA-binding proteins during infection uncovers a role for MKRN2 in influenza mRNA trafficking. *PLOS Pathogens*, 20(5):e1012231, 5 2024.

[115] Sungyul Lee, Young suk Lee, Yeon Choi, Ahyeon Son, Youngran Park, Kyung Min Lee, Jeesoo Kim, Jong Seo Kim, and V. Narry Kim. The SARS-CoV-2 RNA interactome. *Molecular Cell*, 81(13):2838–2850, 7 2021.

[116] Nikoleta G. Tsvetanova, Daniel M. Klass, Julia Salzman, and Patrick O. Brown. Proteome-Wide Search Reveals Unexpected RNA-Binding Proteins in Saccharomyces cerevisiae. *PLOS ONE*, 5(9):e12671, 2010.

[117] Tanja Scherrer, Nitish Mittal, Sarath Chandra Janga, and Andre P. Gerber. A Screen for RNA-Binding Proteins in Yeast Indicates Dual Functions for Many Enzymes. *PLOS ONE*, 5(11):e15499, 2010.

[118] Falk Butter, Marion Scheibe, Mario Mörl, and Matthias Mann. Unbiased RNA-protein interaction screen by quantitative proteomics. *Proceedings of the National Academy of Sciences of the United States of America*, 106(26):10626–10631, 6 2009.

[119] Alfredo Castello, Bernd Fischer, Katrin Eichelbaum, Rastislav Horos, Benedikt M. Beckmann, Claudia Strein, Norman E. Davey, David T. Humphreys, Thomas Preiss, Lars M. Steinmetz, Jeroen Krijgsveld, and Matthias W. Hentze. Insights into RNA Biology from an Atlas of Mammalian mRNA-Binding Proteins. *Cell*, 149(6):1393–1406, 6 2012.

[120] Alexander G. Baltz, Mathias Munschauer, Björn Schwanhäusser, Alexandra

Vasile, Yasuhiro Murakawa, Markus Schueler, Noah Youngs, Duncan Penfold-Brown, Kevin Drew, Miha Milek, Emanuel Wyler, Richard Bonneau, Matthias Selbach, Christoph Dieterich, and Markus Landthaler. The mRNA-bound proteome and its global occupancy profile on protein-coding transcripts. *Molecular cell*, 46(5):674–690, 6 2012.

[121] Joel I. Perez-Perri, Dunja Ferring-Appel, Ina Huppertz, Thomas Schwarzl, Sudeep Sahadevan, Frank Stein, Mandy Rettel, Bruno Galy, and Matthias W. Hentze. The RNA-binding protein landscapes differ between mammalian organs and cultured cells. *Nature Communications*, 14(1):2074, 12 2023.

[122] Benedikt M. Beckmann, Rastislav Horos, Bernd Fischer, Alfredo Castello, Katrin Eichelbaum, Anne Marie Alleaume, Thomas Schwarzl, Tomaž Curk, Sophia Foehr, Wolfgang Huber, Jeroen Krijgsveld, and Matthias W. Hentze. The RNA-binding proteomes from yeast to man harbour conserved enigmRBPs. *Nature Communications*, 6, 12 2015.

[123] Alex M. Tamburino, Sean P. Ryder, and Albertha J.M. Walhout. A compendium of Caenorhabditis elegans RNA binding proteins predicts extensive regulation at multiple levels. *G3: Genes, Genomes, Genetics*, 3(2):297–304, 2013.

[124] Ana M. Matia-González, Emma E. Laing, and André P. Gerber. Conserved mRNA-binding proteomes in eukaryotic organisms. *Nature Structural and Molecular Biology*, 22(12):1027–1033, 12 2015.

[125] Vladimir Despic, Mario Dejung, Mengting Gu, Jayanth Krishnan, Jing Zhang, Lydia Herzel, Korinna Straube, Mark B. Gerstein, Falk Butter, and Karla M. Neugebauer. Dynamic RNA-protein interactions underlie the zebrafish maternal-to-zygotic transition. *Genome Research*, 27(7):1184–1194, 7 2017.

[126] Marlene Reichel, Yalin Liao, Mandy Rettel, Chikako Ragan, Maurits Evers, Anne Marie Alleaume, Rastislav Horos, Matthias W. Hentze, Thomas Preiss, and Anthony A. Millar. In planta determination of the mRNA-binding proteome of arabidopsis etiolated seedlings. *Plant Cell*, 28(10):2435–2452, 10 2016.

[127] Zhicheng Zhang, Kurt Boonen, Piero Ferrari, Liliane Schoofs, Ewald Janssens, Vera Noort, Filip Rolland, and Koen Geuten. UV crosslinked mRNA-binding proteins captured from leaf mesophyll protoplasts. *Plant Methods*, 12(1), 11 2016.

[128] Claudius Marondedze, Ludivine Thomas, Natalia L. Serrano, Kathryn S. Lilley, and Chris Gehring. The RNA-binding protein repertoire of Arabidopsis thaliana. *Scientific Reports*, 6:29766, 7 2016.

[129] Evelien M. Bunnik, Gayani Batugedara, Anita Saraf, Jacques Prudhomme, Laurence Florens, and Karine G. Le Roch. The mRNA-bound proteome of the human malaria parasite Plasmodium falciparum. *Genome Biology*, 17(1):147, 7 2016.

[130] Devki Nandan, Sneha A. Thomas, Anne Nguyen, Kyung Mee Moon, Leonard J. Foster, and Neil E. Reiner. Comprehensive Identification of mRNA-Binding Proteins of Leishmania donovani by Interactome Capture. *PLoS ONE*, 12(1):e0170068, 1 2017.

[131] Matthias W. Hentze, Alfredo Castello, Thomas Schwarzl, and Thomas Preiss. A brave new world of RNA-binding proteins. *Nature Reviews Molecular Cell Biology*, 19(5):327–341, 5 2018.

[132] Roosje Van Ende, Sam Balzarini, and Koen Geuten. Single and Combined Methods to Specifically or Bulk-Purify RNA–Protein Complexes. *Biomolecules 2020, Vol. 10, Page 1160*, 10(8):1160, 8 2020.

[133] Xichen Bao, Xiangpeng Guo, Menghui Yin, Muqddas Tariq, Yiwei Lai, Shahzina Kanwal, Jiajian Zhou, Na Li, Yuan Lv, Carlos Pulido-Quetglas, Xiwei Wang, Lu Ji, Muhammad J. Khan, Xihua Zhu, Zhiwei Luo, Changwei Shao, Do Hwan Lim, Xiao Liu, Nan Li, Wei Wang, Minghui He, Yu Lin Liu, Carl Ward, Tong Wang, Gong Zhang, Dongye Wang, Jianhua Yang, Yiwen Chen, Chaolin Zhang, Ralf Jauch, Yun Gui Yang, Yangming Wang, Baoming Qin, Minna Liisa Anko, Andrew P. Hutchins, Hao Sun, Huating Wang, Xiang Dong Fu, Biliang Zhang,

and Miguel A. Esteban. Capturing the interactome of newly transcribed RNA. *Nature Methods*, 15(3):213–220, 3 2018.

[134] Rongbing Huang, Mengting Han, Liying Meng, and Xing Chen. Capture and Identification of RNA-binding Proteins by Using Click Chemistry-assisted RNA-interactome Capture (CARIC) Strategy. *Journal of Visualized Experiments : JoVE*, 2018(140):58580, 10 2018.

[135] Claudio Asencio, Aindrila Chatterjee, and Matthias W. Hentze. Silica-based solid-phase extraction of cross-linked nucleic acid–bound proteins. *Life Science Alliance*, 1(3), 6 2018.

[136] Vadim Shchepachev, Stefan Bresson, Christos Spanos, Elisabeth Petfalski, Lutz Fischer, Juri Rappsilber, and David Tollervey. Defining the RNA interactome by total RNA -associated protein purification . *Molecular Systems Biology*, 15(4):8689, 4 2019.

[137] Byungil Kim, Sarah Arcos, Katherine Rothamel, Jeffrey Jian, Kristie L. Rose, W. Hayes McDonald, Yuqi Bian, Seth Reasoner, Nicholas J. Barrows, Shelton Bradrick, Mariano A. Garcia-Blanco, and Manuel Ascano. Discovery of Widespread Host Protein Interactions with the Pre-replicated Genome of CHIKV Using VIR-CLASP. *Molecular Cell*, 78(4):624–640, 5 2020.

[138] Jakob Trendel, Thomas Schwarzl, Rastislav Horos, Ananth Prakash, Alex Bateman, Matthias W. Hentze, and Jeroen Krijgsveld. The Human RNA-Binding Proteome and Its Dynamics during Translational Arrest. *Cell*, 176(1-2):391–403, 1 2019.

[139] Rayner M.L. Queiroz, Tom Smith, Eneko Villanueva, Maria Marti-Solano, Mie Monti, Mariavittoria Pizzinga, Dan Mircea Mirea, Manasa Ramakrishna, Robert F. Harvey, Veronica Dezi, Gavin H. Thomas, Anne E. Willis, and Kathryn S. Lilley. Comprehensive identification of RNA–protein interactions in any organism using orthogonal organic phase separation (OOPS). *Nature Biotechnology*, 37(2):169–178, 2 2019.

[140] Erika C. Urdaneta and Benedikt M. Beckmann. Fast and unbiased purification of RNA-protein complexes after UV cross-linking. *Methods*, 178:72–82, 6 2020.

[141] Xiaohan Luan, Lei Wang, Guangji Song, and Wen Zhou. Innate immune responses to RNA: sensing and signaling. *Frontiers in Immunology*, 15:1287940, 1 2024.

[142] Peter D. Nagy. Viral Sensing of the Subcellular Environment Regulates the Assembly of New Viral Replicase Complexes during the Course of Infection. *Journal of Virology*, 89(10):5196, 5 2015.

[143] Elias A. Said, Nicolas Tremblay, Mohammed S. Al-Balushi, Ali A. Al-Jabri, and Daniel Lamarre. Viruses Seen by Our Cells: The Role of Viral RNA Sensors. *Journal of Immunology Research*, 2018:9480497, 2018.

[144] Anke Liepelt, Isabel S. Naarmann-De Vries, Nadine Simons, Katrin Eichelbaum, Sophia Föhr, Stuart K. Archer, Alfredo Castello, Bjorn Usadel, Jeroen Krijgsveld, Thomas Preiss, Gernot Marx, Matthias W. Hentze, Dirk H. Ostareck, and Antje Ostareck-Lederer. Identification of RNA-binding Proteins in Macrophages by Interactome Capture. *Molecular & Cellular Proteomics : MCP*, 15(8):2699, 8 2016.

[145] Louisa Iselin, Natasha Palmalux, Wael Kamel, Peter Simmonds, Shabaz Mohammed, and Alfredo Castello. Uncovering viral RNA–host cell interactions on a proteome-wide scale. *Trends in Biochemical Sciences*, 47(1):23–38, 1 2022.

[146] Byungil Kim, Sarah Arcos, Katherine Rothamel, Jeffrey Jian, Kristie L. Rose, W. Hayes McDonald, Yuqi Bian, Seth Reasoner, Nicholas J. Barrows, Shelton Bradrick, Mariano A. Garcia-Blanco, and Manuel Ascano. Discovery of Widespread Host Protein Interactions with the Pre-Replicated Genome of CHIKV using VIR-CLASP. *Molecular cell*, 78(4):624, 5 2020.

[147] Autumn T. Lapointe, Joaquín Moreno-Contreras, and Kevin J. Sokoloski. Increasing the Capping Efficiency of the Sindbis Virus nsP1 Protein Negatively

Affects Viral Infection. *mBio*, 9(6), 11 2018.

[148] Natasha N. Gebhart, Richard W. Hardy, and Kevin J. Sokoloski. Comparative analyses of alphaviral RNA:Protein complexes reveals conserved host-pathogen interactions. *PLOS ONE*, 15(8):e0238254, 8 2020.

[149] Alfredo Castelló, David Franco, Pablo Moral-López, Juan J. Berlanga, Enrique Álvarez, Eckard Wimmer, and Luis Carrasco. HIV- 1 Protease Inhibits Cap- and Poly(A)-Dependent Translation upon eIF4GI and PABP Cleavage. *PLoS ONE*, 4(11):e7997, 11 2009.

[150] Iván Ventoso, Miguel Angel Sanz, Susana Molina, Juan José Berlanga, Luis Carrasco, and Mariano Esteban. Translational resistance of late alphavirus mRNA to eIF2α phosphorylation: a strategy to overcome the antiviral effect of protein kinase PKR. *Genes & Development*, 20(1):87, 1 2006.

[151] Yanhui Hu, Aram Comjean, Jonathan Rodiger, Weihang Chen, Ah Ram Kim, Mujeeb Qadiri, Chenxi Gao, Jonathan Zirin, Stephanie E. Mohr, and Norbert Perrimon. FlyRNAi.org 2025 update—expanded resources for new technologies and species. *Nucleic Acids Research*, 53(D1):D958–D965, 1 2025.

[152] Christopher S. Hughes, Sophie Moggridge, Torsten Müller, Poul H. Sorensen, Gregg B. Morin, and Jeroen Krijgsveld. Single-pot, solid-phase-enhanced sample preparation for proteomics experiments. *Nature Protocols 2018 14:1*, 14(1):68–85, 11 2018.

[153] Peptides package - RDocumentation.

[154] Marco Necci, Damiano Piovesan, Zsuzsanna Doszt Anyi, and Silvio C E Tosatto. MobiDB-lite: fast and highly specific consensus prediction of intrinsic disorder in proteins.

[155] Philip Jones, David Binns, Hsin-Yu Chang, Matthew Fraser, Weizhong Li, Craig Mcanulla, Hamish Mcwilliam, John Maslen, Alex Mitchell, Gift Nuka, Sebastien Pesseat, Antony F Quinn, Amaia Sangrador-Vegas, Maxim Scheremetjew, Siew-Yit Yong, Rodrigo Lopez, Sarah Hunter, and Alfonso

Valencia. InterProScan 5: genome-scale protein function classification. 30(9):1236–1240, 2014.

[156] Matthias Blum, Hsin-Yu Chang, Sara Chuguransky, Tiago Grego, Swaathi Kandasaamy, Alex Mitchell, Gift Nuka, Typhaine Paysan-Lafosse, Matloob Qureshi, Shriya Raj, Lorna Richardson, Gustavo A Salazar, Lowri Williams, Alan Bridge, Julian Gough, Daniel H Haft, Ivica Letunic, Aron Marchler-Bauer, Huaiyu Mi, Darren A Natale, Marco Necci, Christine A Orengo, Arun P Pandurangan, Catherine Rivoire, Christian J A Sigrist, Ian Sillitoe, Narmada Thanki, Paul D Thomas, Silvio C E Tosatto, Cathy H Wu, Alex Bateman, and Robert D Finn. The InterPro protein families and domains database: 20 years on. *Nucleic Acids Research*, 49, 2021.

[157] Alfredo Castello, Rastislav Horos, Claudia Strein, Bernd Fischer, Katrin Eichelbaum, Lars M. Steinmetz, Jeroen Krijgsveld, and Matthias W. Hentze. System-wide identification of RNA-binding proteins by interactome capture. *Nature protocols*, 8(3):491–500, 2 2013.

[158] Alfredo Castello, Bernd Fischer, Katrin Eichelbaum, Rastislav Horos, Benedikt M. Beckmann, Claudia Strein, Norman E. Davey, David T. Humphreys, Thomas Preiss, Lars M. Steinmetz, Jeroen Krijgsveld, and Matthias W. Hentze. Insights into RNA Biology from an Atlas of Mammalian mRNA-Binding Proteins. *Cell*, 149(6):1393–1406, 6 2012.

[159] Jürgen Cox and Matthias Mann. MaxQuant enables high peptide identification rates, individualized p.p.b.-range mass accuracies and proteome-wide protein quantification. *Nature Biotechnology*, 26(12):1367–1372, 12 2008.

[160] Gordon K. Smyth. Linear models and empirical bayes methods for assessing differential expression in microarray experiments. *Statistical Applications in Genetics and Molecular Biology*, 3(1), 2004.

[161] Gideon Dreyfuss, V. Narry Kim, and Naoyuki Kataoka. Messenger-RNA-binding proteins and the messages they carry. *Nature reviews. Molecular Cell Biology*,

3(3):195–205, 3 2002.

[162] RBPbase - a comprehensive database of eukaryotic RNA-binding proteins (RBPs) with their RBP annotations.

[163] Kate B. Cook, Hilal Kazan, Khalid Zuberi, Quaid Morris, and Timothy R. Hughes. RBPDB: a database of RNA-binding specificities. *Nucleic Acids Research*, 39(Database issue):D301, 1 2010.

[164] Maiwen Caudron-Herger, Ralf E. Jansen, Elsa Wassmer, and Sven Diederichs. RBP2GO: a comprehensive pan-species database on RNA-binding proteins, their interactions and functions. *Nucleic Acids Research*, 49(D1):D425–D436, 1 2021.

[165] Yuan Zhang, Minhao Wang, Mingliu Huang, and Jinyi Zhao. Innovative strategies and challenges mosquito-borne disease control amidst climate change. *Frontiers in Microbiology*, 15:1488106, 11 2024.

[166] Scott C. Weaver and William K. Reisen. Present and Future Arboviral Threats. *Antiviral research*, 85(2):328, 2 2009.

[167] Mayra Diosa-Toro, K. Reddisiva Prasanth, Shelton S. Bradrick, and Mariano A. Garcia Blanco. Role of RNA-binding proteins during the late stages of Flavivirus replication cycle. *Virology Journal*, 17(1):60, 4 2020.

[168] Alexandra Wilson, Wael Kamel, Kelsey Davies, Zaydah R. De Laurent, Rozeena Arif, Lesley Bell-Sakyi, Douglas Lamont, Yana Demyanenko, Marko Noerenberg, Alain Kohl, Shabaz Mohammed, Alfredo Castello, and Benjamin Brennan. Uukuniemi virus infection causes a pervasive remodelling of the RNA-binding proteome in tick cell cultures. *bioRxiv*, page 2024.09.06.611624, 9 2024.

[169] Samara Rosendo Machado, Jieqiong Qu, Werner J.H. Koopman, and Pascal Miesen. The DEAD-box RNA helicase Dhx15 controls glycolysis and arbovirus replication in Aedes aegypti mosquito cells. *PLOS Pathogens*, 18(11), 11 2022.

[170] Wai Suet Lee, Julie A. Webster, Eugene T. Madzokere, Eloise B. Stephenson, and Lara J. Herrero. Mosquito antiviral defense mechanisms: a delicate balance between innate immunity and persistent viral infection. *Parasites & Vectors 2019 12:1*, 12(1):1–12, 4 2019.

[171] Ibraheem Alshareedah, Mahdi Muhammad Moosa, Matthew Pham, Davit A. Potoyan, and Priya R. Banerjee. Programmable viscoelasticity in protein-RNA condensates with disordered sticker-spacer polypeptides. *Nature communications*, 12(1), 12 2021.

[172] Emma Persson and Erik L.L. Sonnhammer. InParanoid-DIAMOND: faster orthology analysis with the InParanoid algorithm. *Bioinformatics*, 38(10):2918–2919, 5 2022.

[173] Elaine C. Meng, Thomas D. Goddard, Eric F. Pettersen, Greg S. Couch, Zach J. Pearson, John H. Morris, and Thomas E. Ferrin. UCSF ChimeraX: Tools for structure building and analysis. *Protein Science*, 32(11), 11 2023.

[174] Ulrich Bodenhofer, Enrico Bonatesta, Christoph Horejš Kainrath, and Sepp Hochreiter. msa: an R package for multiple sequence alignment.

[175] Yijia Ren, Hongyu Liao, Jun Yan, Hongyu Lu, Xiaowei Mao, Chuan Wang, Yi Fei Li, Yu Liu, Chong Chen, Lu Chen, Xiangfeng Wang, Kai Yu Zhou, Han Min Liu, Yi Liu, Yi Min Hua, Lin Yu, and Zhihong Xue. Capture of RNA-binding proteins across mouse tissues using HARD-AP. *Nature Communications*, 15(1):8421, 12 2024.

[176] Robin Van Der Lee, Marija Buljan, Benjamin Lang, Robert J Weatheritt, Gary W Daughdrill, A Keith Dunker, Monika Fuxreiter, Julian Gough, Joerg Gsponer, David T Jones, Philip M Kim, Richard W Kriwacki, Christopher J Oldfield, Rohit V Pappu, Peter Tompa, Vladimir N Uversky, Peter E Wright, and M Madan Babu. Classification of Intrinsically Disordered Regions and Proteins. 2014.

[177] Hao Guo, Jin Xu, Peiqi Xing, Qilong Li, Donghai Wang, Chao Tang, Bruno Palhais, Juliette Roels, Jiaxu Liu, Sa Pan, Jinyan Huang, Zhaoqi Liu, Ping

Zhu, Tom Taghon, Guoliang Qing, Pieter Van Vlierberghe, and Hudan Liu. RNA helicase DHX15 exemplifies a unique dependency in acute leukemia. *Haematologica*, 108(8):2029, 8 2023.

[178] Sourav Saha, Yilun Sun, Shar yin Naomi Huang, Simone Andrea Baechler, Lorinc Sandor Pongor, Keli Agama, Ukhyun Jo, Hongliang Zhang, Yuk Ching Tse-Dinh, and Yves Pommier. DNA and RNA Cleavage Complexes and Repair Pathway for TOP3B RNA- and DNA-Protein Crosslinks. *Cell Reports*, 33(13), 12 2020.

[179] Stefanie Gerstberger, Markus Hafner, and Thomas Tuschl. A census of human RNA-binding proteins. *Nature Reviews Genetics*, 15(12):829–845, 1 2014.

[180] Jie Jia, Abul Arif, Partho S. Ray, and Paul L. Fox. WHEP Domains Direct Noncanonical Function of Glutamyl-Prolyl tRNA Synthetase in Translational Control of Gene Expression. *Molecular Cell*, 29(6):679–690, 3 2008.

[181] William E. Walden, Anna I. Selezneva, Jérôme Dupuy, Anne Volbeda, Juan C. Fontecilla-Camps, Elizabeth C. Theil, and Karl Volz. Structure of dual function iron regulatory protein 1 complexed with ferritin IRE-RNA. *Science (New York, N.Y.)*, 314(5807):1903–1908, 12 2006.

[182] Joel I. Perez-Perri, Birgit Rogell, Thomas Schwarzl, Frank Stein, Yang Zhou, Mandy Rettel, Annika Brosig, and Matthias W. Hentze. Discovery of RNA-binding proteins and characterization of their dynamic responses by enhanced RNA interactome capture. *Nature Communications*, 9(1):4408, 12 2018.

[183] Aino I. Järvelin, Marko Noerenberg, Ilan Davis, and Alfredo Castello. The new (dis)order in RNA regulation. *Cell communication and signaling : CCS*, 14(1), 4 2016.

[184] Benedikt M. Beckmann, Rastislav Horos, Bernd Fischer, Alfredo Castello, Katrin Eichelbaum, Anne Marie Alleaume, Thomas Schwarzl, Tomaž Curk, Sophia Foehr, Wolfgang Huber, Jeroen Krijgsveld, and Matthias W. Hentze. The RNA-

binding proteomes from yeast to man harbour conserved enigmRBPs. *Nature Communications*, 6:10127, 12 2015.

[185] Alfredo Castello, Lucía Álvarez, Wael Kamel, Louisa Iselin, and Janosch Hennig. Exploring the expanding universe of host-virus interactions mediated by viral RNA. *Molecular Cell*, 84(19):3706–3721, 10 2024.

[186] Martin R. Jakobsen, Rasmus O. Bak, Annika Andersen, Randi K. Berg, Søren B. Jensen, Tengchuan Jin, Anders Laustsen, Kathrine Hansen, Lars Østergaard, Katherine A. Fitzgerald, T. Sam Xiao, Jacob G. Mikkelsen, Trine H. Mogensen, and Søren R. Paludan. IFI16 senses DNA forms of the lentiviral replication cycle and controls HIV-1 replication. *Proceedings of the National Academy of Sciences*, 110(48):E4571–E4580, 11 2013.

[187] Byungil Kim, Sarah Arcos, Katherine Rothamel, and Manuel Ascano. Viral crosslinking and solid-phase purification enables discovery of ribonucleoprotein complexes on incoming RNA virus genomes. *Nature protocols*, 16(1):516–531, 1 2021.

[188] Marco Grodzki, Andrew P. Bluhm, Moritz Schaefer, Abderrahmane Tagmount, Max Russo, Amin Sobh, Roya Rafiee, Chris D. Vulpe, Stephanie M. Karst, and Michael H. Norris. Genome-scale CRISPR screens identify host factors that promote human coronavirus infection. *Genome Medicine*, 14(1):1–18, 12 2022.

[189] Lucie Cappuccio and Carine Maisse. Infection of Mammals and Mosquitoes by Alphaviruses: Involvement of Cell Death. *Cells*, 9(12), 12 2020.

[190] Anthony C. Fredericks, Tiffany A. Russell, Louisa E. Wallace, Andrew D. Davidson, Ana Fernandez-Sesma, and Kevin Maringer. Aedes aegypti (Aag2)-derived clonal mosquito cell lines reveal the effects of pre-existing persistent infection with the insect-specific bunyavirus Phasi Charoen-like virus on arbovirus replication. *PLoS Neglected Tropical Diseases*, 13(11):e0007346, 2019.

[191] Wolfgang Huber, Anja Von Heydebreck, Holger Sültmann, Annemarie Poustka,

and Martin Vingron. Variance stabilization applied to microarray data calibration }and to the quantification of differential expression. *Bioinformatics*, 18(suppl_1):S96–S104, 7 2002.

[192] Maintainer Gordon Smyth. Package 'limma' Title Linear Models for Microarray and Omics Data. 2025.

[193] Korbinian Strimmer. fdrtool: a versatile R package for estimating local and tail area-based false discovery rates. *Bioinformatics*, 24(12):1461–1462, 6 2008.

[194] Autumn C. Holmes, Katherine Basore, Daved H. Fremont, and Michael S. Diamond. A molecular understanding of alphavirus entry. *PLOS Pathogens*, 16(10):e1008876, 10 2020.

[195] Jüri Reimand, Meelis Kull, Hedi Peterson, Jaanus Hansen, and Jaak Vilo. g:Profiler—a web-based toolset for functional profiling of gene lists from large-scale experiments. *Nucleic Acids Research*, 35(Web Server issue):W193, 7 2007.

[196] Jelke J. Fros and Gorben P. Pijlman. Alphavirus Infection: Host Cell Shut-Off and Inhibition of Antiviral Responses. *Viruses 2016, Vol. 8, Page 166*, 8(6):166, 6 2016.

[197] Anna Fernanda Vasconcellos, Reynaldo Magalhães Melo, Samuel Coelho Mandacaru, Lucas Silva de Oliveira, Athos Silva de Oliveira, Emily Caroline dos Santos Moraes, Monique Ramos de Oliveira Trugilho, Carlos André Ornelas Ricart, Sônia Nair Báo, Renato Oliveira Resende, and Sébastien Charneau. Aedes aegypti Aag-2 Cell Proteome Modulation in Response to Chikungunya Virus Infection. *Frontiers in Cellular and Infection Microbiology*, 12:920425, 6 2022.

[198] Megan B. Kingsolver, Zhijing Huang, and Richard W. Hardy. Insect antiviral innate immunity: pathways, effectors, and connections. *Journal of molecular biology*, 425(24):4921, 12 2013.

[199] J A Lemm and C M Rice. Roles of nonstructural polyproteins and cleavage products in regulating Sindbis virus RNA replication and transcription. *Journal of Virology*, 67(4):1916, 4 1993.

[200] Iván Ventoso, Juan José Berlanga, René Toribio, and Irene Díaz-López. Translational Control of Alphavirus–Host Interactions: Implications in Viral Evolution, Tropism and Antiviral Response. *Viruses*, 16(2):205, 2 2024.

[201] Rodion Gorchakov, Elena Frolova, Bryan R. G. Williams, Charles M. Rice, and Ilya Frolov. PKR-Dependent and -Independent Mechanisms Are Involved in Translational Shutoff during Sindbis Virus Infection. *Journal of Virology*, 78(16):8455, 8 2004.

[202] Gerald M. McInerney, Nancy L. Kedersha, Randal J. Kaufman, Paul Anderson, and Peter Liljeström. Importance of eIF2α Phosphorylation and Stress Granule Assembly in Alphavirus Translation Regulation. *Molecular Biology of the Cell*, 16(8):3753, 8 2005.

[203] Ivan Akhrymuk, Sergey V. Kulemzin, and Elena I. Frolova. Evasion of the Innate Immune Response: the Old World Alphavirus nsP2 Protein Induces Rapid Degradation of Rpb1, a Catalytic Subunit of RNA Polymerase II. *Journal of Virology*, 86(13):7180–7191, 7 2012.

[204] Rodion Gorchakov, Natalia Garmashova, Elena Frolova, and Ilya Frolov. Different Types of nsP3-Containing Protein Complexes in Sindbis Virus-Infected Cells. *Journal of Virology*, 82(20):10088, 10 2008.

[205] John W. Schoggins and Charles M. Rice. Interferon-stimulated genes and their antiviral effector functions. *Current Opinion in Virology*, 1(6):519, 2011.

[206] Svetlana Atasheva, Natalia Garmashova, Ilya Frolov, and Elena Frolova. Venezuelan Equine Encephalitis Virus Capsid Protein Inhibits Nuclear Import in Mammalian but Not in Mosquito Cells. *Journal of Virology*, 82(8):4028, 4 2008.

[207] Carol D. Blair. Mosquito RNAi is the major innate immune pathway controlling arbovirus infection and transmission. *Future microbiology*, 6(3):265, 3 2011.

[208] Esther Schnettler, Mark G. Sterken, Jason Y. Leung, Stefan W. Metz, Corinne Geertsema, Rob W. Goldbach, Just M. Vlak, Alain Kohl, Alexander A. Khromykh, and Gorben P. Pijlman. Noncoding Flavivirus RNA Displays RNA Interference Suppressor Activity in Insect and Mammalian Cells. *Journal of Virology*, 86(24):13486–13500, 12 2012.

[209] G. P. Göertz, J. J. Fros, P. Miesen, C. B. F. Vogels, M. L. van der Bent, C. Geertsema, C. J. M. Koenraadt, R. P. van Rij, M. M. van Oers, and G. P. Pijlman. Noncoding Subgenomic Flavivirus RNA Is Processed by the Mosquito RNA Interference Machinery and Determines West Nile Virus Transmission by Culex pipiens Mosquitoes. *Journal of Virology*, 90(22):10145–10159, 11 2016.

[210] Yingjun Cui, Pei Liu, Brian P. Mooney, and Alexander W.E. Franz. Quantitative proteomic analysis of chikungunya virus-infected Aedes aegypti reveals proteome modulations indicative of persistent infection. *Journal of proteome research*, 19(6):2443, 6 2020.

[211] Vincenzo Ruscica, Louisa Iselin, Ryan Hull, Azman Embarc-Buh, Samyukta Narayanan, Natasha Palmalux, Namah Raut, Quan Gu, Honglin Chen, Marko Noerenberg, Zaydah R. de Laurent, Josmi Joseph, Michelle Noble, Catia Igreja, David L. Robertson, Joseph Hughes, Shabaz Mohammed, Vicent Pelechano, Ilan Davis, and Alfredo Castello. XRN1 supplies free nucleotides to feed alphavirus replication. *bioRxiv*, page 2024.12.09.625895, 12 2024.

[212] Gerard Terradas and Elizabeth A. McGraw. Using genetic variation in Aedes aegypti to identify candidate anti-dengue virus genes. *BMC Infectious Diseases*, 19(1):580, 7 2019.

[213] Sandra E. Pérez, Monika Gooz, and Eduardo N. Maldonado. Mitochondrial Dysfunction and Metabolic Disturbances Induced by Viral Infections. *Cells*, 13(21):1789, 11 2024.

[214] Tatiana El-Bacha and Andrea T. Da Poian. Virus-induced changes in mitochondrial bioenergetics as potential targets for therapy. *The International Journal of Biochemistry & Cell Biology*, 45(1):41–46, 1 2013.

[215] M. Gabriella Santoro, Antonio Rossi, and Carla Amici. NF-κB and virus infection: who controls whom. *The EMBO Journal*, 22(11):2552–2560, 6 2003.

[216] Haoxiong Zhou, Sizhe Wan, Yujun Luo, Huiling Liu, Jie Jiang, Yunwei Guo, Jia Xiao, and Bin Wu. Hepatitis B virus X protein induces ALDH2 ubiquitin-dependent degradation to enhance alcoholic steatohepatitis. *Gastroenterology Report*, 11:goad006, 2023.

[217] Meihui Huang, Yucong Li, Yuxiao Li, and Shuiping Liu. C-Terminal Binding Protein: Regulator between Viral Infection and Tumorigenesis. *Viruses 2024, Vol. 16, Page 988*, 16(6):988, 6 2024.

[218] Abul Arif, Peng Yao, Fulvia Terenzi, Jie Jia, Partho Sarothi Ray, and Paul L. Fox. The GAIT translational control system. *Wiley Interdisciplinary Reviews. RNA*, 9(2):e1441, 3 2017.

[219] Bishnu P. De, Sanhita Gupta, Hong Zhao, Judith A. Drazba, and Amiya K. Banerjee. Specific Interaction in Vitro and in Vivo of Glyceraldehyde-3-phosphate Dehydrogenase and LA Protein with Cis-acting RNAs of Human Parainfluenza Virus Type 3. *Journal of Biological Chemistry*, 271(40):24728–24735, 10 1996.

[220] Aashir Awan. GAPDH, Interferon γ, and Nitric Oxide: Inhibitors of Coronaviruses. *Frontiers in Virology*, 1:682136, 9 2021.

[221] Norman E. Davey, Gilles Travé, and Toby J. Gibson. How viruses hijack cell regulation. *Trends in Biochemical Sciences*, 36(3):159–169, 3 2011.

[222] Manuel Garcia-Moreno, Aino I. Järvelin, and Alfredo Castello. Unconventional RNA-binding proteins step into the virus–host battlefront. *Wiley Interdisciplinary Reviews. RNA*, 9(6):e1498, 11 2018.

[223] Allyn Spear, Nidhi Sharma, and James Bert Flanegan. Protein-RNA Tethering: The Role of Poly(C) Binding Protein 2 in Poliovirus RNA Replication. *Virology*, 374(2):280, 5 2008.

[224] Le Ann P. Nguyen, Kelly S. Aldana, Emily Yang, Zhenlan Yao, and Melody M.H. Li. Alphavirus Evasion of Zinc Finger Antiviral Protein (ZAP) Correlates with CpG Suppression in a Specific Viral nsP2 Gene Sequence. *Viruses*, 15(4):830, 4 2023.

[225] Irma Sánchez-Vargas, Jaclyn C. Scott, B. Katherine Poole-Smith, Alexander W.E. Franz, Valérie Barbosa-Solomieu, Jeffrey Wilusz, Ken E. Olson, and Carol D. Blair. Dengue Virus Type 2 Infections of Aedes aegypti Are Modulated by the Mosquito's RNA Interference Pathway. *PLOS Pathogens*, 5(2):e1000299, 2 2009.

[226] Esther Schnettler, Claire L. Donald, Stacey Human, Mick Watson, Ricky W.C. Siu, Melanie McFarlane, John K. Fazakerley, Alain Kohl, and Rennos Fragkoudis. Knockdown of piRNA pathway proteins results in enhanced Semliki Forest virus production in mosquito cells. *The Journal of General Virology*, 94(Pt 7):1680, 7 2013.

[227] Corey L. Campbell, Kimberly M. Keene, Douglas E. Brackney, Ken E. Olson, Carol D. Blair, Jeffrey Wilusz, and Brian D. Foy. Aedes aegypti uses RNA interference in defense against Sindbis virus infection. *BMC Microbiology*, 8:47, 2008.

[228] Isabelle Dietrich, Xiaohong Shi, Melanie McFarlane, Mick Watson, Anne Lie Blomström, Jessica K. Skelton, Alain Kohl, Richard M. Elliott, and Esther Schnettler. The Antiviral RNAi Response in Vector and Non-vector Cells against Orthobunyaviruses. *PLOS Neglected Tropical Diseases*, 11(1):e0005272, 1 2017.

[229] Shwetha Shivaprasad, Kuo Feng Weng, Yaw Shin Ooi, Julia Belk, Jan E. Carette, Ryan Flynn, and Peter Sarnow. Loquacious modulates flaviviral RNA

replication in mosquito cells. *PLOS Pathogens*, 18(4):e1010163, 4 2022.

[230] John P. Burand and Wayne B. Hunter. RNAi: Future in insect management. *Journal of Invertebrate Pathology*, 112(SUPPL.1), 3 2013.

[231] Mallikarjuna R. Joga, Moises J. Zotti, Guy Smagghe, and Olivier Christiaens. RNAi Efficiency, Systemic Properties, and Novel Delivery Methods for Pest Insect Control: What We Know So Far. *Frontiers in Physiology*, 7(NOV):553, 11 2016.

[232] Neema Agrawal, P. V. N. Dasaradhi, Asif Mohmmed, Pawan Malhotra, Raj K. Bhatnagar, and Sunil K. Mukherjee. RNA Interference: Biology, Mechanism, and Applications. *Microbiology and Molecular Biology Reviews*, 67(4):657–685, 12 2003.

[233] Claire L. Donald, Alain Kohl, and Esther Schnettler. New Insights into Control of Arbovirus Replication and Spread by Insect RNA Interference Pathways. *Insects*, 3(2):511, 2012.

[234] Gregory J. Hannon. RNA interference. *Nature*, 418(6894):244–251, 7 2002.

[235] Anders Fjose, Ståle Ellingsen, Anna Wargelius, and Hee Chan Seo. RNA interference: Mechanisms and applications. *Biotechnology Annual Review*, 7:31–57, 2001.

[236] Shantanu Karkare, Saurabha Daniel, and Deepak Bhatnagar. RNA interference silencing the transcriptional message: Aspects and applications. *Applied Biochemistry and Biotechnology - Part A Enzyme Engineering and Biotechnology*, 119(1):1–12, 2004.

[237] M. McFarlane, M. Laureti, T. Levée, S. Terry, A. Kohl, and E. Pondeville. Improved transient silencing of gene expression in the mosquito female Aedes aegypti. *Insect Molecular Biology*, 30(3):355–365, 6 2021.

[238] Zach N. Adelman, Irma Sanchez-Vargas, Emily A. Travanty, Jon O. Carlson, Barry J. Beaty, Carol D. Blair, and Ken E. Olson. RNA Silencing of Dengue

Virus Type 2 Replication in Transformed C6/36 Mosquito Cells Transcribing an Inverted-Repeat RNA Derived from the Virus Genome. *Journal of Virology*, 76(24):12925, 12 2002.

[239] Jaclyn C. Scott, Doug E. Brackney, Corey L. Campbell, Virginie Bondu-Hawkins, Brian Hjelle, Greg D. Ebel, Ken E. Olson, and Carol D. Blair. Comparison of Dengue Virus Type 2-Specific Small RNAs from RNA Interference-Competent and –Incompetent Mosquito Cells. *PLoS Neglected Tropical Diseases*, 4(10):e848, 10 2010.

[240] Li He, Yanna Huang, and Xueming Tang. RNAi-based pest control: Production, application and the fate of dsRNA. *Frontiers in Bioengineering and Biotechnology*, 10:1080576, 11 2022.

[241] Sonja Mehlhorn, Vera S. Hunnekuhl, Sven Geibel, Ralf Nauen, and Gregor Bucher. Establishing RNAi for basic research and pest control and identification of the most efficient target genes for pest control: a brief guide. *Frontiers in Zoology*, 18(1):60, 12 2021.

[242] Olivier Christiaens, Steve Whyard, Ana M. Vélez, and Guy Smagghe. Double-Stranded RNA Technology to Control Insect Pests: Current Status and Challenges. *Frontiers in Plant Science*, 11:451, 4 2020.

[243] Raja Sekhar Nandety, Yen Wen Kuo, Shahideh Nouri, and Bryce W. Falk. Emerging strategies for RNA interference (RNAi) applications in insects. *Bioengineered*, 6(1):8, 2014.

[244] Anastasia M.W. Cooper, Kristopher Silver, Jianzhen Zhang, Yoonseong Park, and Kun Yan Zhu. Molecular mechanisms influencing efficiency of RNA interference in insects. *Pest Management Science*, 75(1):18–28, 1 2019.

[245] Zhi Xiong Chong, Swee Keong Yeap, and Wan Yong Ho. Transfection types, methods and strategies: A technical review. *PeerJ*, 9:e11165, 4 2021.

[246] Bodunrin Omokungbe, Alejandra Centurión, Sabrina Stiehler, Antonia Morr, Andreas Vilcinskas, Antje Steinbrink, and Kornelia Hardes. Gene silencing in

the aedine cell lines C6/36 and U4.4 using long double-stranded RNA. *Parasites & Vectors*, 17(1):255, 12 2024.

[247] Adolf Michael Sandbichler, Teresa Aschberger, and Bernd Pelster. A Method to Evaluate the Efficiency of Transfection Reagents in an Adherent Zebrafish Cell Line. *BioResearch Open Access*, 2(1):20, 2 2013.

[248] Derek Walsh, Michael B. Mathews, and Ian Mohr. Tinkering with Translation: Protein Synthesis in Virus-Infected Cells. *Cold Spring Harbor Perspectives in Biology*, 5(1):a012351, 1 2013.

[249] Derek Walsh and Ian Mohr. Viral subversion of the host protein synthesis machinery. *Nature Reviews. Microbiology*, 9(12):860, 12 2011.

[250] Roberta Marchione, Serge A. Leibovitch, and Jean Luc Lenormand. The translational factor eIF3f: the ambivalent eIF3 subunit. *Cellular and Molecular Life Sciences : CMLS*, 70(19):3603–3616, 1 2013.

[251] Sebastian Fenn, Zhihua Du, John K. Lee, Richard Tjhen, Robert M. Stroud, and Thomas L. James. Crystal structure of the third KH domain of human poly(C)-binding protein-2 in complex with a C-rich strand of human telomeric DNA at 1.6 A resolution. *Nucleic acids research*, 35(8):2651–2660, 4 2007.

[252] Aleksandr V. Makeyev and Stephen A. Liebhaber. The poly(C)-binding proteins: a multiplicity of functions and a search for mechanisms. *RNA*, 8(3):265, 2002.

[253] Haiyan Gu, Jing Yang, Jiayu Zhang, Ying Song, Yao Zhang, Pengfei Xu, Yuanxiang Zhu, Liangliang Wang, Pengfei Zhang, Lin Li, Dahua Chen, and Qinmiao Sun. PCBP2 maintains antiviral signaling homeostasis by regulating cGAS enzymatic activity via antagonizing its condensation. *Nature Communications*, 13(1):1564, 12 2022.

[254] Phillida A. Charley and Jeffrey Wilusz. Standing your ground to exoribonucleases: Function of Flavivirus long non-coding RNAs. *Virus Research*, 212:70, 1 2015.

[255] Yessica Y. Llamas-González, Dalkiria Campos, Juan M. Pascale, Juan Arbiza, and José González-Santamaría. A Functional Ubiquitin-Proteasome System is Required for Efficient Replication of New World Mayaro and Una Alphaviruses. *Viruses 2019, Vol. 11, Page 370*, 11(4):370, 4 2019.

[256] Maria Velez-Brochero, Padmanava Behera, Kazi Sabrina Afreen, Abby Odle, and Ricardo Rajsbaum. Ubiquitination in viral entry and replication: Mechanisms and implications. *Advances in Virus Research*, 119:1–38, 1 2024.

[257] Honglin Luo. Interplay between the virus and the ubiquitin–proteasome system: molecular mechanism of viral pathogenesis. *Current Opinion in Virology*, 17:1–10, 4 2016.

[258] Alex Goeun Choi, Jerry Wong, David Marchant, and Honglin Luo. The ubiquitin-proteasome system in positive-strand RNA virus infection. *Reviews in Medical Virology*, 23(2):85, 3 2012.

[259] Sukanya Chakravarty, Gayatri Subramanian, Sonam Popli, Manoj Veleeparambil, Shumin Fan, Ritu Chakravarti, and Saurabh Chattopadhyay. Interferon-stimulated gene TDRD7 interacts with AMPK and inhibits its activation to suppress viral replication and pathogenesis. *mBio*, 14(5), 10 2023.

[260] Gayatri Subramanian, Teodora Kuzmanovic, Ying Zhang, Cara Beate Peter, Manoj Veleeparambil, Ritu Chakravarti, Ganes C. Sen, and Saurabh Chattopadhyay. A new mechanism of interferon's antiviral action: Induction of autophagy, essential for paramyxovirus replication, is inhibited by the interferon stimulated gene, TDRD7. *PLOS Pathogens*, 14(1):e1006877, 1 2018.

[261] Nicholas S. Heaton and Glenn Randall. Dengue Virus-Induced Autophagy Regulates Lipid Metabolism. *Cell Host & Microbe*, 8(5):422–432, 11 2010.

[262] Rodolphe Hamel, Ophélie Dejarnac, Sineewanlaya Wichit, Peeraya Ekchariyawat, Aymeric Neyret, Natthanej Luplertlop, Manuel Perera-Lecoin, Pornapat Surasombatpattana, Loïc Talignani, Frédéric Thomas, Van-Mai Cao-Lormeau, Valérie Choumet, Laurence Briant, Philippe Desprès, Ali Amara,

Hans Yssel, and Dorothée Missé. Biology of Zika Virus Infection in Human Skin Cells. *Journal of Virology*, 89(17):8880–8896, 9 2015.

[263] Rastislav Horos, Magdalena Büscher, Rozemarijn Kleinendorst, Anne Marie Alleaume, Abul K. Tarafder, Thomas Schwarzl, Dmytro Dziuba, Christian Tischer, Elisabeth M. Zielonka, Asli Adak, Alfredo Castello, Wolfgang Huber, Carsten Sachse, and Matthias W. Hentze. The Small Non-coding Vault RNA1-1 Acts as a Riboregulator of Autophagy. *Cell*, 176(5):1054–1067, 2 2019.

[264] Michela Mazzon, Cecilia Castro, Bastian Thaa, Lifeng Liu, Margit Mutso, Xiang Liu, Suresh Mahalingam, Julian L. Griffin, Mark Marsh, and Gerald M. McInerney. Alphavirus-induced hyperactivation of PI3K/AKT directs pro-viral metabolic changes. *PLOS Pathogens*, 14(1):e1006835, 1 2018.

[265] Zhenlu Zhang, Guijuan He, Natalie A. Filipowicz, Glenn Randall, George A. Belov, Benjamin G. Kopek, and Xiaofeng Wang. Host lipids in positive-strand RNA virus genome replication. *Frontiers in Microbiology*, 10(FEB):440841, 2 2019.

[266] Markus C. Wahl, Cindy L. Will, and Reinhard Lührmann. The Spliceosome: Design Principles of a Dynamic RNP Machine. *Cell*, 136(4):701–718, 2 2009.

[267] Constantin Cretu, Jana Schmitzová, Almudena Ponce-Salvatierra, Olexandr Dybkov, Evelina I. De Laurentiis, Kundan Sharma, Cindy L. Will, Henning Urlaub, Reinhard Lührmann, and Vladimir Pena. Molecular Architecture of SF3b and Structural Consequences of Its Cancer-Related Mutations. *Molecular Cell*, 64(2):307–319, 10 2016.

[268] Alfredo Castello and Wael Kamel. Nuclear RNA-binding proteins meet cytoplasmic viruses. *RNA*, 31(3):444, 3 2025.

[269] Ali Shilatifard. The COMPASS family of histone H3K4 methylases: Mechanisms of regulation in development and disease pathogenesis. *Annual Review of Biochemistry*, 81(Volume 81, 2012):65–95, 7 2012.

[270] Brian M. Ortmann, Natalie Burrows, Ian T. Lobb, Esther Arnaiz, Niek Wit, Peter S.J. Bailey, Louise H. Jordon, Olivia Lombardi, Ana Peñalver, James McCaffrey, Rachel Seear, David R. Mole, Peter J. Ratcliffe, Patrick H. Maxwell, and James A. Nathan. The HIF complex recruits the histone methyltransferase SET1B to activate specific hypoxia-inducible genes. *Nature genetics*, 53(7):1022, 7 2021.

[271] Eva Neugebauer, Aura M. Bastidas-Quintero, Daniel Weidl, and Florian Full. Pioneer factors in viral infection. *Frontiers in Immunology*, 14:1286617, 10 2023.

[272] T. Walker, P. H. Johnson, L. A. Moreira, I. Iturbe-Ormaetxe, F. D. Frentiu, C. J. McMeniman, Y. S. Leong, Y. Dong, J. Axford, P. Kriesner, A. L. Lloyd, S. A. Ritchie, S. L. O'Neill, and A. A. Hoffmann. The wMel Wolbachia strain blocks dengue and invades caged Aedes aegypti populations. *Nature*, 476(7361):450–455, 8 2011.

[273] Wai Suet Lee, Julie A. Webster, Eugene T. Madzokere, Eloise B. Stephenson, and Lara J. Herrero. Mosquito antiviral defense mechanisms: a delicate balance between innate immunity and persistent viral infection. *Parasites & Vectors*, 12(1):165, 4 2019.

[274] Margus Varjak, Claire L. Donald, Timothy J. Mottram, Vattipally B. Sreenu, Andres Merits, Kevin Maringer, Esther Schnettler, and Alain Kohl. Characterization of the Zika virus induced small RNA response in Aedes aegypti cells. *PLOS Neglected Tropical Diseases*, 11(10):e0006010, 10 2017.

[275] Shuaikun Su, Yutong Xue, Alexei Sharov, Yongqing Zhang, Seung Kyu Lee, Jennifer L. Martindale, Wen Li, Wai Lim Ku, Keji Zhao, Supriyo De, Weiping Shen, Payel Sen, Myriam Gorospe, Dongyi Xu, and Weidong Wang. A dual-activity topoisomerase complex regulates mRNA translation and turnover. *Nucleic Acids Research*, 50(12):7013, 7 2022.

[276] Seung Kyu Lee, Yutong Xue, Weiping Shen, Yongqing Zhang, Yuyoung Joo, Muzammil Ahmad, Madoka Chinen, Yi Ding, Wai Lim Ku, Supriyo De, Elin

Lehrmann, Kevin G. Becker, Elissa P. Lei, Keji Zhao, Sige Zou, Alexei Sharov, and Weidong Wang. Topoisomerase 3β interacts with RNAi machinery to promote heterochromatin formation and transcriptional silencing in Drosophila. *Nature Communications*, 9(1):4946, 12 2018.

[277] Sowmya Pattabhi, Megan L. Knoll, Michael Gale, and Yueh Ming Loo. DHX15 Is a Coreceptor for RLR Signaling That Promotes Antiviral Defense Against RNA Virus Infection. *Journal of Interferon and Cytokine Research*, 39(6):331–346, 6 2019.

[278] Kenta Mosallanejad, Yusuke Sekine, Seiko Ishikura-Kinoshita, Kazuo Kumagai, Tetsuo Nagano, Atsushi Matsuzawa, Kohsuke Takeda, Isao Naguro, and Hidenori Ichijo. The DEAH-Box RNA helicase DHX15 activates NF-κB and MAPK signaling downstream of MAVS during antiviral responses. *Science Signaling*, 7(323), 4 2014.

[279] Matthias W. Hentze, Pia Sommerkamp, Venkatraman Ravi, and Fátima Gebauer. Rethinking RNA-binding proteins: Riboregulation challenges prevailing views. *Cell*, 188(18):4811–4827, 9 2025.

[280] Jerome M Molleston, Sara Cherry, Karen Beemon, and Robert Hogg. Attacked from All Sides: RNA Decay in Antiviral Defense. *Viruses 2017, Vol. 9, Page 2*, 9(1):2, 1 2017.

[281] Vishvanath Nene, Jennifer R. Wortman, Daniel Lawson, Brian Haas, Chinnappa Kodira, Zhijian Tu, Brendan Loftus, Zhiyong Xi, Karyn Megy, Manfred Grabherr, Quinghu Ren, Evgeny M. Zdobnov, Neil F. Lobo, Kathryn S. Campbell, Susan E. Brown, Maria F. Bonaldo, Jingsong Zhu, Steven P. Sinkins, David G. Hogenkamp, Paolo Amedeo, Peter Arensburger, Peter W. Atkinson, Shelby Bidwell, Jim Biedler, Ewan Birney, Robert V. Bruggner, Javier Costas, Monique R. Coy, Jonathan Crabtree, Matt Crawford, Becky DeBruyn, David DeCaprio, Karin Eiglmeier, Eric Eisenstadt, Hamza El-Dorry, William M. Gelbart, Suely L. Gomes, Martin Hammond, Linda I. Hannick, James R. Hogan, Michael H. Holmes, David Jaffe, J. Spencer Johnston, Ryan C. Kennedy, Hean

Koo, Saul Kravitz, Evgenia V. Kriventseva, David Kulp, Kurt LaButti, Eduardo Lee, Song Li, Diane D. Lovin, Chunhong Mao, Evan Mauceli, Carlos F.M. Menck, Jason R. Miller, Philip Montgomery, Akio Mori, Ana L. Nascimento, Horacio F. Naveira, Chad Nusbaum, Sinéad O'Leary, Joshua Orvis, Mihaela Pertea, Hadi Quesneville, Kyanne R. Reidenbach, Yu Hui Rogers, Charles W. Roth, Jennifer R. Schneider, Michael Schatz, Martin Shumway, Mario Stanke, Eric O. Stinson, Jose M.C. Tubio, Janice P. VanZee, Sergio Verjovski-Almeida, Doreen Werner, Owen White, Stefan Wyder, Qiandong Zeng, Qi Zhao, Yongmei Zhao, Catherine A. Hill, Alexander S. Raikhel, Marcelo B. Soares, Dennis L. Knudson, Norman H. Lee, James Galagan, Steven L. Salzberg, Ian T. Paulsen, George Dimopoulos, Frank H. Collins, Bruce Birren, Claire M. Fraser-Liggett, and David W. Severson. Genome sequence of Aedes aegypti, a major arbovirus vector. *Science (New York, N.Y.)*, 316(5832):1718–1723, 6 2007.

[282] Benjamin J. Matthews, Olga Dudchenko, Sarah B. Kingan, Sergey Koren, Igor Antoshechkin, Jacob E. Crawford, William J. Glassford, Margaret Herre, Seth N. Redmond, Noah H. Rose, Gareth D. Weedall, Yang Wu, Sanjit S. Batra, Carlos A. Brito-Sierra, Steven D. Buckingham, Corey L. Campbell, Saki Chan, Eric Cox, Benjamin R. Evans, Thanyalak Fansiri, Igor Filipović, Albin Fontaine, Andrea Gloria-Soria, Richard Hall, Vinita S. Joardar, Andrew K. Jones, Raissa G.G. Kay, Vamsi K. Kodali, Joyce Lee, Gareth J. Lycett, Sara N. Mitchell, Jill Muehling, Michael R. Murphy, Arina D. Omer, Frederick A. Partridge, Paul Peluso, Aviva Presser Aiden, Vidya Ramasamy, Gordana Rašić, Sourav Roy, Karla Saavedra-Rodriguez, Shruti Sharan, Atashi Sharma, Melissa Laird Smith, Joe Turner, Allison M. Weakley, Zhilei Zhao, Omar S. Akbari, William C. Black, Han Cao, Alistair C. Darby, Catherine A. Hill, J. Spencer Johnston, Terence D. Murphy, Alexander S. Raikhel, David B. Sattelle, Igor V. Sharakhov, Bradley J. White, Li Zhao, Erez Lieberman Aiden, Richard S. Mann, Louis Lambrechts, Jeffrey R. Powell, Maria V. Sharakhova, Zhijian Tu, Hugh M. Robertson, Carolyn S. McBride, Alex R. Hastie, Jonas Korlach, Daniel E. Neafsey, Adam M. Phillippy, and Leslie B. Vosshall. Improved reference genome of Aedes aegypti

informs arbovirus vector control. *Nature*, 563(7732):501–507, 11 2018.

[283] Samara Rosendo Machado, Tom van der Most, and Pascal Miesen. Genetic determinants of antiviral immunity in dipteran insects – Compiling the experimental evidence. *Developmental & Comparative Immunology*, 119:104010, 6 2021.

[284] F. Li, X. Zhao, M. Li, K. He, C. Huang, Y. Zhou, Z. Li, and J. R. Walters. Insect genomes: progress and challenges. *Insect molecular biology*, 28(6):739–758, 12 2019.

[285] Jay D. Evans, Susan J. Brown, Kevin J.J. Hackett, Gene Robinson, Stephen Richards, Daniel Lawson, Christine Elsik, Jonathan Coddington, Owain Edwards, Scott Emrich, Toni Gabaldon, Marian Goldsmith, Glenn Hanes, Bernard Misof, Monica Muñoz-Torres, Oliver Niehuis, Alexie Papanicolaou, Michael Pfrender, Monica Poelchau, Mary Purcell-Miramontes, Hugh M. Robertson, Oliver Ryder, Denis Tagu, Tatiana Torres, Evgeny Zdobnov, Guojie Zhang, and Xin Zhou. The i5K Initiative: Advancing Arthropod Genomics for Knowledge, Human Health, Agriculture, and the Environment. *Journal of Heredity*, 104(5):595, 9 2013.

[286] Ina Huppertz, Jan Attig, Andrea D'Ambrogio, Laura E. Easton, Christopher R. Sibley, Yoichiro Sugimoto, Mojca Tajnik, Julian König, and Jernej Ule. iCLIP: Protein–RNA interactions at nucleotide resolution. *Methods (San Diego, Calif.)*, 65(3):274, 2014.

[287] Lucas Henrique Figueiredo Prates, Jakob Fiebig, Henrik Schlosser, Eleni Liapi, Tanja Rehling, Célia Lutrat, Jeremy Bouyer, Qiang Sun, Han Wen, Zhiyong Xi, Marc F. Schetelig, and Irina Häcker. Challenges of Robust RNAi-Mediated Gene Silencing in Aedes Mosquitoes. *International Journal of Molecular Sciences*, 25(10):5218, 5 2024.

[288] Kathryn E. Kistler, Leslie B. Vosshall, and Benjamin J. Matthews. Genome Engineering with CRISPR-Cas9 in the Mosquito Aedes aegypti. *Cell Reports*,

11(1):51–60, 4 2015.

[289] Louis Lambrechts and Maria Carla Saleh. Manipulating Mosquito Tolerance for Arbovirus Control. *Cell Host and Microbe*, 26(3):309–313, 9 2019.